Spatiotemporal Patterns and Dominant Controls of Riverine Nutrient Export Across Catchments

Dissertation

zur Erlangung des akademischen Grades einer
Doktorin der Naturwissenschaften
(Dr. rer. nat.)

an der Fakultät für
Biologie, Chemie und Geowissenschaften
der Universität Bayreuth

vorgelegt von

Pia Ebeling

aus Hannover

Bayreuth, 2022

Die vorliegende Arbeit wurde in der Zeit von Juli 2018 bis April 2022 in Leipzig am Helmholtz-Zentrum für Umweltforschung unter Betreuung von Herrn Prof. Dr. Jan H. Fleckenstein angefertigt.

Die Arbeiten dieser Dissertation wurden durch die Deutsche Forschungsgemeinschaft (DFG) gefördert unter der Projektnummer DFG 392886738 Dominant controls on catchment water quality dynamics – a Germany-wide analysis using data-driven models.

Vollständiger Abdruck der von der Fakultät für Biologie, Chemie und Geowissenschaften der Universität Bayreuth genehmigten Dissertation zur Erlangung des akademischen Grades einer Doktorin der Naturwissenschaften (Dr. rer. nat.).

Dissertation eingereicht am:	27.04.2022
Zulassung durch Promotionskommission:	11.05.2022
Wissenschaftliches Kolloquium:	06.10.2022

Amtierender Dekan: Prof. Dr. Benedikt Westermann

Prüfungsausschuss:

Prof. Dr. Jan Fleckenstein	(Gutachter)
Prof. Dr. Gudrun Massmann	(Gutachterin)
Prof. Dr. Eva Lehndorff	(Vorsitz)
Prof. Dr. Thomas Köllner	

Acknowledgment

Throughout my doctorate, I have received great support from my supervisors, colleagues, family and friends. Thanks to this, I had a great time and stayed motivated even at more difficult times.

Andreas Musolff and Jan H. Fleckenstein, thank you very much for your incredible support and belief in me and my work and your great supervision. Due to your support, I could develop scientifically and personally both at the UFZ and around the world during my research stay in Rennes and several conferences, trainings and networking events in Potsdam, Munich, Halle, Birmingham, Vienna, Gainesville, New Hampshire, Strasbourg, New Orleans and virtually. I always felt appreciated and free to develop.

Andreas, I especially thank you for your awesome supervision, your scientific curiosity and motivation that always inspire me. Thank you for sharing your experience and your eye for the bigger picture that helped me enhance and appreciate my research. I also appreciate your interest and support in my personal development, patience and trust.

Rémi Dupas, thank you very much for your invitation to Rennes, our fruitful discussions and collaboration. This helped me enlarge my scientific self-confidence and have a great time in Brittany!

Rohini Kumar, thank you very much for your enthusiasm and the engaged discussions. I also thank the whole mQM team for their commitment and collaboration.

I thank the whole HDG team for the great time together, scientific discussions as well as personal exchange during paper cakes and other activities. I thank my fellow PhD students for fruitful scientific exchange, fun distractions and friendships developed. I thank the PhD team for machine learning for the fun and active group spirit and curiosity to learn together! I would like to thank all people providing helpful comments and inspiration.

Finally, I would like to deeply thank my family and friends. I especially thank my parents and grandparents, Philipp and Lea - without you, your love and trust in me throughout my life I would certainly never have come to write these lines.

Table of Contents

Abstract

Human activities have affected the quality of water resources globally, threatening both ecosystem and human health. One major threat arises from excess nutrients, largely stemming from agriculture and waste water, causing eutrophication in receiving surface water bodies. For effective water quality management, knowledge of catchment functioning in terms of water and solute dynamics and the interplay of natural and anthropogenic controls is crucial. Catchments are both the focus of management as well as integrators of various interacting hydrological and biogeochemical processes. While most studies focus on specific processes and individual catchments, overarching spatiotemporal patterns of nutrient export from streams and their prevailing control mechanisms still need to be better understood to tailor improved water quality management.

The aim of this thesis is to increase the understanding of spatiotemporal patterns of riverine nutrient export at catchment scale and to identify their dominant controls and underlying processes across a wide range of catchments on the basis of a newly assembled data set. Study 1 targets at the spatial patterns and controls of mean riverine nitrate, phosphate and total organic carbon concentrations and export dynamics across 797 German catchments. Study 2 explores spatiotemporal patterns of joint riverine nitrate concentration and discharge seasonality and controls across 290 German and French catchments. Study 3 aims to enable future knowledge gains beyond this thesis by providing the novel large-sample data set of water quality combined with data on water quantity, meteorology, nutrient input and catchment attributes for 1386 German catchments.

To compile the consistent large-sample data set, water quality and quantity data from the environmental authorities of the German federal states and France were processed along with various spatial data sets characterizing the catchments. Data-driven analyses were applied to determine catchment archetypes (i.e., to classify catchments) regarding their nutrient export dynamics and identify similarities and differences across catchments. More specifically, catchment responses were characterized from riverine nutrient concentrations and discharge and subsequently linked to catchment characteristics using multivariate methods. In Study 1, mean concentrations and concentration-discharge relationships were determined to classify the catchments. Nutrient source heterogeneity was parameterized

from horizontal landscape patterns and vertical nitrate concentration profiles to evaluate their impact on nutrient export dynamics. In Study 2, long-term trajectories of nitrate concentration seasonality were classified, considering seasonally variable response times. This classification allowed to evaluate if concentrations during high-flow season respond faster to management changes as shallow nitrogen sources are affected first and predominantly activated during high flow.

The large-sample analysis of nutrient export dynamics across Germany (Study 1) identified regional patterns and nutrient-specific ranges with about 70 % of the catchments classified as the respective predominant class. Nitrate and total organic carbon concentrations mostly increased with increasing discharge, while phosphate was predominantly diluted. The variability of both mean nitrate concentrations and export dynamics across the catchments increased with the share of agriculture and was linked to the share of sedimentary aquifers within the catchments. The results suggest that subsurface denitrification can buffer high diffuse inputs, causing vertical concentration heterogeneity across different flow paths. In agricultural lowland catchments with deep sedimentary aquifers, predominant in northern Germany, this leads to low mean riverine nitrate concentrations and strong enrichment patterns. For phosphate, anthropogenic sources dominated, although cycling processes likely caused substantial variability, decoupling the instream concentrations from the catchment source configuration. Phosphate export dynamics were surprisingly strongly controlled by diffuse sources, suggesting that losses from legacy stores in agricultural soils are more dominant than expected and need to be better considered for sustainable phosphorus management. Riverine total organic carbon concentrations were dominated by natural sources from riparian wetlands and by hydrologic controls.

Nitrate and discharge varied synchronously in the majority of the German and French catchments (84 %) with seasonal maxima during winter (Study 2). The trajectories of nitrate seasonality on the contrary were more diverse, with a similar number of catchments with low-flow and high-flow concentrations responding first to changes in nutrient inputs. The lack of a consistent link between the different trajectories and controls suggests complex underlying processes.

In synthesis, consistent spatial patterns of nitrate-discharge relationships and seasonality imply that nitrate export predominantly varies at a seasonal time scale. Although nitrate export dynamics can exhibit significant long-term trends, their spatial variability among catchments was larger and better explained by catchment characteristics, implying persistence of spatial patterns and thus of underlying processes.

Overall, this thesis advanced the understanding of spatiotemporal patterns of nutrient export dynamics and their dominant controls across a wide range of different catchments

and enables further research by providing data products. Knowledge on regional similarities and differences of catchment archetypes and controls can inform catchment models of water and solute transport, provide context for ungauged basins and future catchment trajectories and help to adapt water quality management.

Zusammenfassung

Menschliches Handeln beeinträchtigt die Wasserqualität weltweit, was die Gesundheit von Ökosystemen und Menschen bedroht. Eine wesentliche Gefahr entsteht durch Nährstoffüberschüsse, die zum Großteil aus der Landwirtschaft und Abwässern stammen und zur Eutrophierung von Oberflächengewässern führen können. Für eine wirksame Wasserqualitätsbewirtschaftung sind Kenntnisse über die Funktionsweise von Einzugsgebieten hinsichtlich der Dynamik von Wasser- und Stoffflüssen und des Zusammenspiels von natürlichen und anthropogenen Einflussfaktoren entscheidend. Einzugsgebiete stehen im Mittelpunkt der Bewirtschaftung und verbinden gleichzeitig eine Vielzahl interagierender hydrologischer und biogeochemischer Prozesse. Viele Studien konzentrieren sich auf spezifische Prozesse und einzelne Einzugsgebiete, allerdings müssen übergreifende raum-zeitliche Muster des Nährstoffexports in Fließgewässern und die vorherrschenden Kontrollmechanismen besser verstanden werden, um die Bewirtschaftung der Wasserqualität zu verbessern.

Ziel dieser Arbeit ist es, das Verständnis der raum-zeitlichen Muster des Nährstoffexports in Flüssen auf Einzugsgebietsebene zu verbessern und die vorherrschenden Einflussfaktoren und zugrunde liegenden Prozesse über eine Vielzahl von Einzugsgebieten anhand eines neu zusammengestellten Datensatzes zu identifizieren. Studie 1 befasst sich mit den räumlichen Mustern und Einflussfaktoren der mittleren Konzentrationen von Nitrat, Phosphat und organischem Gesamtkohlenstoff in Flüssen sowie die Exportdynamik in 797 deutschen Einzugsgebieten. Studie 2 untersucht die raum-zeitlichen Muster der gemeinsamen Saisonalität der Nitratkonzentration in Flüssen und des Abflusses in 290 deutschen und französischen Einzugsgebieten. Studie 3 hat das Ziel, einen über diese Arbeit hinausgehenden Wissenszuwachs zu ermöglichen, indem sie den neuen, groß angelegten Datensatz zur Wasserqualität zusammen mit Daten zu Abfluss, Meteorologie, Nährstoffeintrag und Einzugsgebietsmerkmalen für 1386 deutsche Einzugsgebiete bereitstellt.

Um einen konsistenten Datensatz mit vielen Einzugsgebieten zu erstellen, wurden Wasserqualitäts- und -quantitätsdaten der Umweltbehörden der deutschen Bundesländer und Frankreichs und verschiedene räumliche Datensätze zur Charakterisierung der Einzugsgebiete verarbeitet. Mittels datengestützter Analysen, wurden Einzugsgebietsarchetypen

bezüglich ihrer Nährstoffexportdynamik bestimmt (d. h. Einzugsgebiete klassifiziert) und Ähnlichkeiten und Unterschiede zwischen den Einzugsgebieten ermittelt. Konkret wurde das Verhalten der Einzugsgebiete anhand von Nährstoffkonzentrationen im Fluss und Abfluss charakterisiert und anschließend mit multivariaten Methoden mit den Einzugsgebietsmerkmalen verknüpft. In Studie 1 wurden die mittleren Konzentrationen und die Beziehungen zwischen Konzentration und Abfluss bestimmt, um die Einzugsgebiete zu klassifizieren. Die Heterogenität der Nährstoffquellen wurde anhand von horizontalen Landschaftsmustern und vertikalen Nitratkonzentrationsprofilen parametrisiert, um deren Einfluss auf die Nährstoffexportsdynamik zu ermitteln. In Studie 2 wurden Langzeitverläufe der Nitratsaisonalität unter Berücksichtigung saisonal variabler Reaktionszeiten klassifiziert. Die Klassifizierung ermöglichte es zu beurteilen, ob die Konzentrationen bei saisonal höheren Abflüssen schneller auf Änderungen der Bewirtschaftung reagieren, da oberflächennahe Stickstoffquellen zuerst betroffen sind und überwiegend bei hohen Abflüssen aktiviert werden.

Die groß angelegte Analyse der Nährstoffexportdynamik in Deutschland (Studie 1) ergab regionale Muster und nährstofftypische Wertebereiche, wobei etwa 70 % der Einzugsgebiete in die jeweils vorherrschende Klasse eingestuft wurden. Die Konzentrationen von Nitrat und organischem Gesamtkohlenstoff stiegen überwiegend mit zunehmendem Abfluss, während Phosphat überwiegend verdünnt wurde. Die Variabilität der mittleren Nitratkonzentrationen und Exportdynamik in den Einzugsgebieten nahm mit dem Anteil der Landwirtschaft zu und war mit dem Anteil sedimentärer Grundwasserleiter im Einzugsgebiet verknüpft. Die Ergebnisse deuten darauf hin, dass Nitratabbau hohe diffuse Einträge abpuffern und zu einer Konzentrationsheterogenität im Untergrund über verschiedene Fließwege führen kann. In landwirtschaftlichen Einzugsgebieten im Flachland mit tiefgründigen, sedimentären Grundwasserleitern, wie in Norddeutschland vorherrschend, führt dies zu niedrigen mittleren Nitratkonzentrationen in den Flüssen und starken Anreicherungsmuster. Bei Phosphat dominierten anthropogene Quellen, obwohl Umsatzprozesse wahrscheinlich eine erhebliche Variabilität verursachten und die Konzentrationen im Fluss von der Quellenkonfiguration im Einzugsgebiet entkoppelten. Die Phosphatexportdynamik wurde überraschend stark von diffusen Quellen bestimmt, was darauf hindeutet, dass Verluste aus akkumulierten Einträgen in landwirtschaftliche Böden dominanter sind als erwartet und daher für ein nachhaltiges Phosphor-Management besser berücksichtigt werden müssen. Die Konzentrationen des organischen Gesamtkohlenstoffs in den Flüssen wurden von natürlichen Quellen aus flussnahen Feuchtgebieten und hydrologischen Einflüssen bestimmt.

Nitrat und Abfluss variierten in den deutschen und französischen Einzugsgebieten mehrheitlich synchron (84 %) mit saisonalen Maxima im Winter (Studie 2). Die Langzeitverläufe der Nitratsaisonalität waren dagegen vielfältiger: Konzentrationen in den Jahreszeiten mit höheren und niedrigeren Abflüssen reagierten in einer ähnlichen Anzahl von Einzugsgebieten zuerst auf Veränderungen der Nährstoffeinträge. Das Fehlen einer konsistenten Verbindung zwischen den Langzeitverläufen und Einzugsgebietsmerkmalen lässt auf komplexe zugrunde liegende Prozesse schließen.
In der Synthese deuten die konsistenten räumlichen Muster der Nitrat-Abfluss-Beziehungen und -Saisonalität darauf hin, dass der Nitratexport überwiegend auf einer saisonalen Zeitskala variiert. Obwohl die Nitratexportdynamik signifikante langfristige Trends aufweisen kann, war die räumliche Variabilität zwischen den Einzugsgebieten größer und besser durch Einzugsgebietsmerkmale erklärbar, was auf eine Beständigkeit der räumlichen Muster und damit der zugrunde liegenden Prozesse hinweist.
Insgesamt erweitert diese Arbeit das Verständnis der raum-zeitlichen Muster der Nährstoffexportdynamik und ihrer vorherrschenden Einflussfaktoren über viele verschiedene Einzugsgebiete und ermöglicht weitere Forschungsarbeiten durch die bereitgestellten Datenprodukte. Die Kenntnis regionaler Ähnlichkeiten und Unterschiede von Einzugsgebietstypen und Einflussfaktoren kann Wasser- und Stofftransportmodelle unterrichten, Kontext für unbeobachtete Einzugsgebiete und zukünftige Entwicklungen liefern und helfen die Bewirtschaftung der Wasserqualität zu verbessern.

Chapter 1

Introduction

1.1 Water quality challenges in the Anthropocene

Human interventions with the major biogeochemical cycles have affected most of the Earth's ecosystems and drastically changed their functioning (Abbott et al., 2019; Vitousek et al., 1997). In 1997, Vitousek et al. (1997) stated that "Beyond any doubt, humanity is a major biogeochemical force on Earth.", which is a characteristic of the Anthropocene with humans as a dominant driver on the global biogeochemical cycles (Crutzen, 2002). Human activities such as land conversion, mining, fossil fuel burning, agricultural practices, and various other changes in biogeochemical cycles have substantial impacts on ecosystems, global climate and biodiversity (Vitousek et al., 1997). Among the altered cycles are those of the macronutrients carbon, nitrogen (N) and phosphorus (P) and the water cycle (Vitousek et al., 1997). The resulting impacts on water quality pose a major challenge for water management.

Macronutrients are essential components for all living organisms. Generally, they transform between organic and inorganic forms during assimilation and mineralization processes. N and P are therefore applied as organic or mineral fertilizers to increase agricultural food production in the face of a growing world population. With the discovery of the Haber-Bosch process in the beginning of the 20th century, synthetic N fixation from the air for fertilizer production became possible. Synthetic N fixation increased rapidly along with population growth, but at an even higher rate, especially since the 1950s (Galloway and Cowling, 2002; Galloway et al., 2004). Through the cultivation of N fixing crops such as legumes and the burning of fossil fuels, humans generate additional reactive N (as opposed to nonreactive N_2, Galloway et al., 2004). Since 1965, N fixation by humans for food and energy production exceeds the natural fixation by the terrestrial ecosystems (Galloway and Cowling, 2002). By 1990, N fixation had increased about tenfold compared

to 1860 with inorganic fertilizers accounting for the largest share (Galloway et al., 2003). Similarly, global P fertilizer applications have drastically increased in the 20th century (fourfold from 1961 to 2015) and are expected to further increase, although accessible P resources are limited (Bindraban et al., 2020). In Europe, peak fertilization was reached during the 1980s, but fertilization levels remain high (Schoumans et al., 2015). Moreover, about half of the applied nutrients are not taken up by cultivated crops and even more (about 80-90 %) are not eventually consumed by humans, which implies overfertilization (Cordell et al., 2009; Galloway and Cowling, 2002; Smil, 2000). Those nutrients are mostly lost to the environment, either emitted to the atmosphere in the case of N, to ground- and surface waters, or to long term stores in soils (Cordell et al., 2009; Galloway and Cowling, 2002). The largest part of anthropogenic N and P demand serves the food production, although P is also used for industrial products such as detergents and thus enters the domestic and industrial wastewater (Smil, 2000). During the 1970s, about 60-75 % of P inputs to streams originated from wastewater in populated catchments, but these inputs have declined due to restrictions on P in detergents and improved wastewater treatment (Smil, 2000).

Levels of reactive N and P in the environment therefore dramatically exceed the natural planetary boundaries today (Rockström et al., 2009; Steffen et al., 2015). These boundaries define a "safe operating space for humanity" (Rockström et al., 2009) and exceedance is expected to continue in the future (Conijn et al., 2018). The impacts are far-reaching for ecosystems, climate as well as for human life (Galloway et al., 2003). Nutrient pollution threatens the health and resilience of ecosystems (Steffen et al., 2015) and are a major reason for degraded water quality (Jenny et al., 2020; EEA et al., 2021). The excess nutrients can cause severe eutrophication in streams, lakes and coastal ecosystems all over the world, leading to toxic algal blooms, hypoxic "dead zones" in lakes and marine environments, and biodiversity loss, changes in ecosystem structure and functioning including species compositions (Jenny et al., 2020; Le Moal et al., 2019; Diaz and Rosenberg, 2008; Galloway et al., 2003; Smith, 2003; Peñuelas et al., 2013). Excess nitrogen can also cause acidification and greenhouse gas emissions such as nitrous oxide (N_2O) contributing to global warming and reducing ozone (Galloway et al., 2003). Moreover, deteriorated water quality is a risk for drinking water supplies and human health that comes with high economical costs e. g. for drinking water treatment (Le Moal et al., 2019).

Although plants directly take up carbon dioxide (CO_2) from the atmosphere for photosynthesis and no carbon fertilization is required, human activities strongly impact the global carbon cycle in multiple ways (Vitousek et al., 1997; Rockström et al., 2009). Fossil fuel combustion and land use changes, for example, to convert pristine into arable land,

are major contributors to greenhouse gas emissions (Vitousek et al., 1997). Furthermore, agricultural activities modify the sources and transport of organic carbon (OC) in various ways, affecting both the amount and composition of OC sources exported to streams (Graeber et al., 2015; Stanley et al., 2012). OC is an energy source for heterotrophic organisms and plays an important role for stream ecosystem structure and functioning including species compositions, nutrient uptake, availability of light and toxins, and acidity (Stanley et al., 2012). The ecological implications vary and are not yet fully understood including effects of complex interactions with nutrients and light (Solomon et al., 2015). Due to its modulating role, OC is relevant for water quality management (Stanley et al., 2012) and it can also impair drinking water resources (Solomon et al., 2015).
Although nutrient pollution has been recognized as a threat to ecosystem health and resilience since decades, it still remains one of today's major water management challenges (EEA et al., 2021). Mitigation measures have not yielded the desired improvements in water quality (EEA et al., 2018; Bouraoui and Grizzetti, 2011), which will be also further addressed in the following section. Nutrient management must balance the potentially conflicting interests of ecosystem health, climate change mitigation and water and food security. All of which are part of the sustainable development goals and increasingly under pressure as population growth continues and the demand for resources increases (Langhans et al., 2022). Hence, effective integrated management efforts are needed to overcome these challenges, especially as the adverse effects of deteriorated water quality might continue or increase with future changes like global warming (Jenny et al., 2020; Vörösmarty et al., 2010).

1.2 Lack of success in improving water quality

Several national and European regulations and directives address water quality challenges resulting from excess nutrients. The first regulations, adopted in the 1970s (USA) and 1980s (e. g. Germany), focused on reducing point sources by restricting P amounts in detergents and improving wastewater treatment (BGBI.1, 1980; EC, 1991*a*; Copeland, 2016). These were followed by regulations for diffuse pollution mainly targeting agricultural N (EC, 1991*b*; Copeland, 2016). With the Water Framework Directive (WFD), the perspective evolved towards a more ecologically oriented assessment of water quality and towards sustainable and integrated catchment management (EC, 2000). The target was to jointly address several water management objectives (EC, 2000; EEA et al., 2021). With the European Green Deal (EC, 2019), the European Union set itself the goal to

become climate-neutral by 2050 and to achieve a sustainable economy, food sector and environmental management. This includes biodiversity and "zero-pollution" targets, i. e. also protecting and preserving aquatic ecosystems (EEA et al., 2021).
Although regulations and mitigation measures have been put into place to curb nutrient pollution, improvements in water quality are often small or even absent. In Europe, 60 % of the surface and 26 % of the groundwater bodies do not achieve a good ecological or chemical status, respectively (EEA et al., 2018). The status improved only little from the first assessment of the WFD in 2009 to the second in 2015, with diffuse pollution remaining one of the major causes of poor water quality (EEA et al., 2018). The situation is especially pronounced in western and central European catchments, e. g. in Germany only 8 % of the surface water bodies achieve a good ecological status (EEA et al., 2018).
The lack of success in improving water quality can be partially explained by time lags up to several decades between implemented measures and the catchment response in water quality (Bouraoui and Grizzetti, 2011; Meals et al., 2010; Sharpley et al., 2013; Van Meter et al., 2016). These time lags can be caused by long retention and transport times of diffuse nutrient sources in soils, vadose zones, groundwater and stream networks as well as the biological response to changes in concentrations (Ascott et al., 2017; Bouraoui and Grizzetti, 2011; Meals et al., 2010; Sharpley et al., 2013; Van Meter et al., 2016). The accumulation of nutrient inputs in catchments as legacy stores can be considered a biogeochemical legacy in soils and a hydrological legacy in mobile form transported along water flow paths (Van Meter et al., 2016, 2021). Nutrient legacies from past inputs pose a long-term challenge for water quality management, because a slow release of nutrients from such storage can potentially sustain high nutrient levels in streams. In addition to average concentration levels, the nutrient export dynamics are also relevant for the ecological conditions in aquatic ecosystems. For example, nutrient export dynamics can affect the temporal variability of nutrients available for autotrophic and heterotrophic assimilation, the overall pressure and reversibility of effects as well as loads transported to downstream water bodies (Withers and Jarvie, 2008; Conley et al., 2009). Finally, a sound understanding of catchment functioning in terms of nutrient concentrations, export dynamics, and their response time scales to changes in the management are crucial to improving water quality management.

1.3 Catchments integrate hydrology and biogeochemistry

Catchments are both complex systems and the landscape element of main interest in hydrology (Sivapalan, 2006; Wagener et al., 2007). At the catchment scale, water quality managers implement and evaluate measures as processes determine the ecological conditions and exported nutrient loads transported to downstream water bodies (Bouraoui and Grizzetti, 2011). Therefore, knowledge of controls is needed at this catchment scale, particularly regarding interactions between the natural and anthropogenic controls. Although biogeochemical and hydrological processes are intensely studied at small scales, there is still a lack of knowledge on how to upscale or transfer the gained process understanding to larger scales of catchments or landscapes (e. g., Pinay et al., 2015).
The complexity of a catchment is the result of the interacting biogeochemical and hydrological processes at different spatial and temporal scales. Catchments integrate these processes and heterogeneities into water quality and quantity responses at the catchment outlet (e. g., Sivapalan, 2006; Wagener et al., 2007). Inversely, learning from (i. e. analyzing) the integrated catchment response can reveal catchment functioning in a "pattern-to-process" approach (Sivapalan, 2006). For example, relationships between concentration and discharge (C-Q relationships) can be used to characterize systems with transport- or supply-limited solute export (Basu et al., 2010; Zarnetske et al., 2018). Variability of riverine concentrations with discharge (Q) generally results from interactions of source and discharge generating zones and potential reactions along the flow paths (Musolff et al., 2017; Seibert et al., 2009). Increasing concentrations with discharge indicate that additional sources get activated (i. e. causing enrichment patterns), while decreasing concentrations emerge without additional sources as discharge increases (i. e., dilution patterns; Godsey et al., 2009; Thompson et al., 2011). Such data-driven approaches in catchment hydrology can be used to gain knowledge on underlying processes from observed response patterns at the catchment outlet. In this sense, data-driven top-down approaches contribute to our understanding of riverine nutrient export dynamics resulting from the interplay of sources, mobilization and retention processes. Anthropogenic activities interact with natural controls and can affect this interplay determining the land-to-stream transfer of solutes in various ways. Examples of this are the modification of source areas and nutrient loads added to the catchment (e. g. Stanley et al., 2012), the modification of hydrological pathways and travel times due to artificial drainage and altered stream morphology (Van der Velde et al., 2010; Stanley et al., 2012; Withers and Jarvie, 2008), and the modification of erosion risk (Withers and Jarvie, 2008; Schoumans et al., 2014). These controls inter-

act with climatic, topographical, pedological and lithological controls (e. g. Musolff et al., 2015; Minaudo et al., 2019; Moatar et al., 2017).
As reactive processes vary in space and time, locations and times with comparatively high reaction rates are referred to as hot spots and hot moments (McClain et al., 2003). Although this concept is often connected to relatively local and short-term perspectives, it can be adapted to different scales including the catchment scale by identifying dominant controls, e. g. wetland coverage (McClain et al., 2003). The hierarchy of processes that determine the overall catchment functioning varies among catchments and may also vary at different time scales within a catchment, e. g. seasonally or on long-term (Dupas, Minaudo, Gruau, Ruiz and Gascuel-Odoux, 2018; Ehrhardt et al., 2019; Winter et al., 2021). Because data-driven investigations generally allow to derive hypotheses on integrated processes underlying the patterns represented in the data, great value lies in a large spatial and temporal coverage. Long-term time series of concentrations, even at low sampling frequency, for example, can inform about trends in catchment functioning in response to changes in regulations and nutrient management (Burt et al., 2011; Howden et al., 2010). They thus allow to investigate general long-term changes in catchment functioning and can additionally set the context for sites with shorter monitoring periods (Burt et al., 2011).
To understand relevant processes and their dynamics at larger scales of whole catchments or landscapes, dominant controls of the hydrological and biogeochemical processes and their interactions need to be identified. This should include both natural and anthropogenic controls to identify potential control mechanisms for water quality management.

1.4 Large-sample hydrology to identify dominant processes

Large-sample hydrology investigates similarities and differences among numerous catchments, allowing to derive hypotheses on dominant controls and underlying processes (Gupta et al., 2014; Addor et al., 2020). In this way, it can increase the knowledge on catchment functioning across various environmental and anthropogenic conditions and spatiotemporal scales and thus contribute to overcome water quality problems. Large-sample hydrology opens opportunities to move forward beyond the single catchment to identify general hydrological principles (Gupta et al., 2014). In this context, to "balance depth with breadth" means to move beyond the understanding of small scale and detailed processes in intensively studied catchments to overarching perspectives across

a broad variety of catchments (Gupta et al., 2014). The variability of response patterns across catchments can be linked to catchment characteristics to identify dominant controls. Large-sample hydrology follows the idea of comparative hydrology by drawing inferences from the similarities and differences of a significant number of catchments (Addor et al., 2020).

The broader perspective of large-sample hydrology can particularly support understanding overarching trends and inform catchment management beyond the single catchment scale (Kingston et al., 2020). The characterization of similar and different catchment functioning can be used to classify catchments based on archetypal behavior. Such schemes could become quantitative frameworks for catchment typologies which support moving towards a more unified hydrological theory, i. e. a more holistic understanding of hydrological processes (Sivapalan, 2006). Further, knowledge on dominant controls and underlying processes from spatial variability can improve predictions in ungauged basins as well as of future trajectories following a trading-space-for-time concept (Singh et al., 2011; Peel and Blöschl, 2011; Wagener et al., 2007). The trading-space-for-time concept transfers the process understanding derived from spatial variability to temporal variability, e. g. accounting for changing controls such as the climate (Singh et al., 2011; Peel and Blöschl, 2011). Therefore, similarly to temporal coverage, spatial coverage can be of high value to understand general hydrological principles (Gupta et al., 2014). More generally, the knowledge transfer in space and time includes the exploration of proxies or other predictors to make use of their larger availability and value, which Blöschl et al. (2019) identified as part of the unresolved problems in hydrology. However, more understanding is required to assess and exploit the potential of the spatial and temporal transferability (Blöschl et al., 2019).

One of the major challenges for large-sample hydrologic studies is still the limited availability and accessibility of consistent data sets (Kingston et al., 2020). This is especially true for water quality and even more so for combined data of water quality, water quantity and catchment characteristics. Although large-sample data sets have become increasingly available, these do usually either not include water quality data (such as the CAMELS data sets with the first one presented for the USA, Addor et al. (2017)) or focus on water quality disregarding water quantity and catchment attributes (e. g. Virro et al., 2021). Therefore, efforts are needed to increase the availability of consistent catchment hydrological data sets including water quality and to ultimately inform hydrological theories.

Chapter 2

Research goals and design

Following the introductory chapter, this Chapter 2 defines the research goals and design, including a summary of the approaches of each study of this thesis and linkages between the studies. Chapter 3 summarizes the key findings from the individual studies. The studies are synthesized in Chapter 4 and implications and further research questions are identified. Subsequently, the single studies are included together with indications of own contributions, followed by a list of publications.

2.1 Research goals

The overall aim of this thesis was to increase the understanding of spatiotemporal patterns of nutrient export dynamics and underlying dominant processes across a large range of catchments at different temporal scales. More specifically, the overarching research questions were:

R. 1 Can catchments be classified in terms of archetypes of riverine nutrient export dynamics?

R. 2 What are the dominant controls and underlying processes?

For the latter, interactions between natural and anthropogenic controls should be considered. This knowledge is crucial for practitioners to improve water quality management and for water quality modelers to potentially reduce the complexity of water quality models. To address the research questions, the thesis was designed to present a comprehensive analysis of nutrient export dynamics and their dominant controls, for which a novel data set of water quality, quantity and catchment characteristics covering a large number and variety of catchments was assembled. Thus, the objectives were to:

O. 1 Assemble and provide a consistent, comprehensive data set of riverine water quality, quantity and catchment attributes for Germany and consistently extend it to French catchments with available long-term water quality data.

O. 2 Determine catchment archetypes regarding nitrate (NO_3^-), phosphate (PO_4^{3-}) and total organic carbon (TOC) concentration levels and export dynamics (spatial patterns) using quantitative classification frameworks and identify dominant controls by linking response patterns to catchment characteristics.

O. 3 Determine catchment archetypes regarding average NO_3^- and discharge seasonality and the long-term trajectories of NO_3^- seasonality (spatiotemporal patterns) using quantitative classification frameworks and identify controls from linkages to catchment characteristics.

The conducted studies are based on the following principles:

P. 1 Nutrient export dynamics are linked to catchment characteristics.

P. 2 Concentration variability reflects past and present inputs, variable flow paths and retention.

P. 3 Large-sample hydrology allows to assess generalities as well as differences in catchment functioning.

2.2 Research design

The overall research design of this thesis is shown in Figure 1. Within the framework of this thesis, a comprehensive data set of water quality, quantity and catchment characteristics was assembled for 1386 German catchments, addressing Objective 1. All studies used parts of this German data set, while its entirety was presented in Study 3. The catchment characteristics were also derived for 486 French catchments with long-term concentration data available, which were combined with the German data set in Study 2. The goal and approach of each study and the links to the other studies are explained in the following.

Study 1 aimed at classifying German catchments based on recent data (starting in year 2000) in terms of their mean nitrate-N (NO_3^--N), phosphate-P (PO_4^{3-}-P) and TOC concentrations and export dynamics, revealing spatial patterns and archetypes, and identifying dominant controls. It is therefore tailored to address Objective 2. Prior to the investigation, the data of water quality, quantity and catchment characteristics for Germany

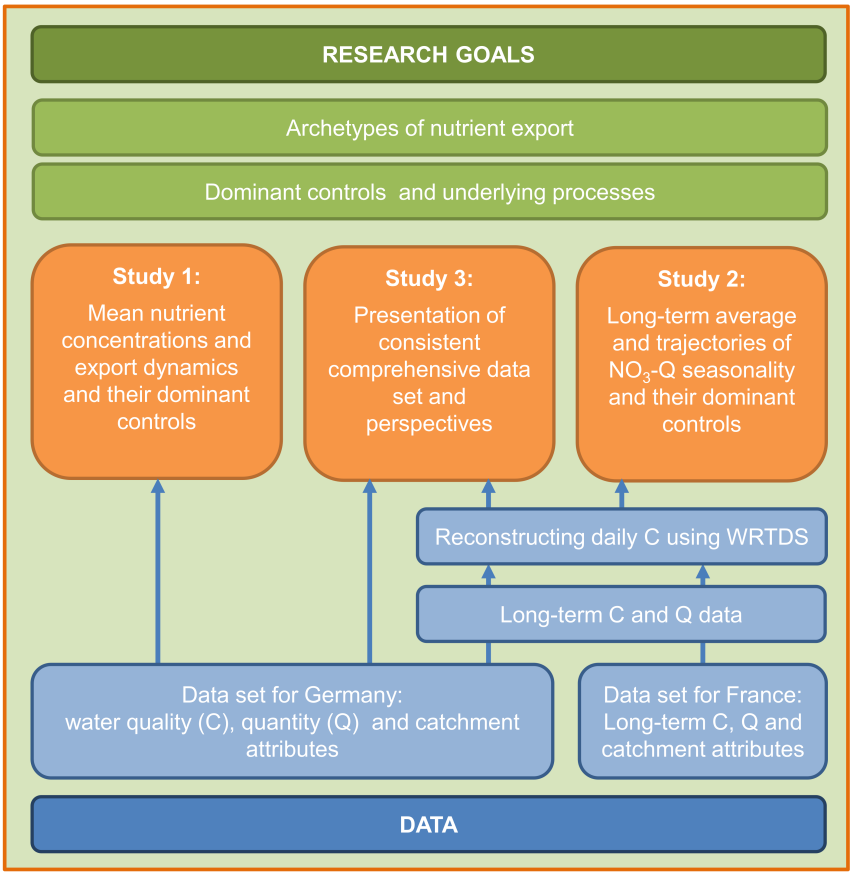

Figure 1: Overview of the study design of this thesis: the overarching research goals, the studies and their respective linkages to data sets used.

were assembled, processed and quality checked addressing Objective 1. The classification of export dynamics based on data-driven analyses in terms of C-Q relationships. Slope b of the linear regression between concentration and discharge in logarithmic space distinguishes the export patterns enrichment ($b > 0$), neutral ($b \approx 0$) and dilution ($b < 0$). The concentration variability relative to discharge is quantified by the ratio of the variation coefficients (CV_C/CV_Q), characterizing the export regimes as chemostatic ($CV_C/CV_Q < 0.5$) or as chemodynamic ($CV_C/CV_Q > 0.5$). Dominant controls were identified by linking water quality metrics to a comprehensive set of catchment characteristics with partial least square regression and random forest regression models. The characteristics included the topography, land cover, nutrient sources, lithology, top soil texture and chemistry and hydroclimate. The main hypothesis was that the degree of spatial heterogeneity of diffuse nutrient sources dominantly controls the variability of export dynamics among catchments. To test this hypothesis, a parameterization of the heterogeneity of nutrient sources within the catchment was developed for both the horizontal and the vertical di-

rection and the derived indices included as descriptors. In this study, the novel data set of water quality, quantity and catchment attributes for Germany was analyzed for the first time to provide a comprehensive picture of prevailing export dynamics in Germany. The compiled data set and findings about the dominant controls of NO_3^- export (see Chapter 3) serve as a basis for the other studies.

Study 2 aimed at classifying long-term average NO_3^- and discharge seasonality and their trajectories across French and German catchments, disclosing spatiotemporal patterns of NO_3^- export dynamics and identifying dominant controls. This study thus addresses Objective 3 and also Objective 1 as it extended the assembled data set. Daily flow-normalized NO_3^--N concentrations were reconstructed using Weighted Regressions on Time, Discharge, and Season (WRTDS) from long-term NO_3^--N and discharge time series to fill data gaps and to focus the analysis on long-term trends independent of interannual climate variability (Hirsch et al., 2015). To classify trajectories of C-Q seasonality, a novel hysteresis approach based on time series of concentrations separated for low- and high-flow seasons was proposed. The hysteresis determines catchments with seasonally variable response times with either preceding high-flow or low-flow concentrations. Study 2 subsequently linked the calculated metrics to catchment characteristics using rank correlations, Wilcoxon and Kruskal-Wallis tests and a random forest classification model. Within the study, three selected catchments are discussed more closely for dominant controls. Two main hypotheses were tested. Firstly, catchments with a long-term average NO_3^- maximum during winter high-flow season would predominate. Secondly, catchments with high-flow concentrations responding first to external input changes compared to low-flow concentrations would dominate. This based on the assumption that shallow N sources are affected first by diffuse input changes to soils and activated during high flow.
Study 2 used a smaller number of catchments (n=290) due to the required long-term data, but covers a larger variety of landscapes and hydroclimate by expanding the study area of Study 1. It also adds the long-term evolution of export dynamics to the investigation presented in Study 1. The metrics used in Study 1 and 2 to characterize export dynamics are shown to be interrelated (refer to Methods, Study 2).

Study 3 aimed at providing a comprehensive, freely available data set of water quality and quantity, meteorological and nutrient input forcing data and catchment attributes to facilitate further large-sample water quality investigations at a national scale and beyond. This addresses Objective 1. In this Study 3, the newly assembled data for 1386 German catchments were combined, extended and jointly presented in a structured way.

Both preprocessed observed and reconstructed long-term (WRTDS model output) data of the species of the macronutrients N, P and OC were presented for the stations fulfilling the selection criteria (e. g. regarding the data availability). Data were generally aggregated to annual time scales and thus homogenized; while for the catchments with a data availability high enough to run WRTDS models monthly aggregated data were additionally provided. Thus, Study 3 combined and complemented the data sets analyzed in Studies 1 and 2 by presenting and providing data from more stations, more water quality compounds, and more ancillary data in a comprehensive data set for Germany. Study 3 increases the accessibility of the assembled data set to facilitate further research.

The approaches and motivation of all three studies are in line with the idea of large-sample hydrology to infer similarities and differences from a large sample of catchments. Study 1 and 2 both characterized spatial and temporal patterns of riverine nutrient dynamics, classified the catchments and used statistical and machine learning techniques to identify links between catchment responses and descriptors. Study 3 provided the data set and a comprehensive overview for future large-sample water quality and quantity studies to further advance our understanding of spatial and temporal water quality patterns and dominant controls at catchment scale.

Chapter 3

Key findings and conclusions

3.1 Study 1: Nutrient levels and export dynamics across German catchments

Title: Archetypes and Controls of Riverine Nutrient Export Across German Catchments

The comprehensive analysis of average concentrations and C-Q relationships across Germany revealed archetypal ranges of export dynamics for the macro-nutrients NO_3^-, PO_4^{3-}, and TOC and underlying dominant controls (Figure 2). While enrichment patterns prevailed for NO_3^- and TOC, dilution patterns predominated for PO_4^{3-}. For each compound about 70 % of the catchments were classified into the respective predominant pattern. The analysis revealed spatial differences in prevailing mean concentration levels and export dynamics, which could be partially explained by catchment characteristics and their spatial organization.

Mean NO_3^- concentrations were positively correlated to the fraction of agricultural areas in the catchments. However, agricultural catchments could also exhibit relatively low mean NO_3^- concentrations combined with a relatively high variability (Figure 2a, Figure 6 in Study 1). These catchments were mostly located in lowland areas with deep sedimentary aquifers and higher vertical concentration heterogeneity representing the potential vertical NO_3^- heterogeneity between soils and groundwater as catchment average. This finding does not support the generality of the hypothesis from previous studies that agricultural catchments are subject to source homogenization resulting in chemostatic export (Basu et al., 2010; Thompson et al., 2011). Even though overall chemostatic catchments prevailed, the fraction of chemodynamic export increased with agricultural area (Figure 6b and c in Study 1) accounting for 34 % of the catchments with at least 50 % agricul-

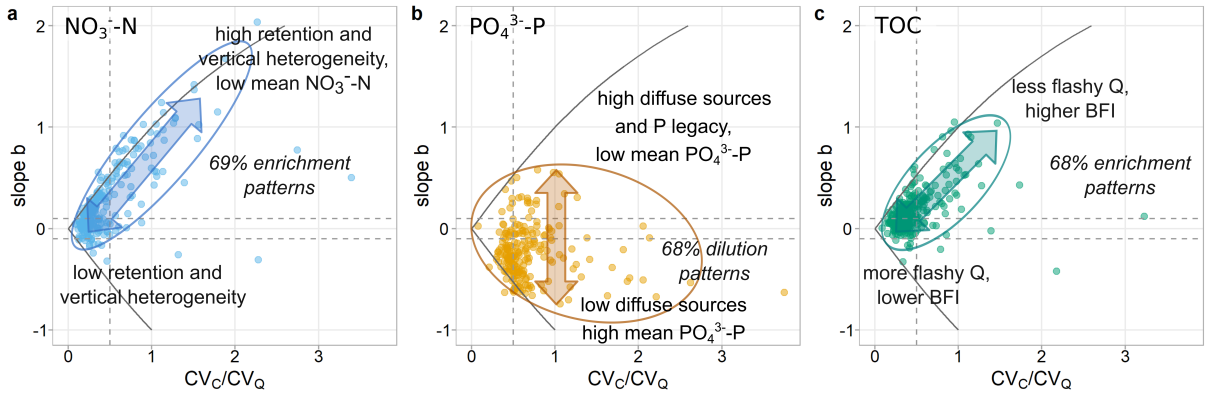

Figure 2: Summary of archetypal ranges of export dynamics of the macronutrients NO_3^-, PO_4^{3-}, TOC and their dominant controls.

tural areas compared to 17 % of the catchments with smaller share of agriculture. Study 1 suggests that anthropogenic inputs from agricultural areas can be buffered by natural subsurface attenuation (removal by denitrification), which is in line with high denitrification potential in deep sedimentary aquifers with long travel times and anaerobic conditions especially in northern Germany (Knoll et al., 2020; Kunkel et al., 2004; Wendland et al., 2008). In consequence, low mean NO_3^- concentrations and pronounced enrichment patterns under high inputs could inversely indicate effective subsurface denitrification.

Mean PO_4^{3-} concentrations were linked to point sources in line with previous literature (e. g., Minaudo et al., 2019; Westphal et al., 2019). However, the inter-catchment variability of export patterns could rather be explained by the degree of diffuse sources, which was linked to enrichment patterns (Figure 2b). This was surprising, as most studies discuss a dominant impact of point sources causing contrasting seasonal PO_4^{3-} and discharge cycles, i. e. dilution patterns (e. g., Bowes et al., 2015; Minaudo et al., 2019; Moatar et al., 2017). Since nevertheless dilution patterns prevailed for PO_4^{3-}, Study 1 suggests that both point source dilution and diffuse source mobilization are relevant and both export mechanisms interact with variable hierarchies. Catchments with dominant PO_4^{3-} mobilization (11 %, enrichment patterns) in northwestern and southeastern Germany coincided with areas of high diffuse inputs (Häußermann et al., 2019) with potentially high P legacies and risk of P loss from P saturated soils to the streams (Fischer et al., 2017; Sharpley et al., 2013). This mechanism is likely not exclusive to those regions in Germany (Fischer et al., 2017), but seems to be more dominant here than dilution mechanisms. A relatively low degree of explained variability for mean PO_4^{3-} concentrations and export patterns among catchments (between 34 and 47 %) suggests that processes were not fully represented by aggregated catchment characteristics. For example, controls at different

spatial and temporal scales may cause additional, unexplained variability of the PO_4^{3-} response at the catchment outlet. P cycling including in-stream retention, transformation and remobilization is known to strongly vary in space and time and to be able to reshape P concentration dynamics (Jarvie et al., 2012). This reshaping decouples the instream P concentration from the catchment's source configuration and land-to-stream transfer hampering predictions at the catchment outlet. This suggests that small-scale controls significantly interact with the anthropogenic source controls at catchment scale.

Mean TOC concentrations were dominantly controlled by the topography, suggesting that natural, terrestrial sources dominate instream TOC across large scales. Higher mean TOC concentrations emerged in lowland areas with higher probability of accumulation of organic matter in riparian wetlands and potential export, which is in line with previous studies from small boreal headwater catchments (e. g. Bishop et al., 2004; Laudon et al., 2004) and recent large-sample analyses in small forested, mountainous German catchments (Musolff et al., 2018) and various catchments across the US (Zarnetske et al., 2018). The dominance of enrichment patterns (68 %) together with the predictive power of the topographic wetness index (as a proxy for riparian wetlands) for mean TOC concentrations suggest horizontal heterogeneity of sources within the catchments and regions in the study area and vertical heterogeneity in near-stream sources to control export dynamics. However, the inter-catchment variability of the export metrics could not be well explained by topography, land cover nor climate. Adding hydrological catchment characteristics to the analysis for a subset of catchments revealed the flashiness, discharge seasonality and base flow index as better predictors with more equilibrated discharge patterns linking to more dynamic TOC export (Figure 2c). Additionally, TOC concentrations were more closely linked to discharge (higher R^2 in C-Q relationships) in lowland catchments with more equilibrated discharge and higher base flow indices. Moreover, antecedent conditions, especially soil temperature and moisture, are known to control OC production and thus potential export during hot moments (Wen et al., 2020; Winterdahl et al., 2011). Together, this might indicate that more flashy hydrologic conditions could cause more variable antecedent conditions and thus create larger scatter in C-Q relationships and lower slope b values in the catchments.

Overall, NO_3^- and PO_4^{3-} catchment responses were dominantly controlled by anthropogenic inputs and buffered or reshaped by natural controls, while TOC was dominated by natural topographic controls. The gained knowledge on regional similarities and differences and underlying processes can support water quality modeling and management.

3.2 Study 2: Long-term trajectories of nitrate-discharge seasonality

Title: Long-Term Nitrate Trajectories Vary by Season in Western European Catchments

The analysis of long-term trajectories of NO_3^--Q seasonality in 290 French and German catchments revealed commonalities and differences in the catchment responses and linkages to catchment characteristics. NO_3^- and discharge varied synchronously in the majority of the catchments (84 %) with seasonal maxima during winter. The trajectories of NO_3^- seasonality on the contrary were more diverse, with a similar number of catchments with low-flow and high-flow concentrations responding first to changes in nutrient inputs. The spatial, inter-catchment variability in seasonal NO_3^- dynamics was found to be larger than the temporal, intra-catchment variability, while the spatial patterns were also more closely linked to catchment characteristics than the spatiotemporal patterns.

For long-term average NO_3^- and discharge seasonality, three distinct catchment archetypes were identified. The archetype with synchronous variations of NO_3^- and discharge and their maxima in winter occurred most frequently, entailing a predominant enrichment archetype. This is in line with existing literature (e. g. Moatar et al., 2017; Musolff et al., 2015) and confirms our first hypothesis. The other two archetypes were characterized by asynchronous seasonal NO_3^- and discharge variations with either large seasonal variations in NO_3^- and a clear dilution patterns or relatively little seasonal variations and high mean NO_3^- concentrations. The three archetypes were clearly spatially organized and distinguishable by topographical and hydroclimatic controls (Figure 3a). Strong dilution was observed in mountainous catchments in southern Germany and France likely resulting from the spatial disconnection between main discharge generating zones upstream and main agricultural source zones downstream. Weaker dilution or rather chemostatic export and high concentration levels in the Armorican Massif suggest large N legacies (Dupas et al., 2020) and potentially bottom-loaded NO_3^- profiles with higher concentrations in deeper groundwater discharging during low flow (Martin et al., 2004), although other mechanisms such as bypassing of denitrifying riparian zones during low flows are possible (Fovet et al., 2018).
For long-term trajectories of seasonal NO_3^- concentrations, the number of catchments with high-flow and with low-flow concentrations responding first to long-term changes was similar (about 30 % each, Figure 3b). Thus, our second hypothesis of predominantly preceding high-flow concentrations was not confirmed. Although it was shown that high-

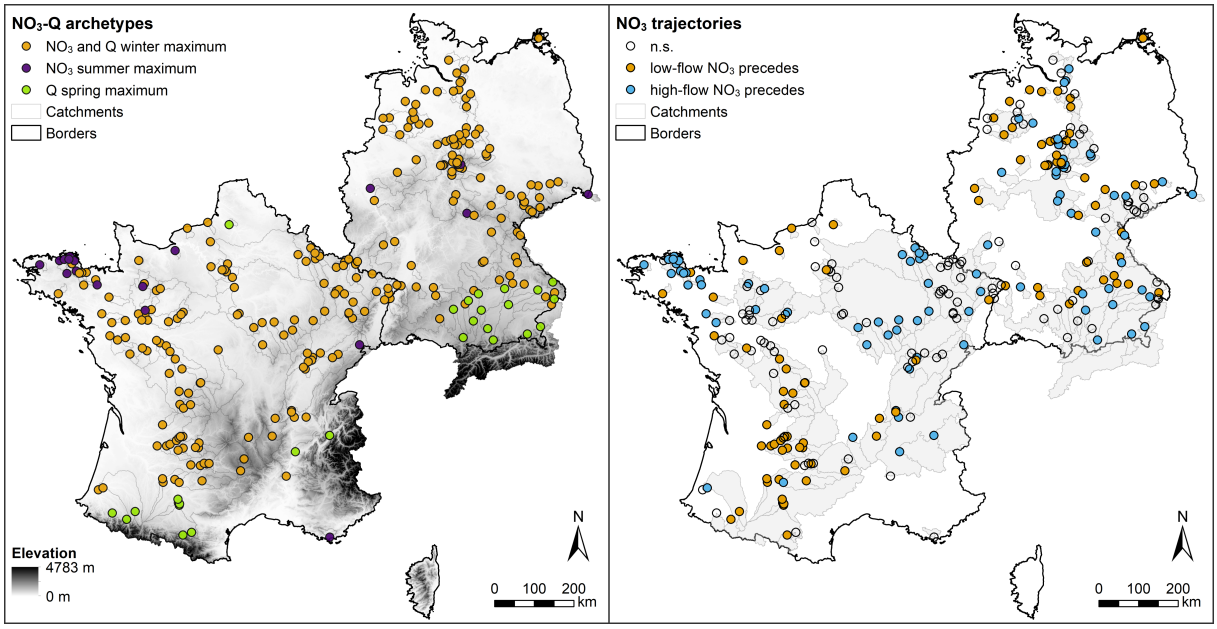

Figure 3: Catchment classification of French and German catchments regarding the average NO_3^--Q seasonality (left) and the trajectories of NO_3^- seasonality (right). Q - discharge, n. s. - not significant.

flow concentrations may respond first in catchments where diffuse sources dominate and that low-flow concentrations may respond first in catchments with strong point source influence, this consistency was not found across the whole set of catchments. The reason could be complexity and interactions in controls and underlying processes. Interestingly, in 20 % of the catchments, a reversal in NO_3^- seasonality between low- and high-flow seasons was found, so ecological conditions probably changed drastically in the last decades.

Although, the majority of catchments showed significant hysteresis patterns (59 %) and trends in NO_3^- seasonality regarding low-flow and high-flow seasons (76 %), the spatial variability of NO_3^- seasonality among catchments was larger than the temporal variability within the catchments. Thus, the concept of spatial persistence, previously discussed for seasonal concentration variability (Abbott et al., 2018; Dupas et al., 2019), was extended to long-term trajectories of NO_3^- seasonality in Study 2. At the same time, spatial variability was better explained by catchment characteristics.

Overall, Study 2 characterized archetypes of average NO_3^- and Q seasonality and their long-term trajectories and linkages to controls, with average seasonality being explained well by catchment characteristics in contrast to their temporal variability. For the latter, complex interacting controls were discussed. Study 2 thus increased the understanding of regional similarities and differences and underlying processes of seasonal NO_3^- and discharge dynamics across a wide range of catchments.

3.3 Study 3: Large-sample data set of water quality for Germany

Title: Water quality, discharge and catchment attributes for large-sample studies in Germany - QUADICA

The presented data set is the first large-sample data set of riverine water quality combined with water quantity, meteorological and nutrient forcing data, and catchment attributes for Germany. The data set covers 1386 German and transboundary catchments across a wide range of landscapes, hydroclimatic and anthropogenic conditions. QUADICA (water QUAlity, DIscharge and Catchment Attributes for large-sample studies in Germany) thus facilitates large-sample hydrological studies, for example, to identify spatiotemporal patterns of water quality dynamics and dominant controls and to infer underlying processes or to calibrate and validate models of water and solute transport.

The data set contains time series of macronutrient concentrations (species of N, P and OC), discharge, precipitation, potential evapotranspiration and mean air temperature and diffuse N input in form of N surplus, atmospheric deposition and fixation at catchment level and catchment attributes. Generally, the time series were aggregated to an annual time scale. Additionally, for 140 stations with high data availability, i. e. long-term water quality data of at least 20 years and daily discharge data, time series of concentrations, flow-normalized concentrations, and mean fluxes derived from WRTDS were aggregated to a monthly time scale. The catchment attributes characterize the topography, hydroclimate, land cover, population density, lithology and hydrogeology, textural and chemical soil properties and nutrient sources.
An overview of the spatial and temporal coverage of the data set is given in Figure 4. Out of the total 1386 stations, 324 stations have a co-located discharge station and 140 stations have a high data availability for at least one of the water quality compounds. The distribution and density of the stations varies regionally due to data availability and robustness of the catchment delineation from topography. The compounds TOC, PO_4^{3-}, NO_3^- have the highest number of stations and highest data densities in most recent years (data set covers until 2015). The earliest time series (disregarding one isolated value in 1900) started in 1954 for NO_3^- and mineral N, in 1965 for P species and in the 1970s for OC, although median start was in the 1990s. The stations have median time series lengths between 15 and 21 years and median number of samples between 139 and 165. The forcing data extends from 1950 to 2015 for diffuse N inputs and to 2018 for meteorological data.

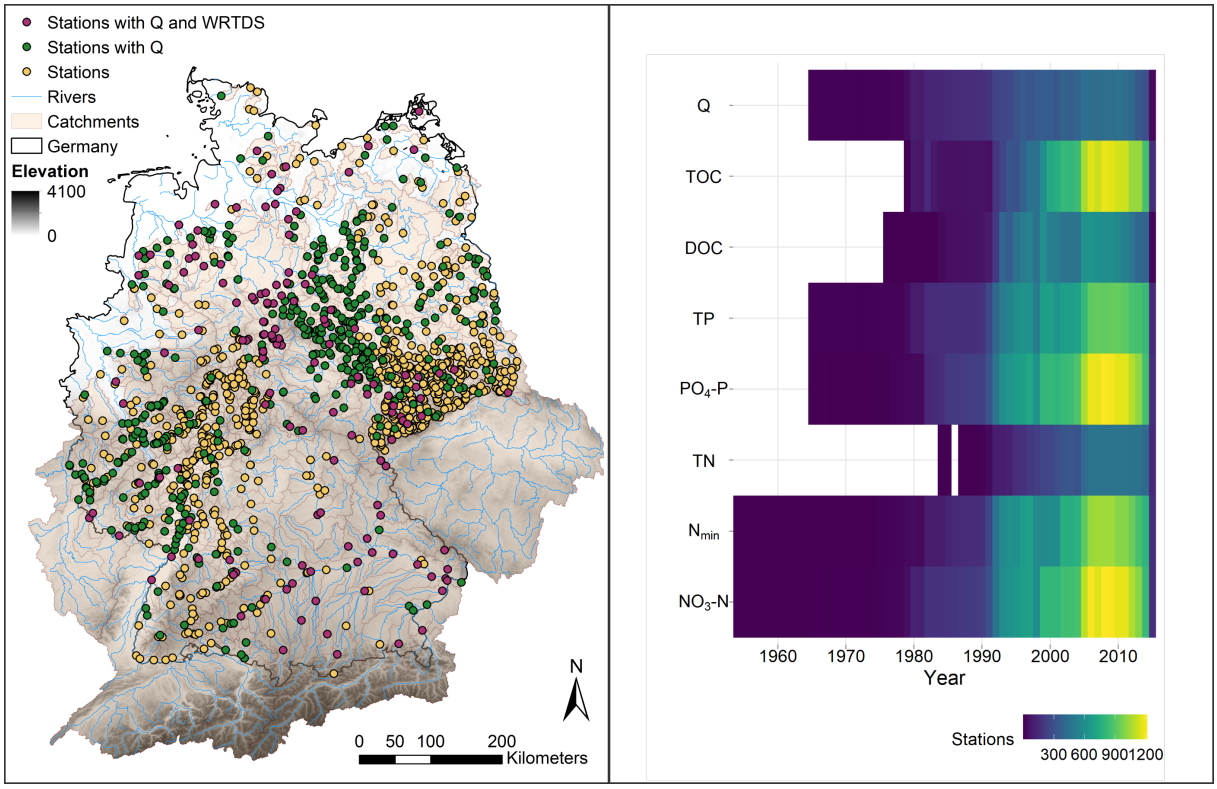

Figure 4: Overview of the data set: the 1386 stations and catchments (left) and station density with data per year and compound (right). Q - discharge, WRTDS - Weighted Regressions on Time, Discharge, and Season (Hirsch et al., 2015).

Altogether, this comprehensive, homogenized data set of water quality combined with water quantity, driving forces and catchment attributes opens up several further research opportunities for data-driven and modeling large-sample assessments of water quality. Study 3 also calls for the compilation and provision of similar data sets and open data and science policies.

Chapter 4

Synthesis and outlook

The aim of this thesis was to advance the understanding of spatiotemporal patterns of nutrient export at catchment scale and dominant controls to infer underlying processes. The controls should include natural and anthropogenic ones to identify the human impact on nutrient export. To this end, archetypal response patterns were characterized and catchments classified using data-driven quantitative frameworks and principles of large-sample hydrology (Gupta et al., 2014). Subsequently, linking catchment characteristics to the response patterns revealed dominant controls and allowed to discuss underlying processes.

4.1 Archetypes of riverine nutrient export

Spatial patterns and archetypal ranges of nutrient export dynamics were identified for the three macronutrients NO_3^-, PO_4^{3-}, TOC across a wide range of catchments in Germany (Study 1). Continuous compound-specific ranges of export patterns (slope b, Figure 2) were found, from which about 70 % of the catchments classified into the dominant class of export patterns: enrichment for NO_3^- and TOC and dilution for PO_4^{3-}. Regionally, enrichment patterns prevailed in north-western and partially also north-eastern Germany for all the macronutrients (Figure 5). In south-eastern Germany, NO_3^- dilution patterns contrasted to PO_4^{3-} and TOC enrichment patterns, while patterns were generally more variable in central Germany.

In general, PO_4^{3-} export was more chemodynamic (majority $CV_C/CV_Q > 0.5$) than NO_3^- and TOC export, although the range in slope b values was similar for the three nutrients. This indicates a higher variability of PO_4^{3-} concentrations unrelated to discharge. The link between PO_4^{3-} export patterns (slope b) and regimes (CV_C/CV_Q) was therefore not as clear as for the other nutrients. Instead, PO_4^{3-} export patterns were linked to

mean PO_4^{3-} concentrations, as catchments with dilution patterns had significantly higher mean concentrations than the ones with enrichment patterns. For NO_3^-, catchments with chemodynamic export linked to strong enrichment patterns and had lower mean concentrations than the chemostatic group. The highest mean NO_3^- concentrations were found in eastern Germany, where more neutral but less consistent export patterns emerged. For TOC, the highest mean concentrations occurred in northern German lowlands coinciding with dominant enrichment patterns.

Consistent regional patterns were determined for average NO_3^- and discharge seasonality from investigations of long-term time series with a smaller catchment density but across a larger spatial extent as French catchments were added to the German data set (Study 2). This implies that NO_3^- export dynamics are predominantly determined by the seasonal rather than the pure event time scale. A synthesis of both classifications for NO_3^- export dynamics is shown in Figure 5. The link between the ratio of seasonal concentrations in relation to discharge during low- and high-flow seasons and the regression slope b between concentration and discharge in logarithmic space was demonstrated and discussed in Study 2. A simple linear regression between the two metrics yields a coefficient of determination of R^2=0.79 for the overlapping German catchments (n=120). Differences in the two metrics can result from, for example, existing long-term trends and different analysis periods, discharge variability apart from average seasonal variations and ambivalent C-Q relationships (Minaudo et al., 2019). Generally, the dominance of enrichment patterns and synchronous seasonal variability of NO_3^- and discharge agree with existing literature (e. g. Moatar et al., 2017; Musolff et al., 2015), as does the dominant seasonal time scale in NO_3^--Q variability (Minaudo et al., 2019).

The good agreement between the two classifications of NO_3^- dynamics from Study 1 and 2 is also consistent with the finding that spatial variability is larger than temporal variability (Study 2) indicating that differences between the catchments are larger than the changes of general functioning over two or more decades in most catchments. When spatial variability prevails, persistence in general spatial patterns resulting in good agreement of water quality metrics can be expected even if the covered time periods differ.

However, this does not imply that there are no significant temporal changes in NO_3^- export dynamics, which the majority of significant trends in the logarithmic seasonal ratio between low-flow and high-flow concentrations (74 %) and hysteresis patterns (59 %) clearly demonstrated (Study 2). Both types of hysteresis were observed equally often (about 30 % each) with a dominance of preceding high-flow concentrations in northwestern and -eastern France and southeastern Germany (Figure 3). This trajectory archetype often showed declining seasonal concentration ratios, although overall increasing ratios

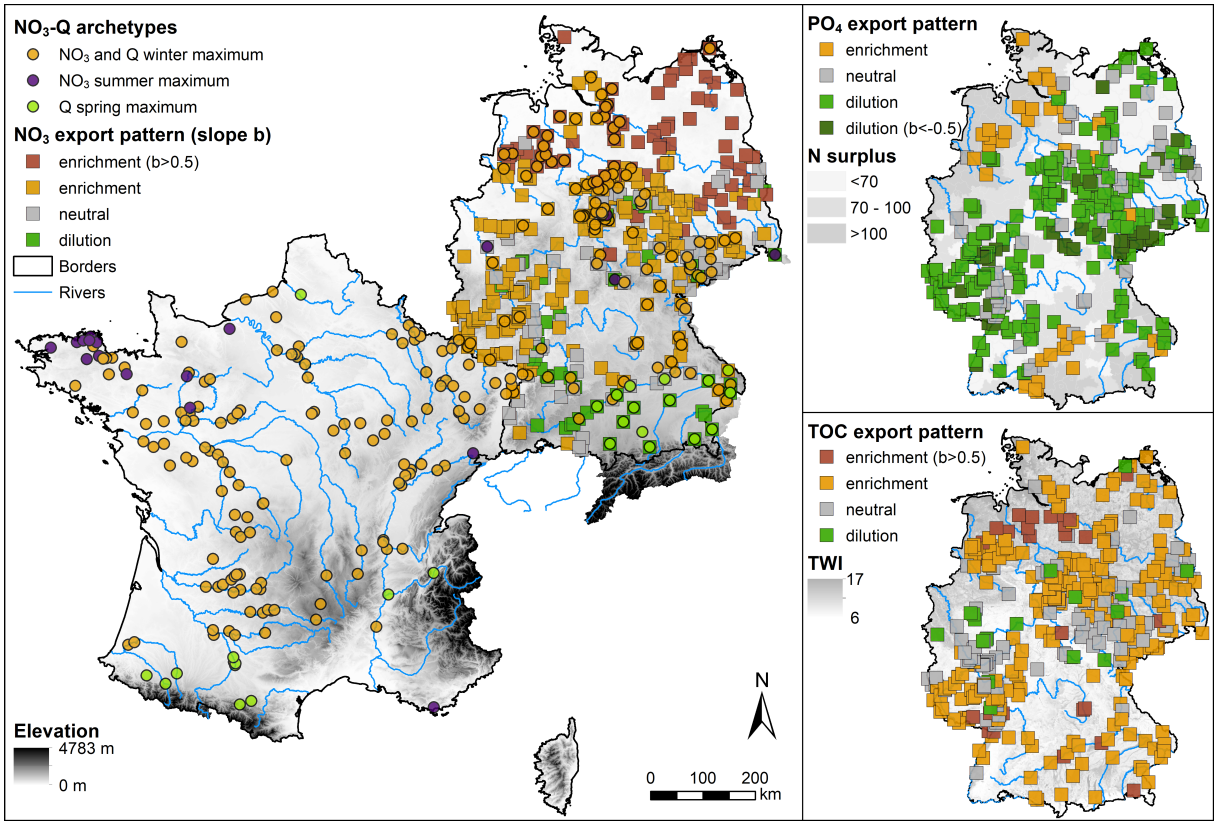

Figure 5: Synthesis of catchment archetypes: NO_3^- export patterns from Study 1 (n=441 all catchments) and average seasonality archetype from Study 2 (n=290) with elevation (left), PO_4^{3-} export patterns (n=391) with N surplus [kg ha^{-}1 y^{-1}] (top right), and TOC export patterns (n=407) with topographic wetness index (TWI) aggregated to a 2 km grid (bottom right).

(45 % of the catchments) were more often. Additionally, about 20 % of the catchments experienced a reversal in NO_3^- seasonality between low- and high-flow concentrations, indicating fundamental long-term changes in inter-annual export dynamics.

The results suggest that NO_3^- trajectories are rather variable, which is generally in line with the large-sample analyses by Ehrhardt et al. (2021) who found that peak response times to input changes varied strongly with a median response time of five and maximum of 34 years among a subset of the same study catchments. Thus, both Ehrhardt et al. (2021) and Study 2 confirmed that long-term NO_3^- trajectories are variable in western European catchments although input trajectories have been more similar in time following the European regulations. The existing regional similarities suggest a linkage to the spatial patterns of controls.

4.2 Dominant controls and underlying processes

4.2.1 Nitrate

Findings from this thesis showed that mean NO_3^- concentrations and export dynamics are dominantly controlled by the interplay between diffuse inputs from agriculture and vertical concentration heterogeneity potentially resulting from natural attenuation (removal by denitrification). Inputs define an upper limit for concentration levels, but mean concentrations in catchments with intense agriculture can still be substantially lower often combined with pronounced chemodynamic enrichment patterns. This catchment archetype was predominant in lowlands with deep sedimentary aquifers in northern Germany with high vertical concentration heterogeneity. This heterogeneity was argued to result from high inputs to soils and high subsurface denitrification in such areas (Knoll et al., 2020; Kunkel et al., 2004; Wendland et al., 2008) sustaining low concentrations in flow paths with long travel times. In lowlands, longer travel times in the stream network and denitrification in riparian wetlands interacting with the carbon cycle could also lower NO_3^- concentrations especially in summer. Additionally, the vertical heterogeneity could be related to dilution with pre-industrial water with low NO_3^- concentrations in large aquifers. In contrast, horizontal source heterogeneity in terms of distance to the stream was not a dominant control.

Across larger scales, topography and related hydroclimatic variability were identified as dominant controls of discharge seasonality and thus archetypes of NO_3^--Q seasonality (Study 2). Even though climatic variables were not a primary control of export dynamics across Germany (Study 1), this is consistent with the topographic controls identified and because the descriptors are interlinked.

Prevalent enrichment patterns and synchronous seasonality of NO_3^- and discharge indicate that additional sources are dominantly activated with increasing hydrological connectivity. This agrees with shallow sources of top-loaded profiles being mainly mobilized by younger water during high flow (Seibert et al., 2009). Artificial drainage could amplify the heterogeneity effect by facilitating the discharge of young water during high flows and the bypassing of potential retention zones (Musolff et al., 2015; Van der Velde et al., 2010; Van Meter and Basu, 2017). Additionally, seasonal variations in biogeochemical processes could reinforce the enrichment pattern, e. g. increased riparian and in-stream retention processes such as nutrient uptake or denitrification during summer low flows with longer travel times and higher temperatures (Lutz et al., 2020; Nogueira et al., 2021). The archetype of asynchronous seasonality and NO_3^- dilution with low mean NO_3^- concen-

tration in mountainous catchments (Q maximum in spring or summer) likely results from high specific discharge and spatial separation between main discharge generating zones at high elevations and downstream source areas. The archetype of asynchronous seasonality and only light dilution with high mean NO_3^- concentration in northwestern France (NO_3^- maximum in summer) could be caused by bottom-loaded concentration profiles. This is in agreement with the identified dominant control of vertical concentration heterogeneity on NO_3^- export dynamics across Germany.

The hysteresis approach, based on seasonally variable response times, allowed testing for dominant long-term changes in concentration heterogeneity in the catchment affecting trajectories of NO_3^- export dynamics. This approach is based on the understanding that different water ages contribute to discharge with varying intensities during different seasons (Benettin et al., 2017; Yang et al., 2018). Fundamental changes in concentration heterogeneity could be linked to the migration of concentration fronts along flow paths and thus aging water (Dupas et al., 2016; Ehrhardt et al., 2019). Such significant long-term changes in catchment functioning have been described for meso-scale catchments (Dupas et al., 2016; Ehrhardt et al., 2019; Winter et al., 2021), but the expected trajectories with high-flow concentrations preceding low-flow concentrations only emerged in 30 % of the catchments. This suggests that downward migrating concentration fronts, which fundamentally alter subsurface source distributions and are associated with delayed responses in low-flow nitrate concentrations and dominant hydrological legacies, are not predominant across the investigated landscapes. This is consistent with the non-dominant hydrological legacies discussed by Ehrhardt et al. (2021) for the study area. For the long-term trajectories of export dynamics, no consistent relationship to controls was found, although regional patterns and significant trends were observed. This suggests that controls are complex and that different settings and interactions of constant and time-variant controls can potentially lead to similar long-term trajectories.

Comparing the hysteresis classes from Study 2 to N retention (i. e. "missing N" retained in legacies or denitrified and not exported to streams) patterns (overlap n=232, Ehrhardt et al., 2021) shows that retention was significantly smaller (i. e. exported N higher, $p < 0.01$ Kruskal-Wallis and Wilcoxon test for pairwise comparisons) for the class of catchments with preceding high-flow NO_3^- concentrations compared to the other classes. Their median retention was significantly lower (67 %, n=73) than the median retention for catchments with preceding low-flow concentrations (73 %, n=68). Differences in the values were more pronounced for lower values: 25 % of the catchments with preceding high-flow concentrations had retention below 50 %, whereas only 4 % of the catchments with preceding low-flow concentrations were below 50 % and their lower quartile was at 69 %. This could

mean that the overall N export relates to the seasonal response times and thus different trajectories: In catchments with higher N export, processes related to relatively faster response times in high-flow concentrations seem to be more dominant. As both metrics characterize the integrated catchment response, different mechanisms (e. g. biogeochemical and hydrological legacies and denitrification) and their interplay could affect both metrics in different ways. Ehrhardt et al. (2021) found that higher N export (i. e. lower retention) was linked to hydrologic and subsurface properties favoring lower denitrification and shorter travel times of the water, which could enhance the N export especially of shallow sources with younger water fractions dominating during high flow. It could also enhance the potential of migrating N concentration fronts and impact the relative seasonal response times.

Although chemostatic catchments prevailed and linked to higher mean NO_3^- concentrations, this thesis showed that high long-term N inputs do not necessarily lead to chemostatic NO_3^- export from agricultural catchments, as had been hypothesized earlier (Basu et al., 2010; Thompson et al., 2011). Pronounced and more frequent chemodynamic enrichment patterns in catchments with intense agriculture as well as prevailing positive trends in seasonal NO_3^- ratios with predominant synchronous NO_3^--Q seasonality (i. e., prevailing increase in export dynamics) do not support the generality of this hypothesis of chemostasis.

One can conclude that natural attenuation (resulting from the joint effect of reaction rates and travel times) is able to buffer high diffuse anthropogenic N inputs in some areas and their interplay determine the variability of mean NO_3^- concentrations and export dynamics via vertical concentration heterogeneity. However, current retention capacities can decrease if finite bioavailable electron donors in the subsurface are continuously depleted by excess NO_3^- inputs (Wilde et al., 2017; Merz et al., 2009). If this natural buffer is irreversibly used up, the pressure of anthropogenic diffuse N sources on water quality may increase in the future in those areas. Horizontal source heterogeneity regarding the distance to stream was not controlling export dynamics in Study 1 but the general catchment structure with a spatial separation of main discharge generating and source zones caused asynchronous NO_3^- and discharge seasonality on average in Study 2.

Altogether, the thesis showed that across large scales, anthropogenic activities strongly affect the N cycle including especially the N transfer from land to stream. NO_3^- export is dominantly controlled by diffuse anthropogenic N inputs and subsurface properties favoring natural attenuation and thus vertical concentration heterogeneity and spatial separation of discharge generation and sources, all associated with different topography.

4.2.2 Phosphate

For PO_4^{3-}, both point and diffuse sources were relevant controls. Mean PO_4^{3-} concentrations were linked to point sources and dilution patterns, which were predominant and are also typical for point sources (Bowes et al., 2015; Moatar et al., 2017). However, diffuse sources, which were related to the fewer enrichment patterns, better explained the variability in export patterns. The enrichment was dominant in areas with high P soil saturation in agricultural soils (Fischer et al., 2017) suggesting P losses from accumulated P sources (P legacies, Sharpley et al., 2013). P accumulation in soils is a result of continuous excess diffuse P inputs especially from manure and low P use efficiencies (Sharpley et al., 2013). Although mean PO_4^{3-} concentrations were lower in the catchments with enrichment patterns, exported loads can be high during high flows and impact downstream water bodies. The rather weak link between export patterns and regimes implies that hydrology-driven dynamics are altered by highly reactive biogeochemical processes, e. g. strongly variable P cycling processes including retention, transformation and remobilization (Jarvie et al., 2012; Musolff et al., 2015). Remobilization of dissolved P from riverbed or lake sediments or wetland soils when redox conditions change can also mimic point sources and create dilution patterns (Dupas, Tittel, Jordan, Musolff and Rode, 2018; Smolders et al., 2017). Altogether, the anthropogenic impact on mean PO_4^{3-} concentrations and export dynamics is dominant, although riverine concentration dynamics are reshaped by natural highly variable biogeochemical processes. However, these biogeochemical transformation processes can still be induced or altered by human activities as higher P loads circulate in the environment. For example, eutrophication can result in oxygen depletion, changed redox conditions and remobilization of P from sediments.

4.2.3 Total organic carbon

Topography was found to dominantly control mean TOC concentrations across Germany, as it regulates the humidity that favors the accumulation of organic matter, such as in riparian wetlands (Clark et al., 2010). TOC export was dominated by mobilization processes likely from these near-stream sources as enrichment patterns were also most pronounced in lowland areas. The export was also generally more hydrology-driven in lowland areas. Hydrological characteristics also partly explained the variability in export patterns among catchments with more equilibrated discharge patterns linking to stronger enrichment patterns. Within riparian zones, which are hot spots for biogeochemical processes, interactions with other nutrients can occur, e. g. during denitrification where NO_3^- is reduced and OC is the electron donor.

Together, this suggests that more variable hydrology, entailing variable antecedent conditions and lower or less constant TOC sources, create higher variability in TOC export in terms of more ambivalent C-Q relationships. On the other hand, well-connected near-stream sources are mobilized increasingly with increasing discharge, indicating a control of vertical and horizontal source heterogeneity across catchments and regions. TOC export is dominated by natural controls determining the occurrence of terrestrial sources and hydrological variability, although humans alter the landscapes relevant for OC, such as wetlands, as well as transport pathways and processes with diverse impacts (Stanley et al., 2012).

4.3 Implications

This thesis improved the understanding of spatiotemporal patterns of nutrient export, their dominant controls and underlying dominant processes, which can support practitioners and water quality modelers. The findings can assist water quality managers to adapt monitoring and management strategies and define priorities. The identified differences and similarities and dominant controls of water quality patterns across large scales provide context for other catchments and changing conditions. This context provides regional guidance, e. g. for ungauged basins, and can facilitate temporal transfer using the concept of "trading-space-for-time" (Peel and Blöschl, 2011). Strong NO_3^- enrichment patterns under high inputs could indicate natural attenuation based on the dominant control of vertical concentration heterogeneity on export dynamics and its link to subsurface properties favoring conditions for denitrification. Subsequently, trends in export dynamics could also indicate shifts in catchment functioning regarding nutrient retention, which could result from decreasing subsurface reactivity if electron donors get exhausted (Wilde et al., 2017; Merz et al., 2009). The analysis of long-term trajectories showed that spatial variability in NO_3^- export dynamics was larger than the decadal intra-catchment variability (Study 2). Thus, management strategies and regulations need to consider the prevalent regional differences. PO_4^{3-} enrichment patterns were linked to diffuse sources in areas with high probabilities of soil P saturation (Fischer et al., 2017; Sharpley et al., 2013). This highlighted the importance of managing and regulating diffuse P sources besides the point sources. These P accumulations in soils (biogeochemical legacies) potentially cause long-term P losses to the streams (Van Meter et al., 2021), especially from near-stream or well-connected areas such as by artificial drainage and preferential flow paths (Osterholz et al., 2020). P legacies in agricultural areas are likely more widespread than in the catchments with emergent enrichment patterns, but could be masked by more

dominant dilution patterns. Fischer et al. (2017) estimated that more than 76 % of agricultural soils in Germany are close to P saturation. Although mean NO_3^- and PO_4^{3-} concentrations of the catchments with chemodynamic enrichment patterns were relatively low, these sites can still be hot spots of exported loads. Both N and P legacies may cause large export time scales up to several decades and impair water quality over the long term (Van Meter et al., 2021; Meals et al., 2010).

For management measures, this implies that nutrient inputs should be further reduced to avoid continuous build-up of nutrient legacies, the risk of depleting buffer capacities and continuous deterioration of aquatic ecosystems. To reduce legacies and losses, nutrient use efficiencies should be increased e. g. using more effective fertilizing strategies to improve plant uptake and recycling nutrients stored in soils (Bindraban et al., 2020; Dupas et al., 2020). Buffer strips or riparian wetlands can create additional retention zones removing NO_3^- via denitrification (Sabater et al., 2003) and trapping P, although there are risks to consider such as the potential remobilization of P under changing redox conditions (Gu et al., 2017) and release of greenhouse gases (Galloway et al., 2003). Improved, sustainable nutrient management is also specifically relevant for P as a limited resource (Bindraban et al., 2020). TOC concentrations were controlled by riparian wetlands. These can be restored to modify ecosystem structure and functions including nutrient uptake and thus potentially improve the water quality, although effects are diverse and not yet fully understood (Stanley et al., 2012).

Water quality modelers can benefit from the identified dominant controls to inform models to better represent relevant processes shaping large-scale spatiotemporal patterns of nutrient export, to reduce model complexity or to adapt strategies to regionalize parameters. This could be by adapting easily available proxies, such as the topographic and land use characteristics. The assembled data set can be used to calibrate and validate models based on concentrations and loads as well as the different export metrics and to verify the model structure. Modeling can further extend the knowledge of catchment functioning and explore management strategies.

This thesis has made an important contribution to the understanding of general catchment functioning including similarities and differences, by presenting a broad „pattern-to-process“ analysis in line with large-sample hydrology (Sivapalan, 2006). Identifying general patterns and relationships within the complexity of catchments can help unite process understanding at different scales and thus advance the understanding of hydrological functions at the catchment scale (Sivapalan, 2006; Wagener et al., 2007). This concept is based on the understanding of catchments as self-organizing systems resulting from principles of landscape genesis (Sivapalan, 2006; Wagener et al., 2007). The

large-sample analysis of this thesis revealed spatiotemporal patterns of nutrient export dynamics, identified dominant controls and underlying processes. It increased the understanding of mechanisms of nutrient export and how human controls interact with natural controls across a wide range of catchments. Overall, this thesis showed that human interference with the biogeochemical cycles has a large impact on the land-to-stream transfer and riverine concentration dynamics of the nutrients.

Reducing nutrient losses to the environment to decrease widespread adverse effects of human activities is crucial to protect aquatic ecosystem and human health. Joint efforts of researchers, practitioners and stakeholders are needed to define and implement best management practices, mediate between conflicting interests and move in a "safe operating space for humanity" (Rockström et al., 2009), especially in the face of a changing world and future challenges.

4.4 Outlook

Follow-up studies could further verify the hypotheses derived from the large sample analyses and help to quantify and disentangle the underlying processes. To understand catchment buffering capacities for nutrient inputs, estimates of large-scale, regional denitrification potential are needed, including potential long-term changes and limits. Similarly, more research on the quantification of N and P soil accumulation and saturation across larger scales is needed. In combination with these estimates, the potential of C-Q relationships to serve as diagnostic tools or proxies for such shifts in catchment functioning could be evaluated. The importance of the different retention mechanisms at catchment scale need to be further disentangled between the legacies and removal by denitrification, but also among the different compartments, namely soils, vadose zone, groundwater, riparian zones and stream network. Moreover, nutrient interactions causing temporal or permanent removal and their impact on responses at the catchment outlet need to be further investigated, especially in riparian zones and in stream networks. The role of tile drains on nutrient export dynamics across larger scales also still remains speculative at the moment (Musolff et al., 2015; Osterholz et al., 2020).
Disentangling the different controls on C-Q trajectories could help to better understand their interacting impact on the different trajectories of low- and high-flow concentrations. More detailed analyses in fewer catchments of different archetypes with higher data availability including point source input time series might forward the understanding. Time series of point source inputs would also allow estimating source apportionment and re-

fining priorities for management. To further investigate long-term trends in catchment functioning, trajectories of PO_4^{3-} and TOC in addition to NO_3^- export dynamics, nutrient ratios and interactions should also be considered. Subsequently, the link between nutrient dynamics on ecological responses needs to be investigated, including algae growth (chlorophyll-a), biodiversity, and the ecological status as a target of the European water quality management according to the WFD (EC, 2000). Here, water quality modeling studies can help to transfer the gained knowledge into water quality predictions including climate and management scenarios.

The proposed approaches including the parameterization of source heterogeneity and hysteresis for seasonality trajectories can be further explored to investigate catchment functioning. They would benefit from comparison to other frameworks and further applications to better understand sensitivities and dependencies. The hysteresis framework informs about catchment response time scales and their seasonal differences reflecting the input history, retention and release processes. It thus allows to discuss different ecological implications as low-flow season is usually more sensitive to eutrophication (Minaudo et al., 2020; Withers and Jarvie, 2008), high flows are more relevant for loads exported to downstream water bodies (Bouraoui and Grizzetti, 2011) and changes in inter-annual export dynamics could imply changes in ecosystem functioning (Penuelas et al., 2020). To characterize long-term changes in catchment functioning, the hysteresis integrates transitional states, including when trends are not monotonic and seasonal response times vary. This transition could include, for example, a temporarily chemostatic ("pseudo-chemostatic") export regime, as described by Ehrhardt et al. (2019). Further applications could, for example, include other water quality compounds and catchments with high data availability.

To address the open questions, the assembled large-sample data set can be used. Nevertheless, further freely available data would be useful. This includes similar large-sample data sets of water quality extending for other regions, but also additional data, particularly on long-term soil nutrient content, groundwater quality, and ecological data. In addition, time series of anthropogenic drivers would be useful, in particular of land and water management at national or larger scales, of point source loads and of P-surplus on agricultural land, as well as improved estimates of e. g. atmospheric deposition or N-surplus. Large-sample studies across a larger extent with higher climate variability could generally increase the opportunities to apply the "trading-space-for-time" concept for climate change scenarios. Moving to cross-continental, global scale analysis of water quality dynamics covering more variable hydroclimatic conditions (including arid areas), landscapes and anthropogenic settings could further advance our understanding of differences

and similarities and dominant controls of catchment responses. This thesis and especially Study 3 therefore calls for open science and data policies to increase data accessibility and consistency and open up further opportunities for water quality research and management.

References

Abbott, B. W., Bishop, K., Zarnetske, J. P., Hannah, D. M., Frei, R. J., Minaudo, C., Chapin, F. S., Krause, S., Conner, L., Ellison, D., Godsey, S. E., Plont, S., Marçais, J., Kolbe, T., Huebner, A., Hampton, T., Gu, S., Buhman, M., Sayedi, S. S., Ursache, O., Chapin, M., Henderson, K. D. and Pinay, G. (2019), 'A water cycle for the Anthropocene', *Hydrological Processes* **3**3(23), 3046–3052.
URL: *https://doi.org/10.1002/hyp.13544*

Abbott, B. W., Gruau, G., Zarnetske, J. P., Moatar, F., Barbe, L., Thomas, Z., Fovet, O., Kolbe, T., Gu, S., Pierson-Wickmann, A.-C., Davy, P. and Pinay, G. (2018), 'Unexpected spatial stability of water chemistry in headwater stream networks', *Ecology Letters* **2**1(2), 296–308.
URL: *https://onlinelibrary.wiley.com/doi/abs/10.1111/ele.12897*

Addor, N., Do, H. X., Alvarez-Garreton, C., Coxon, G., Fowler, K. and Mendoza, P. A. (2020), 'Large-sample hydrology: recent progress, guidelines for new datasets and grand challenges', *Hydrological Sciences Journal* **6**5(5), 712–725.
URL: *https://doi.org/10.1080/02626667.2019.1683182*

Addor, N., Newman, A. J., Mizukami, N. and Clark, M. P. (2017), 'The CAMELS data set: catchment attributes and meteorology for large-sample studies', *Hydrology and Earth System Sciences* **2**1(10), 5293–5313.
URL: *https://doi.org/10.5194/hess-21-5293-2017*

Ascott, M. J., Gooddy, D. C., Wang, L., Stuart, M. E., Lewis, M. A., Ward, R. S. and Binley, A. M. (2017), 'Global patterns of nitrate storage in the vadose zone', *Nature Communications* **8**(1), 1416.
URL: *https://doi.org/10.1038/s41467-017-01321-w*

Basu, N. B., Destouni, G., Jawitz, J. W., Thompson, S. E., Loukinova, N. V., Darracq, A., Zanardo, S., Yaeger, M., Sivapalan, M., Rinaldo, A. and Rao, P. S. C. (2010), 'Nutrient loads exported from managed catchments reveal emergent biogeochemical stationarity',

Geophysical Research Letters **37**(23).
URL: *https://agupubs.onlinelibrary.wiley.com/doi/full/10.1029/2010GL045168*

Benettin, P., Bailey, S. W., Rinaldo, A., Likens, G. E., McGuire, K. J. and Botter, G. (2017), 'Young runoff fractions control streamwater age and solute concentration dynamics', *Hydrological Processes* **31**(16), 2982–2986.
URL: *https://onlinelibrary.wiley.com/doi/abs/10.1002/hyp.11243*

BGBI.1 (1980), 'Verordnung über Höchstmengen für Phosphate in Wasch-und Reinigungsmitteln vom 4.6.1980: PHöchstMengV; 1980'.

Bindraban, P. S., Dimkpa, C. O. and Pandey, R. (2020), 'Exploring phosphorus fertilizers and fertilization strategies for improved human and environmental health', *Biology and Fertility of Soils* **56**(3), 299–317.
URL: *https://doi.org/10.1007/s00374-019-01430-2*

Bishop, K., Seibert, J., Köhler, S. and Laudon, H. (2004), 'Resolving the Double Paradox of rapidly mobilized old water with highly variable responses in runoff chemistry', *Hydrological Processes* **18**(1), 185–189.
URL: *https://onlinelibrary.wiley.com/doi/abs/10.1002/hyp.5209*

Blöschl, G., Bierkens, M. F. P., Chambel, A., Cudennec, C., Destouni, G., Fiori, A., Kirchner, J. W., McDonnell, J. J., Savenije, H. H. G., Sivapalan, M., Stumpp, C., Toth, E., Volpi, E., Carr, G., Lupton, C., Salinas, J., Széles, B., Viglione, A., Aksoy, H., Allen, S. T., Amin, A., Andréassian, V., Arheimer, B., Aryal, S. K., Baker, V., Bardsley, E., Barendrecht, M. H., Bartosova, A., Batelaan, O., Berghuijs, W. R., Beven, K., Blume, T., Bogaard, T., Borges de Amorim, P., Böttcher, M. E., Boulet, G., Breinl, K., Brilly, M., Brocca, L., Buytaert, W., Castellarin, A., Castelletti, A., Chen, X., Chen, Y., Chen, Y., Chifflard, P., Claps, P., Clark, M. P., Collins, A. L., Croke, B., Dathe, A., David, P. C., de Barros, F. P. J., de Rooij, G., Di Baldassarre, G., Driscoll, J. M., Duethmann, D., Dwivedi, R., Eris, E., Farmer, W. H., Feiccabrino, J., Ferguson, G., Ferrari, E., Ferraris, S., Fersch, B., Finger, D., Foglia, L., Fowler, K., Gartsman, B., Gascoin, S., Gaume, E., Gelfan, A., Geris, J., Gharari, S., Gleeson, T., Glendell, M., Gonzalez Bevacqua, A., González-Dugo, M. P., Grimaldi, S., Gupta, A. B., Guse, B., Han, D., Hannah, D., Harpold, A., Haun, S., Heal, K., Helfricht, K., Herrnegger, M., Hipsey, M., Hlaváčiková, H., Hohmann, C., Holko, L., Hopkinson, C., Hrachowitz, M., Illangasekare, T. H., Inam, A., Innocente, C., Istanbulluoglu, E., Jarihani, B., Kalantari, Z., Kalvans, A., Khanal, S., Khatami, S., Kiesel, J., Kirkby, M., Knoben,

W., Kochanek, K., Kohnová, S., Kolechkina, A., Krause, S., Kreamer, D., Kreibich, H., Kunstmann, H., Lange, H., Liberato, M. L. R., Lindquist, E., Link, T., Liu, J., Loucks, D. P., Luce, C., Mahé, G., Makarieva, O., Malard, J., Mashtayeva, S., Maskey, S., Mas-Pla, J., Mavrova-Guirguinova, M., Mazzoleni, M., Mernild, S., Misstear, B. D., Montanari, A., Müller-Thomy, H., Nabizadeh, A., Nardi, F., Neale, C., Nesterova, N., Nurtaev, B., Odongo, V. O., Panda, S., Pande, S., Pang, Z., Papacharalampous, G., Perrin, C., Pfister, L., Pimentel, R., Polo, M. J., Post, D., Prieto Sierra, C., Ramos, M.-H., Renner, M., Reynolds, J. E., Ridolfi, E., Rigon, R., Riva, M., Robertson, D. E., Rosso, R., Roy, T., Sá, J. H. M., Salvadori, G., Sandells, M., Schaefli, B., Schumann, A., Scolobig, A., Seibert, J., Servat, E., Shafiei, M., Sharma, A., Sidibe, M., Sidle, R. C., Skaugen, T., Smith, H., Spiessl, S. M., Stein, L., Steinsland, I., Strasser, U., Su, B., Szolgay, J., Tarboton, D., Tauro, F., Thirel, G., Tian, F., Tong, R., Tussupova, K., Tyralis, H., Uijlenhoet, R., van Beek, R., van der Ent, R. J., van der Ploeg, M., Van Loon, A. F., van Meerveld, I., van Nooijen, R., van Oel, P. R., Vidal, J.-P., von Freyberg, J., Vorogushyn, S., Wachniew, P., Wade, A. J., Ward, P., Westerberg, I. K., White, C., Wood, E. F., Woods, R., Xu, Z., Yilmaz, K. K. and Zhang, Y. (2019), 'Twenty-three unsolved problems in hydrology (UPH) – a community perspective', *Hydrological Sciences Journal* **6**4(10), 1141–1158.
URL: *https://doi.org/10.1080/02626667.2019.1620507*

Bouraoui, F. and Grizzetti, B. (2011), 'Long term change of nutrient concentrations of rivers discharging in European seas', *Science of The Total Environment* **4**09(23), 4899–4916.
URL: *https://doi.org/10.1016/j.scitotenv.2011.08.015*

Bowes, M. J., Jarvie, H. P., Halliday, S. J., Skeffington, R. A., Wade, A. J., Loewenthal, M., Gozzard, E., Newman, J. R. and Palmer-Felgate, E. J. (2015), 'Characterising phosphorus and nitrate inputs to a rural river using high-frequency concentration–flow relationships', *Science of The Total Environment* **5**11, 608–620.
URL: *http://www.sciencedirect.com/science/article/pii/S0048969714017975*

Burt, T. P., Howden, N. J. K., Worrall, F. and McDonnell, J. J. (2011), 'On the value of long-term, low-frequency water quality sampling: avoiding throwing the baby out with the bathwater', *Hydrological Processes* **2**5(5), 828–830.
URL: *https://onlinelibrary.wiley.com/doi/abs/10.1002/hyp.7961*

Clark, J. M., Bottrell, S. H., Evans, C. D., Monteith, D. T., Bartlett, R., Rose, R., Newton, R. J. and Chapman, P. J. (2010), 'The importance of the relationship between

scale and process in understanding long-term DOC dynamics', *Science of The Total Environment* **4**08(13), 2768–2775.
URL: *http://www.sciencedirect.com/science/article/pii/S0048969710002160*

Conijn, J. G., Bindraban, P. S., Schröder, J. J. and Jongschaap, R. E. E. (2018), 'Can our global food system meet food demand within planetary boundaries?', *Agriculture, Ecosystems & Environment* **2**51, 244–256.
URL: *https://www.sciencedirect.com/science/article/pii/S0167880917302438*

Conley, D. J., Paerl, H. W., Howarth, R. W., Boesch, D. F., Seitzinger, S. P., Havens, K. E., Lancelot, C. and Likens, G. E. (2009), 'Controlling Eutrophication: Nitrogen and Phosphorus', *Science* **3**23(5917), 1014–1015.
URL: *https://science.sciencemag.org/content/sci/323/5917/1014.full.pdf*

Copeland, C. (2016), 'Clean Water Act: A Summary of the Law'.
URL: *https://fas.org/sgp/crs/misc/RL30030.pdf*

Cordell, D., Drangert, J.-O. and White, S. (2009), 'The story of phosphorus: Global food security and food for thought', *Global Environmental Change* **1**9(2), 292–305.
URL: *https://www.sciencedirect.com/science/article/pii/S095937800800099X*

Crutzen, P. J. (2002), 'Geology of mankind', *Nature* **4**15(6867), 23.
URL: *https://doi.org/10.1038/415023a*

Diaz, R. J. and Rosenberg, R. (2008), 'Spreading Dead Zones and Consequences for Marine Ecosystems', *Science* **3**21(5891), 926–929.
URL: *https://science.sciencemag.org/content/sci/321/5891/926.full.pdf*

Dupas, R., Ehrhardt, S., Musolff, A., Fovet, O. and Durand, P. (2020), 'Long-term nitrogen retention and transit time distribution in agricultural catchments in western France', *Environmental Research Letters* **1**5(11), 115011.
URL: *http://dx.doi.org/10.1088/1748-9326/abbe47*

Dupas, R., Jomaa, S., Musolff, A., Borchardt, D. and Rode, M. (2016), 'Disentangling the influence of hydroclimatic patterns and agricultural management on river nitrate dynamics from sub-hourly to decadal time scales', *Science of The Total Environment* **5**71, 791–800.
URL: *https://doi.org/10.1016/j.scitotenv.2016.07.053*

Dupas, R., Minaudo, C. and Abbott, B. W. (2019), 'Stability of spatial patterns in water chemistry across temperate ecoregions', *Environmental Research Letters* **1**4(7), 74015.
URL: *http://dx.doi.org/10.1088/1748-9326/ab24f4*

Dupas, R., Minaudo, C., Gruau, G., Ruiz, L. and Gascuel-Odoux, C. (2018), 'Multidecadal Trajectory of Riverine Nitrogen and Phosphorus Dynamics in Rural Catchments', *Water Resources Research* **5**4(8), 5327–5340.
URL: *https://agupubs.onlinelibrary.wiley.com/doi/abs/10.1029/2018WR022905*

Dupas, R., Tittel, J., Jordan, P., Musolff, A. and Rode, M. (2018), 'Non-domestic phosphorus release in rivers during low-flow: Mechanisms and implications for sources identification', *Journal of Hydrology* **5**60, 141–149.
URL: *https://doi.org/10.1016/j.jhydrol.2018.03.023*

EC (1991*a*), 'Council Directive 91/271/EEC of 21 May 1991 concerning urban waste water treatment', *Official Journal of the European Communities* .

EC (1991*b*), 'Council Directive 91/676/EEC of 12 December 1991 concerning the protection of waters against pollution caused by nitrates from agricultural sources', *Official Journal of the European Communities* .

EC (2000), 'Directive 2000/60/EC of the European Parliament and of the Council of 23 October 2000 establishing a framework for Community action in the field of water policy', *Official Journal of the European Communities* **L** 327, 1–73.

EC (2019), 'Communication from the Commission to the European Parliament, the European Council, the Council, the European Economic and Social Committee and the Committee of the Regions, The European Green Deal', **C**OM(2019).

EEA, Kristensen, P., Kampa, E., Völker, J., Stein, U. and Mohaupt, V. (2021), Drivers of and pressures arising from selected key water management challenges - A European overview, Technical report.
URL: *https://data.europa.eu/doi/10.2800/059069*

EEA, Zal, N., Whalley, C., Christiansen, T., Kristensen, P. and Néry, F. (2018), European waters. Assessment of status and pressures 2018, Technical report.
URL: *https://www.eea.europa.eu/publications/state-of-water*

Ehrhardt, S., Ebeling, P., Dupas, R., Kumar, R., Fleckenstein, J. H. and Musolff, A. (2021), 'Nitrate Transport and Retention in Western European Catchments

Are Shaped by Hydroclimate and Subsurface Properties', *Water Resources Research* **5**7(10), e2020WR029469.
URL: *https://agupubs.onlinelibrary.wiley.com/doi/abs/10.1029/2020WR029469*

Ehrhardt, S., Kumar, R., Fleckenstein, J. H., Attinger, S. and Musolff, A. (2019), 'Trajectories of nitrate input and output in three nested catchments along a land use gradient', *Hydrol. Earth Syst. Sci.* **2**3(9), 3503–3524.
URL: *https://www.hydrol-earth-syst-sci.net/23/3503/2019/*

Fischer, P., Pöthig, R. and Venohr, M. (2017), 'The degree of phosphorus saturation of agricultural soils in Germany: Current and future risk of diffuse P loss and implications for soil P management in Europe', *Science of The Total Environment* **5**99-600, 1130–1139.
URL: *http://www.sciencedirect.com/science/article/pii/S0048969717306629*

Fovet, O., Humbert, G., Dupas, R., Gascuel-Odoux, C., Gruau, G., Jaffrezic, A., Thelusma, G., Faucheux, M., Gilliet, N., Hamon, Y. and Grimaldi, C. (2018), 'Seasonal variability of stream water quality response to storm events captured using high-frequency and multi-parameter data', *Journal of Hydrology* **5**59, 282–293.
URL: *https://doi.org/10.1016/j.jhydrol.2018.02.040*

Galloway, J. N., Aber, J. D., Erisman, J. W., Seitzinger, S. P., Howarth, R. W., Cowling, E. B. and Cosby, B. J. (2003), 'The Nitrogen Cascade', *BioScience* **5**3(4), 341–356.
URL: *https://doi.org/10.1641/0006-3568(2003)053[0341:TNC]2.0.CO;2*

Galloway, J. N. and Cowling, E. B. (2002), 'Reactive Nitrogen and The World: 200 Years of Change', *AMBIO: A Journal of the Human Environment* **3**1(2), 8,64–71.
URL: *https://doi.org/10.1579/0044-7447-31.2.64*

Galloway, J. N., Dentener, F. J., Capone, D. G., Boyer, E. W., Howarth, R. W., Seitzinger, S. P., Asner, G. P., Cleveland, C. C., Green, P. A., Holland, E. A., Karl, D. M., Michaels, A. F., Porter, J. H., Townsend, A. R. and Vöosmarty, C. J. (2004), 'Nitrogen Cycles: Past, Present, and Future', *Biogeochemistry* **7**0(2), 153–226.
URL: *https://doi.org/10.1007/s10533-004-0370-0*

Godsey, S. E., Kirchner, J. W. and Clow, D. W. (2009), 'Concentration-discharge relationships reflect chemostatic characteristics of US catchments', *Hydrological Processes* **2**3(13), 1844–1864.
URL: *https://doi.org/10.1002/hyp.7315*

Graeber, D., Boëchat, I. G., Encina-Montoya, F., Esse, C., Gelbrecht, J., Goyenola, G., Gücker, B., Heinz, M., Kronvang, B., Meerhoff, M., Nimptsch, J., Pusch, M. T., Silva, R. C. S., von Schiller, D. and Zwirnmann, E. (2015), 'Global effects of agriculture on fluvial dissolved organic matter', *Scientific Reports* **5**(1), 16328.
URL: *https://doi.org/10.1038/srep16328*

Gu, S., Gruau, G., Dupas, R., Rumpel, C., Creme, A., Fovet, O., Gascuel-Odoux, C., Jeanneau, L., Humbert, G. and Petitjean, P. (2017), 'Release of dissolved phosphorus from riparian wetlands: Evidence for complex interactions among hydroclimate variability, topography and soil properties', *Sci Total Environ* **5**98, 421–431.
URL: *https://www.ncbi.nlm.nih.gov/pubmed/28448934*

Gupta, H. V., Perrin, C., Blöschl, G., Montanari, A., Kumar, R., Clark, M. and Andréassian, V. (2014), 'Large-sample hydrology: a need to balance depth with breadth', *Hydrol. Earth Syst. Sci.* **1**8(2), 463–477.
URL: *https://www.hydrol-earth-syst-sci.net/18/463/2014/*

Häußermann, U., Bach, M., Klement, L. and Breuer, L. (2019), 'Stickstoff-Flächenbilanzen für Deutschland mit Regionalgliederung Bundesländer und Kreise – Jahre 1995 bis 2017. Methodik, Ergebnisse und Minderungsmaßnahmen', *Texte* **1**31/2019.
URL: *https://www.umweltbundesamt.de/sites/default/files/medien/1410/publikationen/2019-10-28_texte_131-2019_stickstoffflaechenbilanz.pdf*

Hirsch, R. M., Archfield, S. A. and De Cicco, L. A. (2015), 'A bootstrap method for estimating uncertainty of water quality trends', *Environmental Modelling & Software* **7**3, 148–166.
URL: *http://www.sciencedirect.com/science/article/pii/S1364815215300220*

Howden, N. J. K., Burt, T. P., Worrall, F., Whelan, M. J. and Bieroza, M. Z. (2010), 'Nitrate concentrations and fluxes in the River Thames over 140 years (1868–2008): are increases irreversible?', *Hydrological Processes* **2**4(18), 2657–2662.
URL: *https://onlinelibrary.wiley.com/doi/abs/10.1002/hyp.7835*

Jarvie, H. P., Sharpley, A. N., Scott, J. T., Haggard, B. E., Bowes, M. J. and Massey, L. B. (2012), 'Within-River Phosphorus Retention: Accounting for a Missing Piece in the Watershed Phosphorus Puzzle', *Environmental Science & Technology* **4**6(24), 13284–13292.
URL: *https://doi.org/10.1021/es303562y*

Jenny, J.-P., Anneville, O., Arnaud, F., Baulaz, Y., Bouffard, D., Domaizon, I., Bocaniov, S. A., Chèvre, N., Dittrich, M., Dorioz, J.-M., Dunlop, E. S., Dur, G., Guillard, J., Guinaldo, T., Jacquet, S., Jamoneau, A., Jawed, Z., Jeppesen, E., Krantzberg, G., Lenters, J., Leoni, B., Meybeck, M., Nava, V., Nõges, T., Nõges, P., Patelli, M., Pebbles, V., Perga, M.-E., Rasconi, S., Ruetz, C. R., Rudstam, L., Salmaso, N., Sapna, S., Straile, D., Tammeorg, O., Twiss, M. R., Uzarski, D. G., Ventelä, A.-M., Vincent, W. F., Wilhelm, S. W., Wängberg, S.-Å. and Weyhenmeyer, G. A. (2020), 'Scientists' Warning to Humanity: Rapid degradation of the world's large lakes', *Journal of Great Lakes Research* **4**6(4), 686–702.
URL: *http://www.sciencedirect.com/science/article/pii/S0380133020300988*

Kingston, D. G., Massei, N., Dieppois, B., Hannah, D. M., Hartmann, A., Lavers, D. A. and Vidal, J. (2020), 'Moving beyond the catchment scale: Value and opportunities in large-scale hydrology to understand our changing world', *Hydrological Processes* **3**4(10), 2292–2298.
URL: *https://doi.org/10.1002/hyp.13729*

Knoll, L., Breuer, L. and Bach, M. (2020), 'Nation-wide estimation of groundwater redox conditions and nitrate concentrations through machine learning', *Environmental Research Letters* **1**5(6), 64004.
URL: *http://dx.doi.org/10.1088/1748-9326/ab7d5c*

Kunkel, R., Bach, M., Behrendt, H. and Wendland, F. (2004), 'Groundwater-borne nitrate intakes into surface waters in Germany', *Water Science and Technology* **4**9(3), 11–19.
URL: *https://doi.org/10.2166/wst.2004.0152*

Langhans, C., Beusen, A. H. W., Mogollón, J. M. and Bouwman, A. F. (2022), 'Phosphorus for Sustainable Development Goal target of doubling smallholder productivity', *Nature Sustainability* **5**(1), 57–63.
URL: *https://doi.org/10.1038/s41893-021-00794-4*

Laudon, H., Köhler, S. and Buffam, I. (2004), 'Seasonal TOC export from seven boreal catchments in northern Sweden', *Aquatic Sciences* **6**6(2), 223–230.
URL: *https://doi.org/10.1007/s00027-004-0700-2*

Le Moal, M., Gascuel-Odoux, C., Ménesguen, A., Souchon, Y., Étrillard, C., Levain, A., Moatar, F., Pannard, A., Souchu, P., Lefebvre, A. and Pinay, G. (2019), 'Eutrophication: A new wine in an old bottle?', *Science of The Total Environment* **6**51, 1–11.
URL: *https://doi.org/10.1016/j.scitotenv.2018.09.139*

Lutz, S. R., Trauth, N., Musolff, A., Van Breukelen, B. M., Knöller, K. and Fleckenstein, J. H. (2020), 'How Important is Denitrification in Riparian Zones? Combining End-Member Mixing and Isotope Modeling to Quantify Nitrate Removal from Riparian Groundwater', *Water Resources Research* **5**6(1), e2019WR025528.
URL: *https://agupubs.onlinelibrary.wiley.com/doi/abs/10.1029/2019WR025528*

Martin, C., Aquilina, L., Gascuel-Odoux, C., Molénat, J., Faucheux, M. and Ruiz, L. (2004), 'Seasonal and interannual variations of nitrate and chloride in stream waters related to spatial and temporal patterns of groundwater concentrations in agricultural catchments', *Hydrological Processes* **1**8(7), 1237–1254.
URL: *https://onlinelibrary.wiley.com/doi/abs/10.1002/hyp.1395*

McClain, M. E., Boyer, E. W., Dent, C. L., Gergel, S. E., Grimm, N. B., Groffman, P. M., Hart, S. C., Harvey, J. W., Johnston, C. A., Mayorga, E., McDowell, W. H. and Pinay, G. (2003), 'Biogeochemical Hot Spots and Hot Moments at the Interface of Terrestrial and Aquatic Ecosystems', *Ecosystems* **6**(4), 301–312.
URL: *https://doi.org/10.1007/s10021-003-0161-9*

Meals, D. W., Dressing, S. A. and Davenport, T. E. (2010), 'Lag Time in Water Quality Response to Best Management Practices: A Review', *Journal of Environmental Quality* **3**9(1), 85–96.
URL: *http://dx.doi.org/10.2134/jeq2009.0108*

Merz, C., Steidl, J. and Dannowski, R. (2009), 'Parameterization and regionalization of redox based denitrification for GIS-embedded nitrate transport modeling in Pleistocene aquifer systems', *Environmental Geology* **5**8(7), 1587.
URL: *https://doi.org/10.1007/s00254-008-1665-6*

Minaudo, C., Abonyi, A., Leitão, M., Lançon, A. M., Floury, M., Descy, J.-P. and Moatar, F. (2020), 'Long-term impacts of nutrient control, climate change, and invasive clams on phytoplankton and cyanobacteria biomass in a large temperate river', *Science of The Total Environment* p. 144074.
URL: *https://doi.org/10.1016/j.scitotenv.2020.144074*

Minaudo, C., Dupas, R., Gascuel-Odoux, C., Roubeix, V., Danis, P.-A. and Moatar, F. (2019), 'Seasonal and event-based concentration-discharge relationships to identify catchment controls on nutrient export regimes', *Advances in Water Resources* **1**31, 103379.
URL: *https://doi.org/10.1016/j.advwatres.2019.103379*

Moatar, F., Abbott, B. W., Minaudo, C., Curie, F. and Pinay, G. (2017), 'Elemental properties, hydrology, and biology interact to shape concentration-discharge curves for carbon, nutrients, sediment, and major ions', *Water Resources Research* **5**3(2), 1270–1287.
URL: *https://doi.org/10.1002/2016wr019635*

Musolff, A., Fleckenstein, J. H., Opitz, M., Büttner, O., Kumar, R. and Tittel, J. (2018), 'Spatio-temporal controls of dissolved organic carbon stream water concentrations', *Journal of Hydrology* **5**66, 205–215.
URL: *https://doi.org/10.1016/j.jhydrol.2018.09.011*

Musolff, A., Fleckenstein, J. H., Rao, P. S. C. and Jawitz, J. W. (2017), 'Emergent archetype patterns of coupled hydrologic and biogeochemical responses in catchments', *Geophysical Research Letters* **4**4(9), 4143–4151.
URL: *https://doi.org/10.1002/2017gl072630*

Musolff, A., Schmidt, C., Selle, B. and Fleckenstein, J. H. (2015), 'Catchment controls on solute export', *Advances in Water Resources* **8**6, 133–146.
URL: *https://doi.org/10.1016/j.advwatres.2015.09.026*

Nogueira, G. E. H., Schmidt, C., Brunner, P., Graeber, D. and Fleckenstein, J. H. (2021), 'Transit-Time and Temperature Control the Spatial Patterns of Aerobic Respiration and Denitrification in the Riparian Zone', *Water Resources Research* **5**7(12), e2021WR030117.
URL: *https://agupubs.onlinelibrary.wiley.com/doi/abs/10.1029/2021WR030117*

Osterholz, W. R., Hanrahan, B. R. and King, K. W. (2020), 'Legacy phosphorus concentration–discharge relationships in surface runoff and tile drainage from Ohio crop fields', *Journal of Environmental Quality* **4**9(3), 675–687.
URL: *https://acsess.onlinelibrary.wiley.com/doi/abs/10.1002/jeq2.20070*

Peel, M. C. and Blöschl, G. (2011), 'Hydrological modelling in a changing world', *Progress in Physical Geography: Earth and Environment* **3**5(2), 249–261.
URL: *https://journals.sagepub.com/doi/abs/10.1177/0309133311402550*

Penuelas, J., Janssens, I. A., Ciais, P., Obersteiner, M. and Sardans, J. (2020), 'Anthropogenic global shifts in biospheric N and P concentrations and ratios and their impacts on biodiversity, ecosystem productivity, food security, and human health', *Global Change Biology* **2**6(4), 1962–1985.
URL: *https://onlinelibrary.wiley.com/doi/abs/10.1111/gcb.14981*

Peñuelas, J., Poulter, B., Sardans, J., Ciais, P., van der Velde, M., Bopp, L., Boucher, O., Godderis, Y., Hinsinger, P., Llusia, J., Nardin, E., Vicca, S., Obersteiner, M. and Janssens, I. A. (2013), 'Human-induced nitrogen–phosphorus imbalances alter natural and managed ecosystems across the globe', *Nature Communications* **4**, 2934.
URL: *https://doi.org/10.1038/ncomms3934*

Pinay, G., Peiffer, S., De Dreuzy, J.-R., Krause, S., Hannah, D. M., Fleckenstein, J. H., Sebilo, M., Bishop, K. and Hubert-Moy, L. (2015), 'Upscaling Nitrogen Removal Capacity from Local Hotspots to Low Stream Orders' Drainage Basins', *Ecosystems* **1**8(6), 1101–1120.
URL: *https://doi.org/10.1007/s10021-015-9878-5*

Rockström, J., Steffen, W., Noone, K., Persson, Å., Chapin, F. S., III, E. L., Lenton, T. M., Scheffer, M., Folke, C., Schellnhuber, H., Nykvist, B., Wit, C. A. D., Hughes, T., van der Leeuw, S., Rodhe, H., Sörlin, S., Snyder, P. K., Costanza, R., Svedin, U., Falkenmark, M., Karlberg, L., Corell, R. W., Fabry, V. J., Hansen, J., Walker, B., Liverman, D., Richardson, K., Crutzen, P. and Foley, J. (2009), 'Planetary boundaries: exploring the safe operating space for humanity', *Ecology and Society* **1**4(2)(32).

Sabater, S., Butturini, A., Clement, J.-C., Burt, T., Dowrick, D., Hefting, M., Matre, V., Pinay, G., Postolache, C., Rzepecki, M. and Sabater, F. (2003), 'Nitrogen Removal by Riparian Buffers along a European Climatic Gradient: Patterns and Factors of Variation', *Ecosystems* **6**(1), 20–30.
URL: *https://doi.org/10.1007/s10021-002-0183-8*

Schoumans, O. F., Bouraoui, F., Kabbe, C., Oenema, O. and van Dijk, K. C. (2015), 'Phosphorus management in Europe in a changing world', *Ambio* **4**4(2), 180–192.
URL: *https://doi.org/10.1007/s13280-014-0613-9*

Schoumans, O. F., Chardon, W. J., Bechmann, M. E., Gascuel-Odoux, C., Hofman, G., Kronvang, B., Rubaek, G. H., Ulen, B. and Dorioz, J. M. (2014), 'Mitigation options to reduce phosphorus losses from the agricultural sector and improve surface water quality: a review', *Sci Total Environ* **4**68-469, 1255–1266.
URL: *https://www.ncbi.nlm.nih.gov/pubmed/24060142*

Seibert, J., Grabs, T., Köhler, S., Laudon, H., Winterdahl, M. and Bishop, K. (2009), 'Linking soil- and stream-water chemistry based on a Riparian Flow-Concentration Integration Model', *Hydrol. Earth Syst. Sci.* **1**3(12), 2287–2297.
URL: *https://www.hydrol-earth-syst-sci.net/13/2287/2009/*

Sharpley, A., Jarvie, H. P., Buda, A., May, L., Spears, B. and Kleinman, P. (2013), 'Phosphorus Legacy: Overcoming the Effects of Past Management Practices to Mitigate Future Water Quality Impairment', *Journal of Environmental Quality* **4**2(5), 1308–1326.
URL: *https://acsess.onlinelibrary.wiley.com/doi/abs/10.2134/jeq2013.03.0098*

Singh, R., Wagener, T., van Werkhoven, K., Mann, M. E. and Crane, R. (2011), 'A trading-space-for-time approach to probabilistic continuous streamflow predictions in a changing climate – accounting for changing watershed behavior', *Hydrol. Earth Syst. Sci.* **1**5(11), 3591–3603.
URL: *https://hess.copernicus.org/articles/15/3591/2011/*

Sivapalan, M. (2006), Pattern, Process and Function: Elements of a Unified Theory of Hydrology at the Catchment Scale, *in* M. G. Anderson and J. J. McDonnell, eds, 'Encyclopedia of Hydrological Sciences'.
URL: *https://onlinelibrary.wiley.com/doi/abs/10.1002/0470848944.hsa012*

Smil, V. (2000), 'PHOSPHORUS IN THE ENVIRONMENT: Natural Flows and Human Interferences', *Annual Review of Energy and the Environment* **2**5(1), 53–88.
URL: *https://www.annualreviews.org/doi/abs/10.1146/annurev.energy.25.1.53*

Smith, V. H. (2003), 'Eutrophication of freshwater and coastal marine ecosystems a global problem', *Environmental Science and Pollution Research* **1**0(2), 126–139.
URL: *https://doi.org/10.1065/espr2002.12.142*

Smolders, E., Baetens, E., Verbeeck, M., Nawara, S., Diels, J., Verdievel, M., Peeters, B., De Cooman, W. and Baken, S. (2017), 'Internal Loading and Redox Cycling of Sediment Iron Explain Reactive Phosphorus Concentrations in Lowland Rivers', *Environmental Science & Technology* **5**1(5), 2584–2592.
URL: *https://doi.org/10.1021/acs.est.6b04337*

Solomon, C. T., Jones, S. E., Weidel, B. C., Buffam, I., Fork, M. L., Karlsson, J., Larsen, S., Lennon, J. T., Read, J. S., Sadro, S. and Saros, J. E. (2015), 'Ecosystem Consequences of Changing Inputs of Terrestrial Dissolved Organic Matter to Lakes: Current Knowledge and Future Challenges', *Ecosystems* **1**8(3), 376–389.
URL: *https://doi.org/10.1007/s10021-015-9848-y*

Stanley, E. H., Powers, S. M., Lottig, N. R., Buffam, I. and Crawford, J. T. (2012), 'Contemporary changes in dissolved organic carbon (DOC) in human-dominated rivers:

is there a role for DOC management?', *Freshwater Biology* **57**(s1), 26–42.
URL: *https://onlinelibrary.wiley.com/doi/abs/10.1111/j.1365-2427.2011.02613.x*

Steffen, W., Richardson, K., Rockstrom, J., Cornell, S. E., Fetzer, I., Bennett, E. M., Biggs, R., Carpenter, S. R., de Vries, W., de Wit, C. A., Folke, C., Gerten, D., Heinke, J., Mace, G. M., Persson, L. M., Ramanathan, V., Reyers, B. and Sorlin, S. (2015), 'Sustainability. Planetary boundaries: guiding human development on a changing planet', *Science* **3**47(6223), 1259855.
URL: *https://www.ncbi.nlm.nih.gov/pubmed/25592418*

Thompson, S. E., Basu, N. B., Lascurain, J., Aubeneau, A. and Rao, P. S. C. (2011), 'Relative dominance of hydrologic versus biogeochemical factors on solute export across impact gradients', *Water Resources Research* **47**(10).
URL: *https://agupubs.onlinelibrary.wiley.com/doi/full/10.1029/2010WR009605*

Van der Velde, Y., de Rooij, G. H., Rozemeijer, J. C., van Geer, F. C. and Broers, H. P. (2010), 'Nitrate response of a lowland catchment: On the relation between stream concentration and travel time distribution dynamics', *Water Resources Research* **4**6(11).
URL: *https://doi.org/10.1029/2010WR009105*

Van Meter, K. J. and Basu, N. B. (2017), 'Time lags in watershed-scale nutrient transport: an exploration of dominant controls', *Environmental Research Letters* **1**2(8), 84017.
URL: *http://dx.doi.org/10.1088/1748-9326/aa7bf4*

Van Meter, K. J., Basu, N. B., Veenstra, J. J. and Burras, C. L. (2016), 'The nitrogen legacy: emerging evidence of nitrogen accumulation in anthropogenic landscapes', *Environmental Research Letters* **1**1(3), 35014.
URL: *http://dx.doi.org/10.1088/1748-9326/11/3/035014*

Van Meter, K. J., McLeod, M. M., Liu, J., Tenkouano, G. T., Hall, R. I., Van Cappellen, P. and Basu, N. B. (2021), 'Beyond the Mass Balance: Watershed Phosphorus Legacies and the Evolution of the Current Water Quality Policy Challenge', *Water Resources Research* **57**(10), e2020WR029316.
URL: *https://agupubs.onlinelibrary.wiley.com/doi/abs/10.1029/2020WR029316*

Virro, H., Amatulli, G., Kmoch, A., Shen, L. and Uuemaa, E. (2021), 'GRQA: Global River Water Quality Archive', *Earth Syst. Sci. Data* **1**3(12), 5483–5507.
URL: *https://doi.org/10.5194/essd-13-5483-2021*

Vitousek, P. M., Mooney, H. A., Lubchenco, J. and Melillo, J. M. (1997), 'Human Domination of Earth's Ecosystems', *Science* **2**77(5325), 494–499.
URL: *https://science.sciencemag.org/content/sci/277/5325/494.full.pdf*

Vörösmarty, C. J., McIntyre, P. B., Gessner, M. O., Dudgeon, D., Prusevich, A., Green, P., Glidden, S., Bunn, S. E., Sullivan, C. A., Liermann, C. R. and Davies, P. M. (2010), 'Global threats to human water security and river biodiversity', *Nature* **4**67(7315), 555–561.
URL: *https://doi.org/10.1038/nature09440*

Wagener, T., Sivapalan, M., Troch, P. and Woods, R. (2007), 'Catchment Classification and Hydrologic Similarity', *Geography Compass* **1**(4), 901–931.
URL: *https://compass.onlinelibrary.wiley.com/doi/abs/10.1111/j.1749-8198.2007.00039.x*

Wen, H., Perdrial, J., Abbott, B. W., Bernal, S., Dupas, R., Godsey, S. E., Harpold, A., Rizzo, D., Underwood, K., Adler, T., Sterle, G. and Li, L. (2020), 'Temperature controls production but hydrology regulates export of dissolved organic carbon at the catchment scale', *Hydrol. Earth Syst. Sci.* **2**4(2), 945–966.
URL: *https://www.hydrol-earth-syst-sci.net/24/945/2020/*

Wendland, F., Blum, A., Coetsiers, M., Gorova, R., Griffioen, J., Grima, J., Hinsby, K., Kunkel, R., Marandi, A., Melo, T., Panagopoulos, A., Pauwels, H., Ruisi, M., Traversa, P., Vermooten, J. S. A. and Walraevens, K. (2008), 'European aquifer typology: a practical framework for an overview of major groundwater composition at European scale', *Environmental Geology* **5**5(1), 77–85.
URL: *https://doi.org/10.1007/s00254-007-0966-5*

Westphal, K., Graeber, D., Musolff, A., Fang, Y., Jawitz, J. W. and Borchardt, D. (2019), 'Multi-decadal trajectories of phosphorus loading, export, and instream retention along a catchment gradient', *Science of The Total Environment* **6**67, 769–779.
URL: *http://www.sciencedirect.com/science/article/pii/S0048969719309404*

Wilde, S., Hansen, C. and Bergmann, A. (2017), 'Nachlassender Nitratabbau im Grundwasser und deren Folgen – abgestufte modellgestützte Bewertungsansätze (engl. Decreasing denitrification capacity in aquifers: scaled model-based evaluation)', *Grundwasser* **2**2(4), 293–308.
URL: *https://doi.org/10.1007/s00767-017-0373-0*

Winter, C., Lutz, S. R., Musolff, A., Kumar, R., Weber, M. and Fleckenstein, J. H. (2021), 'Disentangling the Impact of Catchment Heterogeneity on Nitrate Export Dynamics From Event to Long-Term Time Scales', *Water Resources Research* **57**(1), e2020WR027992.
URL: *https://agupubs.onlinelibrary.wiley.com/doi/abs/10.1029/2020WR027992*

Winterdahl, M., Futter, M., Köhler, S., Laudon, H., Seibert, J. and Bishop, K. (2011), 'Riparian soil temperature modification of the relationship between flow and dissolved organic carbon concentration in a boreal stream', *Water Resources Research* **47**(8).
URL: *https://agupubs.onlinelibrary.wiley.com/doi/abs/10.1029/2010WR010235*

Withers, P. J. A. and Jarvie, H. P. (2008), 'Delivery and cycling of phosphorus in rivers: A review', *Science of The Total Environment* **400**(1), 379–395.
URL: *https://doi.org/10.1016/j.scitotenv.2008.08.002*

Yang, J., Heidbüchel, I., Musolff, A., Reinstorf, F. and Fleckenstein, J. H. (2018), 'Exploring the Dynamics of Transit Times and Subsurface Mixing in a Small Agricultural Catchment', *Water Resources Research* **54**(3), 2317–2335.
URL: *https://onlinelibrary.wiley.com/doi/abs/10.1002/2017WR021896*

Zarnetske, J. P., Bouda, M., Abbott, B. W., Saiers, J. and Raymond, P. A. (2018), 'Generality of Hydrologic Transport Limitation of Watershed Organic Carbon Flux Across Ecoregions of the United States', *Geophysical Research Letters* **45**(21), 11,702–711,711.
URL: *https://agupubs.onlinelibrary.wiley.com/doi/abs/10.1029/2018GL080005*

Study 1: Archetypes and Controls of Riverine Nutrient Export Across German Catchments

Status:	Published in Water Resources Research
DOI:	10.1029/2020WR028134
Authors:	Pia Ebeling, Rohini Kumar, Michael Weber, Lukas Knoll, Jan H. Fleckenstein, Andreas Musolff

PE carried out the study, prepared visualizations of results and wrote the manuscript. PE and AM conceptualized and designed the study. PE processed and curated the data with contributions from several authors: AM collected the original data from the environmental authorities, RK provided the gridded meteorological time series and atmospheric deposition data, MW provided time series of N surplus data for the catchments and contributed to quality checks, LK calculated the grid of vertical concentration heterogeneity. All authors contributed to the reviewing and editing of the manuscript.

Own contribution:

Study concept and design:	70 %
Data analysis:	90 %
Preparation of figures and tables:	100 %
Interpretation of the results:	80 %
Preparation of the manuscript:	90 %

AGU ADVANCING EARTH AND SPACE SCIENCE

Water Resources Research

RESEARCH ARTICLE
10.1029/2020WR028134

Archetypes and Controls of Riverine Nutrient Export Across German Catchments

Pia Ebeling[1], Rohini Kumar[2], Michael Weber[2], Lukas Knoll[3], Jan H. Fleckenstein[1,4], and Andreas Musolff[1]

[1]Department of Hydrogeology, Helmholtz Centre for Environmental Research—UFZ, Leipzig, Germany, [2]Department of Computational Hydrosystems, Helmholtz Centre for Environmental Research—UFZ, Leipzig, Germany, [3]Institute for Landscape Ecology and Resources Management (ILR), Research Centre for BioSystems, Land Use and Nutrition (iFZ), Justus Liebig University Giessen, Giessen, Germany, [4]Bayreuth Center of Ecology and Environmental Research (BayCEER), University of Bayreuth, Bayreuth, Germany

Key Points:

- Riverine NO_3^- dynamics are controlled by vertical concentration heterogeneity, which can result from subsurface denitrification
- Diffuse P sources exert a strong control on the spatial variability of PO_4^{3-} export patterns in contrast to point sources
- Share of riparian wetlands controls the mean TOC concentrations in German catchments

Supporting Information:

Supporting Information may be found in the online version of this article.

Correspondence to:

P. Ebeling,
pia.ebeling@ufz.de

Citation:

Ebeling, P., Kumar, R., Weber, M., Knoll, L., Fleckenstein, J. H., & Musolff, A. (2021). Archetypes and controls of riverine nutrient export across German catchments. *Water Resources Research*, *57*, e2020WR028134. https://doi.org/10.1029/2020WR028134

Received 10 JUN 2020
Accepted 6 MAR 2021

Author Contributions:

Conceptualization: Pia Ebeling, Andreas Musolff
Data curation: Pia Ebeling, Rohini Kumar, Michael Weber, Lukas Knoll, Andreas Musolff
Formal analysis: Pia Ebeling, Rohini Kumar, Michael Weber, Andreas Musolff
Funding acquisition: Andreas Musolff
Investigation: Pia Ebeling
Methodology: Pia Ebeling, Rohini Kumar, Andreas Musolff
Supervision: Jan H. Fleckenstein, Andreas Musolff
Validation: Pia Ebeling
Visualization: Pia Ebeling

Abstract Elevated nutrient inputs challenge the health and functioning of aquatic ecosystems. To improve riverine water quality management, it is necessary to understand the underlying biogeochemical and physical processes, anthropogenic drivers and their interactions at catchment scale. We hypothesize that the spatial heterogeneity of nutrient sources dominantly controls the variability of in-stream concentration dynamics among catchments. We investigated controls of mean nitrate (NO_3^-), phosphate (PO_4^{3-}), and total organic carbon (TOC) concentrations and concentration-discharge (*C*-*Q*) relationships in 787 German catchments of a newly assembled data base, covering a wide range of physiographic and anthropogenic settings. We linked water quality metrics to catchment characteristics using partial least squares regressions and random forests. We found archetypal *C*-*Q* patterns with enrichment dominating NO_3^- and TOC, and dilution dominating PO_4^{3-} export. Both the mean NO_3^- concentrations and their variance among sites increased with agricultural land use. We argue that subsurface denitrification can buffer high nitrogen inputs and cause a decline in concentration with depth, resulting in chemodynamic, strongly positive *C*-*Q* patterns. Mean PO_4^{3-} concentrations were related to point sources, though the low predictive power suggests effects of unaccounted in-stream processes. In contrast, high diffuse agricultural inputs explained observed positive PO_4^{3-} *C*-*Q* patterns. TOC levels were positively linked to the abundance of riparian wetlands, while hydrological descriptors were important for explaining TOC dynamics. Our study shows a strong modulation of anthropogenic inputs by natural controls for NO_3^- and PO_4^{3-} concentrations and dynamics, while for TOC only natural controls dominate observed patterns across Germany.

Plain Language Summary Phosphorus, nitrogen, and organic carbon are key elements of plants and all living organisms. Humans are altering the nutrient cycles especially, to improve agricultural productivity and through domestic and industrial wastewater. Excess nutrients in surface waters have harmed many aquatic ecosystems by causing toxic algal blooms and a loss of biodiversity. Low nutrient concentrations and habitat variability are similarly important to those ecosystems, but human interference with natural drivers is not yet fully understood. To better understand and disentangle natural or human controls, we investigated nutrient concentrations and their variability across German catchments with varying landscapes and anthropogenic conditions. The human impact is clearly visible for mean nitrate concentrations, while the (natural) subsurface properties mainly controlled the variability of riverine nitrate. In the past, phosphate inputs were usually linked to wastewater, yet we found the control of agricultural activities on concentration dynamics to be unexpectedly high. Organic carbon was mainly associated with natural sources related to riparian wetlands where interactions with other nutrients are possible. This understanding of dominant controls is important in order to adapt management strategies to ensure healthy aquatic ecosystems.

1. Introduction

Elevated nutrient inputs from human sources such as fertilizers and wastewater put aquatic ecosystems under pressure. The health and functioning of stream ecosystems and the eutrophication risk are strongly linked to nutrient concentrations (Conley et al., 2009; Galloway et al., 2003; Vitousek et al., 1997), while

Water Resources Research 10.1029/2020WR028134

Writing – original draft: Pia Ebeling
Writing – review & editing: Pia Ebeling, Rohini Kumar, Michael Weber, Lukas Knoll, Jan H. Fleckenstein, Andreas Musolff

their temporal variability can additionally affect the pressure and reversibility of effects (Withers & Jarvie, 2008) and primary production via for example stoichiometric shifts (Conley et al., 2009). Moreover, the dynamics of nutrient concentrations in concert with discharge variability control nutrient loads exported from catchments to downstream water bodies and cause eutrophication in many receiving rivers, lakes, and estuaries around the globe (e.g., Bricker et al., 1999; EEA, 2018; Jenny et al., 2020).

Several national and European regulations have been adopted to reduce water quality problems with a major focus on the macronutrients nitrogen (N) and phosphorous (P). Initially, the regulations in Europe and the USA focused on reducing nutrient inputs related to point sources (BGBI.1, 1980; Copeland, 2016; EEC, 1991a), but later additionally addressed nonpoint-source pollution (Copeland, 2016; EEC, 1991b, 2000). In Europe, the Water Framework Directive (WFD, EEC, 2000) set water quality aims and guidelines including the reduction of diffuse N and P pollution and the demand for a river basin and ecology-oriented perspective for water quality management. Still, many surface water bodies worldwide lack a good ecological status, with diffuse agricultural sources being one of the main pressures (Damania et al., 2019; EEA, 2018; EPA, 2017). Even though regulations do not focus on regulating the macronutrient organic carbon (Stanley et al., 2012), it affects aquatic ecosystem structure and functioning (for example via energy input and biogeochemical interactions) and can impair drinking water resources (Solomon et al., 2015).

Measures to improve water quality are usually implemented and evaluated at catchment scale (Bouraoui & Grizzetti, 2011). Catchments are complex systems with various biogeochemical and hydrological processes interacting at different spatial and temporal scales (Bouwman et al., 2013; Clark et al., 2010) and finally integrating into water quantity and quality responses at the catchment outlet (Bouraoui & Grizzetti, 2011). A considerable amount of nutrients can be retained or transformed in different compartments, such as soils, groundwater, riparian zones, and streams, altogether considered as successive filters which alter specific loads transported downstream (Bouwman et al., 2013). The importance of processes on transported loads generally depends on the interplay between transport and reaction time scales (Musolff et al., 2017; Oldham et al., 2013). Hierarchies and interactions among processes and different scales as well as differences among catchments are still not properly understood, and upscaling of small-scale processes to the catchment scale remains a challenging task (Bol et al., 2018; Pinay et al., 2015). The integrated signal of concentration (C), discharge (Q) and their relationship observed at the catchment outlet can be used to characterize catchment functioning, to reveal generalities and differences among solutes and catchments and thereby to interpret underlying processes (Sivapalan, 2006).

Mean concentrations indicate the general levels of nutrient stress, while concentration-discharge (C-Q) relationships classify solute export dynamics in terms of export regimes and patterns (Musolff et al., 2015). A chemostatic regime can be defined as low C variability compared to high Q variability, while a chemodynamic regime refers to a high C to Q variability using e.g. the coefficients of variation (CV) (Thompson et al., 2011). Export patterns characterize the direction and strength of influence of Q on C. Enrichment patterns describe increasing C with increasing Q, while dilution describes decreasing C with increasing Q, which prevail in supply limited systems. When comparing C-Q relationships among different solutes and catchments, generalities and key controls of solute export can be identified (Minaudo et al., 2019; Musolff et al., 2015; Zarnetske et al., 2018). C-Q relationships have been widely applied at different temporal scales, that is at event, inter- and intra-annual scales (Dupas et al., 2016; Minaudo et al., 2019; Rose et al., 2018; Westphal et al., 2019), and spatial scales, i.e. from hillslopes and headwaters (e.g. Bishop et al., 2004; Herndon et al., 2015; Hunsaker & Johnson, 2017) to numerous, large and nested catchments (e.g. Basu et al., 2010; Evans et al., 2014; Moatar et al., 2020).

To understand riverine nutrient export dynamics, we require process understanding of the major components of catchment scale transport—input, mobilization and retention. Mean nitrate (NO_3) concentrations in general increase with higher shares of agricultural land (e.g., Evans et al., 2014; Hansen et al., 2018; Minaudo et al., 2019; Musolff et al., 2015). However, elevated N inputs can be counteracted by removal, for example via denitrification under anoxic conditions and sufficient availability of electron donors, as observed in wetlands (Hansen et al., 2018), riparian zones (Pinay et al., 2015; Sabater et al., 2003) and groundwater (Rivett et al., 2008). Elevated phosphate (PO_4^{3-}) concentrations have been mainly related to point sources (Minaudo et al., 2019; Westphal et al., 2019), though with significant point source reductions diffuse P emissions from agricultural soils become increasingly relevant (Bol et al., 2018; Le Moal et al., 2019; Schoumans

Water Resources Research 10.1029/2020WR028134

et al., 2014). P retention and delivery to streams are closely linked to sorption in soils influenced by abiotic factors such as pH and redox conditions (Withers & Jarvie, 2008). Riparian wetlands are usually considered as sinks for agricultural P, but can also act as a source during rewetting after warm periods or under anoxic conditions (Dupas, Gruau, et al., 2015; Gu et al., 2017). For organic carbon, sources are linked to zones of organic matter accumulation, where biomass production exceeds removal via decomposition, such as in wetlands and peatlands (Clark et al., 2010). Riparian zones are important source areas for dissolved organic carbon (DOC) (Clark et al., 2010; Laudon et al., 2011; Musolff et al., 2018), which are usually hydrologically connected to the stream, whereas more distant DOC source areas might not intersect discharge generating zones (Bishop et al., 2004). Riparian zones are thus potential hot spots of biogeochemical processes, such as denitrification, DOC production and consumption and both P trapping and release, which are often linked to redox conditions and hence to water table dynamics. After the delivery to the stream, in-stream processes such as redox reactions and uptake can further remove, retain, transform or remobilize the nutrients before they reach the catchment outlet (Battin et al., 2008; Gomez-Velez et al., 2015).

Generally, the interplay between the solute source areas and hydrological connectivity has been found to be the major control of solute export dynamics (e.g., Herndon et al., 2015; Musolff et al., 2017; Seibert et al., 2009; Thompson et al., 2011; Tunaley et al., 2017). If solute source areas are uniformly distributed in a catchment, a chemostatic regime is established, as is typical for geogenic solutes (Thompson et al., 2011). Previous studies have found evidence that NO_3 often exhibits a chemostatic export regime in agricultural catchments (e.g., Basu et al., 2010, 2011; Dupas et al., 2016). This chemostatic regime is attributed to the built-up legacy of high N inputs in the past, causing spatial homogenization of sources (Basu et al., 2010; Thompson et al., 2011), which suggests a significant anthropogenic impact on NO_3 export dynamics. Similarly, excess P inputs have led to P legacies in soils and sediments (Jarvie et al., 2013; Schoumans et al., 2015; Sharpley et al., 2013). Legacy effects may hamper mitigation measures designed to reduce exported nutrient loads by dampening concentration responses and creating time lags up to several decades (Bouraoui & Grizzetti, 2011; Howden et al., 2010; Meals et al., 2010; Van Meter & Basu, 2015). In contrast, chemodynamic regimes are related to heterogeneously distributed source areas and variable discharge generating zones (Musolff et al., 2017; Zhi et al., 2019). Source heterogeneity can be linked, for example, to distinct production zones and the resulting vertical soil distribution profiles (Seibert et al., 2009), to vegetation and soil organic matter patterns (as shown for DOC by Herndon et al., 2015), and to heterogeneous land use patterns connected to inputs such as fertilizers (Musolff et al., 2017). Chemodynamic exports can also result from reactions along different flow paths. Flow paths with longer travel times, dominating during low flow conditions, are affected more than shorter ones. Thus removal along flow paths leads to depleted low-flow concentrations and thus enrichment patterns (Musolff et al., 2017) while production or accumulation processes lead to dilution patterns (Ameli et al., 2017; Musolff et al., 2017). Moreover, transient processes can cause temporal variations in source zones, for example long-term input changes from fertilizer applications (Ehrhardt et al., 2019) or temporally variable dissolution of accumulated phosphorus (Gu et al., 2017). However, spatial variability in export patterns of different archetypal catchments (catchments with different functioning) can collapse into a chemostatic downstream signal if concentrations vary asynchronously (Abbott et al., 2018). In summary, chemodynamic regimes signal variable combinations of discharge generating zones with different solute source strengths, travel times and reactivity along the flow paths within a catchment.

The anthropogenic impact on nutrient cycles and their effects on nutrient levels in streams (e.g., Gruber & Galloway, 2008; Hansen et al., 2018; Howden et al., 2010) as well as on nutrient export regimes have been discussed in several studies. However, to draw general and transferable conclusions a large sample size is required (Gupta et al., 2014). So far, only few studies consider a large number of catchments and different solutes (e.g., Basu et al., 2010; Moatar et al., 2017; Zarnetske et al., 2018). It thus remains uncertain how general and wide-spread the anthropogenic impact and resulting homogeneity or heterogeneity of sources is over a wide range of landscapes compared to natural controls, heterogeneity and reactivity (Ehrhardt et al., 2019; Van Meter & Basu, 2017). Therefore, we seek to understand (1) what drives nutrient concentration levels and dynamics across a large variety of catchments, and (2) how do anthropogenic impacts such as nutrient inputs interact with natural factors such as the hydroclimate, topography, and subsurface conditions. Our exploratory analysis is guided by the hypothesis that the differences of nutrient export dynamics

Water Resources Research 10.1029/2020WR028134

among catchments are dominantly controlled by the degree of spatial heterogeneity of diffuse sources, as opposed to geologic, climatic or topographic controls or the mere input load of nutrients to the catchment.

To this end, we analyze a newly assembled Germany-wide water quantity and quality data base (Musolff, 2020; Musolff et al., 2020). We use mean *C* and *C*-*Q* relationships of NO_3-N, PO_4-P and total organic carbon (TOC) to classify riverine nutrient dynamics in 787 independent catchments covering a wide range of ecoregions and large gradients in physical and hydroclimatic properties. We then disentangle the predictive role of anthropogenic and natural catchment properties to infer dominant controls and to hypothesize about the underlying processes by linking the descriptors to *C*-*Q* export metrics. Potential predictors include topography, land cover, geology, and hydroclimate, as well as diffuse and point sources and proxies for spatial source heterogeneity. Knowledge on dominant controls of nutrient export can serve to improve nutrient export models aiming at the catchment scale and to better tailor water quality management.

2. Materials and Methods

2.1. Water Quality and Quantity Data Set

Water quality data from river stations across Germany were gathered from the German federal state environmental authorities (Musolff, 2020; Musolff et al., 2020). The authorities regularly monitor the surface water quality in the context of the WFD (EEC, 2000), taking grab samples with a biweekly to seasonal frequency. Here, we focused on the three major nutrients: Nitrate-N concentrations as the dominant form of dissolved N (NO_3^--N), the biologically available dissolved orthophosphate phosphorus (PO_4^{3-}-P) and TOC concentrations. For brevity we use NO_3-N, PO_4-P without charges in the text. We used TOC instead of DOC because of better data availability and a strong correlation with a regression slope of about 0.87 between mean DOC and TOC concentrations (see Figure S1), and DOC representing about 81.3 (±7.9) % of TOC on average. Daily mean discharge time series at the water quality locations were partly provided together with the quality data (Musolff, 2020; Musolff et al., 2020).

Out of the initial pool of 6,000 sites of the newly assembled Germany-wide data base, water quality time series were selected based on the following criteria concerning the quality and availability of concentration and spatial data:

1) Data availability of at least three years in the target period from 2000 to 2015. This time period excludes major changes in the 1990s when major improvements of wastewater treatment were put into place (Westphal et al., 2019)
2) Minimum of 70 concentration samples after outlier removal. As the large number of sites demanded a cost-effective method, only extreme outliers likely to be typographical errors were removed (following Oelsner et al., 2017). We defined outliers as concentrations greater than mean $C + 4$*standard deviation in logarithmic space (confidence level >99.99% assuming lognormal distribution of concentrations) for all elements and as PO_4-P concentrations >100 mg l^{-1}, and TOC concentrations >1,000 mg l^{-1} in terms of absolute values
3) Seasonal coverage of the concentration data, that is the samples from all possible three consecutive months constitute at least 10% of the samples on average. This includes stations with data systematically missing in one month
4) Left-censored data of the concentration time series (values below the detection limit) must be less than 50% of the samples
5) Catchment area must be delineable from topography, that is we excluded stations with major deviations between location of real river network and topography-based basin area. The catchments were delineated based on flow accumulation derived from a digital elevation model (EEA, 2013) of 25 m resolution resampled to 100 m and the river network from the CCM River and Catchment Database (version 2.1, De Jager & Vogt, 2007), with some manual adaptations of river segments which drastically improve the match between catchments and the real river network

Water Resources Research 10.1029/2020WR028134

6) Independence of catchments, which was defined as nested catchments sharing less than 20% of their catchment area with any upstream station
7) Station must not be directly located at the outlet of a reservoir or lake (about 5 km), because the water quality in the vicinity of a lake or reservoir is expected to be mainly a result of lake dynamics, thus likely masking the effect of catchment processes
8) Data availability of catchment characteristics. This leads to the criterion that a minimum of 70% of the catchment area must fall within the borders of Germany, as some of the geodata were limited to Germany, such as N-surplus and point sources (see Section 2.3)

Applying the above criteria resulted in a set of 787 catchments with 759 NO_3-N, 695 PO_4-P, and 722 TOC time series. At 278 sites out of those catchments, observed discharge data were available. Altogether, the analyzed data base consists of a total of 110,603 concentration samples for combinations of dates and locations with an average between 135 (TOC) and 142 (NO_3-N) samples per site (from 2000 to 2015).

2.2. Metrics of Water Quality Dynamics

We used arithmetic mean concentrations and metrics of the *C*-*Q* relationships to characterize the nutrient concentration levels and dynamics in the different catchments. Before calculating basic statistics at each station, that is mean concentrations and the standard deviation, we replaced the concentration values falling below the detection limit (left-censored data) with half of the detection limit (see e.g., Hunsaker & Johnson, 2017; Underwood et al., 2017).

The relationship between concentration (C) and discharge (Q) can be described as: $\log(C) = \log(a) + b\log(Q) + \varepsilon$ with ε as a normal-distributed error term (Vogel et al., 2005). As described by Godsey et al. (2009), we fit the model without an error term (equals power law relationship $C = aQ^b$) to estimate the parameter slope b for each station, separately. Slope b characterizes the export pattern of a constituent such that $b > 0$ indicates an enrichment pattern, $b < 0$ a dilution pattern, while $b \approx 0$ describes a non-significant, neutral *C*-*Q* pattern (Musolff et al., 2017). Thompson et al. (2011) note that the power law *C*-*Q* model and metrics as R^2 and *f*-statistics become uninformative when b approaches zero. The separation of the three export pattern classes is therefore based on the significant difference of the slope b from zero (*t*-test, 95% confidence level). We consider this approach as an alternative to a classification based on fixed ranges of slope b (M. Botter et al., 2020; Herndon et al., 2015; Zimmer et al., 2019). We excluded left censored values (below the detection limit) from the regression analysis and limited the censored fraction to 20% assuming that otherwise parts of the *C*-*Q* relationship could be underrepresented.

We aggregated low-frequency data over different seasons and hydroclimatic conditions to obtain general *C*-*Q* relationships. Generally, ambivalent *C*-*Q* relationships can cause dispersion in regression estimates toward increased chemostatic export (Burns et al., 2019; Minaudo et al., 2019). Several studies have therefore applied models deviating from a simple power-law *C*-*Q* relationship (Minaudo et al., 2019; Moatar et al., 2017; Underwood et al., 2017). In several catchments, segmented models yielded better performances than the simple power-law (Diamond & Cohen, 2018; Marinos et al., 2020). However, the direction of segmented *C*-*Q* relationships rarely changed, for example from upward to downward (Moatar et al., 2017), which suggests that the general behavior of slope b can be preserved in a simple power law approach. To further test if a single power law was justified for our case domain, we compared the simple (power law) model to segmented regression models in log space using the Akaike information criterion (Akaike, 1974) as presented by Marinos et al. (2020). A single power law was superior in about 75% of the study catchments (Table S1), that is an increase in model complexity was not justified. In the other 25% of the study catchments, we noticed on average an increase in the R^2 by 10%. Based on these results and for the sake of consistency across the study catchments, we selected the parsimonious single power law model for further investigations.

Additionally, we used the ratio of the coefficients of variation of concentration and discharge CV_C/CV_Q to characterize export regimes (Thompson et al., 2011). The export regime is considered as chemostatic for small CV_C/CV_Q (<0.5) and as chemodynamic for high CV_C/CV_Q (Musolff et al., 2015).

Water Resources Research 10.1029/2020WR028134

The combination of both statistics (slope b and CV_C/CV_Q) leads to six distinct C-Q export classes (Figure S2) characterizing the distinct combinations of chemostatic and chemodynamic regimes within the different export patterns. This distinction is especially important for non-significant C-Q relationships ($b \approx 0$), which can still demonstrate a chemodynamic export with C variability ($CV_C/CV_Q \geq 0.5$) related to other factors than Q. Such dynamics can result from highly reactive export such as fast turnover in the streams (Musolff et al., 2015). Differences in mean concentrations between the export patterns and regimes were tested for significance ($\alpha = 0.05$) using a Kruskal-Wallis rank sum test. In case of significant differences between the C-Q patterns, the Wilcoxon rank sum test was used for pairwise comparisons to identify the difference in patterns.

2.3. Catchment Characteristics

The 278 C-Q catchments with available discharge data cover 43.7% of Germany, while the 787 C catchments cover 65.6%. Catchment sizes vary from 1.9 to 77,099.2 km^2 (4.4–23,162.7 km^2 for C-Q catchments), with 50% of the catchments smaller than 97.1 km^2 (<235.6 km^2) and 95% < 1,257.4 km^2 (<2,540.0 km^2). The catchments intersect all ten hydrogeological regions in Germany (BGR & SGD, 2015) and span a wide range of topographical, hydroclimatic, lithological and soil properties with varying anthropogenic presence. A summary of catchment characteristics is given in Table 1 and represented distributions of selected characteristics (matching mean conditions in Germany) are shown in Figure 1. The catchment characteristics are provided in a data repository (Ebeling, 2021a). The selection of catchment characteristics was inspired by several previous studies (e.g., G. Botter et al., 2013; Dupas, Delmas, et al., 2015; Moatar et al., 2017; Musolff et al., 2018, 2015; Onderka et al., 2012) and limited by data availability over the large scale.

In addition to climatic characteristics available for all catchments, hydrological characteristics were calculated for a smaller subset of catchments where daily discharge measurements were available ($n = 186$). The hydrological variables included mean discharge, mean specific discharge, runoff coefficient, seasonal ratio, base-flow index (BFI, WMO, 2008) and flashiness index based on flow percentiles following Jordan et al. (2005) (for details see Tables S2 and S9–S911).

To test our main hypothesis over a wide range of catchments, we parameterized source heterogeneity from landscape characteristics. Inspired by Musolff et al. (2017), who found "structured heterogeneity"—defined as nonlinear correlation between source concentration and travel time—to dominantly shape C-Q relationships, we aim at connecting discharge generating zones (implicitly related to travel times and water ages) with source distributions. Thereby, we focused on parameterizing the prevailing structured heterogeneity in each catchment as opposed to random variability and considered both horizontal and a vertical parameterization component as visualized in the supporting information (Figure S3).

For the horizontal component of source heterogeneity of diffuse NO_3-N and PO_4-P sources, we assumed horizontal flow distances from the solute source to the stream network to link to flow paths and thus travel times. Horizontal source heterogeneity is considered as a temporally invariant catchment characteristic and does not account for seasonal or short term variability of nutrient availability within the source but rather represents the catchment setup with regards to spatial land use arrangement. Agricultural diffuse nutrient source areas were defined as seasonal, perennial cropland and grassland estimated based on a highly resolved land use map of 2015 (Pflugmacher et al., 2018). We computed horizontal flow distances along the topographic flow direction toward the stream using the ESRI ArcGIS (version 10.6). The stream grid was derived from the EU-wide EU-Hydro river network (EEA, 2016b). Based on the flow distance grid, we resampled the land cover map with a 30 m resolution to 100 m using the majority method. For each catchment, we then estimated the mean agricultural source area distance to nearest stream (sdist_mean) and the fraction of agricultural source area within classes of flow distances of 400 m each. Subsequently, we fitted a linear regression to the class values of the histogram weighted by the corresponding class frequencies within the catchment. When the slope of this regression is positive (het_h > 0), source areas tend to be located further from the stream, whereas when it is negative (het_h < 0), sources tend to be closer and sources are homogeneously distributed when het_h = 0 (Figure S3). As the EU-Hydro river network partly deviates from delineated catchments and contains different degrees of details, 78 C and 38 C-Q catchments (mostly small ones) resulted in implausible distance distributions. Therefore, het_h was assigned as missing value

Water Resources Research 10.1029/2020WR028134

Table 1
Catchment Descriptors Used in the Analysis, Associated Methods and Data Sources

Category	Variable	Unit	Description and method	Data source
Topography	area	km^2	Catchment area	
	dem_mean	mamsl	Mean elevation of catchment, from DEM (digital elevation model) rescaled from 25 to 100 m resolution using average	EEA, 2013
	slope_mean	°	Mean topographic slope of catchment, from DEM	EEA, 2013
	twi_mean	–	Mean topographic wetness index (TWI, Beven & Kirkby, 1979)	EEA, 2013
	twi_90p	–	90th percentile of the TWI as a proxy for riparian wetlands (following Musolff et al., 2018)	EEA, 2013
	drain_dens	km^{-1}	Average drainage density of the catchment. Gridded drainage density is provided as the length of surface waters (rivers and lakes) per area from a 75 km^2 circular area around each cell center	BMU, 2000
Land cover	f_urban	–	Fraction of artificial land cover	EEA, 2016a
	f_agric	–	Fraction of agricultural land cover	EEA, 2016a
	f_forest	–	Fraction of forested land cover	EEA, 2016a
	f_wetland	–	Fraction of wetland cover	EEA, 2016a
	f_water	–	Fraction of surface water cover	EEA, 2016a
	p_dens	inhabitants km^{-2}	Mean population density	CIESIN, 2017
Nutrient sources	N_surp_00	kg N ha^{-1} y^{-1}	Mean nitrogen surplus per catchment during sampling period (2000–2015) including N surplus on agricultural land and atmospheric deposition on non-agricultural areas	Bach et al., 2016; Häußermann et al., 2019
	N_surp_80	kg N ha^{-1} y^{-1}	Mean N surplus per catchment before and during sampling period (1980–2015) to consider historic (legacy) inputs	Bach et al., 2016; Häußermann et al., 2019
	N_WW	kg N ha^{-1} y^{-1}	Sum of N input from point sources including waste water treatment plants (WWTP) > 2000 person equivalents from the database of the European Environment Agency covering areas beyond Germany and data collected from 13 federal German states covering smaller WWTP within Germany	Büttner, 2020a, 2020b
	P_WW	kg P ha^{-1} y^{-1}	Sum of P input from WWTP analogous to N_WW	Büttner, 2020a, 2020b
	het_h	–	Slope of relative frequency of source areas in classes of flow distances to stream as a proxy for horizontal source heterogeneity (see in text Section 2.3)	Source areas based on Pflugmacher et al., 2018
	sdist_mean	m	Mean lateral flow distance of source areas to stream (see in text Section 2.3)	Source areas based on Pflugmacher et al., 2018
	het_v	–	Mean ratio between potential seepage and groundwater NO_3-N concentrations as proxy for vertical concentration heterogeneity (see in text Section 2.3)	Knoll et al., 2020
Lithology and soils	f_calc	–	Fraction of calcareous rocks	BGR & UNESCO (eds.), 2014
	f_calc_sed	–	Fraction of calcareous rocks and sediments	BGR & UNESCO (eds.), 2014
	f_magma	–	Fraction of magmatic rocks	BGR & UNESCO (eds.), 2014
	f_metam	–	Fraction of metamorphic rocks	BGR & UNESCO (eds.), 2014
	f_sedim	–	Fraction of sedimentary aquifer	BGR & UNESCO (eds.), 2014
	f_silic	–	Fraction of siliciclastic rocks	BGR & UNESCO (eds.), 2014
	f_sili_sed	–	Fraction of siliciclastic rocks and sediments	BGR & UNESCO (eds.), 2014
	dtb	cm	Median depth to bedrock in the catchment	Shangguan et al., 2017
	f_gwsoils	–	Fraction of water-impacted soils in the catchment (from soil map 1:250,000), including stagnosols, semi-terrestrial, semi-subhydric, subhydric and moor soils	BGR, 2018

Water Resources Research 10.1029/2020WR028134

Table 1
Continued

Category	Variable	Unit	Description and method	Data source
	f_sand	–	Mean fraction of sand in soil horizons of the top 100 cm	FAO/IIASA/ISRIC/ISSCAS/JRC, 2012
	f_silt	–	Mean fraction of silt in soil horizons of the top 100 cm	
	f_clay	–	Mean fraction of clay in soil horizons of the top 100 cm	
	water_root	mm	Mean available water content in the root zone from pedo-transfer functions	Livneh et al., 2015; Samaniego et al., 2010; Zink et al., 2017
	theta_S	–	Mean porosity in catchment from pedo-transfer functions	Livneh et al., 2015; Samaniego et al., 2010; Zink et al., 2017
	soil_N	g kg^{-1}	Mean top soil N in catchment	Ballabio et al., 2019
	soil_P	mg kg^{-1}	Mean top soil P in catchment	Ballabio et al., 2019
	soil_CN	–	Mean top soil C/N (Carbon/Nitrogen) ratio in catchment	Ballabio et al., 2019
Climate	P_mm	mm	Mean annual precipitation (period 1986–2015 used for all climatic variables)	Cornes et al., 2018
	P_SIsw	–	Seasonality of precipitation as the ratio between mean summer (Jun-Aug) and winter (Dec-Feb) precipitation	Cornes et al., 2018
	P_lambda	–	Mean precipitation frequency λ as used by G. Botter et al., 2013	Cornes et al., 2018
	PET_mm	mm	Mean potential evapotranspiration	Cornes et al., 2018
	AI	–	Aridity index as AI = PET_mm/P_mm	Cornes et al., 2018
	T_mean	°C	Mean annual air temperature	Cornes et al., 2018

in catchments without intersection with any river segment or a maximum flow distance to stream ≥15 km. We do not expect that results are generally influenced by this limitation as the remaining catchments still represent well the parameter space. However, these missing values lower the sample size, the related variables (het_h and sdist_mean) did not rank among the dominant predictors, nor did they improve model performances; het_h and sdist_mean were therefore excluded from the main analysis (Section 3.3). Results corresponding to the smaller subset including het_h and sdist_mean are presented in the supporting information (Tables S4 and S5).

Similar to the horizontal source heterogeneity, we parameterized the vertical concentration heterogeneity as concentration gradients over depth. We again assume a link between flow paths over depth and travel times. For each catchment, we calculated the mean of the ratio between the potential seepage NO_3 concentrations and groundwater NO_3 concentrations (Figure S3). This ratio resembles the parameter C_{ratio} of soil versus groundwater concentrations used in Zhi et al. (2019). We used the groundwater NO_3 and potential seepage concentrations across Germany presented by Knoll et al. (2020). They estimated groundwater NO_3 concentrations with a resolution of 1 km using a random forest model trained on observed groundwater concentrations (averages over the years 2009–2018) and spatial predictors. Mean groundwater NO_3 concentrations from Knoll et al. (2020) correlated positively with mean riverine NO_3 concentrations in our study ($r = 0.73$) and with average low-flow NO_3 concentrations ($r = 0.63$ for all observations with daily Q below the 10th percentile). The potential seepage NO_3 concentrations (Knoll et al., 2020) were calculated as a ratio of N surplus (Bach et al., 2016; Häußermann et al., 2019) and the seepage rate (BGR, 2003). We note that this approach does not estimate the actual but a potential seepage concentration, as we do not consider denitrification and lateral NO_3 fluxes in the unsaturated zone. This implies that het_v integrates removal processes across both the unsaturated and the saturated zone. Due to data availability, vertical heterogeneity parameterization was calculated for NO_3 only.

Water Resources Research 10.1029/2020WR028134

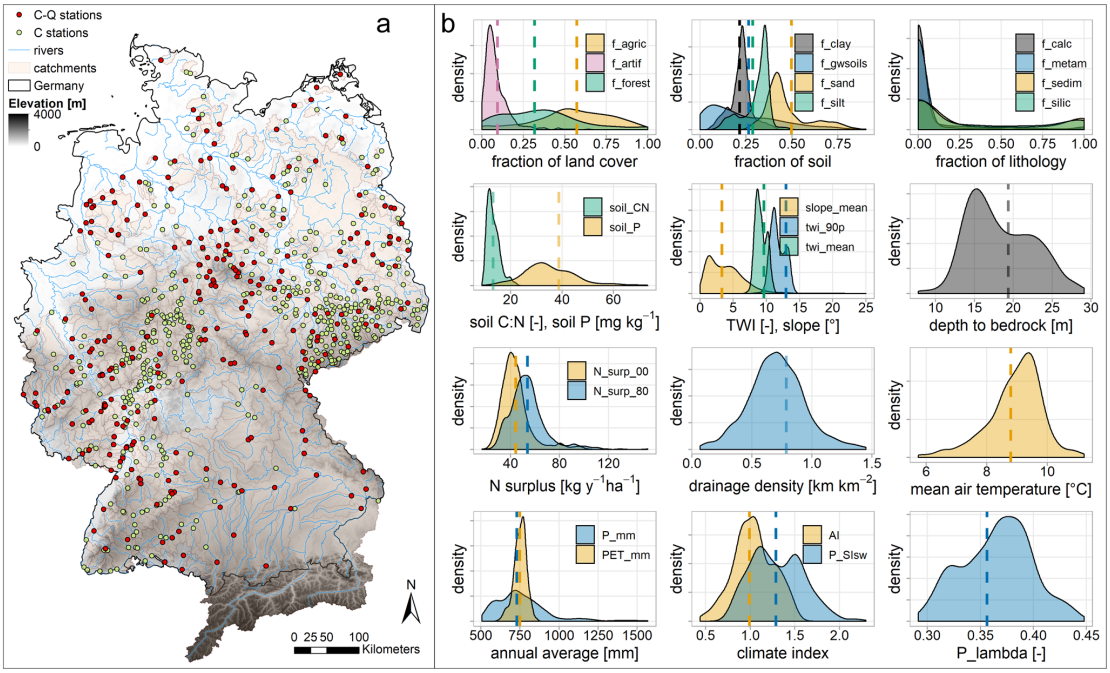

Figure 1. The study area with stations of concentration (*C*) and additional discharge (*C*-*Q*) data and corresponding catchments overlaying elevation (a) and distributions of selected catchment characteristics represented by the *C* catchments (b). TWI, topographic wetness index; P_mm, precipitation; PET_mm, potential evapotranspiration; AI, aridity index; P_SIsw, precipitation seasonality; P_lambda, precipitation frequency. Refer to Table 1 for detailed explanations of the parameters. Vertical dashed lines mark corresponding average values for Germany.

2.4. Linking Water Quality Metrics to Descriptors

Rank-based correlations provide a first indication of existing links between the individual catchment descriptors and the response metrics (Figure S5). Yet, due to inter-correlations among several descriptors (Figure S4), suitable multivariable statistical approaches are required for a proper interpretation of linkages and hierarchies.

We applied Partial Least Squares Regressions (PLSR, Wold et al., 2001) in combination with the Variable Influence of Projection (VIP, Wold et al., 2001) and Random Forests (RF, Breiman, 2001) to identify controls for differences in mean concentrations, export patterns and regimes of NO_3-N, PO_4-P and TOC among the studied catchments. Both PLSR and RF can handle co-linear descriptors as given here and provide variable importance measures to rank descriptors and interpret dominant controls. Still, ambiguity in certain predictors can limit clear linking of the identified dominant controls to drivers and processes. Both models have been applied in water quality studies, for example PLSR for investigating solute export and their predictors (Musolff et al., 2015; Onderka et al., 2012; Wallin et al., 2015) and RF for estimating the spatial distributions of groundwater NO_3 concentrations (Knoll et al., 2019; Ouedraogo et al., 2019; Rodriguez-Galiano et al., 2014) and artificial drainage systems (Møller et al., 2018). While PLSR is based on linear relationships, RF is a non-linear method. Here, we combine the two approaches as a model ensemble to address the uncertainty of data-driven analyses and thus to increase the robustness and interpretability of the results (Schmidt et al., 2020).

One PLSR and one RF model per response variable were set up using the catchment characteristics as descriptors (Table 1, excluding sdist_mean and het_h). In addition, models including either sdist_mean and

Water Resources Research 10.1029/2020WR028134

Table 2
Summary Statistics of the Calculated Metrics of Concentration (C) and Concentration-Discharge (C-Q) Relationships

	Concentration				*C-Q* relationships		
	n *C*-catchments with <50% censored data	Mean [mg l^{-1}]	Median [mg l^{-1}]	CV_C	*n* *C-Q*-catchments with <50% (<20%) censored data	CV_C/CV_Q	*b*
NO_3-N	759	4.06 ± 2.69 (3.71 ± 3.14)	3.86 ± 2.74 (3.4 ± 3.2)	0.38 ± 0.27 (0.29 ± 0.27)	275 (274)	0.47 ± 0.43 (0.33 ± 0.34)	0.26 ± 0.35 (0.16 ± 0.36)
PO_4-P	695	0.12 ± 0.12 (0.08 ± 0.11)	0.10 ± 0.10 (0.07 ± 0.09)	0.68 ± 0.33 (0.60 ± 0.28)	261 (236)	0.70 ± 0.42 (0.58 ± 0.31)	−0.22 ± 0.27 (−0.25 ± 0.35)
TOC	722	5.88 ± 2.96 (4.96 ± 3.35)	5.33 ± 2.81 (4.45 ± 3.19)	0.41 ± 0.16 (0.38 ± 0.17)	256 (255)	0.49 ± 0.33 (0.40 ± 0.23)	0.18 ± 0.22 (0.14 ± 0.23)

Note. Given are the sample size *n* and the mean ± standard deviation of the mean and median concentrations, the coefficients of variation of concentration CV_C and the metrics of *C-Q* relationships (i.e. CV_C/CV_Q, slope *b*). Values in brackets refer to median ± interquartile range.

het_h or hydrological descriptors were run for a smaller number of catchments (due to missing values, Tables S4 and S5). Nutrient-specific point sources were considered only for the corresponding nutrient (i.e., either NO_3-N or PO_4-P). Since for diffuse sources, only N surplus but no P surplus data were available, the former was used as a descriptor for all nutrients because of expected correlations to P surplus (Dupas, Delmas, et al., 2015; Minaudo et al., 2019). N surplus was thus considered as a proxy for agricultural, diffuse P inputs together with the topsoil P content, which also correlate positively ($r = 0.52$ for N_surp_80, Figure S4). All data were standardized to unit variance and zero mean to give the variables the same prior importance and enhance the model stability (Wold et al., 2001). Yeo-Johnson transformations did not change results. Furthermore, we used simple and multiple linear regressions for selected descriptors as parsimonious models to complement the complex PLSR and RF models.

To assess the model performances and to tune the number of components in PLSR, we conducted a three times repeated 10-fold cross-validation (Table S3). The variable importance in RF was assessed based on the mean increase of accuracy based on "out-of-bag" (OOB) samples. The analysis was conducted in *R* (version 3.5.0, Team, 2019) with the *caret* package (version 6.0–84, Kuhn et al., 2019) and partial dependence plots created with the *pdp* package (version 0.7.0., Greenwell, 2017).

For our analyses, we assume stationary general catchment functioning over the analyzed time period (2000–2015). Even if this may not be true in all cases, integrating over this relatively short period should be acceptable and not corrupt the generally observed relationships.

3. Results

3.1. Classification of *C-Q* Metrics and Mean Concentrations

Basic statistics of the catchments' mean concentrations and *C-Q* metrics are given in Table 2. Overall, the averages of mean concentrations over the studied catchments were 4.06 mg l^{-1} NO_3-N, 0.12 mg l^{-1} PO_4-P, and 5.88 mg l^{-1} TOC. The average coefficient of variation of concentration CV_C varied between 0.38 for NO_3-N, 0.41 for TOC, and 0.68 for PO_4-P. In general, *C-Q* metrics covered all types of patterns and regimes, with mean slope $b > 0$ and mean $CV_C/CV_Q < 0.5$ for NO_3-N and TOC and mean slopes $b < 0$ and mean $CV_C/CV_Q > 0.5$ for PO_4-P, while standard deviations of *b* were larger than absolute mean *b* for all nutrients. The *C-Q* power-law regressions showed similar model performances for the three nutrients with mean $R^2 = 0.27 \pm 0.24$ for NO_3-N slightly higher than PO_4-P ($R^2 = 0.21 \pm 0.19$) and TOC ($R^2 = 0.19 \pm 0.20$).

For NO_3-N export, the majority of catchments showed a chemostatic regime (74%, $n = 200$) and an enrichment pattern (69%, $n = 188$), while 45% combined both (Figures 2a and 2b). Highest mean concentrations

Water Resources Research 10.1029/2020WR028134

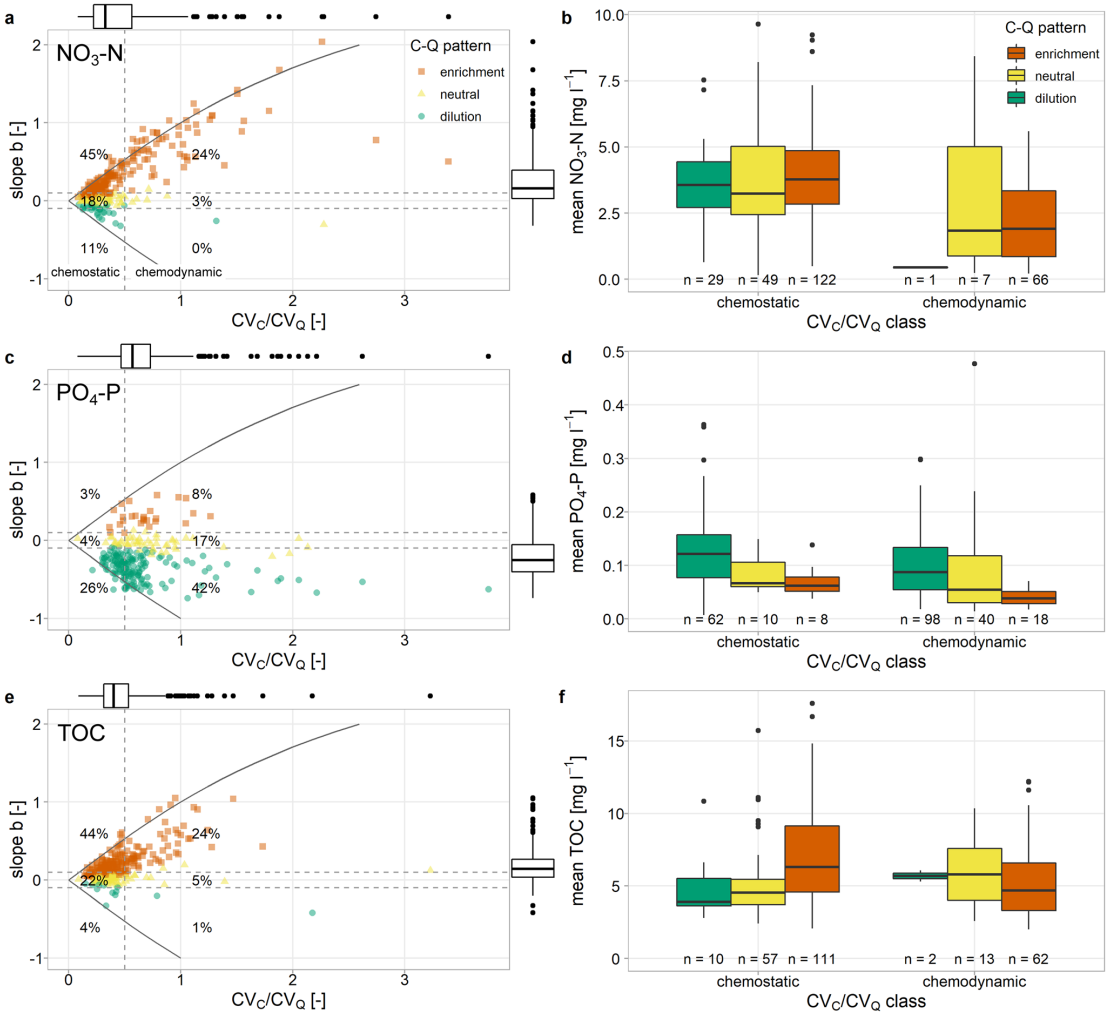

Figure 2. *C-Q* classification schemes composed of CV_C/CV_Q for export regimes and slope *b* for export patterns for NO_3-N (a), PO_4-P (c) and TOC (e), scheme adapted from Musolff et al. (2015). Colors and shape indicate the class of *C-Q* patterns, horizontal dashed lines approximate these class divisions, while the vertical dashed line divides the two classes of *C-Q* regimes with $CV_C/CV_Q < 0.5$ for chemostatic and $CV_C/CV_Q > 0.5$ for chemodynamic regimes. The solid lines indicate the theoretical boundaries between slope *b* and CV_C/CV_Q for $CV_Q = 0.6$ (after Musolff et al., 2015). Percentages indicate the portion of catchments assigned to the corresponding *C-Q* class. Mean concentrations of NO_3-N (b), PO_4-P (d) and TOC (f) are shown as boxplots for each class. n, number of observations in this class.

were observed for chemostatic regimes, while mean concentrations of the group with chemodynamic regimes were significantly lower (Kruskal-Wallis, $p < 0.001$). The mean concentrations between the different *C-Q* patterns did not differ significantly.

For PO_4-P export, the majority of catchments exhibited a chemodynamic regime (67%, $n = 156$) and a dilution pattern (68%, $n = 160$), while the combination of both can be found for 42% of all catchments (Figures 2c and 2d). Independent of the *C-Q* pattern, mean concentrations were significantly lower in the chemodynamic compared to the chemostatic regime (Kruskal-Wallis, $p < 0.001$). Among the *C-Q* patterns,

AGU ADVANCING EARTH AND SPACE SCIENCE
Water Resources Research
10.1029/2020WR028134

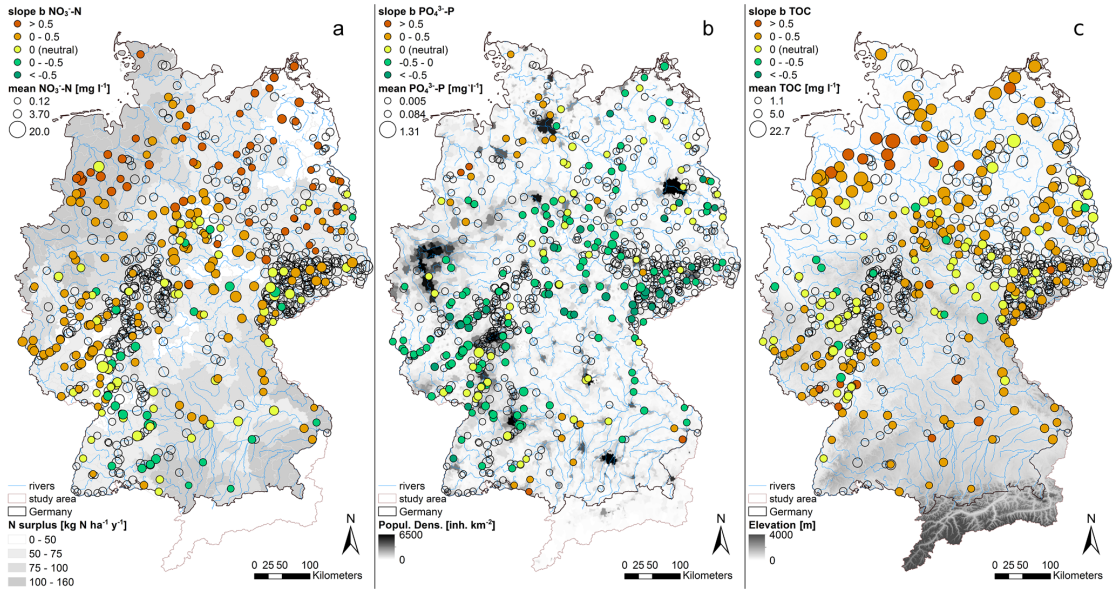

Figure 3. Spatial patterns of *C-Q* slope *b* and mean concentrations across Germany (a) for NO_3-N with average N surplus from 2000 to 2015 on county level (Bach et al., 2016; Häußermann et al., 2019), (b) PO_4-P with population density, and (c) TOC with the elevation as base map. Point size represents mean concentrations, scaled to the respective range across the study catchments with minimum, mean and maximum shown in the legend.

mean concentrations were significantly higher for dilution patterns compared to neutral patterns (Wilcoxon, $p = 0.002$) and to enrichment patterns (Wilcoxon, $p < 0.001$). Catchments with enrichment patterns showed the lowest mean concentrations, though they were not significantly different from catchments with neutral *C-Q* patterns (Wilcoxon, $p = 0.057$).

For TOC, chemostatic export (70%, $n = 178$) and enrichment patterns (68%, $n = 173$) prevailed, with 44% of the catchments combining both (Figures 2e and 2f). Overall, the chemostatic regime showed significantly higher mean TOC concentrations than the chemodynamic regimes (Kruskal-Wallis, $p = 0.014$). The mean concentrations between the *C-Q* patterns also differed significantly (Kruskal-Wallis, $p = 0.007$). The catchments with enrichment patterns had significantly higher mean concentrations than those exhibiting neutral *C-Q* patterns (Wilcoxon, $p = 0.011$), which was mainly apparent within the chemostatic regime (Figure 2f).

3.2. Spatial Patterns of Concentrations and Export Dynamics

The spatial organization of mean concentrations and export patterns of each nutrient are shown in Figure 3. Regional clusters of the export patterns can be observed for all nutrients. NO_3-N showed the strongest enrichment patterns in northern Germany and some dilution patterns in southern and southwestern Germany. The highest mean NO_3-N concentrations were found in the eastern part of Germany. For PO_4-P, dilution and neutral patterns prevailed in central, northeastern and southwestern Germany whereas the few enrichment patterns clustered in the northwest and southeast of Germany. Highest mean PO_4-P concentrations were found in central Germany, though a general spatial organization was not obvious for this metric. TOC also showed strong enrichment patterns in northern Germany, especially in the northwest, but also in the south of Germany, whereas the small number of dilution patterns seemed to cluster more in the west. The highest mean TOC concentrations were found in the lowlands in northern, esp. northwestern Germany, coinciding with the enrichment patterns.

Water Resources Research 10.1029/2020WR028134

Table 3
Ranked Drivers and Model Performances of PLSR With VIP and RF for the Three Nutrients and Metrics

Res-ponse	Mean concentration					*b*					CV_C/CV_Q				
NO_3-N	$n = 759$					$n = 274$					$n = 275$				
	PLSR			**RF**		**PLSR**			**RF**		**PLSR**			**RF**	
	$R^2_{CrossVal} = 0.64$			$R^2_{CrossVal} = 0.69$		$R^2_{CrossVal} = 0.57$			$R^2_{CrossVal} = 0.64$		$R^2_{CrossVal} = 0.60$			$R^2_{CrossVal} = 0.65$	
	$R^2_{train} = 0.66$			$R^2_{OOB} = 0.68$		$R^2_{train} = 0.57$			$R^2_{OOB} = 0.59$		$R^2_{train} = 0.58$			$R^2_{OOB} = 0.56$	
	Variable	**VIP**	**Sign**	**Variable**	**Imp**	**Variable**	**VIP**	**Sign**	**Variable**	**Imp**	**Variable**	**VIP**	**Sign**	**Variable**	**Imp**
	f_forest	1.93	−	f_forest	20.3	het_v	1.66	+	slope_mean	11.5	het_v	1.70	+	het_v	10.2
	f_agric	1.88	+	P_mm	17.4	twi_mean	1.55	+	twi_mean	11.2	f_sedim	1.58	+	twi_mean	9.3
	soil_CN	1.82	−	P_SIsw	16.2	dtb	1.48	+	dem_mean	9.0	dtb	1.42	+	slope_mean	9.3
	het_v	1.40	−	f_sedim	15.8	f_sedim	1.48	+	soil_N	8.1	f_silt	1.40	−	dem_mean	7.4
	f_sand	1.38	+	het_v	14.4	twi_90p	1.47	+	PET_mm	7.7	twi_mean	1.37	+	f_sedim	6.9
	f_clay	1.32	+	f_agric	13.9	dem_mean	1.46	−	P_mm	7.3	f_sand	1.36	+	soil_N	6.6
PO_4-P	$n = 695$					$n = 236$					$n = 261$				
	PLSR			**RF**		**PLSR**			**RF**		**PLSR**			**RF**	
	$R^2_{CrossVal} = 0.34$			$R^2_{CrossVal} = 0.40$		$R^2_{CrossVal} = 0.43$			$R^2_{CrossVal} = 0.47$		$R^2_{CrossVal} = 0.16$			$R^2_{CrossVal} = 0.21$	
	$R^2_{train} = 0.32$			$R^2_{OOB} = 0.30$		$R^2_{train} = 0.52$			$R^2_{OOB} = 0.48$		$R^2_{train} = 0.15$			$R^2_{OOB} = 0.09$	
	Variable	**VIP**	**Sign**	**Variable**	**Imp**	**Variable**	**VIP**	**Sign**	**Variable**	**Imp**	**Variable**	**VIP**	**Sign**	**Variable**	**Imp**
	P_WW	2.04	+	P_WW	23.1	N_surp_00	1.82	+	f_sedim	15.0	f_sedim	1.79	+	T_mean	6.8
	f_artif	1.71	+	dem_mean	9.2	N_surp_80	1.73	+	N_surp_00	13.1	f_sand	1.58	+	thetaS	5.8
	soil_CN	1.67	−	f_silt	8.9	f_sedim	1.61	+	N_surp_80	12.7	het_v	1.55	+	twi_mean	5.6
	pdens	1.60	+	PET_mm	8.2	twi_90p	1.36	+	P_lambda	9.3	dtb	1.54	+	WaterRoots	5.5
	PET_mm	1.53	+	f_silic	7.4	soil_P	1.35	+	twi_90p	9.2	f_silt	1.51	−	dem_mean	5.2
	f_sand	1.53	−	dtb	7.3	P_mm	1.35	+	P_SIsw	8.6	f_water	1.44	+	slope_mean	4.7
TOC	$n = 722$					$n = 255$					$n = 256$				
	PLSR			**RF**		**PLSR**			**RF**		**PLSR**			**RF**	
	$R^2_{CrossVal} = 0.61$			$R^2_{CrossVal} = 0.68$		$R^2_{CrossVal} = 0.19$			$R^2_{CrossVal} = 0.28$		$R^2_{CrossVal} = 0.15$			$R^2_{CrossVal} = 0.21$	
	$R^2_{train} = 0.62$			$R^2_{OOB} = 0.65$		$R^2_{train} = 0.26$			$R^2_{OOB} = 0.26$		$R^2_{train} = 0.23$			$R^2_{OOB} = 0.11$	
	Variable	**VIP**	**Sign**	**Variable**	**Imp**	**Variable**	**VIP**	**Sign**	**Variable**	**Imp**	**Variable**	**VIP**	**Sign**	**Variable**	**Imp**
	twi_90p	1.71	+	dem_mean	14.2	N_surp_00	1.55	+	f_sedim	11.8	f_sedim	1.43	+	drain_dens	8.9
	twi_mean	1.71	+	slope_mean	13.1	N_surp_80	1.46	+	N_surp_00	10.9	f_silic	1.36	−	f_calc	8.5
	f_sedim	1.57	+	twi_mean	13.1	f_sedim	1.43	+	N_surp_80	8.6	soil_N	1.34	−	f_silt	7.7
	slope_mean	1.46	−	twi_90p	12.0	f_silic	1.37	−	dem_mean	8.3	f_calc	1.33	+	P_SIsw	7.1
	dem_mean	1.37	−	PET_mm	11.0	het_v	1.27	−	f_silt	8.0	T_mean	1.33	+	soil_P	5.8
	dtb	1.36	+	f_sedim	9.9	AI	1.18	−	P_mm	7.8	f_gwsoils	1.31	−	P_mm	5.6

Note. Only the six highest ranked variables are shown; the complete results are given in Tables S6–S8 in the supporting information. CrossVal, cross-validation; OOB, out-of-bag samples; LSR, partial least squares regressions; RF, random forests; VIP, variable influence on projection of PLSR; Imp, variable importance in RF models.

3.3. Linking Water Quality Metrics to Catchment Characteristics

The variability in the *C-Q* metrics could be partly explained by the catchment characteristics, albeit not for all investigated nutrients and metrics (Table 3 and Figure S6). The average model performances from cross validation $R^2_{CrossVal}$ varied between 15.0% (PLSR for CV_C/CV_Q of TOC) and 69.2% (RF for mean NO_3-N). The $R^2_{CrossVal}$ were consistently higher for the RF models (on average 5.9%), however, the variance between the folds is high. The standard deviations of $R^2_{CrossVal}$ differed largely between models; they were lowest for

Water Resources Research 10.1029/2020WR028134

mean NO_3-N and mean TOC concentrations (7.3%–9.6%) and highest for slope *b* of TOC in RF (19.0%). The model performances of the final trained models, R^2_{train} for PLSR and R^2_{OOB} for RF (from out-of-bag samples), generally reached similar levels compared to the cross-validation.

All three NO_3-N metrics could be predicted with a reasonably good cross-validated performance, $R^2_{CrossVal} > 0.5$ with the highest value being $R^2_{CrossVal} = 0.69$ for mean NO_3-N concentrations with RF. Performance was substantially lower for PO_4-P: Models for slope *b* of PO_4-P only reached $R^2_{CrossVal} > 0.4$ and mean concentrations $R^2_{CrossVal} > 0.3$, whereas the models CV_C/CV_Q only reached $R^2_{CrossVal} < 0.3$. For TOC, mean concentrations were well explained with $R^2_{CrossVal} > 0.5$, whereas the *C*-*Q* metrics CV_C/CV_Q and slope *b* only reached $R^2_{CrossVal} < 0.3$. The descriptors with the highest ranks are given in Table 3 (Tables S5–S7 for complete results), however, the interpretation of variable importance is limited for models with low overall explained variability.

For mean NO_3-N concentrations, both PLSR and RF models rank the fractions of forest highest, directly followed by agricultural land cover and top soil C/N ratio in PLSR. In the PLSR model, there is a prominent difference in variable importance to the next descriptors, which are the vertical concentration heterogeneity, fractions of sand and clay (all three with a positive direction of influence) and the fraction of sedimentary aquifer. The RF model marks a step in variable importance after the first rank (f_forest), which is followed by mean annual and seasonality of precipitation, fraction of sedimentary aquifer, vertical heterogeneity and fraction of agriculture on rank 6. For explaining the NO_3-N dynamics (*b* and CV_C/CV_Q), the descriptor vertical heterogeneity has the highest importance (first rank in three of the four models). The PLSR model coefficients indicate a positive link, meaning that the slope *b* tends to be higher in areas with high vertical contrast between potential seepage and groundwater NO_3-N concentrations. Only the RF model for slope *b* of NO_3-N ranks the topographic descriptors (slope_mean, twi_mean, dem_mean) highest, which also appear highly ranked in the other models for NO_3-N export dynamics following het_v. The variables depth to bedrock and fraction of sedimentary aquifer also obtain high importance values.

For mean PO_4-P concentrations, the P load from point sources stands out with the highest variable importance in both models, a large step to the second ranked variables and a positive coefficient in PLSR. Slope *b* of the *C*-*Q* relationship is best explained by mean N surplus and the fraction of sedimentary aquifers, all with a positive relationship. After a step in variable importance, these three variables are followed by the 90th percentile of the TWI, the P content in the topsoil and the frequency, amount and seasonality of precipitation.

Mean TOC concentrations are best explained by the TWI (90th percentile and mean) based on PLSR and by mean elevation and topographic slope based on RF. The other respective topographic variables also turn out highly ranked in the models together with the fraction of sedimentary aquifers, potential evapotranspiration and depth to bedrock. The TOC dynamics of the complete set of study catchments were only poorly explained by the available predictors with a maximum $R^2_{CrossVal} = 0.28$ (RF for slope *b*). However, hydrological parameters (Table S11) substantially increased the variance explained by the PLSR and RF models between 11% and 37% (with $R^2_{CrossVal} = 0.44$ for slope *b* in RF and $R^2_{CrossVal} = 0.58$ for CV_C/CV_Q in PLSR) for the smaller subset of catchments ($n = 184$). Especially the flashiness index, seasonal ratio of discharge and BFI ranked high, with a positive direction of influence.

3.4. Relationships Among the Nutrient Export Metrics

All metrics correlated positively for NO_3-N and PO_4-P. This correlation was strongest for CV_C/CV_Q ($r = 0.55$) and lowest for slope *b* ($r = 0.19$, Figure 4). Over the whole range of catchments, the lowest mean NO_3-N and PO_4-P were linked to the highest f_forest (Figure 5a).

For NO_3-N and TOC, mean TOC correlated positively with the NO_3-N export metrics (CV_C/CV_Q $r = 0.58$ and slope *b* $r = 0.52$); this correlation was also apparent for the respective TOC export metrics but was less pronounced. The mean TOC and the slope of NO_3-N also both correlated to the twi_90p ($r = 0.76$ and 0.53 respectively, Figures 5b and S5). Catchments with a high twi_90p tended to have high mean TOC and low mean NO_3-N concentrations (Figure 5c), whereas high NO_3-N concentrations were mostly observed in catchments with lower twi_90p and lower mean TOC concentrations.

Water Resources Research 10.1029/2020WR028134

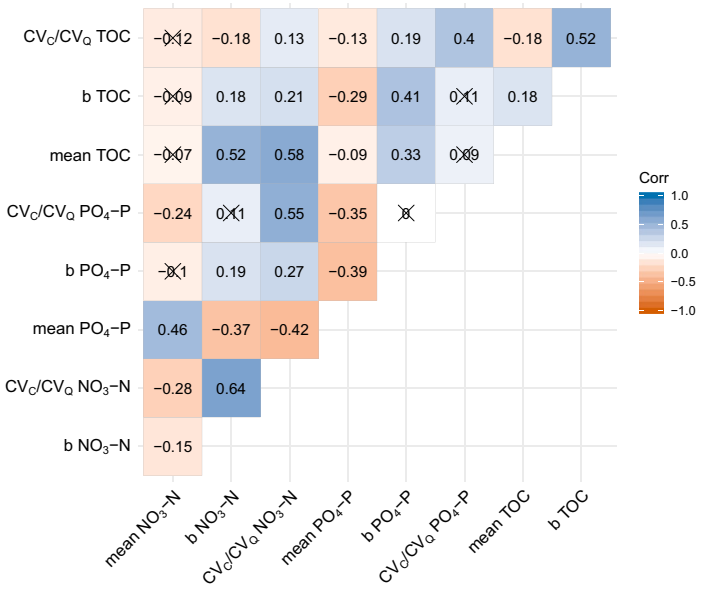

Figure 4. Spearman rank correlation matrix between metrics of the export regimes. Crosses mark non-significant correlations (significance level of 0.05).

For PO_4-P and TOC, slope *b* of PO_4-P correlated positively and mean PO_4-P concentration negatively with all TOC metrics, with the correlation coefficient between the slopes *b* being the highest ($r = 0.41$). *C-Q* slopes *b* of PO_4-P were related to high twi_90p ($r = 0.46$, Figures 5d and S5), which was also a slight tendency for TOC ($r = 0.28$).

4. Discussion

We first discuss the observed export dynamics and their controls for each nutrient individually, followed by a section on nutrient interactions, a synthesis and an implication section.

4.1. Nutrient-Specific Export and Controls

4.1.1. NO_3-N: Natural Attenuation Buffers Input and Controls Export Regimes

The variability in mean NO_3-N concentrations among the studied catchments was linked to the land use, as the fractions of forest and of agriculture both ranked high in the PLSR and RF models and relate to low and high diffuse N sources, respectively. This agrees with findings of previous studies (e.g., Evans et al., 2014; Hansen et al., 2018; Minaudo et al., 2019; Musolff et al., 2015). The fraction of either forest or agriculture alone could respectively explain 32% or 29% of this variability in a simple linear regression case, while in the PLSR and RF the total variability explained by all descriptors was between 64% and 70%. The correlation with N surplus was lower ($r = 0.39$ N_surp_80, Figure S5) even though it is strongly related to agricultural land ($r = 0.71$, Figure S4). This is related to a few catchments that have exceptionally high N surplus but moderate mean NO_3-N concentrations.

However, the relationship between the fraction of agriculture and the mean NO_3-N concentration is highly heteroscedastic as shown in Figure 6a. We found that deviations from a positive linear relationship between the proxies for N input and N output are related to soil and aquifer properties, as e.g. f_sedim ranked high in the PLSR and RF (Tables 3 and S6). This could indicate buffering of inputs by natural attenuation (removal by denitrification) in the unsaturated and saturated zones. Adding the fraction of sedimentary aquifer as a

Water Resources Research 10.1029/2020WR028134

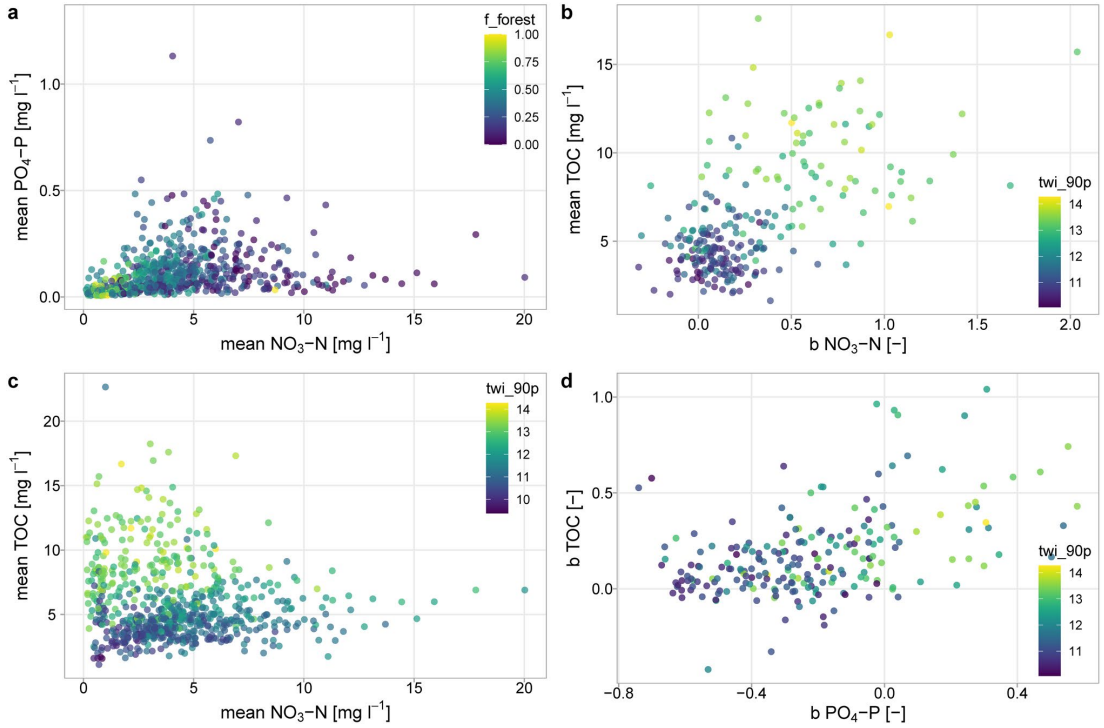

Figure 5. Interaction between metrics of different nutrients: (a) mean PO_4-P against mean NO_3-N concentrations, (b) mean TOC against b NO_3-N, (c) mean TOC against mean NO_3-N concentrations, and (d) slope of PO_4-P against TOC.

secondary factor to the linear model with forest (or agriculture) fractions increased the explained variability by 20%–52% (or 49%) respectively. Previous studies have shown that sedimentary aquifers often exhibit a high denitrification potential (Hannappel et al., 2018; Knoll et al., 2020; Kunkel et al., 2004). Unconsolidated aquifers are usually deep, low-land aquifers linked to long travel times (Merz et al., 2009; Wendland et al., 2008) with anaerobic conditions and organic carbon or pyrite deposits providing electron donors for denitrification, especially in the lowlands of northern Germany (Kunkel et al., 2004; Wendland et al., 2008). Both long residence times and favorable conditions for denitrification increase the potential for NO_3 removal along the flow path (Rivett et al., 2008). This link is supported by het_v (ranked 4th and 5th) representing the vertical NO_3 concentration contrast. This contrast likely results from denitrification under anaerobic subsurface conditions (Knoll et al., 2020) and correlates positively with f_sedim ($r = 0.68$, Figures S4, and 6d). Denitrification in riparian wetlands, which are more abundant in lowlands, could additionally buffer NO_3-N inputs and create a link to the carbon cycle (see also Section 4.2.) (Pinay et al., 2015; Sabater et al., 2003). Apart from effective N removal by denitrification, the decrease in concentration could also be linked to the large groundwater storages of deep, sedimentary aquifers causing high dilution by old (pre-industrial) water fractions low in NO_3-N concentrations and the resultant contrast in vertical concentrations. In such cases, the system would not be equilibrated in terms of its N balance within the investigated time frame (Ehrhardt et al., 2019). Additionally, in-stream retention could also be higher in areas with low slopes due to longer residence times in the river network.

Godsey et al. (2019) showed a general hydroclimatic modification of average concentrations of geogenic solutes. Here, we find a similar pattern with the annual mean and seasonality of precipitation which ranked high in the RF model. Climatic characteristics like the lowest mean annual precipitation, a relatively high ratio between summer to winter precipitation (P_SIsw), and the highest aridity are found in eastern

Water Resources Research 10.1029/2020WR028134

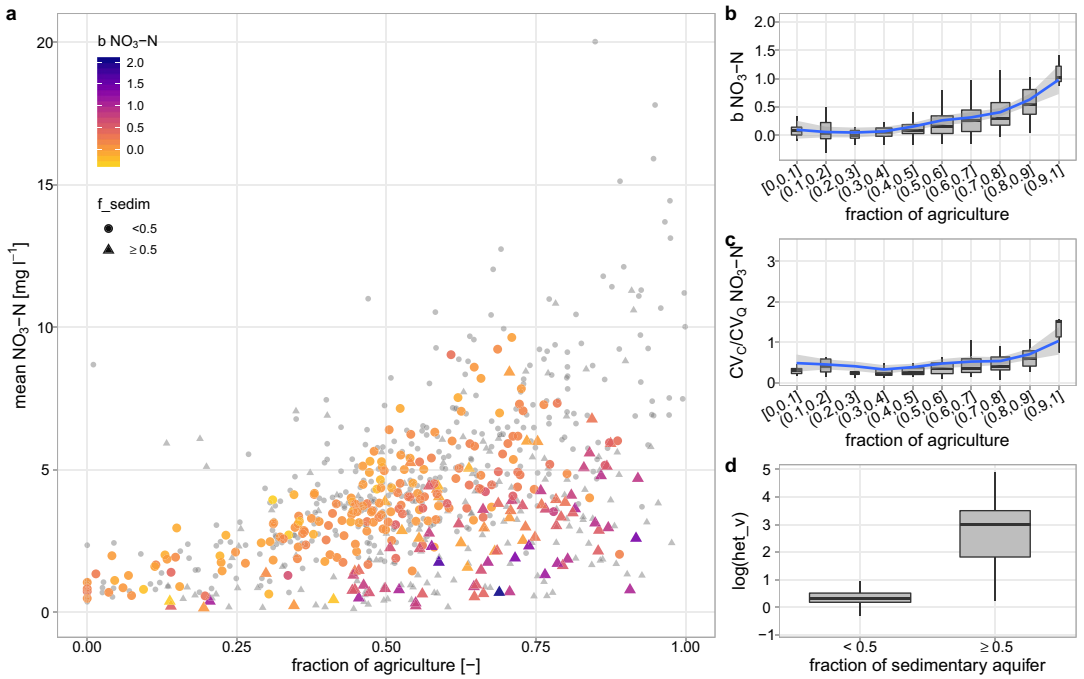

Figure 6. Relationship between the fraction of agriculture as a proxy for diffuse source strength of N and (a) mean NO_3-N concentrations in combination with aquifer type (f_sedim) and NO_3-N export patterns, (b) slope *b* of NO_3-N as binned boxplots, (c) CV_C/CV_Q as binned boxplots, and (d) the link between the fraction of sediments and vertical concentration heterogeneity. In panel (a) the colors indicate the slope *b* of the *C*-*Q* relationship, small gray dots belong to catchments without slope *b* due to missing *Q* data. The shape indicates whether the sedimentary aquifer type dominates. For (b), (c), and (d) the boxplot width is defined by sample size. Blue line with gray shading in (b) and (c) indicate a LOESS regression with confidence interval (confidence level 0.95).

Germany which coincides with highest mean NO_3-N. This suggests an imprint of regional hydro-climate on a lower dilution potential in eastern German catchments.

Altogether, this clearly indicates that the anthropogenic N-input from diffuse sources is a first order control for mean riverine NO_3-N concentrations, while natural attenuation is able to buffer the high inputs (especially in lowlands with deep aquifers), whereas hydroclimatic conditions seem to play a subordinate role.

We found significantly higher mean NO_3-N concentrations for the class of catchments with low concentration variability, that is chemostatic regimes ($CV_C/CV_Q < 0.5$, Figure 2b). This finding agrees with those of Thompson et al. (2011), who found significantly lower CV_C/CV_Q for the group of catchments with higher NO_3-N export and hypothesized that such behavior was due to the homogenization of sources in highly managed catchments. However, in our study, we found that part of the intensively managed catchments exhibited surprisingly low mean NO_3-N concentrations combined with high concentration variability (Figure 6a). For our data set, these agricultural catchments with very high concentration variability led to a tendency of catchments with higher fraction of agriculture linking to higher slope *b* and CV_C/CV_Q (Figures 6b and 6c), although overall chemostatic export prevailed for the majority of the study catchments. More specifically, around 34% of the agriculturally dominated catchments (f_agric ≥ 0.5) exhibited chemodynamic export regimes, out of which 89% were combined with enrichment patterns, compared to 17% of chemodynamic catchments for less agricultural catchments (f_agric < 0.5). Our study therefore does not support the generality of the hypothesis that highly managed, agricultural catchments are necessarily subject to homogenization of sources and thus to chemostatic export regimes (Basu et al., 2010; Thompson et al., 2011). Thus, we recognize that there are agricultural catchments in our study that exhibit chemostatic export, but high fractions of agriculture did not necessarily induce chemostasis and neutral *C*-*Q* patterns. The agricultural chemodynamic catchments widely coincided with catchments where a high abundance of

Water Resources Research 10.1029/2020WR028134

sedimentary aquifers and strong vertical concentration heterogeneity prevailed, as also evident in PLSR and RF models (Table 3, Figure 6a and 6d).

The variability in the export dynamics, that is regimes (CV_C/CV_Q) and patterns (slope *b*), between the studied catchments was positively linked to the descriptor het_v representing the average vertical NO_3-N heterogeneity from soils to groundwater within each catchment. This means that the larger the concentration gradient is over depth within the catchments subsurface, the more chemodynamic and enriching the NO_3-N export. This concentration gradient can be a result of subsurface reactivity such as denitrification in groundwater. In contrast, the variables of horizontal source heterogeneity het_h and sdist_mean did not explain differences in concentration dynamics among the catchments. Accordingly, our results from this data-driven approach confirm findings from previous modeling studies: Zhi et al. (2019) found vertical concentration gradients in combination with end-member mixing, and Musolff et al. (2017) found the concentration gradient over travel times (a more general, indirect measure of solute source heterogeneity) to control *C*-*Q* patterns. The linkage between vertical concentration heterogeneity and export patterns is plausible considering that agricultural and atmospheric N inputs enter the subsurface from the top. A top-loaded profile in combination with the dominance of young water contribution to discharge from upper soil layers during high flows and the dominance of old water fractions at base flow conditions (exponential saturated hydraulic conductivity profile) causes a positive *C*-*Q* slope. This interpretation coincides with the concept of juxtaposition of discharge generation and concentration profiles by Seibert et al. (2009) and with the scenario of higher concentrations linked to shorter travel times described by Musolff et al. (2017). Additionally, tile drainages can enhance the effect of concentration heterogeneity by increasing the younger water fraction during high-flows and by avoiding potential retention zones (Musolff et al., 2015; Van der Velde et al., 2010; Van Meter & Basu, 2017). As geoinformation on drainages over the large study region is not available, we cannot prove the role of this additional flow path in this study.

We found that both the diffuse input and the reactivity (the combined effect of reaction rates and residence times) resulting in NO_3-N attenuation along the flow paths might determine the strength of vertical concentration heterogeneity. Consequently, chemodynamic export with enrichment patterns could indicate natural attenuation and effective denitrification under high inputs. In turn, chemostasis could be an indication of missing reactivity in the catchment in concert with large legacy N pools (Basu et al., 2010). Chemodynamic export may also occur when vertical concentration contrasts emerge in large groundwater bodies not yet in temporal equilibrium (as stated above). However, concentration gradients will only be maintained over a longer term if subsurface attenuation occurs or input changes. The relationship between input, attenuation and export patterns (Figure 6) also indicates that catchments with relatively low mean NO_3-N concentrations but high inputs and steep positive *C*-*Q* patterns might still be "hot spots" in terms of exported loads, eutrophication risk, and large N legacies. Here, the natural attenuation might buffer inputs in terms of mean riverine and groundwater concentrations but not necessarily the exported loads during high flows when concentrations are considerably higher.

4.1.2. PO_4-P: Unexpected Strong Control of Diffuse Sources on Export Patterns

Mean PO_4-P concentrations were positively linked to direct anthropogenic input from point sources, although the overall explained variance in the PLSR and RF models was surprisingly low ($R^2_{CrossVal} = 0.34$ and 0.40). Previous studies have also demonstrated the strong control of point sources on average riverine total P concentrations (Minaudo et al., 2019; Westphal et al., 2019; Withers & Jarvie, 2008), with their contributions remaining high even after significant reductions of inputs from point sources (Behrendt et al., 1999; Westphal et al., 2019). However, even in a densely populated catchments (about 460 inhabitants km^{-2}), contributions of point sources to total P can be similar to diffuse sources, for example about 60% at load peak and 40% with modern wastewater treatment (Westphal et al., 2019).

In general, PO_4-P is subject to P cycling including retention, transformation and remobilization processes in the stream (Jarvie et al., 2012; Smolders et al., 2017; Withers & Jarvie, 2008), all of which may vary strongly in space and time (Withers & Jarvie, 2008). In-stream retention capacities were estimated to 36% of the P loads (Westphal et al., 2019) and even up to 50% of PO_4-P and 60% of total P in other catchments (Withers & Jarvie, 2008). P cycling thus affects both the timing and the load of exported P and potentially reshapes direct inputs and delivery from land-stream transfer at catchment scale (Casquin et al., 2020; Jarvie et al., 2012). This could explain why mean PO_4-P concentrations are linked to the inputs but are hardly

Water Resources Research 10.1029/2020WR028134

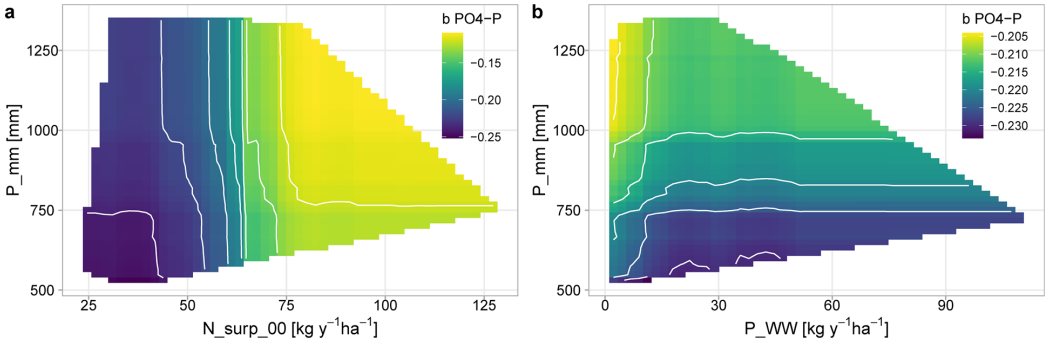

Figure 7. Partial dependence plots for RF model for slope *b* of PO_4-P showing the interaction between (a) N surplus (N_surp_00) and (b) P loads from point sources (P_WW) with mean annual precipitation (P_mm). Colors indicate the range of predicted *b* values with mean values for the other descriptors, which differ for (a) and (b) due to different sensitivities. White areas are outside the covered parameter space (without extrapolation). RF, random forests.

predictable by average catchment characteristics which do not adequately represent controls of in-stream processes. Other reasons for the low predictability could be uncertainties related to (1) the point source data which do not account for potential temporal variations in the loading and small rural point sources (e.g., from farmyards or septic tanks, Withers & Jarvie, 2008), or (2) the sampling frequency of *C* which potentially misses moments of peak concentrations and leads to an underestimation of mean PO_4-P, as shown by Hunsaker and Johnson (2017).

For PO_4-P export dynamics, dilution patterns prevailed in two thirds of the catchments, a finding which agrees with previous studies on association with point-source dilution (Bowes et al., 2015; Moatar et al., 2017) or biogeochemical processes releasing PO_4-P during summer low-flows and thus mimicking point sources in riparian zones (Dupas et al., 2018) and riverbed sediments (Smolders et al., 2017). In 11% of the catchments, we found enrichment patterns of PO_4-P which have also been observed in other cases, for example through mobilization of diffuse sources from agricultural areas (Bieroza & Heathwaite, 2015; Rose et al., 2018) and from a nutrient-rich O-horizon in a forested catchment (Hunsaker & Johnson, 2017) during storm events.

N surplus and the fraction of sedimentary aquifers turned out to be the dominant predictive variables for slope *b* of PO_4-*Q* relationships and were positively linked to it, even with prevailing dilution patterns (Figure 7a, Table 3). Both variables together explain 42% of the variability in slope *b*, and individually 27% and 26% respectively based on a linear model. This constitutes a large part of the explained variability of all descriptors ($R^2_{CrossVal}$ spans 0.43–0.47). Especially in northwestern and southeastern Germany, catchments with high N surplus tended to show enrichment patterns for PO_4-P (Figure 3). High P applications (especially from manure) and low P use efficiencies led to widespread P accumulation (legacy) on agricultural soils, increasing the risk of P losses (Osterholz et al., 2020; Schoumans et al., 2015; Sharpley et al., 2013). Areas with prevailing enrichment patterns coincide with regions of intense manure applications from livestock farms (Häußermann et al., 2019) and high degrees of P saturation (Fischer et al., 2017), which could be the reason for the enhanced PO_4-P land-to-stream transfer. This is reflected in the PLSR model as the topsoil P content (soil_P) positively linked to slope *b* and ranks order 5. Furthermore, Fischer et al. (2017) found widespread (>76%) high risks of dissolved P loss from German agricultural soils, so that the process of diffuse P mobilization is likely to occur in more than 11% of the catchments but might be less pronounced in catchments where dilution prevails. P saturation in the topsoil can be considered as source heterogeneity with a top-loaded profile. The high ranks of f_sedim and twi_90p in the PLSR, explaining slope *b* of PO_4-P, could indicate the additional influence of tile drains in wet lowland soils. Tile drains and preferential flow paths were shown to enhance the land-to-stream transfer of P and cause positive *C*-*Q* patterns by increasing the connectivity of soil P sources and bypassing of potential sinks in the soil matrix (Gentry et al., 2007; Osterholz et al., 2020).

Water Resources Research 10.1029/2020WR028134

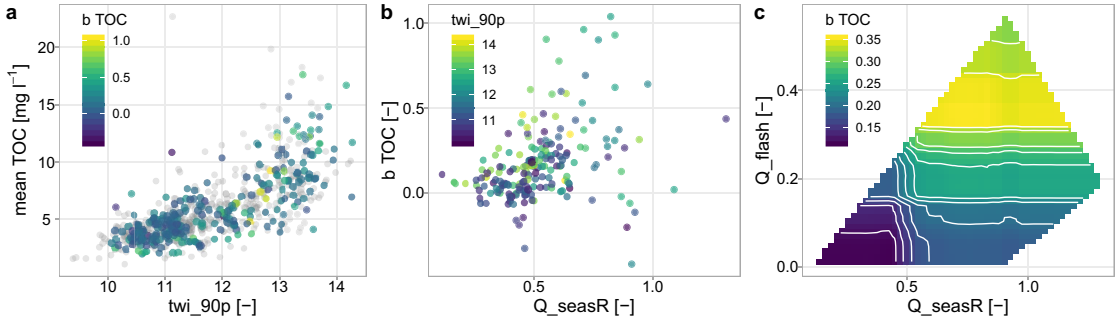

Figure 8. Observed mean TOC concentrations against twi_90p with colors according to slope *b* of TOC (a), observed slope b of TOC against seasonality of discharge (Q_seasR, see Table S2) with colors representing the twi_90p (b), and partial dependence plot of slope *b* TOC from RF model for the variables seasonality and flashiness of discharge (Q_seasR, Q_flash) (c). Note that gray dots in (a) belong to catchments without *Q* data. RF, random forests.

Climatic controls were also ranked high in the PLSR and RF models, for example mean annual precipitation (P_mm) showed a positive impact on slope *b* of PO_4-P (Figure 7, Table 3). The PLSR and RF models including additional hydrological descriptors indicate that a lower seasonal *Q* ratio (i.e. low summer *Q* compared to winter) relate to lower slope *b* and takes over the rank of P_mm in these models (Table S7). This suggests that the impact of P_mm relates to a stronger dilution of low-flow concentrations during the summer and thus less pronounced PO_4-P dilution export patterns.

Although point sources (P_WW) were not part of the highly ranked predictors, the correlations of slope *b* with mean PO_4-P concentrations ($r = -0.39$, see Figure 5), together with the fact that point sources also partly explain mean PO_4-P concentrations, suggest some influence of point sources on slope *b*. This is reflected in the partial dependence plots showing the higher impact of N surplus on slope *b* compared to point sources and climatic drivers (Figure 7). The impact of point sources is only visible for low P loads (<15 kg ha^{-1} y^{-1}), suggesting possible threshold behavior. The lack of an expected clear relationship between point sources and slope *b* fits to the above interpretation that in-stream P cycling can significantly reshape P concentration dynamics (Casquin et al., 2020; Jarvie et al., 2012). The still prevailing dilution patterns of PO_4-P could thus be related to biogeochemically induced P release (see above, Dupas et al., 2018; Smolders et al., 2017) besides the climatic controls.

4.1.3. TOC: Flat Topography Strengthens Sources and Hydrology-Driven Export

Topography related characteristics appeared to dominantly control mean TOC, for example twi_90p and twi_mean alone already explain 52% of the variability in a linear model (Figure 8a). This topography control agrees with previous results by Zarnetske et al. (2018), who found the topographic slope and the share of wetlands followed by mean annual precipitation to best predict DOC concentration levels across the contiguous USA. Musolff et al. (2018) also reported the twi_90p as a good predictor for median DOC concentrations in small mountainous, mainly forested German catchments. The twi_90p can also be interpreted as a proxy for the extent of riparian, well-connected wetlands (Musolff et al., 2018), source areas of organic matter and thus TOC (Bishop et al., 2004; Laudon et al., 2004). Mean TOC concentrations across the studied catchments were not connected to wastewater point sources, suggesting that on a larger spatial extent, terrestrial sources overwhelm potential point source inputs. This is in line with findings of Gücker et al. (2006) on TOC inputs from modern wastewater treatment plants, indicating no consistent effect on downstream TOC concentrations.

Most catchments across Germany classified as enrichment patterns and chemostatic regimes for TOC, which align along the findings of previous studies on dominance of enrichment patterns and transport-limited export for DOC and TOC (Moatar et al., 2017; Musolff et al., 2018; Zarnetske et al., 2018). Zarnetske et al. (2018) found hydrologically well-connected wetlands to control these patterns, while Musolff et al. (2018) found high twi_90p, soluble reactive phosphorus, pH and aridity index to relate to high DOC variability. The near stream, well-connected wetlands can be interpreted as horizontal source heterogeneity

Water Resources Research 10.1029/2020WR028134

and could cause the observed enrichment patterns. However, the fraction of wetland, the twi_90p and the climatic characteristics, together with the other characteristics used, could not satisfactorily explain the variability in the export metrics observed across German catchments. In Moatar et al. (2017), DOC-*Q* slopes correlated with various hydrological variables and, in Musolff et al. (2015), the variability in TOC dynamics were well explained by the BFI (+), artificial drainages (−) and topographic slope (+). In agreement, the subset analysis with hydrological descriptors (Table S11) showed that catchments with more equilibrated discharge patterns (i.e., less flashy, similar summer and winter *Q* with Q_seasR close to 1, and higher base flow) tend to mobilize TOC more dynamically with *Q* but also show a higher variability in the export patterns (Figures 8b and 8c). Antecedent conditions (especially riparian soil temperatures and moisture) are known to control DOC production and therefore could shape the export patterns in combination with temporally variable hydrological connectivity (Wen et al., 2020; Winterdahl et al., 2011). Variable antecedent conditions can cause variable source heterogeneity, resulting in export variability in time and space. The identified hydrological controls (flashiness, seasonality, and BFI) quantify the temporal variability of hydrological conditions and thus might implicitly represent the variability of antecedent conditions within a catchment.

However, even with hydrological descriptors, part of the variability in TOC export dynamics between the studied catchments remains unexplained. This may be linked to other drivers of TOC export besides *Q*, such as the temperature (Musolff et al., 2018; Winterdahl et al., 2014). However, the influence of mean air temperature on the *C*-*Q* relationships cannot be found in our study catchments. We observed that discharge strongly controls the TOC concentrations (high R^2 in the *C*-*Q* relationships) only in study catchments with flatter topography: for TOC-*Q* relationships with $R^2 \geq 0.5$, the topographic slope was <2.1° and twi_90p > 12.2, whereas the catchments with lower R^2 had a higher mean topographic slope = 4.3° and lower mean twi_90p = 11.7.

4.2. N-P-OC: Do Riparian Wetlands Control Observed Nutrient Interactions?

Riparian wetlands are potential hot spots of biogeochemical processes due to high hydrologic connectivity to the streams and variable redox conditions during dry and wet cycles with changing water tables (Burt, 2005; McClain et al., 2003). The twi_90p, a proxy for the extent of riparian wetlands (Musolff et al., 2018), was found to be an important predictor for several of the export metrics (mean TOC concentrations and slope *b* of NO_3-N and PO_4-P) and could be linked to some covariance (Figure 5).

Mean NO_3-N and PO_4-P showed a positive, heteroscedastic relationship with the lowest values of both nutrients in the most forested, pristine catchments (Figure 5a). A negative relationship would be expected in catchments with high twi_90p if reductive mobilization prevailed (Dupas, Gruau, et al., 2015; Gu et al., 2017), however, even catchments without point source influence exhibited a positive relationship. We argue that the anthropogenic impact (in terms of N and P inputs) dominates in the studied catchments and that potential biogeochemical interactions between NO_3-N and PO_4-P do not control the spatial variability of mean concentrations among catchments.

The catchments with the highest twi_90p mostly exhibited relatively high mean TOC and low mean NO_3-N concentrations (Figure 5c). This relationship could be linked to denitrification under anoxic conditions, that is, the redox reaction with DOC as the electron donor and NO_3 as acceptor, as has been observed and discussed in several previous studies (e.g., Cabezas et al., 2013; Taylor & Townsend, 2010). Thus, riparian wetland denitrification could be part of the high natural NO_3-N attenuation in lowlands (see Section 4.1.1.) and intensify positive NO_3-*Q* relationships due to reduced summer low-flow concentrations. However, as the twi_90p is also correlated to het_v ($r = 0.75$), which was the dominant control of slope *b* of NO_3-N, the additional contribution of this interaction within riparian wetland cannot be fully disentangled here.

The positive link between slope *b* of PO4-P and TOC with the twi_90p (Figure 5d) suggests that both nutrients could be mobilized in riparian wetlands, however with a high variability. The mobilization could be linked to iron dissolution under reducing conditions, e.g. due to decreasing NO_3 concentrations as redox buffers, as discussed for example by Cabezas et al. (2013).

Water Resources Research 10.1029/2020WR028134

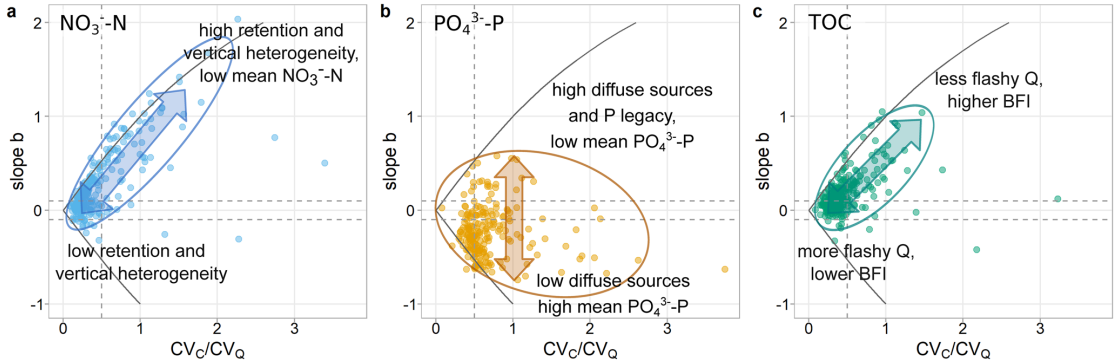

Figure 9. Archetypal ranges of solute-specific export patterns and regimes with arrows along the main axis of variability explained by the identified dominant characteristics (labels at the end) for (a) NO_3-N, (b) PO_4-P, and (c) TOC. The ellipses surround the archetypal ranges including most of the catchments. BFI, base-flow index.

4.3. Archetypal Ranges of Nutrient Export

Over the wide range of investigated catchments, we found solute-specific ranges of export metrics (Figures 2 and 9). The classification of the export dynamics revealed that about 70% of the catchments group into the respective dominant class for each nutrient. This solute-specific prevalence of one pattern or regime has also been reported previously, for example by Minaudo et al. (2019), Moatar et al. (2017) and Zarnetske et al. (2018). The consistency of export type of a specific nutrient might be surprising, considering the multitude of processes affecting nutrient cycling, mobilization, transport, and retention. The properties such as the solubility of each constituent have a major control over processes that lead to mobilization, transport and reactivity, and thus define the archetypal range of export dynamics. The variability within these ranges can be partly linked to catchment characteristics such as the source strength and its spatial arrangement as shown and addressed by PLSR and RF (see Section 3.3).

The dominant controls of the spatial variability of export dynamics and prevailing characteristics for specific areas within the solute-specific ranges (discussed in the preceding sections) are synthesized in Figure 9. For NO_3-N, we found a strong interaction between anthropogenic and natural controls: while agricultural inputs define a baseline for mean NO_3-N concentrations, natural attenuation creates deviations lowering the mean NO_3-N. This attenuation likely increases vertical concentration heterogeneity, and is thus reflected in chemodynamic enrichment patterns. For PO_4-P, anthropogenic footprints from point sources (shaping mean PO_4-P) and diffuse sources (shaping positive *C*-*Q* slopes) seem to interact with more natural controls of P cycling, reshaping the in-stream concentration dynamics and creating a wide range of variability. For TOC, interaction between anthropogenic and natural controls was not apparent, as the topography strongly controlled mean TOC and as the spatial variability of export dynamics was partly explained by hydrological variability.

In summary, we found the hypothesis that diffuse source heterogeneity widely controls export dynamics to be partially confirmed for analyzed nutrients in the study catchments. For NO_3-N, export dynamics were widely controlled by vertical concentration heterogeneity which might be a result of subsurface reactivity as the dominant process (Section 4.1.1). Strong enrichment patterns occurred in areas with high concentration heterogeneity, whereas, chemostatic export prevailed with concentration homogeneity. For PO_4-P, the strength of diffuse sources was dominant, suggesting that heterogeneity in P soil status between top soil and deeper subsurface layers drives export patterns. The generally positive TOC-*Q* relationships could be linked to heterogeneously distributed, near stream sources, however, the extent of riparian wetlands could not explain the variability among the catchments. The hydrology might control variations in source strength and heterogeneity causing temporal variability in the *C*-*Q* relationships. For both PO_4-P and TOC, directly hydrologically connected areas are prerequisite for translating vertical source heterogeneity to chemodynamic

Water Resources Research 10.1029/2020WR028134

export due to their strong sorption tendency. This connectivity can be more pronounced in drained, lowland areas (preferential flow paths) or in locations close to the stream such as riparian zones.

4.4. Implications

Our countrywide analysis of nutrient export dynamics revealed regions of dominant chemostatic and chemodynamic export regimes within Germany (Figure 3), which were partly explained by regionally varying catchment characteristics. Our findings can thus provide orientation for water quality managers about what range of nutrient responses can be expected under specific settings. It could also support decision making for targeted monitoring programmes, as more dynamic systems require higher measurement frequencies to capture their *C*-*Q* variability (Moatar et al., 2020). Observed catchment responses can be used to adapt a targeted management: if chemostatic NO_3-N export is observed, low subsurface denitrification capacity might be the reason and, in consequence, efforts to reduce inputs might be crucial to protect the water quality. In a catchment with apparent effective attenuation and chemodynamic NO_3-N export, the exported loads might still be high and the retention capacity by denitrification might decrease over time, possibly leading to an increase in concentrations in the future. If a system was temporally not in equilibrium (input/output balance), it might exhibit long recovery times. Controlling the inputs thus seems vital in all cases. We found that diffuse sources of PO_4-P can play a large role for P export in German agricultural settings, which demonstrates the need to focus on them in P management besides point sources. The diffuse source mobilization could result in high exported loads, affecting downstream water bodies. Water quality modelers can benefit from the identified dominant controls informing the models to better represent the large-scale observed patterns of different *C*-*Q* dynamics.

As some of the identified controls (especially the anthropogenic ones) have developed over time, the catchment responses may also follow long term trajectories of water quality. For PO_4-P, reductions in point sources and increasing P legacies in agricultural soils might have led to the visibility of enrichment patterns by shifting the dominance of processes. NO_3-N could follow trajectories from more chemodynamic to more chemostatic export if subsurface reactivity decreased over time (Wilde et al., 2017). With rising temperatures and heavier storm events due to climate change (EEA, 2019), biogeochemical interactions linked to temperatures and redox conditions might change. For example, TOC exports might increase with prolonged production times and more variable hydrological connectivity, potentially also enhanced by lower NO_3 redox buffers when depositions and concentrations decrease (Clark et al., 2010).

To further elucidate drivers of nutrient concentrations (including the unexplained variability at catchment scale), the newly assembled data base can be yet explored in terms of nutrient interactions and temporal patterns and their controls. To advance the understanding of the generality of our findings, investigations could be pushed to an even larger, cross-continental scale by adding other national data bases—allowing for greater diversity in hydro-climatic conditions. To complement this national-scale study, studies of selected mesoscale catchments from regions with different observed archetypes using high-frequency data or modeling strategies could further test our derived hypothesis and clarify more of the unexplained variability (Kirchner et al., 2004). Experiments are needed to better characterize and quantify regional denitrification patterns, for example by isotope or trace gas methods.

5. Conclusions

To infer drivers of nutrient export over a wide range of catchments, we analyzed surface water quality and quantity data from a newly assembled, Germany-wide data base. We linked metrics of NO_3-N, PO_4-P, and TOC concentrations and *C*-*Q* relationships of 787 independent catchments to catchment characteristics using multivariate statistical methods. We found that enrichment patterns and chemostatic regimes prevailed for NO_3-N and TOC export, whereas dilution and chemodynamic export prevailed for PO_4-P.

For NO_3-N, we found that subsurface natural attenuation likely buffers anthropogenic diffuse inputs in some catchments reducing mean NO_3-N concentrations and causes vertical concentration heterogeneity

Water Resources Research 10.1029/2020WR028134

which controls export dynamics. This heterogeneity was largest in lowland areas with deep sedimentary aquifers. Accordingly, enrichment patterns in agricultural areas could indicate effective subsurface reactivity.

Anthropogenic diffuse and point sources were found relevant for PO_4-P concentrations even if the spatial variability in responses was hardly predictable by catchment characteristics. Mean PO_4-P were only weakly linked to point sources, while the variability in PO_4-P dynamics was better explained by diffuse agricultural sources and associated P saturation in the top soils. Probably, natural P cycling significantly reshapes in-stream PO_4-P concentrations, which decouples them from the catchments' source configuration and land-stream transfer processes and thus hampers predictions at catchment scale.

Natural topographic settings dominantly controlled TOC concentrations: mean TOC were strongly linked to the abundance of riparian wetlands as source areas. Hydrological descriptors (especially relatively higher summer low-flow discharges and lower flashiness) increased the explained variability of export metrics; however the unexplained part remained high.

Our main hypothesis that diffuse source heterogeneity controls the spatial variability of export patterns was supported for NO_3-N in terms of concentration heterogeneity over depth and for PO_4-P in terms of topsoil P saturation as a top-loaded profile. For TOC, the hypothesis is only indirectly confirmed by the prevalence of enrichment patterns possibly evolving from near stream and thus heterogeneously distributed source areas.

Altogether, we found that NO_3-N and PO_4-P concentrations and dynamics are dominated by anthropogenic inputs, but natural controls significantly buffer or reshape the responses observed at the catchment outlet. For TOC, natural controls dominated.

Our results improve the understanding of controls of nutrient export dynamics and their regional differences. Thus, they can support water quality modeling and management. Further research on large scale subsurface reactivity to test our hypothesis and on temporal changes in export dynamics would deepen our understanding of dominant processes at catchment scale.

Conflict of Interest

The authors declare no conflict of interest.

Acknowledgments
The authors thank the federal authorities for providing water sample data and all contributors to setting up the used data base, including T. Grau, T. Nitz, and J. Dehaspe. The authors thank four anonymous reviewers and the editor for their valuable comments. The authors appreciate Martin Bach and Uwe Häußermann for providing the N surplus data and Soohyun Yang and Olaf Büttner for providing the data of small water treatment plants in Germany. The authors acknowledge the E-OBS data set from the EU-FP6 project UERRA (http://www.uerra.eu) and the Copernicus Climate Change Service, and the data providers in the ECA&D project (https://eca.knmi.nl). The authors further acknowledge several organizations for providing data products used in this study, including the BfG, BGR, SGD, EEA, FAO, IIASA, ISRIC, ISSCAS, and JRC. The authors also greatly appreciate the funding by the Initiative and Networking Fund of the Helmholtz Association through the project Advanced Earth System Modeling Capacity (ESM) (www.esm-project.net). Open access funding enabled and organized by Projekt DEAL.

Data Availability Statement

Datasets for this research are available under Ebeling (2021b), Ebeling (2021a), Musolff et al. (2020) [original data in institutional repository] and Musolff (2020). Further original datasets used for this research are referenced in Table 1 and in the text.

References

Abbott, B. W., Gruau, G., Zarnetske, J. P., Moatar, F., Barbe, L., Thomas, Z., et al. (2018). Unexpected spatial stability of water chemistry in headwater stream networks. *Ecology Letters*, *21*(2), 296–308. https://doi.org/10.1111/ele.12897

Akaike, H. (1974). A new look at the statistical model identification. *IEEE Transactions on Automatic Control*, *19*(6), 716–723. https://doi.org/10.1109/tac.1974.1100705

Ameli, A. A., Beven, K., Erlandsson, M., Creed, I. F., McDonnell, J. J., & Bishop, K. (2017). Primary weathering rates, water transit times, and concentration-discharge relations: A theoretical analysis for the critical zone. *Water Resources Research*, *53*(1), 942–960. https://doi.org/10.1002/2016wr019448

Bach, M., Klement, L., & Häußermann, U. (2016). *Bewertung von Maßnahmen zur Verminderung von Nitrateinträgen in die Gewässer auf Basis regionalisierter Stickstoff Überschüsse. Teil I: Beitrag zur Entwicklung einer ressortübergreifenden Stickstoffstrategie Zwischenbericht*. UBA-Texte, 55/2016. Retrieved from http://www.umweltbundesamt.de/publikationen/bewertung-von-massnahmen-zur-verminderung-von

Ballabio, C., Lugato, E., Fernández-Ugalde, O., Orgiazzi, A., Jones, A., Borrelli, P., et al. (2019). Mapping LUCAS topsoil chemical properties at European scale using Gaussian process regression. *Geoderma*, *355*, 113912. https://doi.org/10.1016/j.geoderma.2019.113912

Basu, N. B., Destouni, G., Jawitz, J. W., Thompson, S. E., Loukinova, N. V., Darracq, A., et al. (2010). Nutrient loads exported from managed catchments reveal emergent biogeochemical stationarity. *Geophysical Research Letters*, *37*(23). https://doi.org/10.1029/2010gl045168

Basu, N. B., Thompson, S. E., & Rao, P. S. C. (2011). Hydrologic and biogeochemical functioning of intensively managed catchments: A synthesis of top-down analyses. *Water Resources Research*, *47*. https://doi.org/10.1029/2011wr010800

Battin, T. J., Kaplan, L. A., Findlay, S., Hopkinson, C. S., Marti, E., Packman, A. I., et al. (2008). Biophysical controls on organic carbon fluxes in fluvial networks. *Nature Geoscience*, *1*(2), 95–100. https://doi.org/10.1038/ngeo101

Behrendt, H., Huber, P., Opitz, D., Schmoll, O., Scholz, G., & Uebe, R. (1999). *Nutrient emissions into river basins of Germany*. UBA-Texte, 75/99. Retrieved from https://www.umweltbundesamt.de/en/publikationen/naehrstoffbilanzierung-flussgebiete-deutschlands

Beven, K. J., & Kirkby, M. J. (1979). A physically based, variable contributing area model of basin hydrology/Un modèle à base physique de zone d'appel variable de l'hydrologie du bassin versant. *Hydrological Sciences Bulletin*, *24*(1), 43–69. https://doi.org/10.1080/02626667909491834

BGBl.1. (1980). *Verordnung über Höchstmengen für Phosphate in Wasch-und Reinigungsmitteln vom 4.6.1980*. PHöchstMengV.

BGR. (2003). Mean annual rate of percolation from the soil in Germany (SWR1000), hydrogeologischer atlas von Deutschland. Retrieved from https://www.bgr.bund.de/DE/Themen/Boden/Bilder/Bod_Themenkarten_HAD_4-5_g.html

BGR. (2018). Bodenübersichtskarte der Bundesrepublik Deutschland 1:250.000 (BUEK250). Soil map of Germany 1:250,000. Retrieved from https://produktcenter.bgr.de/terraCatalog/Start.do

BGR & SGD. (2015). Hydrogeologische Raumgliederung von Deutschland (HYRAUM). Retrieved from https://www.bgr.bund.de/DE/Themen/Wasser/Projekte/abgeschlossen/Beratung/Hyraum/hyraum_projektbeschr.html?nn=1557832

BGR & UNESCO. (2014). International hydrogeological map of Europe 1: 1,500,000 (IHME1500). Digital map data v1.1. Retrieved from http://www.bgr.bund.de/ihme1500/

Bieroza, M. Z., & Heathwaite, A. L. (2015). Seasonal variation in phosphorus concentration-discharge hysteresis inferred from high-frequency in situ monitoring. *Journal of Hydrology*, *524*, 333–347. https://doi.org/10.1016/j.jhydrol.2015.02.036

Bishop, K., Seibert, J., Köhler, S., & Laudon, H. (2004). Resolving the Double Paradox of rapidly mobilized old water with highly variable responses in runoff chemistry. *Hydrological Processes*, *18*(1), 185–189. https://doi.org/10.1002/hyp.5209

BMU. (2000). *Hydrologischer atlas von Deutschland* (N. u. R. Bundesministerium Für Umwelt Ed.). Bonn/Berlin: Datenquelle: Hydrologischer Atlas von Deutschland/BfG.

Bol, R., Gruau, G., Mellander, P.-E., Dupas, R., Bechmann, M., Skarbøvik, E., et al. (2018). Challenges of reducing phosphorus based water eutrophication in the agricultural landscapes of northwest Europe. *Frontiers in Marine Science*, *5*(276). https://doi.org/10.3389/fmars.2018.00276

Botter, G., Basso, S., Rodriguez-Iturbe, I., & Rinaldo, A. (2013). Resilience of river flow regimes. *Proceedings of the National Academy of Sciences*, *110*(32), 12925–12930. https://doi.org/10.1073/pnas.1311920110

Botter, M., Li, L., Hartmann, J., Burlando, P., & Fatichi, S. (2020). Depth of solute generation is a dominant control on concentration-discharge relations. *Water Resources Research*, *56*(8), e2019WR026695. https://doi.org/10.1029/2019wr026695

Bouraoui, F., & Grizzetti, B. (2011). Long term change of nutrient concentrations of rivers discharging in European seas. *The Science of the Total Environment*, *409*(23), 4899–4916. https://doi.org/10.1016/j.scitotenv.2011.08.015

Bouwman, A. F., Bierkens, M. F. P., Griffioen, J., Hefting, M. M., Middelburg, J. J., Middelkoop, H., & Slomp, C. P. (2013). Nutrient dynamics, transfer and retention along the aquatic continuum from land to ocean: Towards integration of ecological and biogeochemical models. *Biogeosciences*, *10*(1), 1–22. https://doi.org/10.5194/bg-10-1-2013

Bowes, M. J., Jarvie, H. P., Halliday, S. J., Skeffington, R. A., Wade, A. J., Loewenthal, M., et al. (2015). Characterising phosphorus and nitrate inputs to a rural river using high-frequency concentration-flow relationships. *The Science of the Total Environment*, *511*, 608–620. https://doi.org/10.1016/j.scitotenv.2014.12.086

Breiman, L. (2001). Random Forests. *Machine Learning*, *45*(1), 5–32. https://doi.org/10.1023/a:1010933404324

Bricker, S. B., Clement, C. G., Pirhalla, D. E., Orlando, S. P., & Farrow, D. R. G. (1999). *National estuarine eutrophication assessment: Effects of nutrient enrichment in the nation's estuaries*. NOAA National Ocean Service Special Projects Office and the National Centers for Coastal Ocean Science. Retrieved from https://ian.umces.edu/neea/pdfs/eutro_report.pdf

Burns, D. A., Pellerin, B. A., Miller, M. P., Capel, P. D., Tesoriero, A. J., & Duncan, J. M. (2019). Monitoring the riverine pulse: Applying high-frequency nitrate data to advance integrative understanding of biogeochemical and hydrological processes. *WIREs Water*, *6*(4), e1348. https://doi.org/10.1002/wat2.1348

Burt, T. P. (2005). A third paradox in catchment hydrology and biogeochemistry: Decoupling in the riparian zone. *Hydrological Processes*, *19*(10), 2087–2089. https://doi.org/10.1002/hyp.5904

Büttner, O. (2020a). *DE-WWTP—data collection of wastewater treatment plants of Germany (status 2015, metadata)*. HydroShare. Retrieved from https://doi.org/10.4211/hs.712c1df62aca4ef29688242eeab7940c

Büttner, O. (2020b). *The waste water treatment data collection for Germany 2015 (DE-WWTP)*. UFZ. Retrieved from https://www.ufz.de/record/dmp/archive/7800

Cabezas, A., Gelbrecht, J., & Zak, D. (2013). The effect of rewetting drained fens with nitrate-polluted water on dissolved organic carbon and phosphorus release. *Ecological Engineering*, *53*, 79–88. https://doi.org/10.1016/j.ecoleng.2012.12.016

Casquin, A., Gu, S., Dupas, R., Petitjean, P., Gruau, G., & Durand, P. (2020). River network alteration of C-N-P dynamics in a mesoscale agricultural catchment. *The Science of the Total Environment*, *749*, 141551. https://doi.org/10.1016/j.scitotenv.2020.141551

Center for International Earth Science Information Network - CIESIN - Columbia University. (2017). *Gridded population of the world, version 4 (GPWv4): Population density, Revision 10*. NASA Socioeconomic Data and Applications Center. Retrieved from https://doi.org/10.7927/H4DZ068D

Clark, J. M., Bottrell, S. H., Evans, C. D., Monteith, D. T., Bartlett, R., Rose, R., et al. (2010). The importance of the relationship between scale and process in understanding long-term DOC dynamics. *The Science of the Total Environment*, *408*(13), 2768–2775. https://doi.org/10.1016/j.scitotenv.2010.02.046

Conley, D. J., Paerl, H. W., Howarth, R. W., Boesch, D. F., Seitzinger, S. P., Havens, K. E., et al. (2009). ECOLOGY: Controlling eutrophication: Nitrogen and phosphorus. *Science*, *323*(5917), 1014–1015. https://doi.org/10.1126/science.1167755

Copeland, C. (2016). *Clean water act: A summary of the law* [press release]. Congressional Research Service. Retrieved from https://fas.org/sgp/crs/misc/RL30030.pdf

Cornes, R. C., van der Schrier, G., van den Besselaar, E. J. M., & Jones, P. D. (2018). An ensemble version of the E-OBS temperature and precipitation data sets. *Journal of Geophysical Research: Atmospheres*, *123*(17), 9391–9409. https://doi.org/10.1029/2017jd028200

Damania, R., Desbureaux, S., Rodella, A.-S., Russ, J. D., & Zaveri, E. D. (2019). Quality unknown : The invisible water crisis (Report No 140973). World Bank. Retrieved from https://openknowledge.worldbank.org/handle/10986/32245

De Jager, A., & Vogt, J. (2007). *Rivers and catchments of Europe—catchment characterisation model (CCM)*. Joint Research Centre. Retrieved from http://data.europa.eu/89h/fe1878e8-7541-4c66-8453-afdae7469221

Diamond, J. S., & Cohen, M. J. (2018). Complex patterns of catchment solute-discharge relationships for coastal plain rivers. *Hydrological Processes*, *32*(3), 388–401. https://doi.org/10.1002/hyp.11424

Dupas, R., Delmas, M., Dorioz, J.-M., Garnier, J., Moatar, F., & Gascuel-Odoux, C. (2015). Assessing the impact of agricultural pressures on N and P loads and eutrophication risk. *Ecological Indicators*, *48*, 396–407. https://doi.org/10.1016/j.ecolind.2014.08.007

Dupas, R., Gruau, G., Gu, S., Humbert, G., Jaffrézic, A., & Gascuel-Odoux, C. (2015). Groundwater control of biogeochemical processes causing phosphorus release from riparian wetlands. *Water Research*, *84*, 307–314. https://doi.org/10.1016/j.watres.2015.07.048

Dupas, R., Jomaa, S., Musolff, A., Borchardt, D., & Rode, M. (2016). Disentangling the influence of hydroclimatic patterns and agricultural management on river nitrate dynamics from sub-hourly to decadal time scales. *The Science of the Total Environment*, *571*, 791–800. https://doi.org/10.1016/j.scitotenv.2016.07.053

Dupas, R., Tittel, J., Jordan, P., Musolff, A., & Rode, M. (2018). Non-domestic phosphorus release in rivers during low-flow: Mechanisms and implications for sources identification. *Journal of Hydrology*, *560*, 141–149. https://doi.org/10.1016/j.jhydrol.2018.03.023

Ebeling, P. (2021a). *CCDB—catchment characteristics data base Germany*. HydroShare. https://doi.org/10.4211/hs.0fc1b5b1be4a475aacfd9545e72e6839

Ebeling, P. (2021b). *WQQDB—water quality metrics for catchments across Germany*. HydroShare. https://doi.org/10.4211/hs.9b4deeca259b4f7398ce72121b4e2979

EEA. (2013). DEM over Europe from the GMES RDA project (EU-DEM, resolution 25m)—version 1, Oct. 2013.

EEA. (2016a). CORINE land cover 2012 v18.5. Retrieved from https://land.copernicus.eu/pan-european/corine-land-cover

EEA. (2016b). EU-Hydro river network [geodata]. Retrieved from https://land.copernicus.eu/imagery-in-situ/eu-hydro/eu-hydro-public-beta/eu-hydro-river-network

EEA. (2018). European waters. Assessment of status and pressures 2018 (EEA Report No 7/201). European Environment Agency. Retrieved from https://www.eea.europa.eu/publications/state-of-water

EEA. (2019). The European environment—state and outlook 2020 (ISBN: 978-92-9480-090-9). European Environment Agency. Retrieved from https://www.eea.europa.eu/publications/soer-2020

EEC. (1991a). Council Directive 91/271/EEC of 21 May 1991 concerning urban waste water treatment. European Economic Community.

EEC. (1991b). Council Directive 91/676/EEC of 12 December 1991 concerning the protection of waters against pollution caused by nitrates from agricultural sources. European Economic Community.

EEC. (2000). Directive 2000/60/EC of the European parliament and of the council of 23 October 2000 establishing a framework for community action in the field of water policy. *Official Journal of the European Communities - Legislation*, *327*, 1–73.

Ehrhardt, S., Kumar, R., Fleckenstein, J. H., Attinger, S., & Musolff, A. (2019). Trajectories of nitrate input and output in three nested catchments along a land use gradient. *Hydrology and Earth System Sciences*, *23*(9), 3503–3524. https://doi.org/10.5194/hess-23-3503-2019

EPA. (2017). National water quality inventory: Report to congress. Retrieved from https://www.epa.gov/sites/production/files/2017-12/documents/305brtc_finalowow_08302017.pdf

Evans, D. M., Schoenholtz, S. H., Wigington, P. J., Griffith, S. M., & Floyd, W. C. (2014). Spatial and temporal patterns of dissolved nitrogen and phosphorus in surface waters of a multi-land use basin. *Environmental Monitoring and Assessment*, *186*(2), 873–887. https://doi.org/10.1007/s10661-013-3428-4

FAO/IIASA/ISRIC/ISSCAS/JRC. (2012). Harmonized world soil Database (version 1.2). Retrieved from https://webarchive.iiasa.ac.at/Research/LUC/External-World-soil-database/HTML/

Fischer, P., Pöthig, R., & Venohr, M. (2017). The degree of phosphorus saturation of agricultural soils in Germany: Current and future risk of diffuse P loss and implications for soil P management in Europe. *The Science of the Total Environment*, *599–600*, 1130–1139. https://doi.org/10.1016/j.scitotenv.2017.03.143

Galloway, J. N., Aber, J. D., Erisman, J. W., Seitzinger, S. P., Howarth, R. W., Cowling, E. B., & Cosby, B. J. (2003). The nitrogen cascade. *BioScience*, *53*(4), 341–356. https://doi.org/10.1641/0006-3568(2003)053[0341:tnc]2.0.co;2

Gentry, L. E., David, M. B., Royer, T. V., Mitchell, C. A., & Starks, K. M. (2007). Phosphorus transport pathways to streams in tile-drained agricultural watersheds. *Journal of Environmental Quality*, *36*(2), 408–415. https://doi.org/10.2134/jeq2006.0098

Godsey, S. E., Hartmann, J., & Kirchner, J. W. (2019). Catchment chemostasis revisited: Water quality responds differently to variations in weather and climate. *Hydrological Processes*, *33*(24), 3056–3069. https://doi.org/10.1002/hyp.13554

Godsey, S. E., Kirchner, J. W., & Clow, D. W. (2009). Concentration-discharge relationships reflect chemostatic characteristics of US catchments. *Hydrological Processes*, *23*(13), 1844–1864. https://doi.org/10.1002/hyp.7315

Gomez-Velez, J. D., Harvey, J. W., Cardenas, M. B., & Kiel, B. (2015). Denitrification in the Mississippi river network controlled by flow through river bedforms. *Nature Geoscience*, *8*, 941. https://doi.org/10.1038/ngeo2567

Greenwell, B. M. (2017). pdp: An R package for constructing partial dependence plots. *The R Journal*, *9*(1), 421–436. https://doi.org/10.32614/rj-2017-016

Gruber, N., & Galloway, J. N. (2008). An earth-system perspective of the global nitrogen cycle. *Nature*, *451*, 293. https://doi.org/10.1038/nature06592

Gu, S., Gruau, G., Dupas, R., Rumpel, C., Crème, A., Fovet, O., et al. (2017). Release of dissolved phosphorus from riparian wetlands: Evidence for complex interactions among hydroclimate variability, topography and soil properties. *The Science of the Total Environment*, *598*, 421–431. https://doi.org/10.1016/j.scitotenv.2017.04.028

Gücker, B., Brauns, M., & Pusch, M. T. (2006). Effects of wastewater treatment plant discharge on ecosystem structure and function of lowland streams. *Journal of the North American Benthological Society*, *25*(2), 313–329. https://doi.org/10.1899/0887-3593(2006)25[313:eowtpd]2.0.co;2

Gupta, H. V., Perrin, C., Blöschl, G., Montanari, A., Kumar, R., Clark, M., & Andréassian, V. (2014). Large-sample hydrology: A need to balance depth with breadth. *Hydrology and Earth System Sciences*, *18*(2), 463–477. https://doi.org/10.5194/hess-18-463-2014

Hannappel, S., Köpp, C., & Bach, T. (2018). Charakterisierung des Nitratabbauvermögens der Grundwasserleiter in Sachsen-Anhalt. *Grundwasser*, *23*(4), 311–321. https://doi.org/10.1007/s00767-018-0402-7

Hansen, A. T., Dolph, C. L., Foufoula-Georgiou, E., & Finlay, J. C. (2018). Contribution of wetlands to nitrate removal at the watershed scale. *Nature Geoscience*, *11*(2), 127–132. https://doi.org/10.1038/s41561-017-0056-6

Häußermann, U., Bach, M., Klement, L., & Breuer, L. (2019). *Stickstoff-Flächenbilanzen für Deutschland mit Regionalgliederung Bundesländer und Kreise—Jahre 1995 bis 2017*. Methodik, Ergebnisse und Minderungsmaßnahmen. Texte, 131/2019. Retrieved from https://www.umweltbundesamt.de/sites/default/files/medien/1410/publikationen/2019-10-28_texte_131-2019_stickstoffflaechenbilanz.pdf

Herndon, E. M., Dere, A. L., Sullivan, P. L., Norris, D., Reynolds, B., & Brantley, S. L. (2015). Landscape heterogeneity drives contrasting concentration-discharge relationships in shale headwater catchments. *Hydrology and Earth System Sciences*, *19*(8), 3333–3347. https://doi.org/10.5194/hess-19-3333-2015

Howden, N. J. K., Burt, T. P., Worrall, F., Whelan, M. J., & Bieroza, M. (2010). Nitrate concentrations and fluxes in the river Thames over 140 years (1868–2008): Are increases irreversible? *Hydrological Processes*, *24*(18), 2657–2662. https://doi.org/10.1002/hyp.7835

Hunsaker, C. T., & Johnson, D. W. (2017). Concentration-discharge relationships in headwater streams of the Sierra Nevada, California. *Water Resources Research*, *53*(9), 7869–7884. https://doi.org/10.1002/2016wr019693

Water Resources Research 10.1029/2020WR028134

Jarvie, H. P., Sharpley, A. N., Scott, J. T., Haggard, B. E., Bowes, M. J., & Massey, L. B. (2012). Within-river phosphorus retention: Accounting for a missing piece in the watershed phosphorus puzzle. *Environmental Science and Technology*, *46*(24), 13284–13292. https://doi.org/10.1021/es303562y

Jarvie, H. P., Sharpley, A. N., Withers, P. J. A., Scott, J. T., Haggard, B. E., & Neal, C. (2013). Phosphorus mitigation to control river eutrophication: Murky waters, inconvenient truths, and "postnormal" science. *Journal of Environmental Quality*, *42*(2), 295–304. https://doi.org/10.2134/jeq2012.0085

Jenny, J.-P., Anneville, O., Arnaud, F., Baulaz, Y., Bouffard, D., Domaizon, I., et al. (2020). Scientists' warning to humanity: Rapid degradation of the world's large lakes. *Journal of Great Lakes Research*, *46*(4), 686–702. https://doi.org/10.1016/j.jglr.2020.05.006

Jordan, P., Menary, W., Daly, K., Kiely, G., Morgan, G., Byrne, P., & Moles, R. (2005). Patterns and processes of phosphorus transfer from Irish grassland soils to rivers-integration of laboratory and catchment studies. *Journal of Hydrology*, *304*(1), 20–34. https://doi.org/10.1016/j.jhydrol.2004.07.021

Kirchner, J. W., Feng, X., Neal, C., & Robson, A. J. (2004). The fine structure of water-quality dynamics: The(high-frequency) wave of the future. *Hydrological Processes*, *18*(7), 1353–1359. https://doi.org/10.1002/hyp.5537

Knoll, L., Breuer, L., & Bach, M. (2019). Large scale prediction of groundwater nitrate concentrations from spatial data using machine learning. *The Science of the Total Environment*, *668*, 1317–1327. https://doi.org/10.1016/j.scitotenv.2019.03.045

Knoll, L., Breuer, L., & Bach, M. (2020). Nation-wide estimation of groundwater redox conditions and nitrate concentrations through machine learning. *Environmental Research Letters*, *15*(6), 064004. https://doi.org/10.1088/1748-9326/ab7d5c

Kuhn, M., Wing, J., Weston, S., Williams, A., Keefer, C., Engelhardt, A., et al. (2019). *caret: Classification and regression training*. Astrophysics Source Code Library. Retrieved from https://CRAN.R-project.org/package=caret

Kunkel, R., Bach, M., Behrendt, H., & Wendland, F. (2004). Groundwater-borne nitrate intakes into surface waters in Germany. *Water Science and Technology*, *49*(3), 11–19. https://doi.org/10.2166/wst.2004.0152

Laudon, H., Berggren, M., Ågren, A., Buffam, I., Bishop, K., Grabs, T., et al. (2011). Patterns and dynamics of dissolved organic carbon (DOC) in boreal streams: The role of processes, connectivity, and scaling. *Ecosystems*, *14*(6), 880–893. https://doi.org/10.1007/s10021-011-9452-8

Laudon, H., Köhler, S., & Buffam, I. (2004). Seasonal TOC export from seven boreal catchments in northern Sweden. *Aquatic Sciences: Research Across Boundaries*, *66*(2), 223–230. https://doi.org/10.1007/s00027-004-0700-2

Le Moal, M., Gascuel-Odoux, C., Ménesguen, A., Souchon, Y., Étrillard, C., Levain, A., et al. (2019). Eutrophication: A new wine in an old bottle? *The Science of the Total Environment*, *651*, 1–11. https://doi.org/10.1016/j.scitotenv.2018.09.139

Livneh, B., Kumar, R., & Samaniego, L. (2015). Influence of soil textural properties on hydrologic fluxes in the Mississippi river basin. *Hydrological Processes*, *29*(21), 4638–4655. https://doi.org/10.1002/hyp.10601

Marinos, R. E., Van Meter, K. J., & Basu, N. B. (2020). Is the river a chemostat?: Scale versus land use controls on nitrate concentration-discharge dynamics in the upper Mississippi river basin. *Geophysical Research Letters*, *47*(16), e2020GL087051. https://doi.org/10.1029/2020gl087051

McClain, M. E., Boyer, E. W., Dent, C. L., Gergel, S. E., Grimm, N. B., Groffman, P. M., et al. (2003). Biogeochemical hot spots and hot moments at the interface of terrestrial and aquatic ecosystems. *Ecosystems*, *6*(4), 301–312. https://doi.org/10.1007/s10021-003-0161-9

Meals, D. W., Dressing, S. A., & Davenport, T. E. (2010). Lag time in water quality response to best management practices: A review. *Journal of Environmental Quality*, *39*(1), 85–96. https://doi.org/10.2134/jeq2009.0108

Merz, C., Steidl, J., & Dannowski, R. (2009). Parameterization and regionalization of redox based denitrification for GIS-embedded nitrate transport modeling in Pleistocene aquifer systems. *Environmental Geology*, *58*(7), 1587. https://doi.org/10.1007/s00254-008-1665-6

Minaudo, C., Dupas, R., Gascuel-Odoux, C., Roubeix, V., Danis, P.-A., & Moatar, F. (2019). Seasonal and event-based concentration-discharge relationships to identify catchment controls on nutrient export regimes. *Advances in Water Resources*, *131*, 103379. https://doi.org/10.1016/j.advwatres.2019.103379

Moatar, F., Abbott, B. W., Minaudo, C., Curie, F., & Pinay, G. (2017). Elemental properties, hydrology, and biology interact to shape concentration-discharge curves for carbon, nutrients, sediment, and major ions. *Water Resources Research*, *53*(2), 1270–1287. https://doi.org/10.1002/2016wr019635

Moatar, F., Floury, M., Gold, A. J., Meybeck, M., Renard, B., Ferréol, M., et al. (2020). Stream solutes and particulates export regimes: A new framework to optimize their monitoring. *Frontiers in Ecology and Evolution*, *7*(516). https://doi.org/10.3389/fevo.2019.00516

Møller, A. B., Beucher, A., Iversen, B. V., & Greve, M. H. (2018). Predicting artificially drained areas by means of a selective model ensemble. *Geoderma*, *320*, 30–42.

Musolff, A. (2020). *WQQDB - water quality and quantity data base Germany: Metadata*. HydroShare. https://doi.org/10.4211/hs.a42addcbd59a466a9aa56472dfef8721

Musolff, A., Fleckenstein, J. H., Opitz, M., Büttner, O., Kumar, R., & Tittel, J. (2018). Spatio-temporal controls of dissolved organic carbon stream water concentrations. *Journal of Hydrology*, *566*, 205–215. https://doi.org/10.1016/j.jhydrol.2018.09.011

Musolff, A., Fleckenstein, J. H., Rao, P. S. C., & Jawitz, J. W. (2017). Emergent archetype patterns of coupled hydrologic and biogeochemical responses in catchments. *Geophysical Research Letters*, *44*(9), 4143–4151. https://doi.org/10.1002/2017gl072630

Musolff, A., Grau, T., Weber, M., Ebeling, P., Samaniego-Eguiguren, L., & Kumar, R. (2020). *WQQDB: Water quality and quantity data base Germany*. HydroShare. Retrieved from http://www.ufz.de/record/dmp/archive/7754

Musolff, A., Schmidt, C., Selle, B., & Fleckenstein, J. H. (2015). Catchment controls on solute export. *Advances in Water Resources*, *86*, 133–146. https://doi.org/10.1016/j.advwatres.2015.09.026

Oelsner, G. P., Sprague, L. A., Murphy, J. C., Zuellig, R. E., Johnson, H. M., Ryberg, K. R., et al. (2017). *Water-quality trends in the nation's rivers and streams, 1972–2012—data preparation, statistical methods, and trend results*. U.S. Geological Survey Scientific Investigations. Retrieved from https://doi.org/10.3133/sir20175006

Oldham, C. E., Farrow, D. E., & Peiffer, S. (2013). A generalized Damköhler number for classifying material processing in hydrological systems. *Hydrology and Earth System Sciences*, *17*(3), 1133–1148. https://doi.org/10.5194/hess-17-1133-2013

Onderka, M., Wrede, S., Rodný, M., Pfister, L., Hoffmann, L., & Krein, A. (2012). Hydrogeologic and landscape controls of dissolved inorganic nitrogen (DIN) and dissolved silica (DSi) fluxes in heterogeneous catchments. *Journal of Hydrology*, *450–451*, 36–47. https://doi.org/10.1016/j.jhydrol.2012.05.035

Osterholz, W. R., Hanrahan, B. R., & King, K. W. (2020). Legacy phosphorus concentration-discharge relationships in surface runoff and tile drainage from Ohio crop fields. *Journal of Environmental Quality*, *49*(3), 675–687. https://doi.org/10.1002/jeq2.20070

Ouedraogo, I., Defourny, P., & Vanclooster, M. (2019). Application of random forest regression and comparison of its performance to multiple linear regression in modeling groundwater nitrate concentration at the African continent scale. *Hydrogeology Journal*, *27*(3), 1081–1098. https://doi.org/10.1007/s10040-018-1900-5

Pflugmacher, D., Rabe, A., Peters, M., & Hostert, P. (2018). *Pan-European land cover map of 2015 based on Landsat and LUCAS data*. PANGAEA. Retrieved from https://doi.org/10.1594/PANGAEA.896282
Pinay, G., Peiffer, S., De Dreuzy, J.-R., Krause, S., Hannah, D. M., Fleckenstein, J. H., et al. (2015). Upscaling nitrogen removal capacity from local hotspots to low stream orders' drainage basins. *Ecosystems*, *18*(6), 1101–1120. https://doi.org/10.1007/s10021-015-9878-5
Rivett, M. O., Buss, S. R., Morgan, P., Smith, J. W. N., & Bemment, C. D. (2008). Nitrate attenuation in groundwater: A review of biogeochemical controlling processes. *Water Research*, *42*(16), 4215–4232. https://doi.org/10.1016/j.watres.2008.07.020
Rodriguez-Galiano, V., Mendes, M. P., Garcia-Soldado, M. J., Chica-Olmo, M., & Ribeiro, L. (2014). Predictive modeling of groundwater nitrate pollution using random forest and multisource variables related to intrinsic and specific vulnerability: A case study in an agricultural setting (Southern Spain). *The Science of the Total Environment*, *476–477*, 189–206. https://doi.org/10.1016/j.scitotenv.2014.01.001
Rose, L. A., Karwan, D. L., & Godsey, S. E. (2018). Concentration-discharge relationships describe solute and sediment mobilization, reaction, and transport at event and longer timescales. *Hydrological Processes*, *32*(18), 2829–2844. https://doi.org/10.1002/hyp.13235
Sabater, S., Butturini, A., Clement, J.-C., Burt, T., Dowrick, D., Hefting, M., et al. (2003). Nitrogen removal by Riparian buffers along a European climatic gradient: Patterns and factors of variation. *Ecosystems*, *6*(1), 0020–0030. https://doi.org/10.1007/s10021-002-0183-8
Samaniego, L., Kumar, R., & Attinger, S. (2010). Multiscale parameter regionalization of a grid-based hydrologic model at the mesoscale. *Water Resources Research*, *46*(5). https://doi.org/10.1029/2008wr007327
Schmidt, L., Heße, F., Attinger, S., & Kumar, R. (2020). Challenges in applying machine learning models for hydrological inference: A case study for flooding events across Germany. *Water Resources Research*, *56*, e2019WR025924. https://doi.org/10.1029/2019WR025924
Schoumans, O. F., Bouraoui, F., Kabbe, C., Oenema, O., & van Dijk, K. C. (2015). Phosphorus management in Europe in a changing world. *Ambio*, *44*(2), 180–192. https://doi.org/10.1007/s13280-014-0613-9
Schoumans, O. F., Chardon, W. J., Bechmann, M. E., Gascuel-Odoux, C., Hofman, G., Kronvang, B., et al. (2014). Mitigation options to reduce phosphorus losses from the agricultural sector and improve surface water quality: A review. *The Science of the Total Environment*, *468–469*, 1255–1266. https://doi.org/10.1016/j.scitotenv.2013.08.061
Seibert, J., Grabs, T., Köhler, S., Laudon, H., Winterdahl, M., & Bishop, K. (2009). Linking soil- and stream-water chemistry based on a riparian flow-concentration integration model. *Hydrology and Earth System Sciences*, *13*(12), 2287–2297. https://doi.org/10.5194/hess-13-2287-2009
Shangguan, W., Hengl, T., Mendes de Jesus, J., Yuan, H., & Dai, Y. (2017). Mapping the global depth to bedrock for land surface modeling. *Journal of Advances in Modeling Earth Systems*, *9*(1), 65–88. https://doi.org/10.1002/2016ms000686
Sharpley, A., Jarvie, H. P., Buda, A., May, L., Spears, B., & Kleinman, P. (2013). Phosphorus legacy: Overcoming the effects of past management practices to mitigate future water quality impairment. *Journal of Environmental Quality*, *42*(5), 1308–1326. https://doi.org/10.2134/jeq2013.03.0098
Sivapalan, M. (2006). Pattern, process and function: Elements of a unified theory of hydrology at the catchment scale. In M. G. Anderson, & J. J. McDonnell (Eds.), *Encyclopedia of hydrological sciences*. John Wiley & Sons.
Smolders, E., Baetens, E., Verbeeck, M., Nawara, S., Diels, J., Verdievel, M., et al. (2017). Internal loading and redox cycling of sediment iron explain reactive phosphorus concentrations in lowland rivers. *Environmental Science and Technology*, *51*(5), 2584–2592. https://doi.org/10.1021/acs.est.6b04337
Solomon, C. T., Jones, S. E., Weidel, B. C., Buffam, I., Fork, M. L., Karlsson, J., et al. (2015). Ecosystem consequences of changing inputs of terrestrial dissolved organic matter to lakes: Current knowledge and future challenges. *Ecosystems*, *18*(3), 376–389. https://doi.org/10.1007/s10021-015-9848-y
Stanley, E. H., Powers, S. M., Lottig, N. R., Buffam, I., & Crawford, J. T. (2012). Contemporary changes in dissolved organic carbon (DOC) in human-dominated rivers: is there a role for DOC management?. *Freshwater Biology*, *57*(s1), 26–42. https://doi.org/10.1111/j.1365-2427.2011.02613.x
Taylor, P. G., & Townsend, A. R. (2010). Stoichiometric control of organic carbon-nitrate relationships from soils to the sea. *Nature*, *464*, 1178. https://doi.org/10.1038/nature08985
Team, R. C. (2019). *R: A language and environment for statistical computing*. R Foundation for Statistical Computing. Retrieved from https://www.R-project.org/
Thompson, S. E., Basu, N. B., Lascurain, J., Aubeneau, A., & Rao, P. S. C. (2011). Relative dominance of hydrologic versus biogeochemical factors on solute export across impact gradients. *Water Resources Research*, *47*(10). https://doi.org/10.1029/2010wr009605
Tunaley, C., Tetzlaff, D., & Soulsby, C. (2017). Scaling effects of riparian peatlands on stable isotopes in runoff and DOC mobilisation. *Journal of Hydrology*, *549*, 220–235. https://doi.org/10.1016/j.jhydrol.2017.03.056
Underwood, K. L., Rizzo, D. M., Schroth, A. W., & Dewoolkar, M. M. (2017). Evaluating spatial variability in sediment and phosphorus concentration-discharge relationships using Bayesian inference and self-organizing maps. *Water Resources Research*, *53*(12), 10293–10316. https://doi.org/10.1002/2017wr021353
Van der Velde, Y., Rooij, G. H. d., Rozemeijer, J. C., Geer, F. C. v., & Broers, H. P. (2010). Nitrate response of a lowland catchment: On the relation between stream concentration and travel time distribution dynamics. *Water Resources Research*, *46*(11). https://doi.org/10.1029/2010wr009105
Van Meter, K. J., & Basu, N. B. (2015). Catchment legacies and time lags: A parsimonious watershed model to predict the effects of legacy storage on nitrogen export. *PLoS One*, *10*(5), e0125971. https://doi.org/10.1371/journal.pone.0125971
Van Meter, K. J., & Basu, N. B. (2017). Time lags in watershed-scale nutrient transport: An exploration of dominant controls. *Environmental Research Letters*, *12*(8), 084017. https://doi.org/10.1088/1748-9326/aa7bf4. http://dx.doi.org/10.1088/1748-9326/aa7bf4
Vitousek, P. M., Mooney, H. A., Lubchenco, J., & Melillo, J. M. (1997). Human domination of earth's ecosystems. *Science*, *277*(5325), 494–499. https://doi.org/10.1126/science.277.5325.494
Vogel, R. M., Rudolph, B. E., & Hooper, R. P. (2005). Probabilistic behavior of water-quality loads. *Journal of Environmental Engineering*, *131*(7), 1081–1089. https://doi.org/10.1061/(asce)0733-9372(2005)131:7(1081)
Wallin, M. B., Weyhenmeyer, G. A., Bastviken, D., Chmiel, H. E., Peter, S., Sobek, S., & Klemedtsson, L. (2015). Temporal control on concentration, character, and export of dissolved organic carbon in two hemiboreal headwater streams draining contrasting catchments. *Journal of Geophysical Research: Biogeosciences*, *120*(5), 832–846. https://doi.org/10.1002/2014jg002814
Wen, H., Perdrial, J., Abbott, B. W., Bernal, S., Dupas, R., Godsey, S. E., et al. (2020). Temperature controls production but hydrology regulates export of dissolved organic carbon at the catchment scale. *Hydrology and Earth System Sciences*, *24*(2), 945–966. https://doi.org/10.5194/hess-24-945-2020
Wendland, F., Blum, A., Coetsiers, M., Gorova, R., Griffioen, J., Grima, J., et al. (2008). European aquifer typology: A practical framework for an overview of major groundwater composition at European scale. *Environmental Geology*, *55*(1), 77–85. https://doi.org/10.1007/s00254-007-0966-5

Water Resources Research 10.1029/2020WR028134

Westphal, K., Graeber, D., Musolff, A., Fang, Y., Jawitz, J. W., & Borchardt, D. (2019). Multi-decadal trajectories of phosphorus loading, export, and instream retention along a catchment gradient. *The Science of the Total Environment*, *667*, 769–779. https://doi.org/10.1016/j.scitotenv.2019.02.428

Wilde, S., Hansen, C., & Bergmann, A. (2017). Nachlassender Nitratabbau im Grundwasser und deren Folgen—abgestufte modellgestützte Bewertungsansätze. *Grundwasser*, *22*(4), 293–308. https://doi.org/10.1007/s00767-017-0373-0

Winterdahl, M., Erlandsson, M., Futter, M. N., Weyhenmeyer, G. A., & Bishop, K. (2014). Intra-annual variability of organic carbon concentrations in running waters: Drivers along a climatic gradient. *Global Biogeochemical Cycles*, *28*(4), 451–464. https://doi.org/10.1002/2013gb004770

Winterdahl, M., Futter, M., Köhler, S., Laudon, H., Seibert, J., & Bishop, K. (2011). Riparian soil temperature modification of the relationship between flow and dissolved organic carbon concentration in a boreal stream. *Water Resources Research*, *47*(8). https://doi.org/10.1029/2010wr010235

Withers, P. J. A., & Jarvie, H. P. (2008). Delivery and cycling of phosphorus in rivers: A review. *The Science of the Total Environment*, *400*(1), 379–395. https://doi.org/10.1016/j.scitotenv.2008.08.002

WMO. (2008). *Manual on low-flow estimation and prediction*. World Meteorological Organization. Retrieved from http://library.wmo.int/pmb_ged/wmo_1029_en.pdf

Wold, S., Sjöström, M., & Eriksson, L. (2001). PLS-regression: A basic tool of chemometrics. *Chemometrics and Intelligent Laboratory Systems*, *58*(2), 109–130. https://doi.org/10.1016/s0169-7439(01)00155-1

Zarnetske, J. P., Bouda, M., Abbott, B. W., Saiers, J., & Raymond, P. A. (2018). Generality of hydrologic transport limitation of watershed organic carbon flux across ecoregions of the United States. *Geophysical Research Letters*, *45*(21), 11702–11711. https://doi.org/10.1029/2018gl080005

Zhi, W., Li, L., Dong, W., Brown, W., Kaye, J., Steefel, C., & Williams, K. H. (2019). Distinct source water chemistry shapes contrasting concentration-discharge patterns. *Water Resources Research*, *55*(5), 4233–4251. https://doi.org/10.1029/2018wr024257

Zimmer, M. A., Pellerin, B., Burns, D. A., & Petrochenkov, G. (2019). Temporal variability in nitrate-discharge relationships in large rivers as revealed by high-frequency data. *Water Resources Research*. *55*, 973–989. https://doi.org/10.1029/2018WR023478

Zink, M., Kumar, R., Cuntz, M., & Samaniego, L. (2017). A high-resolution dataset of water fluxes and states for Germany accounting for parametric uncertainty. *Hydrology and Earth System Sciences*, *21*(3), 1769–1790. https://doi.org/10.5194/hess-21-1769-2017

Water Resources Research

Supporting Information for

Archetypes and Controls of Riverine Nutrient Export Across German Catchments

Pia Ebeling[1], Rohini Kumar[2], Michael Weber[2], Lukas Knoll[3], Jan H. Fleckenstein[1,4], Andreas Musolff[1]

[1]Department of Hydrogeology, Helmholtz Centre for Environmental Research - UFZ, Leipzig, Germany.

[2]Department of Computational Hydrosystems, Helmholtz Centre for Environmental Research - UFZ, Leipzig, Germany.

[3]Institute for Landscape Ecology and Resources Management (ILR), Research Centre for BioSystems, Land Use and Nutrition (iFZ), Justus Liebig University Giessen, Giessen, Germany.

[4]Bayreuth Center of Ecology and Environmental Research (BayCEER), University of Bayreuth, Bayreuth, Germany.

Contents of this file

Introduction

This supporting information provides additional text on descriptor co-linearities, figures and tables with complete model results.

Text S1.

Several co-linearities exist among the catchment characteristics quantified for all variables by Spearman rank correlations (Figure S4). The land cover classes fraction of agriculture and forest were strongly negatively correlated as opposing land use classes. Agricultural land fraction also correlated negatively with the topographic slope, water available in the root zone, the C/N ratio and N content in the topsoil and positively with N surplus and soil P content. The topographic variables were strongly correlated among themselves such that higher slopes prevailed in higher elevations and linked to lower TWI. Topography variables also correlated with descriptors of climate and hydrology (e.g., higher topographic slopes related to higher precipitation amount and frequency, specific discharge, runoff coefficient and discharge variability but lower aridity index), lithology (e.g., higher slopes related to lower fractions of sedimentary aquifers and lower depth to bedrock), soil chemistry (e.g., higher slopes related to higher N in the topsoil but less P) and source heterogeneity (e.g., higher slopes related to lower mean source distances to stream and lower vertical concentration contrasts). This means that flat lowland catchments tend to have more agriculture and diffuse sources, more sedimentary aquifers with deeper bedrock, more riparian wetlands and more vertical concentration contrasts but lesser precipitation and lesser discharge.

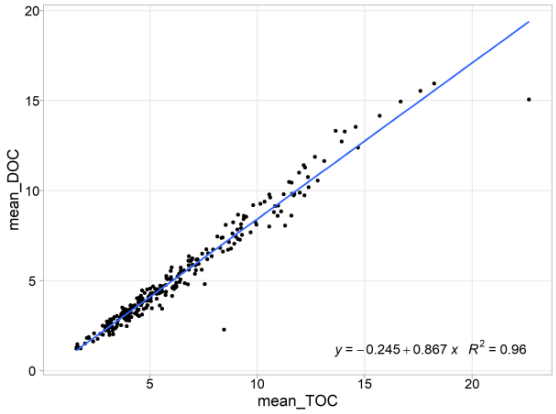

Figure S1. Scatterplot of mean DOC versus TOC concentrations with linear regression equation and coefficient of determination for independent C catchments (n=281).

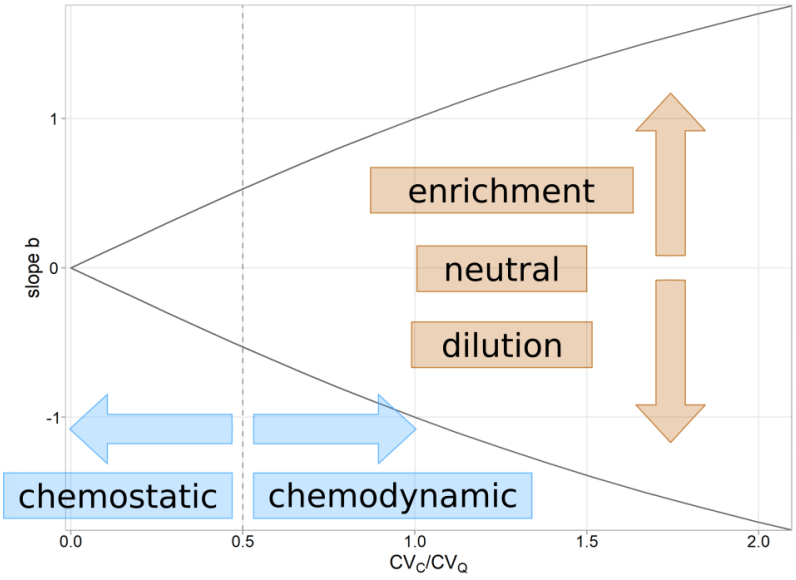

Figure S2. C-Q classification scheme as combinations of export regimes according to CV_C/CV_Q (blue) and export patterns according to slope b of C-Q relationships (orange). The solid lines indicate the theoretical boundaries between slope b and CV_C/CV_Q for CV_Q =0.6 [after Musolff et al., 2015].

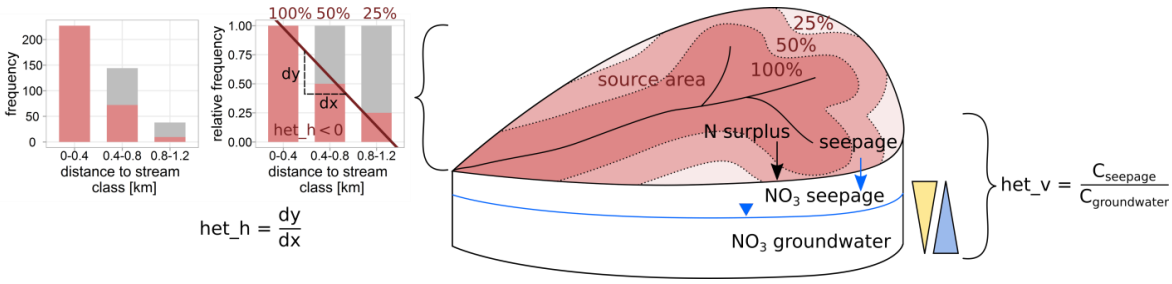

Figure S3. Conceptualized parameterization of horizontal source heterogeneity het_h (saturation of red area represents the fraction of source areas within each distance class) and vertical concentration heterogeneity het_v (yellow – top-loaded concentration profile, blue – bottom-loaded) for a simplified catchment. The example shows a catchment with more source areas close to the stream (the 0-400m distance class contains 100% of source area and the 800-1200m class only 25%). Red fractions in the histograms mark the frequencies of agricultural source area within the distance class. For simplicity, only three flow-distance classes are shown although more classes are used for the real catchments. The slope of the regression of the relative frequency histogram determines het_h, i.e. het_h < 0 represents systems with sources relatively close to the stream, het_h = 0 means that the sources are homogeneously distributed, and when het_h > 0, the sources are relatively far from the stream. For vertical heterogeneity: When het_v < 1 it represents a bottom-loaded, het_v = 1 homogeneous, and het_v > 1 represents a top-loaded concentration profile.

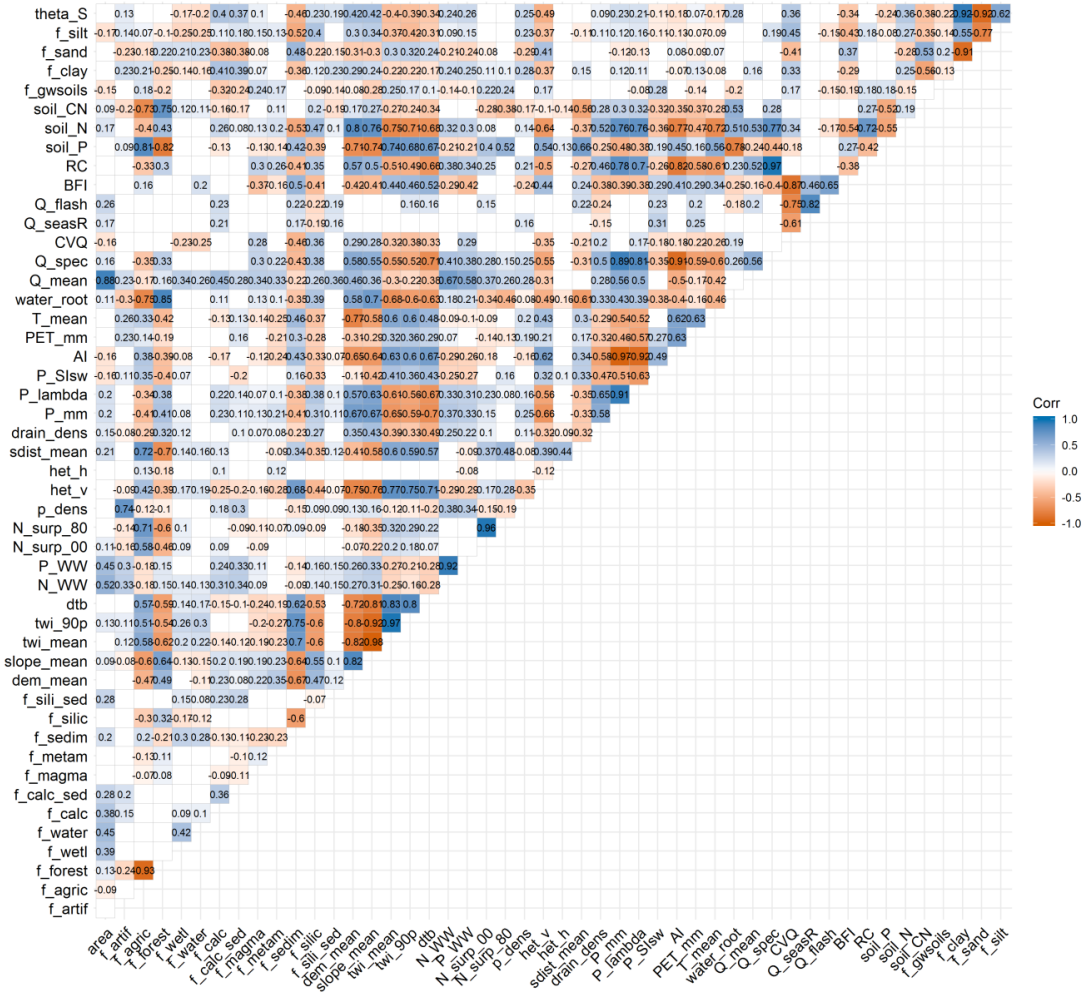

Figure S4. Spearman correlation coefficients among descriptors including horizontal source heterogeneity. Not significant coefficients (confidence level 95%) are shown in blank.

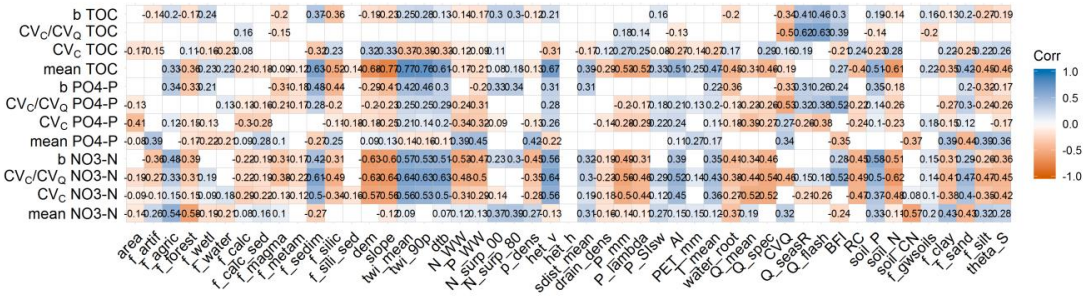

Figure S5. Spearman correlation coefficients between metrics and descriptors including horizontal source heterogeneity. Not significant coefficients (confidence level 95%) are shown in blank.

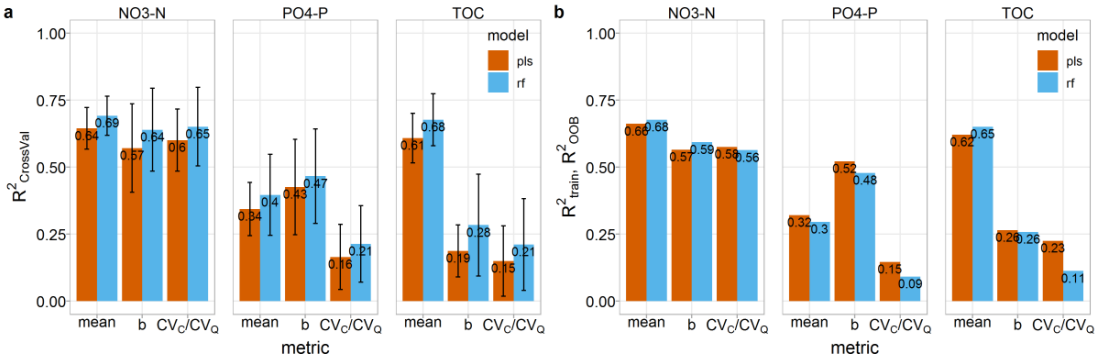

Figure S6. PLSR and RF model performances as mean R^2 of the cross-validation with error bars indicating the standard deviations among the 30 cross-validation folds (a) and of the final trained models, which was calculated from out-of-bag samples for RF models (b).

	NO_3-N	PO_4-P	TOC
Number of C-Q stations	274	236	255
Mean R2 ± standard deviation (median R2 ± interquartile range) of simple logC-logQ regression	0.27 ± 0.24 (0.22 ±0.41)	0.21 ±0.19 (0.15 ±0.30)	0.19 ±0.20 (0.13 ±0.26)
Number (fraction) of C-Q stations with superior segmented model	71 (25.9%)	52 (22.0%)	68 (26.7%)
Average R2 improvement of segmented model	8.0%	10.6%	10.5%

Table S1. Comparison Between Simple Power-Law and Segmented Power-Law Models for C-Q Relationships Using the Akaike Information Criterion (AIC). The more Complex Model was Considered Superior if the Difference in AIC Between the Simple and Segmented Model was >2.

Category	Variable	Unit	Description and method	Data source
Hydrology	Q_mean	$m^3 s^{-1}$	Mean discharge	
	Q_spec	mm	Mean annual specific discharge	
	CVQ	-	Coefficient of variation of discharge based on daily discharge values. Note: only used in correlation analysis, not used in regression models, because it is obviously linked to CV_C/CV_Q	
	RC	-	Runoff coefficient as ratio of specific Q and mean annual precipitation	
	Q_seasR	-	Seasonality index of Q as ratio between summer (May-Oct) and winter median discharge (Nov-Apr)	
	BFI	-	Base flow index using the lfstat package (version 0.9.4) in R	*WMO* [2008]
	Q_flash	km^{-1}	Flashiness index of Q as the ratio between 5% percentile (low-flow) and 95% percentile of Q (high-flow fraction) time series, i.e. the smaller the index, the more flashy the discharge. This index uses percentiles inspired by the *Jordan et al.* [2005]	

Table S2. Hydrological Descriptors Used in the Analysis, Associated Methods and Data Sources.

Model	Tuning			
	Selection Function	Description	Tune parameter	Tune grid
PLSR	tolerance, chooses the most complex model that improves mean RMSE from cross validation >2%	Number of components	ncomp	1:15
RF	-	Number of variables selected randomly at each split	Mtry	11
		Number of trees	ntree	500

Table S3. Parameters and Tuning Settings Used to Train the Models by the Caret Package. Note that for RF we Selected mtry Based on an Exemplary Tuning which Showed Similar Performances for Similar Values.

NO3	Mean concentration					b					CV_C/CV_Q				
Rank	n=684					n=236					n=237				
	PLSR			RF		PLSR			RF		PLSR			RF	
	$R^2_{CrossVal}$=0.65 (0.64)			$R^2_{CrossVal}$=0.69 (0.69)		$R^2_{CrossVal}$=0.55 (0.56)			$R^2_{CrossVal}$=0.58 (0.58)		$R^2_{CrossVal}$=0.61 (0.61)			$R^2_{CrossVal}$=0.67 (0.68)	
	R^2_{train}=0.67 (0.67)			R^2_{OOB}=0.68 (0.68)		R^2_{train}=0.59 (0.61)			R^2_{OOB}=0.51 (0.52)		R^2_{train}=0.57 (0.57)			R^2_{OOB}=0.51 (0.53)	
	Var.	VIP	Sign	Var.	Imp	Var.	VIP	Sign	Var.	Imp	Var.	VIP	Sign	Var.	Imp
1	f_forest	1.92	-	f_forest	20.7	het_v	1.61	+	twi_mean	10.2	het_v	1.69	+	het_v	10.7
2	f_agric	1.88	+	P_SIsw	16.4	twi_mean	1.49	+	slope_mean	9.7	f_sedim	1.65	+	soil_N	8.0
3	soil_CN	1.74	-	f_agric	15.5	dtb	1.47	+	soil_N	8.4	f_water	1.54	+	dem_mean	7.4
4	het_v	1.40	-	dem_mean	14.4	dem_mean	1.41	-	dem_mean	7.8	f_silt	1.47	-	slope_mean	7.2
5	f_sand	1.34	+	f_sedim	14.2	f_sedim	1.40	+	N_WW	7.5	dtb	1.44	+	f_sedim	6.1
6	water_root	1.32	+	P_mm	13.1	twi_90p	1.40	+	f_agric	7.2	f_sand	1.43	+	water_root	5.8
7	f_sedim	1.32	-	soil_CN	12.4	PET_mm	1.34	-	PET_mm	5.7	twi_mean	1.40	+	P_lambda	5.4
8	f_silt	1.24	-	het_v	11.6	soil_P	1.28	+	f_sedim	5.6	twi_90p	1.40	+	P_mm	5.1
9	f_clay	1.24	+	dtb	9.7	slope_mean	1.23	-	p_dens	5.2	P_lambda	1.31	-	twi_mean	5.1
10	f_gwsoils	1.22	+	AI	9.3	soil_N	1.16	-	dtb	5.0	AI	1.30	+	dtb	5.0
11	soil_P	1.16	+	drain_dens	9.0	N_WW	1.16	-	twi_90p	4.9	soil_N	1.28	-	T_mean	4.9
12	P_SIsw	1.12	+	f_magma	8.9	P_mm	1.14	-	soil_P	4.8	theta_S	1.25	-	twi_90p	4.7
13	theta_S	1.07	-	area	8.5	f_sand	1.12	-	T_mean	4.6	dem_mean	1.24	-	AI	3.9
14	P_mm	1.00	+	N_WW	8.4	f_artif	1.11	-	het_v	4.3	P_mm	1.16	-	soil_P	3.7
15	slope_mean	0.99	+	water_root	8.2	theta_S	1.11	+	f_silt	4.1	slope_mean	1.15	-	drain_dens	3.4
16	N_surp_80	0.97	-	P_lambda	8.0	f_silt	1.11	+	AI	3.9	f_clay	1.12	-	area	3.3
17	sdist_mean	0.94	-	soil_N	8.0	p_dens	1.10	-	water_root	3.8	drain_dens	1.02	-	p_dens	2.8
18	AI	0.85	+	slope_mean	7.5	AI	1.07	+	P_mm	3.8	f_forest	0.98	+	f_forest	2.7
19	soil_N	0.85	-	f_silt	7.5	sdist_mean	1.05	+	theta_S	3.8	soil_P	0.97	-	soil_CN	2.6
20	f_magma	0.85	+	f_gwsoils	7.4	water_root	1.04	+	sdist_mean	3.4	f_agric	0.95	-	PET_mm	2.6
21	N_surp_00	0.79	+	soil_P	7.2	P_lambda	1.03	-	N_surp_00	3.0	water_root	0.92	+	f_agric	2.6
22	P_lambda	0.79	+	twi_mean	7.1	f_agric	1.01	+	f_silic	3.0	f_silic	0.87	-	N_WW	2.6
23	T_mean	0.79	+	N_surp_00	7.0	f_clay	0.95	+	P_lambda	2.9	soil_CN	0.80	+	f_silt	2.4
24	f_artif	0.78	-	p_dens	7.0	f_forest	0.93	-	f_magma	2.9	sdist_mean	0.77	-	f_sili_sed	2.0
25	dtb	0.76	+	N_surp_80	7.0	drain_dens	0.82	-	f_clay	2.6	T_mean	0.73	+	N_surp_80	1.8
26	twi_mean	0.74	+	f_clay	6.8	f_silic	0.81	+	f_sand	2.5	N_WW	0.72	-	f_sand	1.7
27	twi_90p	0.74	+	sdist_mean	6.7	T_mean	0.78	-	N_surp_80	2.5	P_SIsw	0.57	+	f_silic	1.5
28	PET_mm	0.73	-	PET_mm	6.3	P_SIsw	0.74	-	drain_dens	2.5	p_dens	0.54	-	f_calc_sed	1.5
29	f_water	0.72	-	theta_S	6.2	f_wetl	0.67	-	f_forest	2.1	f_calc_sed	0.54	-	sdist_mean	1.4
30	drain_dens	0.70	-	f_artif	6.2	soil_CN	0.65	+	f_artif	1.9	f_gwsoils	0.54	-	N_surp_00	1.2
31	dem_mean	0.69	-	f_sand	6.2	f_magma	0.65	-	f_calc_sed	1.8	f_magma	0.51	-	f_clay	1.0
32	f_silic	0.66	+	T_mean	5.6	N_surp_80	0.62	+	f_metam	1.6	area	0.50	-	f_artif	0.9
33	f_calc_sed	0.64	+	twi_90p	5.5	f_calc_sed	0.60	-	P_SIsw	1.4	N_surp_80	0.50	-	f_magma	0.8
34	p_dens	0.63	+	f_silic	5.3	N_surp_00	0.49	+	f_wetl	1.1	f_artif	0.49	-	f_gwsoils	0.3
35	f_calc	0.62	+	f_calc_sed	4.9	f_gwsoils	0.47	-	soil_CN	0.9	PET_mm	0.46	+	P_SIsw	0.3
36	N_WW	0.58	+	f_water	3.9	f_water	0.45	-	area	0.7	N_surp_00	0.45	-	theta_S	0.2
37	f_wetl	0.55	-	het_h	3.7	f_calc	0.42	-	f_sili_sed	0.1	f_calc	0.39	-	f_wetl	0.1
38	f_metam	0.55	+	f_calc	3.4	f_sili_sed	0.40	-	het_h	-0.3	f_sili_sed	0.33	-	f_metam	-1.1
39	f_sili_sed	0.49	-	f_sili_sed	1.8	area	0.38	-	f_water	-1.3	f_metam	0.29	-	f_calc	-1.3
40	area	0.36	-	f_wetl	1.6	f_metam	0.32	-	f_gwsoils	-1.7	het_h	0.28	+	het_h	-1.4
41	het_h	0.34	+	f_metam	-1.7	het_h	0.20	+	f_calc	-3.1	f_wetl	0.12	+	f_water	-2.7

Table S4. PLSR and RF Results and Variable Rankings for NO3-N Metrics Including Variables of Horizontal Source Heterogeneity (sdist_mean, het_h). Values in Brackets Give the Reference Model Performances for the Same Subset of Catchments Without Horizontal Source Heterogeneity.

PO4	Mean concentration					b					CV_C/CV_Q				
Rank	n=626					n=210					n=227				
	PLSR			RF		PLSR			RF		PLSR			RF	
	$R^2_{CrossVal}$=0.40 (0.40)			$R^2_{CrossVal}$=0.40 (0.40)		$R^2_{CrossVal}$=0.33 (0.33)			$R^2_{CrossVal}$=0.38 (0.38)		$R^2_{CrossVal}$=0.22 (0.22)			$R^2_{CrossVal}$=0.21 (0.22)	
	R^2_{train}=0.41 (0.41)			R^2_{OOB}=0.38 (0.37)		R^2_{train}=0.40 (0.41)			R^2_{OOB}=0.36 (0.38)		R^2_{train}=0.23 (0.23)			R^2_{OOB}=0.11 (0.14)	
	Var.	VIP	Sign	Var.	Imp	Var.	VIP	Sign	Var.	Imp	Var.	VIP	Sign	Var.	Imp
1	P_WW	2.26	+	P_WW	21.0	N_surp_00	1.88	+	f_sedim	14.2	f_water	1.90	+	P_WW	8.1
2	p_dens	1.69	+	p_dens	10.8	N_surp_80	1.72	+	N_surp_00	9.4	f_wetl	1.48	+	area	7.3
3	f_artif	1.67	+	PET_mm	10.6	P_mm	1.68	+	twi_90p	8.9	f_sedim	1.47	+	drain_dens	6.2
4	soil_CN	1.64	-	f_silt	10.5	f_sedim	1.63	+	P_lambda	8.5	dtb	1.29	+	f_forest	5.7
5	PET_mm	1.48	+	soil_CN	9.6	twi_90p	1.41	+	N_surp_80	8.5	f_sand	1.28	+	T_mean	5.3
6	f_sand	1.46	-	dem_mean	8.8	twi_mean	1.33	+	PET_mm	7.6	slope_mean	1.28	+	slope_mean	5.3
7	T_mean	1.45	+	dtb	8.8	f_silic	1.33	-	P_SIsw	7.2	het_v	1.26	+	f_sili_sed	5.2
8	f_silt	1.39	+	f_silic	8.7	AI	1.28	-	f_sand	6.5	twi_mean	1.23	+	f_water	5.2
9	theta_S	1.30	+	T_mean	8.4	slope_mean	1.25	-	slope_mean	6.3	twi_90p	1.21	+	water_root	4.9
10	f_clay	1.29	-	f_artif	8.1	soil_N	1.23	+	P_mm	6.2	f_silt	1.20	-	soil_N	4.6
11	f_forest	1.16	-	AI	7.8	soil_P	1.17	+	dtb	6.1	P_lambda	1.18	-	P_lambda	4.3
12	het_v	1.12	-	het_v	7.8	P_lambda	1.17	+	f_silic	5.9	f_clay	1.14	-	f_wetl	4.1
13	AI	1.06	+	f_sand	7.7	dtb	1.17	+	AI	5.8	water_root	1.14	+	f_agric	3.6
14	P_mm	0.98	-	P_mm	7.6	water_root	1.16	-	soil_CN	5.5	AI	1.14	+	N_surp_00	3.6
15	f_calc_sed	0.96	-	f_sedim	7.0	sdist_mean	1.15	+	area	5.3	theta_S	1.12	-	PET_mm	3.5
16	f_sedim	0.92	-	theta_S	6.3	f_agric	1.08	+	soil_P	4.9	drain_dens	1.11	-	f_sedim	3.5
17	soil_P	0.89	+	P_SIsw	6.3	f_forest	1.03	-	twi_mean	4.9	soil_N	1.08	-	N_surp_80	3.5
18	f_agric	0.84	+	soil_P	6.2	dem_mean	0.99	+	p_dens	4.8	soil_P	1.08	-	f_sand	3.5
19	N_surp_00	0.81	-	f_calc_sed	5.9	f_sili_sed	0.99	+	f_calc_sed	4.8	P_WW	1.07	-	twi_mean	3.3
20	N_surp_80	0.79	-	soil_N	5.8	f_silt	0.93	-	dem_mean	4.6	dem_mean	1.02	-	het_v	3.3
21	P_lambda	0.77	-	f_forest	5.7	drain_dens	0.92	+	f_gwsoils	4.5	f_agric	1.01	-	dem_mean	3.2
22	dem_mean	0.76	-	f_clay	5.6	f_gwsoils	0.82	-	f_silt	4.4	P_mm	1.01	-	f_clay	3.1
23	soil_N	0.76	-	f_agric	5.4	het_v	0.80	-	f_magma	3.9	area	0.99	-	P_SIsw	3.1
24	water_root	0.71	-	slope_mean	5.1	PET_mm	0.73	+	f_artif	3.8	f_forest	0.98	+	theta_S	3.1
25	f_silic	0.65	+	twi_90p	5.1	area	0.71	+	soil_N	3.7	P_SIsw	0.94	+	P_mm	2.8
26	slope_mean	0.64	-	P_lambda	4.7	P_SIsw	0.67	+	f_agric	3.6	f_gwsoils	0.89	-	f_silt	2.7
27	dtb	0.62	+	water_root	4.6	f_sand	0.67	+	sdist_mean	3.1	sdist_mean	0.75	-	soil_P	2.2
28	f_water	0.60	-	sdist_mean	4.4	theta_S	0.67	-	water_root	2.6	f_silic	0.74	-	twi_90p	2.1
29	f_wetl	0.59	+	twi_mean	4.1	T_mean	0.60	+	theta_S	2.6	PET_mm	0.70	+	p_dens	2.0
30	sdist_mean	0.58	-	N_surp_00	3.8	f_magma	0.59	-	f_clay	2.3	soil_CN	0.66	+	AI	1.5
31	f_calc	0.57	-	f_gwsoils	3.4	soil_CN	0.54	-	T_mean	2.3	f_calc_sed	0.65	-	soil_CN	1.4
32	twi_90p	0.56	-	het_h	3.4	f_water	0.53	-	f_sili_sed	2.2	f_magma	0.63	-	dtb	1.4
33	twi_mean	0.53	-	area	2.8	P_WW	0.50	-	f_forest	2.2	T_mean	0.60	+	f_gwsoils	1.0
34	P_SIsw	0.52	-	N_surp_80	2.6	f_metam	0.48	-	f_calc	2.1	p_dens	0.45	-	f_calc	1.0
35	drain_dens	0.51	-	f_magma	2.5	f_clay	0.47	+	P_WW	1.8	het_h	0.42	+	f_magma	0.8
36	f_metam	0.48	-	drain_dens	2.3	f_calc	0.41	+	het_v	1.0	f_artif	0.38	-	sdist_mean	0.8
37	f_sili_sed	0.44	+	f_metam	1.8	p_dens	0.36	+	f_metam	0.7	N_surp_80	0.34	-	f_silic	0.1
38	het_h	0.29	-	f_wetl	1.7	f_calc_sed	0.28	-	drain_dens	0.6	N_surp_00	0.29	-	het_h	-0.9
39	area	0.24	-	f_water	1.6	f_artif	0.22	-	het_h	-0.4	f_sili_sed	0.28	-	f_artif	-1.4
40	f_magma	0.21	+	f_calc	1.4	f_wetl	0.21	+	f_water	-1.3	f_metam	0.26	+	f_metam	-1.9
41	f_gwsoils	0.13	-	f_sili_sed	1.3	het_h	0.05	-	f_wetl	-3.0	f_calc	0.25	-	f_calc_sed	-2.1

Table S5. PLSR and RF Results and Variable Rankings for PO4-P Metrics Including Variables of Horizontal Source Heterogeneity (sdist_mean, het_h). Values in Brackets Give the Reference Model Performances for the Same Subset of Catchments Without Horizontal Source Heterogeneity.

NO3	Mean concentration					b					CV_C/CV_Q				
Rank	n=759					n=274					n=275				
	PLSR $R^2_{CrossVal}$=0.64 R^2_{train}=0.66			RF $R^2_{CrossVal}$=0.69 R^2_{OOB}=0.68		PLSR $R^2_{CrossVal}$=0.57 R^2_{train}=0.57			RF $R^2_{CrossVal}$=0.64 R^2_{OOB}=0.59		PLSR $R^2_{CrossVal}$=0.60 R^2_{train}=0.58			RF $R^2_{CrossVal}$=0.65 R^2_{OOB}=0.56	
	Var.	**VIP**	**Sign**	**Var.**	**Imp**	**Var.**	**VIP**	**Sign**	**Var.**	**Imp**	**Var.**	**VIP**	**Sign**	**Var.**	**Imp**
1	f_forest	1.93	-	f_forest	20.3	het_v	1.66	+	slope_mean	11.5	het_v	1.70	+	het_v	10.2
2	f_agric	1.88	+	P_mm	17.4	twi_mean	1.55	+	twi_mean	11.2	f_sedim	1.58	+	twi_mean	9.3
3	soil_CN	1.82	-	P_SIsw	16.2	dtb	1.48	+	dem_mean	9.0	dtb	1.42	+	slope_mean	9.3
4	het_v	1.40	-	f_sedim	15.8	f_sedim	1.48	+	soil_N	8.1	f_silt	1.40	-	dem_mean	7.4
5	f_sand	1.38	+	het_v	14.4	twi_90p	1.47	+	PET_mm	7.7	twi_mean	1.37	+	f_sedim	6.9
6	f_clay	1.32	+	f_agric	13.9	dem_mean	1.46	-	P_mm	7.3	f_sand	1.36	+	soil_N	6.6
7	f_sedim	1.31	-	dem_mean	11.5	slope_mean	1.31	-	soil_P	7.1	twi_90p	1.36	+	soil_P	6.0
8	water_root	1.31	+	soil_CN	11.4	soil_P	1.25	+	f_agric	7.0	AI	1.30	+	P_mm	5.9
9	f_silt	1.27	-	soil_N	10.8	soil_N	1.20	-	water_root	6.6	P_lambda	1.29	-	twi_90p	5.9
10	f_gwsoils	1.20	+	P_lambda	10.7	N_WW	1.19	-	twi_90p	5.9	soil_N	1.26	-	f_agric	5.7
11	P_SIsw	1.13	+	dtb	10.1	f_artif	1.16	-	AI	5.5	f_water	1.25	+	T_mean	5.2
12	theta_S	1.10	+	N_surp_00	9.9	P_mm	1.16	-	f_sedim	5.4	dem_mean	1.25	-	water_root	5.0
13	soil_P	1.05	+	N_WW	9.9	water_root	1.10	+	het_v	5.2	theta_S	1.18	-	P_lambda	4.9
14	N_surp_80	0.94	-	twi_90p	9.8	f_silt	1.09	-	P_lambda	5.0	slope_mean	1.18	-	area	4.8
15	f_magma	0.94	+	AI	9.7	theta_S	1.08	-	f_artif	5.0	P_mm	1.16	-	dtb	4.7
16	P_mm	0.94	+	f_magma	9.3	f_sand	1.06	+	p_dens	4.9	f_clay	1.11	-	AI	4.6
17	slope_mean	0.90	-	soil_P	9.1	AI	1.05	+	theta_S	4.8	f_forest	1.05	+	f_forest	4.5
18	soil_N	0.84	-	f_gwsoils	8.7	PET_mm	1.05	-	N_WW	4.6	f_agric	1.01	-	f_sili_sed	4.0
19	T_mean	0.80	+	f_clay	8.6	p_dens	1.04	-	soil_CN	4.3	soil_P	1.01	-	soil_CN	3.9
20	PET_mm	0.79	-	f_silt	8.5	f_agric	1.04	+	T_mean	4.3	water_root	0.99	+	P_SIsw	3.9
21	AI	0.78	+	f_sand	8.4	P_lambda	0.98	-	f_clay	3.8	f_silic	0.91	-	theta_S	3.8
22	N_surp_00	0.75	+	p_dens	8.0	f_forest	0.93	-	P_SIsw	3.8	drain_dens	0.82	-	N_surp_00	3.4
23	f_water	0.70	-	water_root	7.9	f_silic	0.90	-	f_sand	3.4	T_mean	0.78	+	f_calc_sed	3.3
24	f_artif	0.69	-	area	7.9	f_clay	0.86	-	dtb	3.3	N_WW	0.73	-	f_clay	3.0
25	P_lambda	0.69	+	N_surp_80	7.9	T_mean	0.82	-	f_silt	3.1	soil_CN	0.71	+	p_dens	2.5
26	drain_dens	0.68	-	slope_mean	7.9	N_surp_80	0.71	+	drain_dens	3.1	N_surp_80	0.65	-	f_gwsoils	2.5
27	f_calc_sed	0.67	+	drain_dens	7.8	P_SIsw	0.64	-	N_surp_80	2.7	N_surp_00	0.60	-	N_surp_80	2.4
28	dtb	0.66	+	twi_mean	7.8	N_surp_00	0.61	+	f_calc_sed	2.6	p_dens	0.60	-	N_WW	2.3
29	twi_90p	0.65	-	theta_S	7.3	f_magma	0.60	-	f_magma	2.5	f_gwsoils	0.60	-	f_artif	2.3
30	p_dens	0.64	+	T_mean	6.9	f_gwsoils	0.55	+	f_wetl	2.5	f_calc_sed	0.59	-	f_silic	1.9
31	f_silic	0.63	+	PET_mm	6.4	f_calc_sed	0.54	-	f_silic	2.1	f_artif	0.58	-	PET_mm	1.8
32	twi_mean	0.63	+	f_artif	5.5	drain_dens	0.46	-	N_surp_00	2.0	P_SIsw	0.55	+	f_silt	1.8
33	dem_mean	0.62	-	f_calc_sed	5.2	f_sili_sed	0.45	-	f_metam	1.9	f_magma	0.53	-	f_sand	1.3
34	f_calc	0.57	+	f_water	5.2	f_calc	0.41	-	area	1.6	PET_mm	0.42	+	f_calc	1.2
35	N_WW	0.53	+	f_silic	4.8	f_metam	0.35	-	f_forest	1.5	f_calc	0.42	-	drain_dens	1.1
36	f_metam	0.51	+	f_sili_sed	3.9	f_water	0.34	-	f_sili_sed	0.8	f_sili_sed	0.35	-	f_magma	0.3
37	f_wetl	0.48	-	f_wetl	2.9	soil_CN	0.33	+	f_gwsoils	0.7	f_metam	0.31	-	f_wetl	0.2
38	f_sili_sed	0.44	-	f_calc	1.9	f_wetl	0.22	+	f_calc	-0.5	f_wetl	0.19	+	f_metam	-0.3
39	area	0.26	-	f_metam	-2.5	area	0.14	-	f_water	-1.9	area	0.09	-	f_water	-2.4

Table S6. Complete PLSR and RF Variable Rankings for NO3-N Metrics for the Complete Catchment Selection (Extended Table 3 from Manuscript).

PO4	Mean concentration					b					CV_C/CV_Q				
Rank	n=695					n=236					n=261				
	PLSR $R^2_{CrossVal}$=0.34 R^2_{train}=0.32			RF $R^2_{CrossVal}$=0.40 R^2_{OOB}=0.30		PLSR $R^2_{CrossVal}$=0.43 R^2_{train}=0.52			RF $R^2_{CrossVal}$=0.47 R^2_{OOB}=0.48		PLSR $R^2_{CrossVal}$=0.16 R^2_{train}=0.15			RF $R^2_{CrossVal}$=0.21 R^2_{OOB}=0.09	
	Var.	VIP	Sign	Var.	Imp	Var.	VIP	Sign	Var.	Imp	Var.	VIP	Sign	Var.	Imp
1	P_WW	2.04	+	P_WW	23.1	N_surp_00	1.82	+	f_sedim	15.0	f_sedim	1.79	+	T_mean	6.8
2	f_artif	1.71	+	dem_mean	9.2	N_surp_80	1.73	+	N_surp_00	13.1	f_sand	1.58	+	theta_S	5.8
3	soil_CN	1.67	-	f_silt	8.9	f_sedim	1.61	+	N_surp_80	12.7	het_v	1.55	+	twi_mean	5.6
4	p_dens	1.60	+	PET_mm	8.2	twi_90p	1.36	+	P_lambda	9.3	dtb	1.54	+	water_root	5.5
5	PET_mm	1.53	+	f_silic	7.4	soil_P	1.35	+	twi_90p	9.2	f_silt	1.51	-	dem_mean	5.2
6	f_sand	1.53	-	dtb	7.3	P_mm	1.35	+	P_SIsw	8.6	f_water	1.44	+	slope_mean	4.7
7	f_silt	1.45	+	P_SIsw	7.3	twi_mean	1.31	+	PET_mm	8.0	P_lambda	1.43	-	PET_mm	4.6
8	T_mean	1.39	+	AI	6.6	f_silic	1.30	-	f_silic	7.9	AI	1.42	+	soil_N	4.6
9	f_clay	1.37	+	f_sand	6.5	water_root	1.20	-	f_gwsoils	7.7	f_clay	1.40	-	f_sand	4.4
10	theta_S	1.35	+	p_dens	6.5	slope_mean	1.20	-	soil_CN	7.0	theta_S	1.37	-	N_surp_00	4.4
11	AI	1.15	+	T_mean	6.4	AI	1.16	-	AI	6.9	twi_90p	1.35	+	twi_90p	4.4
12	f_forest	1.12	-	soil_CN	6.3	P_lambda	1.15	+	dem_mean	6.9	twi_mean	1.27	+	f_clay	4.2
13	P_mm	1.02	-	f_artif	6.3	f_agric	1.09	+	soil_P	6.7	soil_N	1.25	-	f_sili_sed	4.0
14	P_lambda	0.93	-	P_mm	6.2	f_forest	1.05	-	slope_mean	6.7	P_WW	1.24	-	soil_P	4.0
15	f_calc_sed	0.91	-	f_sedim	6.1	dtb	1.04	+	f_sand	6.1	P_SIsw	1.07	+	f_agric	4.0
16	het_v	0.88	-	het_v	5.4	f_silt	1.04	-	f_calc_sed	6.0	drain_dens	1.01	-	f_water	3.8
17	f_sedim	0.88	-	f_calc_sed	5.0	soil_N	1.02	+	dtb	5.9	P_mm	0.98	-	f_forest	3.7
18	N_surp_00	0.80	-	water_root	4.8	dem_mean	0.95	-	area	5.7	dem_mean	0.96	-	het_v	3.5
19	drain_dens	0.75	-	soil_P	4.8	PET_mm	0.93	+	f_silt	5.6	f_silic	0.92	-	area	3.3
20	soil_N	0.74	-	slope_mean	4.7	f_gwsoils	0.93	-	twi_mean	5.5	PET_mm	0.87	+	f_sedim	3.2
21	N_surp_80	0.73	-	twi_mean	4.5	theta_S	0.92	-	f_magma	5.3	T_mean	0.78	+	N_surp_80	3.1
22	f_agric	0.68	-	f_agric	4.5	f_sili_sed	0.89	+	P_mm	5.2	f_calc_sed	0.74	-	P_lambda	3.1
23	water_root	0.66	-	theta_S	4.5	f_sand	0.85	+	water_root	4.8	f_wetl	0.74	+	f_silt	3.0
24	f_calc	0.65	-	f_forest	4.4	drain_dens	0.85	+	p_dens	4.7	slope_mean	0.72	-	P_SIsw	2.8
25	f_silic	0.63	+	f_clay	4.1	het_v	0.81	-	theta_S	4.6	f_magma	0.67	-	dtb	2.8
26	soil_P	0.63	+	soil_N	3.7	T_mean	0.74	+	f_clay	4.4	soil_P	0.58	+	f_wetl	2.7
27	slope_mean	0.62	-	N_surp_80	3.1	P_WW	0.72	-	soil_N	4.3	soil_CN	0.48	+	f_gwsoils	2.4
28	dem_mean	0.59	-	N_surp_00	3.1	f_water	0.67	-	f_agric	4.2	p_dens	0.45	-	soil_CN	2.3
29	f_water	0.56	-	f_water	3.1	f_clay	0.67	+	f_sili_sed	4.0	water_root	0.38	-	P_WW	2.2
30	P_SIsw	0.55	-	twi_90p	3.0	f_magma	0.66	-	f_forest	3.7	f_artif	0.35	-	f_calc	2.0
31	dtb	0.54	+	P_lambda	2.9	f_wetl	0.55	-	P_WW	3.6	f_calc	0.35	-	AI	1.9
32	twi_mean	0.54	+	f_metam	1.9	P_SIsw	0.50	-	T_mean	3.5	f_metam	0.27	-	drain_dens	1.4
33	twi_90p	0.51	-	drain_dens	1.8	f_metam	0.50	-	het_v	3.2	f_sili_sed	0.19	-	f_artif	1.2
34	f_wetl	0.50	-	f_sili_sed	1.7	f_calc	0.48	+	drain_dens	2.8	f_agric	0.18	+	f_silic	1.0
35	f_metam	0.40	-	f_wetl	1.3	f_calc_sed	0.36	-	f_calc	2.4	N_surp_80	0.17	+	p_dens	0.9
36	f_magma	0.34	+	area	1.2	p_dens	0.35	+	f_wetl	1.6	f_forest	0.14	-	P_mm	0.5
37	f_sili_sed	0.34	+	f_calc	1.0	soil_CN	0.25	+	f_artif	1.5	N_surp_00	0.13	+	f_calc_sed	0.3
38	area	0.24	-	f_gwsoils	-0.2	area	0.22	+	f_water	0.5	f_gwsoils	0.06	-	f_magma	-1.8
39	f_gwsoils	0.20	-	f_magma	-0.3	f_artif	0.12	+	f_metam	-1.2	area	0.01	+	f_metam	-2.5

Table S7. Complete PLSR and RF Variable Rankings for PO4-P Metrics for the Complete Catchment Selection (Extended Table 3 from Manuscript).

TOC	Mean concentration					b					CV_C/CV_Q				
Rank	n=722					n=255					n=256				
	PLSR $R^2_{CrossVal}$=0.61 R^2_{train}=0.62			RF $R^2_{CrossVal}$=0.68 R^2_{OOB}=0.65		PLSR $R^2_{CrossVal}$=0.19 R^2_{train}=0.26			RF $R^2_{CrossVal}$=0.28 R^2_{OOB}=0.26		PLSR $R^2_{CrossVal}$=0.15 R^2_{train}=0.23			RF $R^2_{CrossVal}$=0.21 R^2_{OOB}=0.11	
	Var.	VIP	Sign	Var.	Imp	Var.	VIP	Sign	Var.	Imp	Var.	VIP	Sign	Var.	Imp
1	twi_90p	1.71	+	dem_mean	14.2	N_surp_00	1.55	+	f_sedim	11.8	f_sedim	1.43	+	drain_dens	8.9
2	twi_mean	1.71	+	slope_mean	13.1	N_surp_80	1.46	+	N_surp_00	10.9	f_silic	1.36	-	f_calc	8.5
3	f_sedim	1.57	+	twi_mean	13.1	f_sedim	1.43	+	N_surp_80	8.6	soil_N	1.34	-	f_silt	7.7
4	slope_mean	1.46	-	twi_90p	12.0	f_silic	1.37	-	dem_mean	8.3	f_calc	1.33	+	P_SIsw	7.1
5	dem_mean	1.37	-	PET_mm	11.0	het_v	1.27	-	f_silt	8.0	T_mean	1.33	+	soil_P	5.8
6	dtb	1.36	+	f_sedim	9.9	AI	1.18	-	P_mm	7.8	f_gwsoils	1.31	-	P_mm	5.6
7	theta_S	1.33	-	soil_N	9.8	soil_P	1.17	+	T_mean	7.4	PET_mm	1.26	+	twi_mean	5.6
8	het_v	1.28	+	het_v	9.2	f_water	1.17	-	twi_90p	7.3	f_silt	1.24	-	f_magma	5.6
9	f_sand	1.28	-	P_lambda	9.1	drain_dens	1.17	-	P_lambda	7.3	f_forest	1.20	+	AI	5.6
10	f_silt	1.26	+	dtb	8.9	f_calc	1.15	+	het_v	7.2	dem_mean	1.19	-	soil_CN	5.5
11	soil_P	1.24	+	AI	8.8	twi_90p	1.14	+	soil_CN	7.1	f_sand	1.19	+	twi_90p	5.5
12	soil_N	1.18	+	T_mean	8.5	theta_S	1.12	-	P_SIsw	6.8	slope_mean	1.15	+	f_sedim	5.5
13	f_clay	1.12	+	f_water	8.4	twi_mean	1.11	+	twi_mean	6.7	f_agric	1.11	-	P_lambda	4.7
14	P_lambda	1.08	-	f_gwsoils	7.8	P_lambda	1.10	+	f_sand	6.7	twi_mean	1.07	-	dem_mean	4.6
15	P_mm	1.05	-	P_SIsw	7.5	P_mm	1.06	+	theta_S	6.3	twi_90p	1.04	-	f_gwsoils	4.5
16	AI	1.04	+	P_mm	7.3	f_silt	1.06	-	water_root	6.1	P_SIsw	1.04	+	f_forest	4.4
17	water_root	1.04	+	soil_P	7.2	PET_mm	1.05	+	PET_mm	6.0	theta_S	1.03	+	het_v	4.3
18	f_silic	1.01	-	f_silt	7.2	f_sand	1.04	+	AI	6.0	f_magma	1.01	-	slope_mean	4.2
19	T_mean	0.90	-	drain_dens	6.8	soil_N	1.01	-	dtb	6.0	soil_CN	1.00	+	f_silic	3.9
20	f_wetl	0.86	+	theta_S	6.3	f_clay	0.97	+	soil_P	5.9	f_clay	0.98	-	soil_N	3.8
21	f_forest	0.84	+	soil_CN	6.2	slope_mean	0.96	+	soil_N	5.7	dtb	0.95	-	PET_mm	3.8
22	PET_mm	0.80	-	N_surp_80	6.0	P_SIsw	0.95	+	f_magma	5.7	drain_dens	0.94	-	T_mean	3.6
23	f_agric	0.80	-	p_dens	6.0	f_artif	0.92	-	slope_mean	5.4	soil_P	0.94	-	f_agric	3.4
24	N_surp_80	0.74	+	water_root	4.5	dem_mean	0.92	+	f_forest	5.4	water_root	0.93	+	water_root	3.2
25	f_water	0.72	+	f_forest	4.4	water_root	0.91	+	f_silic	5.0	P_mm	0.89	+	f_sili_sed	3.2
26	soil_CN	0.70	+	f_silic	4.2	dtb	0.90	-	drain_dens	4.3	N_surp_00	0.80	+	theta_S	3.1
27	N_surp_00	0.69	+	f_magma	4.2	T_mean	0.80	+	f_wetl	4.2	het_v	0.78	-	f_calc_sed	2.9
28	drain_dens	0.68	+	f_sand	4.1	f_agric	0.79	-	f_agric	3.8	AI	0.78	-	N_surp_00	2.9
29	P_SIsw	0.60	+	f_agric	4.0	f_forest	0.79	+	f_calc	3.6	N_surp_80	0.77	+	N_surp_80	2.8
30	f_gwsoils	0.60	+	f_sili_sed	3.6	f_calc_sed	0.72	-	f_calc_sed	3.6	f_artif	0.73	-	f_wetl	1.8
31	f_calc_sed	0.48	-	f_clay	3.5	f_wetl	0.67	+	f_clay	3.5	P_lambda	0.71	+	f_clay	1.8
32	f_calc	0.37	-	N_surp_00	3.5	f_sili_sed	0.67	+	p_dens	2.7	f_calc_sed	0.67	-	f_artif	1.6
33	p_dens	0.35	+	f_calc_sed	3.1	soil_CN	0.62	+	f_sili_sed	1.9	p_dens	0.64	+	p_dens	1.5
34	f_sili_sed	0.34	-	f_wetl	3.0	p_dens	0.57	-	f_artif	1.4	f_metam	0.63	+	f_sand	1.0
35	f_artif	0.30	+	f_artif	1.3	f_gwsoils	0.51	+	f_gwsoils	1.4	f_water	0.51	-	f_water	0.5
36	f_metam	0.28	-	area	1.0	f_metam	0.45	-	area	1.3	f_sili_sed	0.50	+	dtb	-0.1
37	f_magma	0.23	+	f_calc	0.7	f_magma	0.31	-	f_water	0.6	area	0.38	-	f_metam	-1.0
38	area	0.10	-	f_metam	-0.3	area	0.16	-	f_metam	-1.0	f_wetl	0.20	+	area	-1.4

Table S8. Complete PLSR and RF Variable Rankings for TOC Metrics for the Complete Catchment Selection (Extended Table 3 from Manuscript).

NO3	Mean concentration					b					CV_C/CV_Q				
Rank	n=183					n=182					n=183				
	PLSR $R^2_{CrossVal}$=0.65 (0.64) R^2_{train}=0.73 (0.72)			RF $R^2_{CrossVal}$=0.71 (0.71) R^2_{OOB}=0.66 (0.66)		PLSR $R^2_{CrossVal}$=0.57 (0.58) R^2_{train}=0.58 (0.59)			RF $R^2_{CrossVal}$=0.64 (0.65) R^2_{OOB}=0.59 (0.60)		PLSR $R^2_{CrossVal}$=0.67 (0.67) R^2_{train}=0.64 (0.62)			RF $R^2_{CrossVal}$=0.74 (0.69) R^2_{OOB}=0.61 (0.56)	
	Var.	VIP	Sign	Var.	Imp	Var.	VIP	Sign	Var.	Imp	Var.	VIP	Sign	Var.	Imp
1	soil_CN	1.87	-	f_forest	13.2	twi_mean	1.64	+	twi_mean	11.0	f_sedim	1.61	+	het_v	8.7
2	f_forest	1.79	-	f_agric	12.2	f_sedim	1.61	+	slope_mean	10.7	het_v	1.52	+	slope_mean	7.9
3	f_sand	1.75	-	f_sedim	11.1	het_v	1.60	+	dem_mean	10.3	f_silt	1.44	-	f_sedim	7.4
4	f_clay	1.71	+	P_mm	10.6	dtb	1.59	+	twi_90p	7.1	dtb	1.38	+	BFI	7.1
5	het_v	1.70	-	soil_CN	10.0	twi_90p	1.54	+	soil_N	6.8	f_sand	1.38	+	dem_mean	6.3
6	f_sedim	1.69	-	N_WW	9.0	dem_mean	1.49	-	f_agric	6.7	f_water	1.34	+	twi_mean	6.2
7	f_agric	1.66	+	f_clay	8.2	slope_mean	1.45	-	f_sedim	6.5	AI	1.32	+	twi_90p	5.9
8	f_silt	1.62	+	AI	8.2	soil_N	1.29	-	soil_P	5.6	twi_mean	1.32	+	AI	5.6
9	theta_S	1.39	+	P_SIsw	8.1	soil_P	1.28	+	AI	4.5	BFI	1.31	+	P_mm	5.0
10	f_silic	1.12	+	het_v	8.0	PET_mm	1.27	-	theta_S	4.5	twi_90p	1.31	+	Q_seasR	4.5
11	f_water	1.03	-	P_lambda	7.6	P_mm	1.20	-	N_surp_80	4.5	P_lambda	1.31	-	soil_N	4.3
12	f_calc_sed	1.00	+	soil_P	7.4	f_silt	1.12	-	dtb	4.2	soil_N	1.29	-	Q_flash	4.2
13	BFI	0.98	+	dtb	6.9	AI	1.09	+	het_v	4.2	dem_mean	1.24	-	water_root	4.1
14	p_dens	0.93	+	Q_mean	6.9	Q_spec	1.07	-	T_mean	4.0	P_mm	1.22	-	p_dens	4.0
15	water_root	0.92	-	f_silic	6.9	f_agric	1.06	+	water_root	3.8	slope_mean	1.18	-	soil_P	3.9
16	dtb	0.91	-	PET_mm	6.7	N_WW	1.06	-	f_forest	3.7	theta_S	1.17	-	P_lambda	3.5
17	twi_90p	0.91	-	water_root	6.7	theta_S	1.06	-	N_WW	3.5	f_clay	1.13	-	T_mean	3.4
18	N_surp_80	0.89	+	theta_S	6.5	f_sand	1.05	+	f_clay	3.4	Q_flash	1.06	+	f_silt	3.1
19	soil_P	0.80	+	N_surp_00	6.3	T_mean	1.03	-	PET_mm	3.1	Q_spec	1.06	-	dtb	3.1
20	f_artif	0.80	+	twi_90p	6.3	P_lambda	1.03	-	RC	3.0	f_forest	1.05	+	N_WW	3.1
21	N_surp_00	0.79	+	drain_dens	6.1	water_root	1.02	+	P_mm	2.9	RC	1.03	-	f_calc_sed	3.0
22	P_SIsw	0.75	+	f_sand	5.9	f_artif	1.01	-	P_SIsw	2.7	f_agric	1.00	-	Q_spec	3.0
23	N_WW	0.74	-	f_silt	5.9	RC	1.01	-	f_calc_sed	2.7	f_silic	0.97	-	RC	3.0
24	twi_mean	0.74	-	Q_spec	5.8	f_silic	1.00	-	Q_spec	2.7	soil_P	0.97	-	N_surp_00	3.0
25	f_sili_sed	0.74	-	T_mean	5.8	p_dens	0.97	-	N_surp_00	2.6	T_mean	0.92	+	P_SIsw	2.9
26	f_gwsoils	0.73	+	dem_mean	5.4	f_forest	0.92	-	f_sand	2.5	drain_dens	0.91	-	f_silic	2.6
27	f_calc	0.73	+	slope_mean	5.4	BFI	0.86	+	p_dens	2.5	N_WW	0.91	-	f_clay	2.4
28	Q_spec	0.66	-	p_dens	5.4	f_clay	0.84	-	f_artif	2.4	water_root	0.84	+	f_artif	2.4
29	f_metam	0.66	+	twi_mean	5.3	N_surp_80	0.75	+	f_wetl	2.3	p_dens	0.70	-	f_agric	2.3
30	P_lambda	0.65	+	soil_N	5.2	f_magma	0.69	-	P_lambda	2.1	soil_CN	0.67	+	f_calc	2.2
31	soil_N	0.65	-	N_surp_80	4.9	Q_seasR	0.61	-	f_metam	2.0	N_surp_80	0.63	-	f_forest	2.2
32	T_mean	0.63	+	RC	4.1	N_surp_00	0.60	+	drain_dens	1.8	PET_mm	0.60	+	f_wetl	2.1
33	Q_flash	0.61	+	BFI	3.9	f_sili_sed	0.59	-	soil_CN	1.4	Q_seasR	0.59	+	f_sand	2.0
34	P_mm	0.60	-	f_gwsoils	3.3	P_SIsw	0.53	-	f_sili_sed	1.0	N_surp_00	0.58	-	f_gwsoils	2.0
35	dem_mean	0.59	+	f_artif	3.1	drain_dens	0.53	-	f_silt	1.0	f_magma	0.57	-	PET_mm	1.7
36	f_wetl	0.58	-	f_wetl	2.6	Q_mean	0.53	-	f_magma	0.7	f_calc_sed	0.57	-	drain_dens	1.4
37	Q_seasR	0.56	-	f_magma	2.6	Q_flash	0.45	-	f_silic	0.4	f_artif	0.56	-	theta_S	0.7
38	slope_mean	0.56	-	f_calc_sed	2.5	area	0.44	-	area	0.3	f_gwsoils	0.54	-	f_magma	0.7
39	AI	0.55	-	Q_seasR	1.7	f_water	0.42	-	f_gwsoils	0.3	P_SIsw	0.52	+	f_metam	0.6
40	drain_dens	0.52	-	f_sili_sed	1.2	f_calc_sed	0.36	-	f_calc	0.2	f_sili_sed	0.44	-	soil_CN	0.6
41	PET_mm	0.52	-	area	1.1	f_gwsoils	0.35	+	Q_mean	0.1	Q_mean	0.39	-	N_surp_80	0.5
42	RC	0.50	-	f_metam	1.0	f_metam	0.32	-	Q_flash	-0.6	f_metam	0.33	-	f_sili_sed	0.2
43	Q_mean	0.45	-	f_water	0.8	f_calc	0.31	-	f_water	-0.6	area	0.32	-	area	-0.1
44	area	0.36	-	Q_flash	0.1	f_wetl	0.27	+	Q_seasR	-1.1	f_calc	0.30	-	Q_mean	-0.2
45	f_magma	0.23	-	f_calc	-0.1	soil_CN	0.23	+	BFI	-1.3	f_wetl	0.16	+	f_water	-3.0

Table S9. PLSR and RF Results for NO3-N Metrics Including Hydrological Predictors as Descriptors. Values in Brackets Give the Reference Model Performances for the Same Subset of Catchments Without Hydrological Predictors.

PO4	Mean concentration					b					CV_C/CV_Q				
Rank	n=177					n=157					n=175				
	PLSR $R^2_{CrossVal}$=0.39 (0.39) R^2_{train}=0.43 (0.43)			RF $R^2_{CrossVal}$=0.50 (0.49) R^2_{OOB}=0.45 (0.44)		PLSR $R^2_{CrossVal}$=0.48 (0.48) R^2_{train}=0.63 (0.61)			RF $R^2_{CrossVal}$=0.50 (0.47) R^2_{OOB}=0.48 (0.45)		PLSR $R^2_{CrossVal}$=0.35 (0.25) R^2_{train}=0.36 (0.20)			RF $R^2_{CrossVal}$=0.41 (0.30) R^2_{OOB}=0.27 (0.14)	
	Var.	VIP	Sign	Var.	Imp	Var.	VIP	Sign	Var.	Imp	Var.	VIP	Sign	Var.	Imp
1	f_sand	1.78	-	p_dens	10.0	N_surp_00	1.71	+	N_surp_80	12.1	Q_flash	2.17	+	BFI	13.2
2	f_silt	1.76	+	f_artif	7.7	N_surp_80	1.58	+	N_surp_00	11.9	Q_seasR	1.74	+	Q_seasR	9.2
3	f_sedim	1.71	-	T_mean	7.7	f_sedim	1.46	+	f_sedim	10.8	BFI	1.67	+	Q_flash	6.8
4	theta_S	1.58	+	f_silic	7.6	soil_P	1.36	+	Q_seasR	10.2	f_sedim	1.33	+	AI	4.9
5	f_clay	1.57	+	f_forest	7.6	twi_90p	1.29	+	f_gwsoils	8.6	AI	1.31	+	Q_spec	4.6
6	p_dens	1.54	+	f_sand	7.1	twi_mean	1.21	+	P_SIsw	7.6	P_lambda	1.26	-	f_clay	4.0
7	soil_CN	1.34	-	f_silt	6.8	Q_seasR	1.20	+	soil_P	7.3	dtb	1.23	+	soil_N	3.7
8	het_v	1.31	-	f_sedim	6.6	P_mm	1.18	+	twi_90p	6.7	slope_mean	1.23	+	PET_mm	3.6
9	P_WW	1.27	+	dem_mean	6.4	water_root	1.17	-	soil_CN	6.4	twi_mean	1.22	+	het_v	3.6
10	twi_90p	1.26	-	f_clay	6.3	P_WW	1.16	-	dem_mean	6.3	twi_90p	1.21	+	dem_mean	3.6
11	f_artif	1.23	+	Q_spec	6.1	T_mean	1.16	+	dtb	5.6	f_water	1.20	+	T_mean	3.5
12	f_forest	1.19	-	slope_mean	5.9	slope_mean	1.15	+	Q_flash	5.6	soil_N	1.19	-	theta_S	3.3
13	f_silic	1.15	+	RC	5.6	f_silic	1.12	-	P_mm	5.6	f_silt	1.18	-	water_root	3.2
14	twi_mean	1.15	-	theta_S	5.5	theta_S	1.10	+	f_silic	5.6	f_sand	1.15	+	slope_mean	2.7
15	T_mean	1.15	+	P_SIsw	5.5	P_lambda	1.09	+	T_mean	5.3	dem_mean	1.13	+	P_lambda	2.6
16	f_sili_sed	1.08	+	AI	5.5	f_silt	1.05	-	twi_mean	5.2	P_WW	1.10	-	P_SIsw	2.5
17	BFI	1.01	-	het_v	5.3	AI	1.03	-	slope_mean	5.1	P_mm	1.09	-	Q_mean	2.4
18	f_water	0.93	-	P_WW	5.2	P_SIsw	1.02	-	f_magma	4.8	het_v	1.09	+	RC	2.4
19	PET_mm	0.91	+	soil_CN	5.0	dem_mean	1.02	-	Q_mean	4.6	Q_spec	1.04	+	f_silic	2.4
20	f_agric	0.90	+	PET_mm	4.8	f_sand	1.01	-	Q_spec	4.5	theta_S	0.98	-	soil_P	2.3
21	f_calc_sed	0.86	+	dtb	4.7	dtb	0.99	-	P_WW	4.5	drain_dens	0.96	-	f_sand	2.2
22	soil_P	0.84	+	drain_dens	4.5	Q_flash	0.98	-	theta_S	4.4	RC	0.96	+	f_silt	2.1
23	dtb	0.81	-	water_root	4.2	f_sili_sed	0.98	+	AI	4.3	f_clay	0.95	-	P_WW	2.0
24	Q_spec	0.80	-	twi_90p	4.1	Q_spec	0.96	+	f_sand	4.1	soil_P	0.91	-	drain_dens	2.0
25	water_root	0.79	-	f_agric	3.9	f_agric	0.93	-	f_silt	3.8	PET_mm	0.89	+	twi_90p	1.9
26	N_surp_00	0.76	-	P_lambda	3.7	f_forest	0.93	+	BFI	3.8	f_silic	0.87	-	area	1.8
27	N_surp_80	0.76	-	P_mm	3.7	soil_N	0.89	+	soil_N	3.7	T_mean	0.86	+	f_sedim	1.8
28	slope_mean	0.76	+	f_wetl	3.4	f_clay	0.89	+	f_agric	3.5	f_agric	0.85	-	f_calc	1.7
29	dem_mean	0.75	-	soil_P	3.3	f_gwsoils	0.87	-	RC	3.4	f_forest	0.82	+	N_surp_80	1.7
30	P_mm	0.74	-	twi_mean	3.2	RC	0.87	+	f_sili_sed	3.4	P_SIsw	0.78	+	f_sili_sed	1.6
31	soil_N	0.74	-	f_calc_sed	2.9	drain_dens	0.80	+	PET_mm	3.2	f_gwsoils	0.77	-	N_surp_00	1.5
32	AI	0.71	+	soil_N	2.9	het_v	0.80	+	P_lambda	3.2	water_root	0.77	+	f_artif	1.4
33	drain_dens	0.66	-	Q_mean	2.9	f_water	0.79	-	area	3.2	f_magma	0.50	-	P_mm	1.1
34	RC	0.66	-	Q_flash	2.9	BFI	0.79	-	water_root	3.1	f_metam	0.47	-	f_gwsoils	1.0
35	f_metam	0.61	-	f_calc	2.7	PET_mm	0.78	+	p_dens	2.9	f_calc_sed	0.44	-	f_metam	1.0
36	f_wetl	0.56	-	f_water	2.4	f_metam	0.78	+	f_clay	2.7	N_surp_80	0.43	-	f_water	1.0
37	P_lambda	0.53	-	f_gwsoils	2.4	Q_mean	0.74	+	f_forest	2.2	p_dens	0.40	-	f_calc_sed	0.8
38	Q_mean	0.47	-	f_metam	1.6	f_calc_sed	0.74	-	f_calc_sed	2.0	N_surp_00	0.39	-	f_forest	0.6
39	Q_flash	0.47	-	area	1.5	area	0.72	+	drain_dens	1.3	soil_CN	0.37	+	dtb	0.5
40	f_calc	0.44	+	f_magma	1.3	f_magma	0.62	-	f_water	0.8	f_wetl	0.35	+	f_wetl	0.5
41	Q_seasR	0.36	-	Q_seasR	1.1	f_wetl	0.58	-	f_calc	0.6	f_calc	0.34	+	f_magma	0.2
42	area	0.33	-	BFI	0.5	soil_CN	0.45	+	f_wetl	0.5	area	0.33	-	twi_mean	0.1
43	f_magma	0.31	+	f_sili_sed	0.5	f_calc	0.43	-	het_v	0.5	Q_mean	0.32	-	soil_CN	-0.7
44	f_gwsoils	0.26	-	N_surp_00	0.4	f_artif	0.43	-	f_artif	0.4	f_sili_sed	0.30	-	p_dens	-1.3
45	P_SIsw	0.22	-	N_surp_80	-0.1	p_dens	0.30	+	f_metam	-0.7	f_artif	0.22	-	f_agric	-1.4

Table S10. PLSR and RF Results for PO4-P Metrics Including Hydrological Predictors as Descriptors. Values in Brackets Give the Reference Model Performances for the Same Subset of Catchments Without Hydrological Predictors.

TOC	Mean concentration					b					CV_C/CV_Q				
Rank	n=185					n=184					n=184				
	PLSR $R^2_{CrossVal}$=0.70 (0.69) R^2_{train}=0.73 (0.72)			RF $R^2_{CrossVal}$=0.78 (0.77) R^2_{OOB}=0.75 (0.74)		PLSR $R^2_{CrossVal}$=0.39 (0.19) R^2_{train}=0.41 (0.16)			RF $R^2_{CrossVal}$=0.44 (0.33) R^2_{OOB}=0.42 (0.29)		PLSR $R^2_{CrossVal}$=0.58 (0.21) R^2_{train}=0.71 (0.26)			RF $R^2_{CrossVal}$=0.56 (0.26) R^2_{OOB}=0.49 (0.17)	
	Var.	VIP	Sign	Var.	Imp	Var.	VIP	Sign	Var.	Imp	Var.	VIP	Sign	Var.	Imp
1	twi_mean	1.70	+	dem_mean	14.4	Q_flash	2.13	+	Q_flash	13.4	Q_flash	3.60	+	Q_flash	18.2
2	twi_90p	1.65	+	slope_mean	11.1	Q_seasR	1.70	+	Q_seasR	13.1	Q_seasR	2.75	+	Q_seasR	13.0
3	f_sedim	1.60	+	twi_mean	9.3	N_surp_00	1.35	+	N_surp_00	7.6	BFI	2.11	+	BFI	9.2
4	soil_P	1.50	+	AI	8.4	N_surp_80	1.32	+	f_silic	6.7	f_gwsoils	1.35	-	twi_90p	6.8
5	slope_mean	1.43	-	soil_N	7.9	BFI	1.28	+	T_mean	6.2	f_forest	0.98	+	twi_mean	4.9
6	dem_mean	1.37	-	het_v	7.8	f_silic	1.28	-	f_sedim	6.2	f_calc	0.97	+	slope_mean	4.8
7	dtb	1.34	+	T_mean	7.8	f_sedim	1.24	+	twi_90p	6.0	drain_dens	0.94	+	AI	4.5
8	theta_S	1.32	-	P_mm	7.7	f_water	1.21	-	dem_mean	6.0	area	0.89	-	T_mean	3.9
9	f_silt	1.26	-	PET_mm	7.6	theta_S	1.20	-	AI	6.0	f_agric	0.89	-	dem_mean	3.8
10	f_sand	1.25	+	P_lambda	7.5	soil_P	1.19	+	theta_S	5.8	soil_CN	0.88	+	soil_N	3.7
11	het_v	1.23	+	twi_90p	6.5	twi_90p	1.19	+	P_lambda	5.4	f_water	0.87	-	f_silt	3.6
12	soil_N	1.15	-	soil_P	6.4	f_silt	1.18	-	f_silt	5.1	Q_mean	0.86	+	f_calc	3.4
13	water_root	1.13	+	f_sedim	6.1	twi_mean	1.18	+	BFI	5.1	f_silt	0.82	-	f_sedim	3.2
14	f_clay	1.08	-	Q_flash	5.8	f_sand	1.15	+	N_surp_80	5.1	f_sand	0.78	-	RC	2.9
15	P_mm	1.06	-	RC	5.8	AI	1.08	-	twi_mean	4.8	soil_P	0.76	-	drain_dens	2.8
16	f_gwsoils	1.04	+	f_gwsoils	5.8	het_v	1.07	-	f_clay	4.8	P_SIsw	0.76	+	f_wetl	2.8
17	f_wetl	1.02	+	P_SIsw	5.8	water_root	1.04	-	f_sand	4.7	f_clay	0.68	+	Q_spec	2.8
18	N_surp_80	1.01	+	f_sand	5.6	Q_spec	1.03	+	soil_P	4.3	PET_mm	0.68	+	soil_P	2.6
19	f_silic	1.00	-	BFI	5.6	slope_mean	1.01	-	Q_spec	4.2	twi_90p	0.68	-	dtb	2.6
20	f_agric	0.96	+	Q_seasR	5.3	RC	1.01	+	RC	4.2	het_v	0.65	-	PET_mm	2.5
21	P_lambda	0.95	-	Q_spec	5.3	P_mm	1.00	+	P_mm	4.2	twi_mean	0.64	-	P_mm	2.4
22	N_surp_00	0.94	+	theta_S	5.0	f_clay	0.99	+	het_v	4.2	f_sili_sed	0.63	-	water_root	2.2
23	PET_mm	0.94	-	N_surp_80	4.9	dem_mean	0.95	-	water_root	3.9	dem_mean	0.61	-	Q_mean	2.0
24	AI	0.94	+	f_clay	4.7	dtb	0.94	+	f_water	3.8	f_artif	0.59	-	f_clay	1.9
25	T_mean	0.92	-	f_silt	4.5	soil_N	0.92	-	PET_mm	3.8	theta_S	0.57	+	P_SIsw	1.9
26	f_forest	0.92	-	drain_dens	4.4	P_lambda	0.91	+	slope_mean	3.8	N_surp_80	0.56	+	f_artif	1.8
27	Q_spec	0.91	-	N_surp_00	4.1	T_mean	0.85	-	soil_N	3.6	slope_mean	0.56	-	f_agric	1.7
28	Q_flash	0.90	-	f_agric	4.1	f_agric	0.81	+	f_gwsoils	3.1	f_calc_sed	0.56	-	theta_S	1.7
29	RC	0.85	+	dtb	3.5	f_artif	0.76	-	P_SIsw	3.1	water_root	0.54	-	f_silic	1.7
30	BFI	0.77	-	f_forest	3.2	f_forest	0.72	-	f_forest	3.0	f_sedim	0.53	+	f_sand	1.7
31	f_calc_sed	0.68	-	f_water	2.9	p_dens	0.66	-	f_agric	2.6	RC	0.53	+	area	1.6
32	drain_dens	0.66	+	soil_CN	2.9	Q_mean	0.65	-	dtb	2.4	N_surp_00	0.52	+	N_surp_00	1.5
33	soil_CN	0.57	+	f_metam	2.5	f_sili_sed	0.64	+	Q_mean	2.1	f_silic	0.50	-	soil_CN	1.4
34	Q_seasR	0.55	-	f_silic	2.5	f_calc	0.58	+	f_artif	1.9	P_lambda	0.50	+	f_gwsoils	1.3
35	f_calc	0.54	-	water_root	2.2	drain_dens	0.57	-	f_wetl	1.8	soil_N	0.48	-	f_metam	1.3
36	f_magma	0.47	-	area	1.8	PET_mm	0.55	-	drain_dens	1.6	f_metam	0.46	-	f_forest	1.2
37	f_water	0.45	+	f_wetl	1.7	f_wetl	0.55	+	soil_CN	1.4	Q_spec	0.46	+	P_lambda	1.2
38	Q_mean	0.43	-	f_sili_sed	1.5	f_magma	0.51	+	f_magma	0.7	p_dens	0.45	-	f_magma	0.9
39	p_dens	0.41	-	f_calc	1.0	area	0.50	-	f_metam	0.4	AI	0.45	+	N_surp_80	0.8
40	f_sili_sed	0.40	-	f_calc_sed	0.7	P_SIsw	0.49	+	area	0.3	T_mean	0.44	+	f_calc_sed	0.7
41	P_SIsw	0.40	+	Q_mean	0.4	f_calc_sed	0.49	-	f_calc_sed	0.2	dtb	0.42	-	het_v	0.6
42	area	0.36	-	f_artif	0.3	f_gwsoils	0.44	+	p_dens	0.1	f_magma	0.40	-	p_dens	0.2
43	f_metam	0.30	+	f_magma	0.2	soil_CN	0.34	+	f_calc	-0.3	P_mm	0.40	-	f_water	-1.3
44	f_artif	0.29	-	p_dens	-0.2	f_metam	0.32	-	f_sili_sed	-1.7	f_wetl	0.38	+	f_sili_sed	-1.4

Table S11. PLSR and RF Results for TOC Metrics Including Hydrological Predictors as Descriptors. Values in Brackets Give the Reference Model Performances for the Same Subset of Catchments Without Hydrological Predictors.

Jordan, P., W. Menary, K. Daly, G. Kiely, G. Morgan, P. Byrne, and R. Moles (2005), Patterns and processes of phosphorus transfer from Irish grassland soils to rivers—integration of laboratory and catchment studies, *Journal of Hydrology*, *304*(1), 20-34.
Musolff, A., C. Schmidt, B. Selle, and J. H. Fleckenstein (2015), Catchment controls on solute export, *Advances in Water Resources*, *86*, 133-146.
WMO (2008), Manual on Low-flow Estimation and Prediction, World Meteorological Organization.

Study 2: Long-Term Nitrate Trajectories Vary by Season in Western European Catchments

Status:	Published in Global Biogeochemical Cycles
DOI:	10.1029/2021GB007050
Authors:	Pia Ebeling, Rémi Dupas, Benjamin Abbott, Rohini Kumar, Sophie Ehrhardt, Jan H. Fleckenstein, Andreas Musolff

PE carried out the study, prepared visualizations of results and wrote the manuscript. PE, RD and AM conceptualized and designed the study. PE processed and curated the data with contributions from several authors: RK provided the gridded meteorological time series, simulated discharge data for German catchments and atmospheric deposition data, SE conducted the gap filling of discharge data and consistency checks of the N surplus data. All authors contributed to the reviewing and editing of the manuscript.

Own contribution:

Study concept and design:	90 %
Data analysis:	90 %
Preparation of figures and tables:	100 %
Interpretation of the results:	90 %
Preparation of the manuscript:	90 %

Global Biogeochemical Cycles®

RESEARCH ARTICLE
10.1029/2021GB007050

Long-Term Nitrate Trajectories Vary by Season in Western European Catchments

Pia Ebeling[1], Rémi Dupas[2], Benjamin Abbott[3], Rohini Kumar[4], Sophie Ehrhardt[1], Jan H. Fleckenstein[1,5], and Andreas Musolff[1]

[1]Department of Hydrogeology, Helmholtz Centre for Environmental Research-UFZ, Leipzig, Germany, [2]UMR SAS, INRAE, Institut Agro, Rennes, France, [3]Department of Plant and Wildlife Sciences, Brigham Young University, Provo, UT, USA, [4]Department of Computational Hydrosystems, Helmholtz Centre for Environmental Research-UFZ, Leipzig, Germany, [5]Bayreuth Center of Ecology and Environmental Research (BayCEER), University of Bayreuth, Bayreuth, Germany

Key Points:

- Spatial patterns of nitrate and discharge seasonality are linked to topography and hydroclimate with winter maxima dominating for both
- After decreasing nutrient inputs, cases with decreases in river nitrate preceding during low- and high-flow seasons occurred equally often
- Spatial variability of nitrate seasonality is greater and more predictable from catchment characteristics than its long-term variability

Supporting Information:

Supporting Information may be found in the online version of this article.

Correspondence to:

P. Ebeling,
pia.ebeling@ufz.de

Citation:

Ebeling, P., Dupas, R., Abbott, B., Kumar, R., Ehrhardt, S., Fleckenstein, J. H., & Musolff, A. (2021). Long-term nitrate trajectories vary by season in Western European catchments. *Global Biogeochemical Cycles*, *35*, e2021GB007050. https://doi.org/10.1029/2021GB007050

Received 21 APR 2021
Accepted 7 AUG 2021

Abstract Human alteration of nutrient cycles has caused persistent and widespread degradation of water quality around the globe. In many regions, including Western Europe, elevated nitrate (NO_3^-) concentration in surface waters contributes to eutrophication and noncompliance with environmental legislation. Discharge, NO_3^- concentrations and the vulnerability of the aquatic ecosystems to eutrophication often exhibit a distinct seasonality. Understanding spatial patterns and long-term trends in this seasonality is crucial to improve water quality management. Here, we hypothesized that NO_3^- concentrations during high-flow periods would respond faster to changes in nutrient inputs than low-flow concentrations because of greater connectivity of shallow diffuse NO_3^- sources with the river network. To test this hypothesis, we compiled long-term NO_3^- and discharge time series from 290 Western European catchments. To characterize the long-term trajectories of seasonal NO_3^- concentration, we propose a novel hysteresis approach comparing low- and high-flow NO_3^- concentration in the context of multi-decadal N input changes. We found synchronous winter maxima of NO_3^- and discharge in 84% of the study catchments. However, contrary to our hypothesis, there were surprisingly diverse long-term trajectories of seasonal NO_3^- concentration. Both clockwise (faster high-flow NO_3^- response) and counterclockwise hysteresis (faster low-flow NO_3^- response) occurred in similar proportions, potentially due to a high complexity in the underlying processes. Spatial variability of seasonality in NO_3^- concentration across the catchments was more pronounced and better predictable than its long-term variability. This work demonstrates the value of seasonal and inter-annual hydrochemical analysis and provides new tools for water quality monitoring and management.

Plain Language Summary Nitrogen is an essential element of all living organisms and has thus often been used excessively as fertilizer to secure food production. However, surface waters can suffer from elevated nutrients inputs, causing toxic algal blooms and impairing drinking water quality, especially during summer low flows. To manage water quality, it is crucial to understand these seasonal variations of nitrogen and discharge and the underlying processes. We used data from 290 catchments in France and Germany to characterize average seasonality patterns and their long-term evolution across the variety of landscapes and human influences. This allowed classifying catchment behavior and linking them to controls. As expected, both nitrogen and discharge peak during winter in most catchments (84%). However, there are well explainable deviations, for example, in mountainous regions. The long-term evolution of seasonality was more diverse than expected suggesting a complex interplay of various processes with the long input history from fertilization and wastewater being part of the controls. We found that the differences among catchments were greater than the long-term changes of seasonality within most catchments. By identifying catchment typologies, our study increases the understanding of nitrate seasonality patterns across a large extent and thus supports ecological water quality management.

1. Introduction

Many of the Earth's great biogeochemical cycles and nearly all of its ecosystems have been intensely influenced by human activities (Abbott et al., 2019; Vitousek et al., 1997). Some of the most dramatic changes have been associated with global nutrient cycles, with human inputs of reactive nitrogen (N) and phosphorus

Global Biogeochemical Cycles 10.1029/2021GB007050

(P) exceeding natural sources (Steffen et al., 2015). This global nutrient overload has triggered widespread eutrophication, causing toxic cyanobacterial blooms and expansive hypoxic "dead zones" in freshwater and coastal areas and impairing drinking water resources (Diaz & Rosenberg, 2008; Le Moal et al., 2019).

Diffuse agricultural sources are the dominant source of N (e.g., excessive fertilizer application and cultivation of N-fixing crops), but mitigation measures, such as reducing N input, often do not immediately lead to improved riverine water quality (Bouraoui & Grizzetti, 2011). Time lags between changes in N inputs and riverine N concentration can range from immediate to several decades due to legacy storage (e.g., Bouraoui & Grizzetti, 2011; Dupas et al., 2020; Ehrhardt et al., 2020; Meals et al., 2010). Factors that contribute to these time lags include fixation and long transit times in soils (Kumar et al., 2020; Sebilo et al., 2013; Van Meter et al., 2016), in vadose zone (Ascott et al., 2017) and in groundwater (Kolbe et al., 2016; Wang et al., 2016) affecting water quality trajectories of catchments (i.e., the long-term evolution of the catchment's response under changing external forcing) (Hamilton, 2012; Van Meter & Basu, 2015, 2017).

The nutrient-triggered eutrophication in freshwater resources shows a strongly seasonal behavior because its controlling factors light, temperature, and nutrient concentrations fluctuate intra-annually. As aquatic ecological communities are sensitive to those nutrient fluctuations, understanding these seasonal dynamics is necessary to assess and reduce the impact of nutrient pollution. Understanding the factors creating seasonal patterns of riverine N concentrations, discharge and thus flux and their trends could improve our ability to predict response times, long-term pollution trajectories, and priority locations for management interventions (Frei et al., 2020). This calls for large sample approaches to identify catchment typologies (i.e., archetypes) in seasonal water quantity and quality dynamics (e.g., Gupta et al., 2014; Newcomer et al., 2021) and to couple the seasonal time-scale with the long-term trajectories.

Patterns of seasonal N concentration variability are controlled by various interacting physical, climatic, biological, and anthropogenic factors, which vary among catchments. First, the relative contributions of point and diffuse sources can affect concentration seasonality (Van Meter et al., 2020). Point source dominance often leads to highest concentrations during low flow, while diffuse N sources are often exported with higher discharges (Abbott, Moatar, et al., 2018; Van Meter et al., 2020). Second, hydrological connectivity can variably activate heterogeneously distributed solute sources within the catchment as discharge fluctuates at seasonal or event scales (Aubert et al., 2013; Dupas et al., 2016; Seibert et al., 2009). For example, the vertical distribution of solutes in the subsurface can control the concentration-discharge (*C*-*Q*) relationship (Botter et al., 2020; Ebeling et al., 2021; Zhi & Li, 2020) at event, seasonal, and inter-annual scales (Minaudo et al., 2019; Moatar et al., 2017; Musolff et al., 2015; Zarnetske et al., 2018). Third, seasonal variations in hydroclimatic drivers and biogeochemical controls such as riparian or in-stream retention processes can create seasonal variations of riverine N concentrations (Casquin et al., 2020; Kumar et al., 2020; Lutz et al., 2020). For example, during summer low-flow conditions, biological N uptake and removal processes in the benthic and hyporheic zones can more strongly influence water column chemistry because residence times and temperature are higher (Moatar et al., 2017; Wollheim et al., 2017). Conversely, during high-flow periods, the larger flux of nutrients and the disturbance of aquatic nutrient uptake via scouring and sedimentation can result in minimal biological influence on stream chemistry (Blaszczak et al., 2019; Raymond et al., 2016). Among other things, this makes high-flow conditions the most important to nutrient flux, but summer low-flow conditions the most sensitive to eutrophication (e.g., Minaudo et al., 2020; Withers & Jarvie, 2008).

The seasonal variability of N concentrations can be characterized in terms of annual amplitude and timing of the minimum and maximum concentrations. Applied to multi-annual concentration time series this allows identification of long-term controls of seasonality, including strength and type of nutrient loading, which can change through time (Howden et al., 2010; Westphal et al., 2020). For example, decreases in point and diffuse source strength are expected to have greater influence on low-flow and high-flow concentrations, respectively (Abbott, Moatar, et al., 2018). More generally, decreases in point sources may have an immediate effect while diffuse sources are likely to show time lags as described above (Abbott, Moatar, et al., 2018; Westphal et al., 2020). This delayed response can differ between seasons (Ehrhardt et al., 2019; Van Meter & Basu, 2017) according to changes in hydrological connectivity and transit time, with a larger contribution from younger water during high flow periods (Benettin et al., 2017; Yang et al., 2018). Accordingly, Dupas et al. (2016), Ehrhardt et al. (2019) and Winter et al. (2020) demonstrated how changes in N

Global Biogeochemical Cycles 10.1029/2021GB007050

input loading to a catchment can alter long-term N export dynamics, seasonal amplitudes, and even reverse the seasonal timing, in some cases. In other cases, the timing of N seasonality was largely constant even under various concentration trends, potentially due to invariant vertical distributions of the nutrient source zones (Abbott, Moatar, et al., 2018; Dupas et al., 2018). Finally, changes in N seasonality can also be caused by changes in in-stream processes related to other factors, including P concentration (Bowes et al., 2011; Minaudo et al., 2015). As the inter-annual trajectories of low- and high-flow concentrations integrate the input history, retention and release processes at catchment scale, they can be a valuable characteristic and indicator of how catchments respond to changes in nutrient inputs.

Despite a growing body of work on N seasonality, the spatial variability of N concentration seasonality and its long-term trend are still poorly understood across catchments. In this context, we investigated spatio-temporal patterns of nitrate (NO_3^-) seasonality in 290 catchments from two unique datasets of long time series across France and Germany. These catchments cover a wide range of ecohydrological and land use conditions, allowing robust quantification of seasonality and trend parameters on decadal timescales. We hypothesized that in these Western European landscapes where NO_3^- sources are primarily diffuse, most catchments would show (a) a NO_3^- maximum during the winter high-flow season and (b) a faster response of high-flow NO_3^- concentrations to changes in loading compared to low flow because of shallower N sources being affected first and being activated during high flow. To test the hypotheses, we propose a hysteresis approach for long-term trends of NO_3^- seasonality using available low frequency data. We classified the catchments based on their long-term average NO_3^- and discharge seasonality as well as long-term trajectories of NO_3^- seasonality and assessed links between these metrics and potential controls such as mean precipitation and fraction of agricultural land use. This large sample approach allowed us to determine archetypes of spatiotemporal NO_3^- export patterns at continental scale and evaluate underlying processes.

2. Methods

2.1. Databases

We used long-term riverine NO_3^--N (NO_3-N, hereafter) concentration data and daily discharge (Q) data from stations in Germany and France to analyze spatiotemporal patterns of NO_3-N seasonality linking to export dynamics. From the original databases for Germany (Musolff, 2020; Musolff et al., 2020) and France (http://naiades.eaufrance.fr/; http://hydro.eaufrance.fr/; Dupas et al., 2019; Ehrhardt et al. (2021); Minaudo et al., 2019; Moatar et al., 2017) we selected stations based on the following criteria: (a) time series of NO_3-N covering at least 20 years, (b) with at least 150 NO_3-N samples, (c) a maximum sampling gap of 20% of the time series, (d) seasonal coverage, that is at least 10% of the data in each season (all possible quarterly divisions by months), and (e) available corresponding gauge with daily Q data. Discontinuous Q time series at 36 German stations were filled through the support of simulations from the grid-based distributed mesoscale hydrological model mHM (Kumar et al., 2013; Samaniego et al., 2010). Model results with a regression coefficient (R^2) greater than 0.6 with the observed Q were accepted. Next, we used a piece-wise linear regression to reduce bias in modeled Q data, used for gap-filling, following Ehrhardt et al. (2020). The criteria resulted in a set of 290 catchments (165 in France, 125 in Germany) with a median of 336 NO_3-N samples per station and 114,479 in total, which cover various temperate ecoregions, topographic, climatic and land cover settings (Figures 1 and S2). The median time series length was 32 years and the maximum length 46 years starting in 1969. The majority of time series started around 1980 and ended in 2014 or 2015.

We reconstructed daily concentrations (C) and flow-normalized concentrations (C_{FN}) using Weighted Regression on Time, Discharge and Season (WRTDS, Hirsch et al., 2010) as implemented in the R package *EGRET* (version 3.0.2, Hirsch & De Cicco, 2015). Flow-normalization estimates are calculated by averaging C estimates from all observed Q values of the specific day of the year throughout the time series. To focus on concentration trends independent of inter-annual discharge variations we use C_{FN} for our analysis. For data gaps of observed NO_3-N larger than two years, corresponding daily C_{FN} estimates were excluded due to high uncertainties, following Hirsch and De Cicco (2015). Observed and interpolated time series of the Wupper catchment are shown in Figures 2a–2c as an example.

Global Biogeochemical Cycles 10.1029/2021GB007050

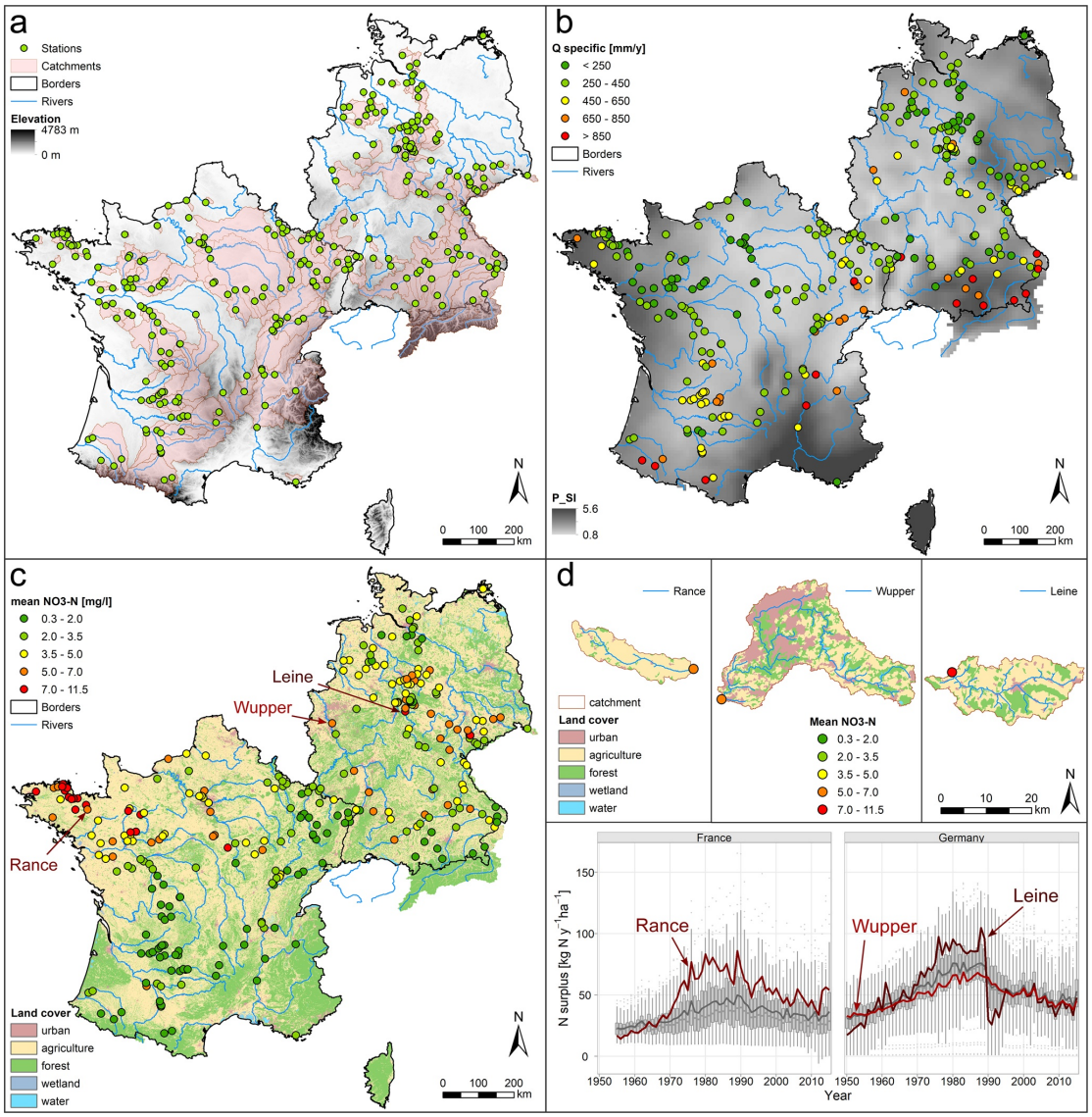

Figure 1. Map of the study area with (a) stations, catchments and elevation (EEA, 2013), (b) specific discharge and precipitation seasonality P_SI (Table S1, Cornes et al., 2018), (c) mean NO_3-N concentrations and land cover classes (CLC, 2006), (d) three selected catchments with mean NO_3-N, land cover, and N surplus time series. N surplus is the diffuse N input from agriculture, atmospheric deposition, and biological fixation in excess of N uptake by plants (for details refer to Ehrhardt et al. (2020) and Ebeling & Dupas, 2021, Table S1). In panel (d) boxplots represent annual N surplus averages of all catchments, gray lines represent mean values over all French and German study catchments, red lines represent single catchment time series.

2.2. Low- and High-Flow Seasons and Average Nitrate Seasonality

We determined the high-flow (HF) and low-flow (LF) seasons for each catchment by calculating the long-term average discharge for three consecutive months and defined the HF and LF seasons as the three wettest and driest months, respectively. Based on the timing of HF we classified the catchments into winter maximum (winMax, center of three wettest months within November–March) and spring or early summer

Global Biogeochemical Cycles 10.1029/2021GB007050

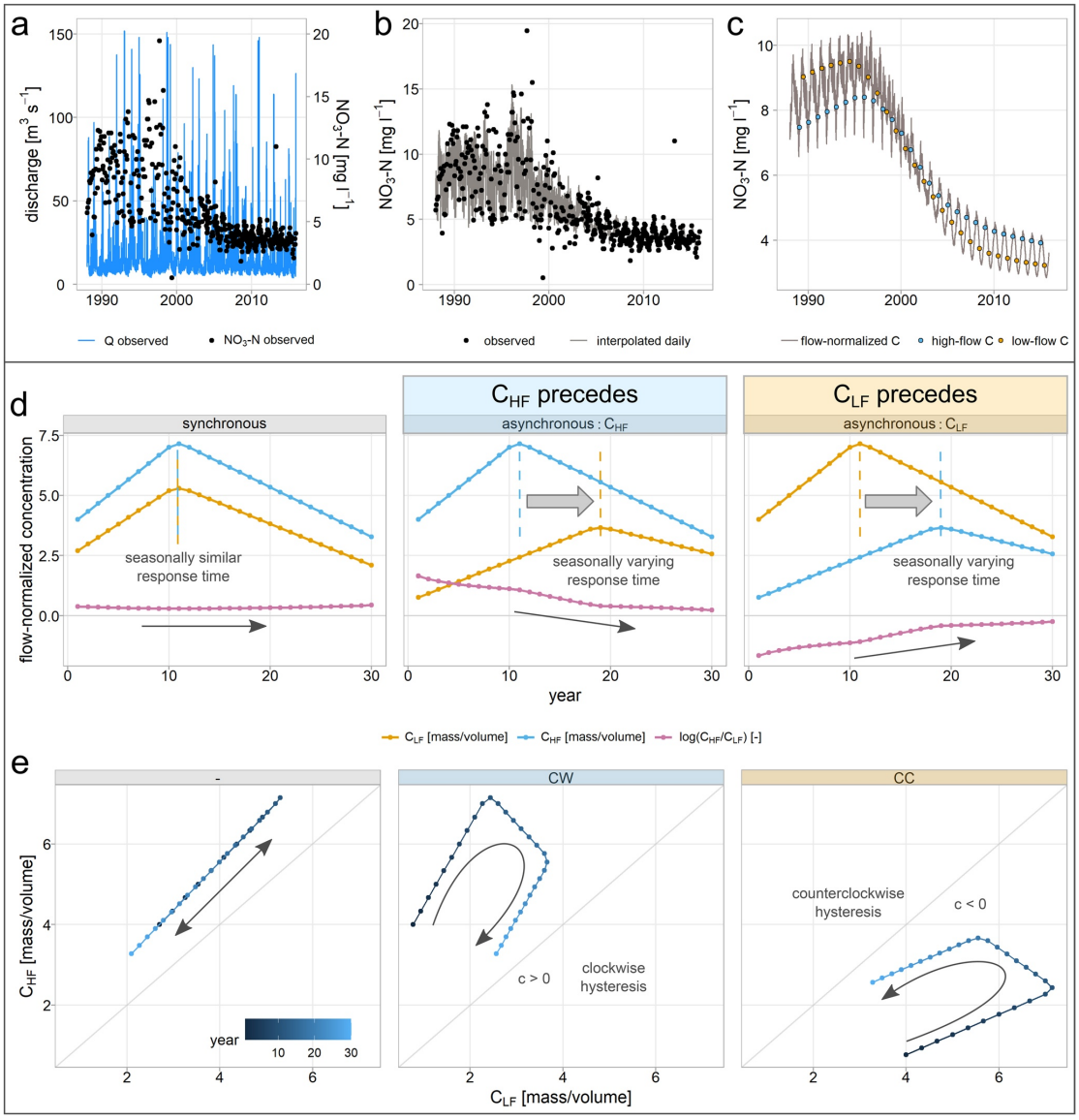

Figure 2. Conceptual framework of hysteresis between annual low-flow (C_{LF}) and high-flow (C_{HF}) concentrations. Upper box: Time series of the Wupper catchment for (a) observed daily discharge and weekly to monthly NO_3-N concentrations, (b) observed and daily WRTDS-interpolated NO_3-N concentrations, and (c) daily flow-normalized NO_3-N concentrations with annual averages during low-flow (C_{LF}) and high-flow (C_{HF}) periods. Lower box: Synthetic (d) time series of annual C_{LF} and C_{HF}, and the seasonal logarithmic ratio $\log(C_{HF}/C_{LF})$, and (e) corresponding long-term hysteresis loops. The three distinct examples of long-term *C*-*Q* trajectories represent from left to right synchronous responses of C_{LF} and C_{HF}, asynchronous responses with C_{HF} preceding and asynchronous responses with C_{LF} preceding. The trajectories with a seasonally varying response times follow a hysteresis loop, while seasonally synchronous responses show no hysteretic behavior. Note that Figure 3 shows trajectories from three study catchments, including the Wupper catchment (as panels a–c), and Figure S1 presents more examples of possible trajectories.

Global Biogeochemical Cycles 10.1029/2021GB007050

Table 1
Metrics Used to Characterize Patterns of Q and NO_3-N Seasonality

Metric	Meaning	Calculation	Unit
seasQmax	Timing of Q seasonal maximum of long-term three months average (high-flow period)	Period of Q_{HF}	Classes: winMax, sprMax
rQseas	Long-term average of relative Q seasonal amplitude	$(Q_{HF} - Q_{LF})/\text{mean}(Q)$	-
C_{FN}	Flow-normalized (FN) concentrations	C_{FN} from WRTDS	mg NO_3-N l^{-1}
seasCmax	Timing of NO_3-N seasonal maximum of long-term months average	Period of maximum monthly NO_3-N C_{FN}	Classes: winMax, sumMax
C_{HF}, C_{LF}	Mean flow-normalized concentrations during HF and LF periods, calculated annually	$C_{HF} = \text{mean}(C_{FN}(HF))$ $C_{LF} = \text{mean}(C_{FN}(LF))$	mg NO_3-N l^{-1}
$\log(C_{HF}/C_{LF})$	Logarithmic seasonal ratio, calculated annually	$\log(C_{HF}/C_{LF})$	-
rCseas	Mean relative NO_3-N seasonal amplitude between HF and LF seasons	$\text{mean}(\text{abs}(C_{HF} - C_{LF}))/\text{mean}(C_{FN})$	-
c	Hysteresis between C_{LF} and C_{HF}	See Equation 1,	Classes:
		$c < 0$	CC,
		$c > 0$	CW,
		$c \approx 0$	n.s.

maximum (sprMax, April–July; metric seasQmax, see Table 1). The LF season was calculated but not used for an additional classification of average Q seasonality. Similarly, we determined the average seasonal concentration pattern at each station. We calculated the maximum monthly averages of C_{FN} to classify the catchments into the ones with their intra-annual maximum during winter (winMax, November–March) and summer (sumMax, April–October; metric seasCmax, see Table 1). The combination of both classifications yields the long-term average C-Q seasonality.

2.3. Hysteresis in Multi-Annual Time Series of Low- and High-Flow Concentrations

We calculated mean C_{FN} during LF (C_{LF}) and HF (C_{HF}) periods (see Section 3.2) for each hydrological year (November–October) and catchment from the WRTDS-interpolated daily C_{FN} time series (Section 2.1, see Figure 2c as example). We only calculated these values with at least 80% daily data coverage over the corresponding time period. As a metric of the strength of C-Q seasonality within each year, we calculated the annual seasonal ratio in logarithmic form $\log(C_{HF}/C_{LF})$. Example trajectories of C_{LF}, C_{HF} and $\log(C_{HF}/C_{LF})$ are shown in Figure 2d.

To identify and characterize the seasonally asynchronous (i.e., phase/time shift between peaks) responses to changes in inputs, we plotted the time series of annual mean C_{LF} and C_{HF} against each other and applied a hysteresis approach (Figure 2e). Accordingly, the hysteresis captures decadal trajectories of the seasonality represented by time series of annual average low- and high-flow concentrations. Systematic changes in the trajectories are considered to be linked to changes in point and diffuse source inputs with mainly increasing inputs before 1990s and decreases mainly after 1990s (Figure 1d) in response to European regulations as drivers (EEC, 1991a, 1991b). If C_{HF} (y-axis) responds faster than C_{LF} (x-axis) hysteresis becomes clockwise (CW), while if C_{LF} responds faster than C_{HF} hysteresis will be counter-clockwise (CC). If C_{HF} and C_{LF} respond simultaneously, no significant hysteresis loop is observed (n.s.). We used a hysteresis method based on the derivative of the X variable $(dX)C_{LF}$ (Krueger et al., 2009; Minaudo et al., 2019). Its advantage for long-term water quality trajectories is that it also works for incomplete hysteresis loops. Incomplete loops are common for example, if (a) sampled time series are too short to cover the complete loop or (b) catchments do not return to their original state due to continued differences in the pressures or changes in their functioning. To this end, we fit the following nonlinear model using the R package *minpack.lm* (version 1.2–1).

$$C_{HF}'(t) = d + mC_{LF}'(t) + c\frac{dC_{LF}'(t)}{dt} \quad (1)$$

Global Biogeochemical Cycles 10.1029/2021GB007050

where t represents the time in years, d is the intercept, m is the slope between C_{HF}' and C_{LF}', and c is the hysteresis coefficient describing the direction and width of the hysteresis ($c < 0$ corresponds to a CC, $c > 0$ to CW, and $c \approx 0$ to a non-significant hysteresis based on a confidence level of 95%). Prior to fitting, we linearly scaled C_{LF} and C_{HF} to vary between 0 and 1 (C_{LF}' and C_{HF}') to make the hysteresis coefficient c of different catchments comparable independent of differences in concentration (Lloyd et al., 2016).

Variations in seasonal response times cause trends in concentration seasonality and export dynamics, that is here $\log(C_{HF}/C_{LF})$ (Figure 2a). Therefore, we use the Mann-Kendall test (R package *Kendall*, version 2.2) and Sen's slope (Sen, 1968) (R package *trend*, version 1.1.2) to detect and quantify monotonic trends in the logarithmic seasonal ratio. Missing annual values at 40 stations were filled by linear interpolation (on average 4.25 interpolated values, maximum eight), for example caused by large gaps in NO_3^-N samples (see Section 2.1).The ratio C_{HF}/C_{LF} is linked to the slope b of the log$C$-log$Q$ regression and is thus another metric of C-Q relationships. The slope b is a widely used metric to characterize solute and particulate export dynamics in terms of C-Q relationships (Godsey et al., 2009).

$$C = aQ^b \tag{2}$$

$$\log(C) = a + b\log(Q) \tag{3}$$

with a being the intercept and b the slope of the log$C$-log$Q$ regression. If we assume a mean Q for HF (Q_{HF}) and another for LF (Q_{LF}) periods, the quotient becomes constant and b dependent on the logarithmic seasonal C_{FN} ratio.

$$b = \frac{\mathrm{dlog}(C)}{\mathrm{dlog}(Q)} = \frac{\log\left(\frac{C_{HF}}{C_{LF}}\right)}{\log\left(\frac{Q_{HF}}{Q_{LF}}\right)} \tag{4}$$

If the ratio of Q_{HF}/Q_{LF} equals Euler's number (~2.718), b becomes equal to $\log(C_{HF}/C_{LF})$. Generally speaking, b behaves proportional to the logarithmic seasonal C_{FN} ratio normalized by the logarithmic seasonal ratio of discharge $\log(Q_{HF}/Q_{LF})$. Though of course, slope b would be more scattered when considering the actual inter-annual Q variability instead of the long-term mean.

Additionally, we assessed and compared both the spatial variability and the long-term temporal variability of NO_3-N seasonality. The spatial variability was determined for each year as the standard deviation of annual $\log(C_{HF}/C_{LF})$ across all stations. The temporal variability was calculated for each station as the standard deviation of annual $\log(C_{HF}/C_{LF})$ over the complete time series including the long-term trends in the seasonality trajectories.

2.4. Linking Metrics and Catchment Characteristics

We tested for relationships between the two classifications of long-term average C-Q seasonality and its trajectory (hysteresis) and catchment descriptors to examine our hypothesis about dominant controls. For the descriptors we used the data sets published and described in Ebeling et al. (2021), Ebeling (2021) and extended to include French catchments in Ebeling and Dupas (2021). The descriptors characterize the hydroclimatic settings, topography, land cover, soil properties, geology, and point and diffuse N sources of the study catchments (Figure S2, Table S1).

The analyzed metrics are partly categorical and partly continuous (Table 1). To test for significant differences among the different classes of long-term average C-Q seasonality and hysteresis trajectories, we used the non-parametric Wilcoxon test for comparing two classes and otherwise the Kruskal-Wallis test. A random forest (RF) classification model was trained for the two significant hysteresis classes (CC and CW) to investigate the joint predictive power of the descriptors while accounting for collinearities (see Figure S3). We used three times repeated tenfold cross-validation to estimate the mean model performance. Subsequently, permutation allows quantifying variable importance and thus identifying the dominant descriptors from the trained RF model. We used the importance permutation by Altmann et al. (2010) to identify significant descriptors from a first RF model using all descriptors (significance level 5%; Table S1), which then served to train a second RF model. We used the R package *mlr3* (version 0.9.0, Lang et al., 2019) to train the RF model and *ranger* (version 0.12.1, Wright & Ziegler, 2017) for permutation variable importance. Spearman

Global Biogeochemical Cycles 10.1029/2021GB007050

Table 2
Summary Statistics of Calculated Metrics of All Catchments (n = 290) From Observations and the WRTDS Models: Median and Interquartile Range (IQR) and the Number of Catchments (n) With Positive (+), Negative (−) or Non-Significant (n.s.) Monotonic Mann-Kendall (MK) Trend

		Specific Q	Rel. seasonal Q amplitude rQseas	Mean NO_3-N C_{FN}	Mean NO_3-N C_{LF}	Mean NO_3-N C_{HF}	Rel. seasonal NO_3-N amplitude rCseas	Mean log (C_{HF}/C_{LF})
		mm y^{-1}	-	mg N l^{-1}	mg N l^{-1}	mg N l^{-1}	-	-
Median		340	1.18	3.23	2.51	3.92	0.37	0.33
IQR		254	0.55	2.95	2.46	3.68	0.45	0.53
n MK trend	+	2		92				124
	−	32		151				95
	n.s.	256		47				71

Note. Q—discharge, FN—flow normalized, LF—low flow, HF—high flow. The Q values used for these statistics was the same time period used for the WRTDS model, that is the overlapping period of NO_3-N and Q time series.

rank correlations served to identify relevant descriptors for the continuous metrics of average Q seasonality (rQseas) and NO_3-N seasonality (mean log(C_{HF}/C_{LF})).

3. Results

3.1. Spatial Patterns of Long-Term Average Discharge and Nitrate Seasonality

The highest specific Q was observed in mountainous catchments (e.g., the Alps) with values up to 1,670 mm y^{-1} (median 340 mm y^{-1} among the study catchments) while lowest specific Q was 63 mm y^{-1}. The relative seasonal Q amplitude (rQseas) was highest in northwestern France (max 2.50) and lowest mostly in southeastern Germany (min 0.11) with a median of 1.18 (see Figure S4). A summary of calculated metrics across the study catchments is presented in Table 2.

Across the catchments, we found a dominance of winter maxima in Q (90.3%) and in flow-normalized NO_3-N concentrations (91.0%) (Figure 3) with occurrence of both in 83.8% of the catchments. The 9.7% of catchments with spring and early summer maxima of Q (sprMax) were apparent in mountainous areas (Figure 3a). The 9.0% of catchments with summer maxima of NO_3-N (sumMax) were observed mainly in northwestern and southern France (Figure 3a). In southern France, these summer NO_3-N maxima coincided with Q minima, while NO_3-N minima coincided with the Q maxima in spring. Catchments with spring maxima of Q in southeastern Germany have lowest Q during autumn or winter, which coincided with maxima in NO_3-N. Figure S5 shows these synchronous and asynchronous long-term average seasonal C and Q variations of the four combined C-Q seasonality classes.

Catchments with the largest positive average seasonal ratios (log(C_{HF}/C_{LF})) were found in western France, northern Germany and northeastern France (Figure 3a). On the other hand, catchments with average log(C_{HF}/C_{LF}) < 0 were observed mainly in southern Germany, southern and western France. The spatial variability of the NO_3-N seasonality among the catchments (standard deviations of log(C_{HF}/C_{LF}) over all stations for each year) ranged from 0.42 to 0.64 with a median of 0.47 and an interquartile range of 0.04.

3.2. Long-Term Trajectories of Nitrate Seasonality

We examplarily visualized the seasonal NO_3-N trajectories of three representative catchments namely the Wupper as an urban and the Leine and the Rance as agricultural rural catchments (Figures 1d and 3c). The Wupper catchment (605.9 km^2) has the highest fraction of artificial surfaces (31%), population density, and load by point sources and ranks under the top three for the fraction of point source loads from the total N input loads (86%) among the studied catchments. The HF season was determined for winter (December–February), LF for summer (May–July). The C_{LF} were higher than the C_{HF} in the beginning, but with C_{LF} decreased from 1994 until C_{LF} < C_{HF} from 1998, indicating a switch in the seasonal timing. The peak

Global Biogeochemical Cycles 10.1029/2021GB007050

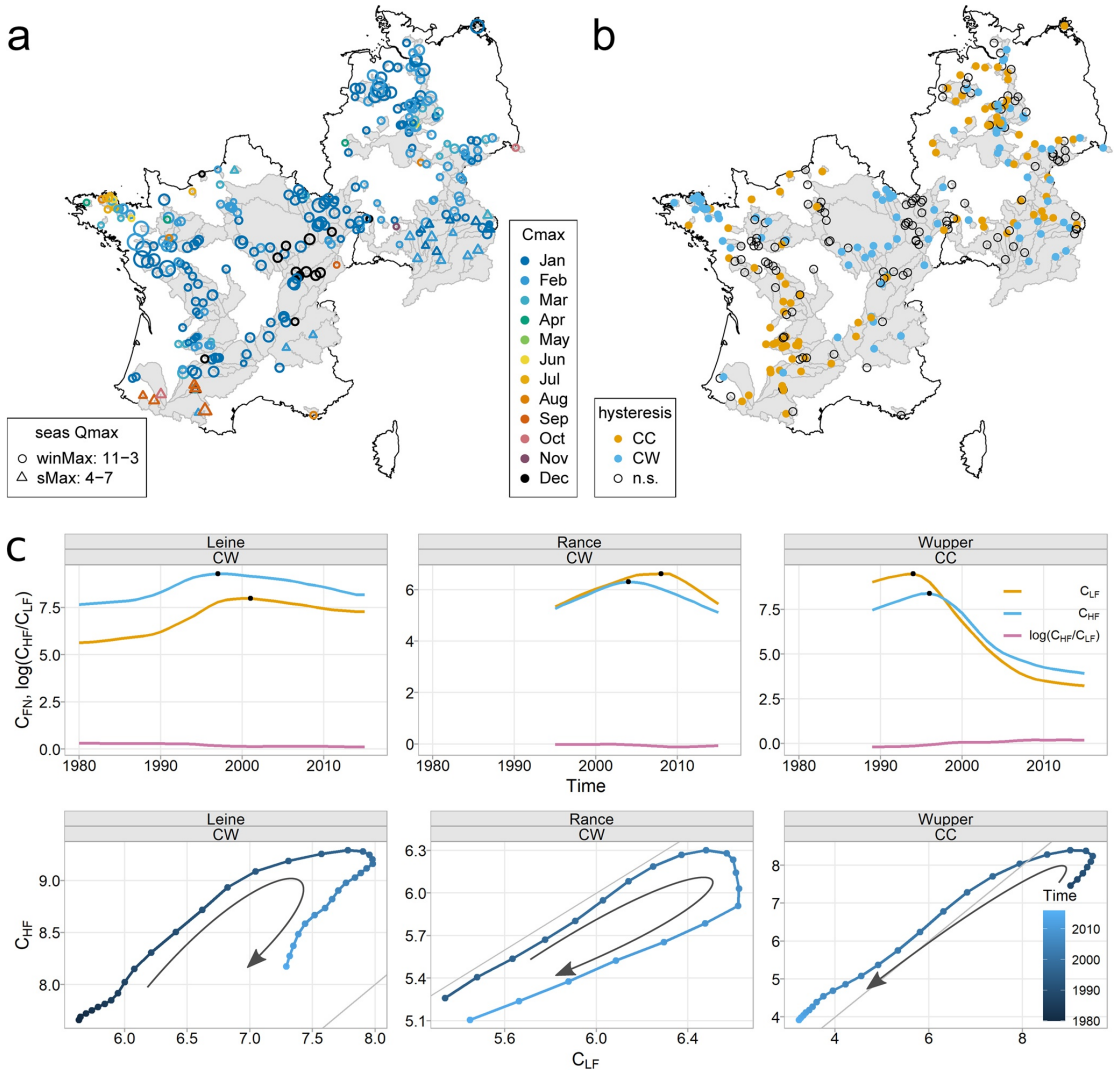

Figure 3. Spatial patterns of (a) average Q and NO_3-N seasonality, color—month with maximum long-term averages of flow normalized concentrations (C_{FN}), shape—timing of maximum average Q (seasQmax), size—absolute average seasonal ratio in log space log(C_{HF}/C_{LF}), and (b) classes of hysteresis between C_{LF} and C_{HF} trajectories, color—hysteresis class, and (c) seasonal NO_3-N concentration trajectories during low-flow (C_{LF}) and high-flow (C_{HF}) periods and the corresponding hysteresis patterns of the three catchments Leine, Range and Wupper, black dots mark the peak concentrations. CC—counterclockwise hysteresis, CW—clockwise hysteresis, Time in years, concentrations in mg NO_3-N l^{-1}.

in C_{LF} is two years before the peak in C_{HF}, which creates a counterclockwise hysteresis. Accordingly, the seasonal ratio log(C_{HF}/C_{LF}) follows a positive trend from a seasonal dilution (log(C_{HF}/C_{LF}) < 0) to enrichment (log(C_{HF}/C_{LF}) > 0) pattern. On the other hand, the two catchments with clockwise hysteresis, Leine (317.4 km²) and Rance (142.6 km²), are selected from catchments with high agricultural impact (65%–90%), strong change in diffuse agricultural N input from before to after 1990 (Figure 1d, and small urban areas (2.6%–6.8%) as well as low fraction of point sources from total N input (below 10%)). The HF season in both catchments is in winter (Leine: January–March; Rance: December–February) and LF season in summer to fall (Leine: August–October; Rance: July–September). In the Leine catchment, C_{HF} peaks in 1997 four years

Global Biogeochemical Cycles 10.1029/2021GB007050

before C_{LF}. In the Rance, C_{HF} peaks in 2004 also four years before C_{LF} with C_{LF} being slightly higher than C_{HF}. Both catchments have a negative trend in the seasonal ratio $\log(C_{HF}/C_{LF})$, which for the Leine means a trend from enrichment to a more neutral export pattern and a decrease in seasonal amplitude and for the Rance from neutral to dilution with an increase in the absolute seasonal amplitude between C_{LF} and C_{HF}.

Although the input trajectories of N surplus are relatively synchronous among the catchments (including the three example catchments) following the EU and national legislation (Figure 1d), the seasonal NO_3-N trajectories observed in the streams differ more prominently among the catchments (Figure S6). Exceptions to this generally synchronous variation in N surplus can be found in East German catchments with a drastic drop in 1990 after the German reunification, including the upper Leine catchment.

For all study catchments, counterclockwise and clockwise hysteresis occurred both in similar proportions ($n = 87$ CC, $n = 85$ CW, about 30% each), while the nonsignificant hysteresis class occurred slightly more often ($n = 116$ n.s., 40%). The fitted hysteresis models had a median performance of $R^2 = 0.84$ and a $R^2 > 0.6$ in 73.8% of the catchments. A spatial organization of the hysteresis patterns was apparent with clusters being more pronounced in France (Figure 3b): counterclockwise hysteresis dominated in central, southern and southwestern France and northern Germany, whereas clockwise hysteresis dominated in Brittany and northeastern France including the Seine catchment and southeastern Germany. In the majority of the catchments (80.3%, $n = 233$) the timing of seasonal C_{FN} maxima and minima remained constant throughout the time series, whereas in 19.7% ($n = 57$) it switched between HF and LF periods (e.g., in the Wupper catchment, Figure 3c). The majority of the switching catchments (54%, $n = 32$) changed once from a seasonality with $C_{LF} > C_{HF}$ to $C_{LF} < C_{HF}$ with the median switch in the year 1991. Most of these catchments had counterclockwise hysteresis patterns (63%, $n = 20$). Some of those catchments (32%, $n = 18$) changed the seasonal timing of concentration maxima more than once.

The C_{LF}-C_{HF}-hysteresis patterns were connected to long-term trends in the annual seasonal ratios $\log(C_{HF}/C_{LF})$ (significance level 5%, Figure S6): 60.9% of the counterclockwise catchments had a positive trend in $\log(C_{HF}/C_{LF})$ and 49.4% of clockwise catchments had a negative trend in $\log(C_{HF}/C_{LF})$. The nonsignificant hysteresis was mostly linked to a significant increase in the seasonal ratio (43.0%). The different trajectories imply a long-term temporal variability in the NO_3-N seasonality. The temporal variability of $\log(C_{HF}/C_{LF})$ at each station varied between 0.01 and 0.54 with a median of 0.09 and an interquartile range of 0.09.

3.3. Linking Seasonality Metrics and Catchment Characteristics

First, we linked the classifications of long-term average *C*-*Q* seasonality and the long-term trajectories to each other: The dominant class with NO_3-N and *Q* winter maxima had similar proportions of all three hysteresis classes (25.9% for CW, 32.1% for CC and 42.0% for n.s.). The two asynchronous NO_3-N and *Q* classes with *Q* winter and NO_3-N summer maxima or *Q* spring/summer and NO_3-N winter maxima both had higher proportions of clockwise hysteresis (63.2% and 47.6% respectively) compared to counterclockwise (10.5% and 14.3%) hysteresis. On the other hand, the asynchronous *C*-*Q* seasonality class in southern France with *Q* spring/summer and NO_3-N summer maxima (LF period) had mostly counterclockwise (57.1%) and no clockwise (0%) hysteresis.

The timing of *Q* seasonality linked to elevation (Figure 4a) and related hydroclimatic descriptors, that is catchments with *Q* spring/summer maxima had significantly higher mean elevations, precipitation and specific discharge and lower mean temperatures. The relative *Q* amplitude (rQseas) also correlated with the hydroclimatic drivers, especially the summer to winter precipitation P_SIsw ($r = -0.63$, Spearman rank, Figure S3) and mean temperature ($r = 0.63$).

The combined timing of NO_3-N and *Q* seasonal maxima (Figure 4a) linked to more characteristics in addition to the controls of only *Q* seasonality. Compared to catchments with maximum NO_3-N concentrations in summer, catchments with winter maxima of NO_3-N tended to be more abundant in catchments with higher ratios of summer to winter precipitation (P_SIsw) and discharge (Q_seasR, not shown) and lower *Q* seasonality (rQseas), although the class of concurrent NO_3-N and *Q* winter maxima contained many catchments with equilibrated summer to winter precipitation (P_SIsw∼1) and smaller precipitation seasonality (P_SI, not shown). Summer maxima in NO_3-N emerged in catchments with consistently lower summer to winter precipitation (P_SIsw < 1, with only one exception) and lower depths to bedrock (dtb). We also found a link

Global Biogeochemical Cycles 10.1029/2021GB007050

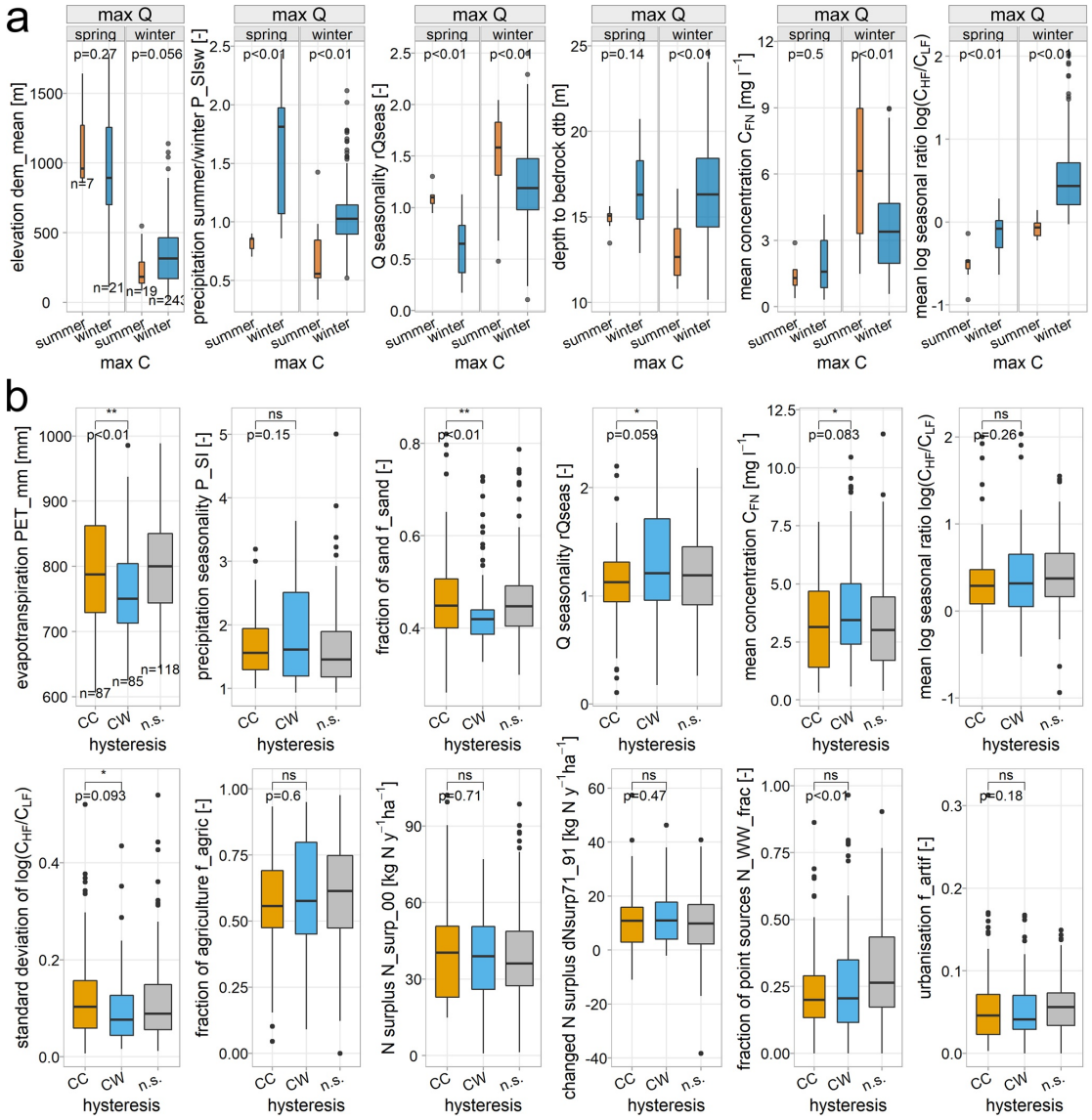

Figure 4. Controls of (a) long-term average NO_3-N and *Q* seasonality and (b) hysteresis classes (n.s. nonsignificant, CC counterclockwise and CW clockwise hysteresis). In panel (a), the classes of maximum NO_3-N concentrations are shown separately for each class of the timing of maximum *Q* (high flow) to distinguish the controls of the different identified combinations of C and *Q* seasonality. Number of samples (*n*) per group is given in the first subplot. The *p* values from Kruskal-Wallis tests for nonparametric comparisons of means for multiple groups and the significance levels from Wilcoxon rank sum tests for the pairwise comparison between CC and CW hysteresis are written above the boxplots (ns - $p > 0.05$, * - $p \leq 0.05$, ** - $p \leq 0.01$). For details on the variables refer to the text, Tables 1 and S1.

of average NO_3-N concentration to long-term average *C*-*Q* seasonality: The mean C_{FN} was lowest for the classes with *Q* spring/summer maxima and highest for *Q* winter maxima with NO_3-N summer maxima (especially in the Armorican Massif). The major class of concurrent NO_3-N and *Q* winter maxima has medium mean C_{FN} values but also a high range. . As expected from the methods, the classes were clearly linked to the

Global Biogeochemical Cycles 10.1029/2021GB007050

strength of the NO_3-N-Q seasonality, quantified by the mean seasonal ratio $\log(C_{HF}/C_{LF})$, with the class of concurrent NO_3-N and Q winter maxima showing mostly positive and the other classes negative values. The mean ratio $\log(C_{HF}/C_{LF})$ was correlated to topographical and hydroclimatic descriptors (slo.mean $r = -0.45$, twi.mean $r = 0.43$, AI $r = 0.41$, specific Q $r = -0.39$) and land use (f_agric $r = 0.39$). Note that the descriptors also correlate with each other (Figure S3).

The RF model for the two significant hysteresis classes reached only a mean accuracy of 0.69 ± 0.12 from cross-validation (compared to 0.5 for random guess). The descriptor relative Q seasonality (rQseas) ranked highest in the feature importance, followed by evapotranspiration (PET_mm), mean C_{FN}, precipitation seasonality (P_SI), ratio of summer to winter discharge (Q_seasR) and fraction of sand (f_sand), although they showed overall relatively low variable importances (Figure S7). Expected links to descriptors of N loading were not found dominant: although N surplus descriptors were significant in the RF model, they only ranked 8th or lower. As shown in Figure 4b, the clockwise hysteresis was mostly noticed in catchments with higher Q and precipitation seasonality (rQseas and P_SI), and mean C_{FN} and lower evapotranspiration (PET_mm), fraction of sand (f_sand), and temporal variability in NO_3-N seasonality (standard deviation of $\log(C_{HF}/C_{LF})$). The clockwise catchments covered a large variability in the fraction of agriculture, N surplus, the difference in N surplus before and after 1990 (dNsurp71_91), the fraction of point source loads (N_WW_frac) and artificial surfaces (f_artif). The nonsignificant hysteresis class contained more catchments with higher fractions of point source loads, albeit with a large variability of values.

4. Discussion

4.1. Spatial Patterns and Controls of Long-Term Average Nitrate and Discharge Seasonality

The long-term average NO_3-N seasonality was linked to average seasonality of Q in combination with climate, topography and geology. Accordingly, we established distinct archetypal patterns across the large range of catchments and provide possible links to the underlying catchment characteristics. The different timing of Q seasonality (seasQmax) across the catchments was controlled by topography and related hydroclimatic variables. This agrees with Kuentz et al. (2017), who found climate was the main driver for several flow characteristics at the European scale, and Gnann et al. (2020), who found catchment aridity to control the timing and magnitude of Q seasonality relative to climate seasonality. The dominance of Q winter maxima (90.3%) and summer low flow (Figure S5) suggests that the seasonal cycle of evapotranspiration strongly affects the Q cycle in the study region. Precipitation seasonality (P_SIsw) with relatively high winter precipitation (as prevalent in France) can add to this pattern, especially in northwestern France with the lowest ratios of summer to winter precipitation (P_SIsw) and relatively low annual evapotranspiration and aridity. In that region, the opposing seasonal precipitation and evapotranspiration cycles in a moist climate lead to strong seasonal Q patterns (rQseas) and short hydrological transport times (Gnann et al., 2020; Kumar et al., 2020), which might also be enhanced by shallow aquifers with shallow depths to bedrock (dtb). The Q maximum is shifted to spring or summer in fewer catchments (9.7%), where winter precipitation is likely retained as snow-pack and discharged with higher temperatures during thawing period. Here, this effect seems to exceed the evapotranspiration control. The spatial patterns of high-flow seasonality (Figures 3a and S4) largely agree with the flood timing reported across the study region, especially the geographical differences between the mountainous, snow-impacted catchments (in the Alps and Pyrenees) and others (Berghuijs et al., 2019; Blöschl et al., 2017).

In combination with the NO_3-N seasonality, we found three archetypal patterns of long-term average C-Q seasonality with different controls and underlying processes:

1. Both NO_3-N and Q have a winter maximum (83.8% of the catchments) and vary mostly synchronously (Figures 3a and S5), which indicates prevalent enrichment patterns (transport limitation) and NO_3-N mobilization processes at a seasonal scale (Minaudo et al., 2019). This supports our first hypothesis that overall synchronous NO_3-N and Q seasonality dominate. The dominance of NO_3-N and Q winter maxima and C-Q enrichment patterns agrees with previous research on temperate catchments (Ebeling et al., 2021; Minaudo et al., 2015; Moatar et al., 2017; Musolff et al., 2015; Zhi & Li, 2020). Moreover, the spatial patterns of the strength of nitrate-discharge seasonality, represented by the average seasonal ratio $\log(C_{HF}/C_{LF})$, are also in line with a previous study of Germany-wide C-Q relationships showing

Global Biogeochemical Cycles 10.1029/2021GB007050

strong enrichment patterns in northern Germany and less pronounced enrichment or neutral patterns in central-eastern Germany (Ebeling et al., 2021). This supports that the seasonal ratio is comparable to the widely used slope b for inter-annual *C*-*Q* relationships (see Equation 4). This is plausible as seasonal NO_3-N variations exceed storm-event induced variations, when considering rather large catchments are usually monitored at low (typically monthly) frequency (Minaudo et al., 2019). Furthermore, our analysis showed the dominant control of topography, climate and land use in shaping the spatial variability of the seasonal ratio, with a tendency of higher ratios in agricultural lowland catchments. With dominant diffuse N sources, a mechanism leading to this synchronous archetype can be variable discharge generating zones, where shallow N sources are activated by younger water dominating during HF and lack of connectivity of sources along with longer reaction times (potentially higher removal) for longer flow paths dominates during LF (Benettin et al., 2020; Musolff et al., 2016; Yang et al., 2018; Zhi & Li, 2020). This interpretation is supported by Ebeling et al. (2021), who additionally found a dominant control of the vertical concentration gradient on the NO_3-N export dynamics in German catchments. Reduced riparian or instream NO_3-N removal during winter following the seasonal biogeochemical cycle (Lutz et al., 2020) could also enhance the pattern of synchronous *C* and *Q* seasonality.

2. The NO_3-N maximum coinciding with the *Q* minimum and vice versa (9.7% of the catchments, Figures 3a and S5) occurred in mountainous catchments, where asynchronous dilution patterns of *C*-*Q* dominate. Spring and summer discharge from mountains stemming from snow melt and summer precipitation could dilute N sources. In these archetypal catchments, mean NO_3-N concentrations are low (Figures 1c and 4a) due to relatively low N input in combination with strong dilution by high specific discharge (Figure 1b). The dominant dilution pattern agrees with *C*-*Q* relationships observed previously in mountainous, snow-dominated German meso-scale catchments (Ebeling et al., 2021). The dilution of N sources is lowest during LF season, that is late summer in southern France and autumn or winter in southern Germany. The dilution pattern of this archetype likely results from the spatial separation of discharge generating zones upstream and dominant agricultural sources downstream, potentially masking other export dynamics in the downstream areas.
3. NO_3-N maxima are reached during summer LF and minima mostly during autumn before the winter HF period (6.6% of the catchments, Figures 3a and S5). This type of NO_3-N seasonality with relatively weak dilution patterns, high mean concentrations and small relative seasonal differences between LF and HF concentration seems to be specific to the Armorican Massif and has been described for several catchments in this region previously (Abbott, Moatar, et al., 2018; Guillemot et al., 2021; Martin et al., 2004). The strong *Q* seasonality in that region and fast hydrological responses (e.g., high flashiness and CVQ) are not reflected in the NO_3-N seasonality, indicating a rather chemostatic export regime (low concentration relative to high *Q* variability) for this archetype. Reasons for this pattern include large legacy stores (Dupas et al., 2020) and bottom-loaded profiles with NO_3^--rich groundwater which is diluted during HF (Martin et al., 2006) in combination with potential bypassing of the riparian zones where removal by denitrification can be high during LF (Fovet et al., 2018). However, riparian zones can also act as NO_3^- sources during LF (Duncan et al., 2015), offering a nonexclusive alternative mechanism for this pattern. Van Meter et al. (2020) found that NO_3^--rich groundwater can lead to an out-of-phase or aseasonal NO_3^- pattern. In case of bottom-loaded profiles, we would expect the catchments to have developed the reverse seasonality over time, as described in for example Ehrhardt et al. (2019), which was indeed observed for some catchments (see Figure S6, crossing the 1:1 line). Alternatively, multiple contributing aquifers with variable response times and sources could be horizontally distributed differently with a longitudinal gradient, with a dominance of nonagricultural wetland soils upstream and agricultural areas downstream. With the upstream discharge diluting downstream sources during HF, this process resembles archetype 2. Another contributing mechanism to this pattern could be the seasonal variation of N inputs as fertilizer is primarily applied in spring or of retention in the soils.

4.2. Long-Term Trajectories of Nitrate Seasonality Integrate Complex Controls

We observed both long-term trajectory types equally often, with annual C_{LF} (counterclockwise hysteresis) or C_{HF} (clockwise hysteresis) changing first. Our hypothesis of dominant clockwise hysteresis for NO_3^- is therefore not supported by the studied catchments. Surprisingly, 20% of the catchments even switched their seasonal timing at least once during the observation period, which imposes substantial changes to aquatic

Global Biogeochemical Cycles 10.1029/2021GB007050

ecosystems over time. As described in the introduction, this could create shifts in nutrient availability and limitation during sensitive time periods for aquatic organisms and ecosystems (Minaudo et al., 2015).

The C_{HF} and C_{LF} are influenced by various controls that may lead to the observed long-term trajectories and hysteresis patterns. For example, in the densely populated Wupper catchment, changes in point sources could have affected C_{LF} more and earlier than C_{HF}, as discussed by Abbott, Moatar, et al. (2018). Reductions in inputs from point sources usually have a more immediate effect on riverine concentrations and have typically been achieved more easily and earlier than reductions in diffuse-source inputs in Western Europe (Le Moal et al., 2019; Westphal et al., 2020). The example catchments Leine and Rance (Figure 3c) are agriculturally managed with few point sources only and show the expected stronger delay in low-flow concentrations (clockwise hysteresis). This suggests that our hypothesis of changes in diffuse sources being reflected first in changes in C_{HF} may be supported for these two catchments but cannot be verified across the entire set of catchments.

Despite the large sample size and rich ancillary data on catchment characteristics, we did not detect fundamental or general controls on hysteresis patterns. Over the whole range of study catchments, the source descriptors (i.e., land cover, N surplus, point sources, population density) did not show consistent relationships with hysteresis. Small differences between the hysteresis classes were apparent in catchment properties describing the hydroclimate and soil data, though they had a relatively low explanatory power. This suggests overall complex controls on the long-term hysteresis patterns over the large extent of the study, with several interacting controls potentially determining the observed trajectories that will be addressed in the following.

The complexity in controls of responses across a wider range of catchments is in line with recent research on the diversity of nutrient retention capacity in various surface and subsurface catchment components (Frei et al., 2020; Kolbe et al., 2019). In particular, the high hydrochemical complexity of the subsurface in combination with relatively sparse subsurface data availability makes regional to continental predictions exceedingly uncertain (Aquilina et al., 2018; Jawitz et al., 2020; Marçais et al., 2018). Moreover, the subsurface reactivity can experience long-term changes if availability of electron donors and thus denitrification potential decreases (Bouwman et al., 2013). Because soil, vadose, and aquifer hydrology and biogeochemistry directly influence both hydrological time lags and active nutrient retention, better characterization of subsurface parameters should be a major research priority (Condon et al., 2020; Li et al., 2021).

The diversity of human activities can also obscure the linkage between catchment characteristics and nutrient dynamics. Catchments with anthropogenic impact often have both point and diffuse N sources, creating complex and time-variant interactions that are not captured by the catchment attributes taken into account here. For example, in diffuse-source-dominated catchments, smaller point sources could still have changed more than diffuse sources and vice versa, hampering predictability of hysteresis by catchment descriptors representing more the source strengths. Point sources could mask changes caused by diffuse source changes especially in larger, more populated catchments (Dupas et al., 2017).

Another unaccounted factor could be long-term changes in in-stream nutrient uptake processes. For example, an increasing C_{LF} while C_{HF} is already decreasing could result from reduced uptake rates during summer. Reduced algal biomass production could be caused by reductions in phosphorus and increasing limitations (Bowes et al., 2011; Minaudo et al., 2015). For example, in the Frome catchment, changes in in-stream processes were even considered to dominantly control changes in NO_3^- seasonal amplitude because concurrent seasonal changes of NO_3^- in groundwater boreholes were not observed (Bowes et al., 2011). Additionally, NO_3^- could be released to the stream by decomposition of biomass in winter and further affect seasonality (Bowes et al., 2011).

The tendency of clockwise catchments to have higher precipitation seasonality (P_SI, Figure 4b) and low evapotranspiration (PET_mm) could relate to their occurance in the Alps and the Armorican Massif (Figure 3b). Conversely, the high relative Q seasonality (rQseas) was common for catchments in northeastern France and the Armorican Massif. This might indicate that pronounced hydroclimatic variability in relatively wet catchments enhances HF concentrations to react faster, whereas high PET_mm links to dominant counterclockwise hysteresis in central and southern France, although this does not seem to be an overall dominant control as predictive power remained low.

Global Biogeochemical Cycles 10.1029/2021GB007050

Interestingly, we found distinct hysteresis patterns in the regions with asynchronous archetypal patterns of long-term average *C*-*Q* seasonality (16.2% of the catchments). For example, in southern France, the strong seasonal dilution pattern was mostly combined with counterclockwise hysteresis, whereas in the Alps and in the Armorican Massif, clockwise hysteresis dominated (Figure 3b). Dilution of downstream sources from upstream discharge generation in mountainous catchments could generally cause a stronger trend in less diluted low-flow concentration when sources change. However, these diluting effects interact with other mechanisms at downstream locations, for example mobilization processes. Possibly, in southern France, the upstream signal dominates, while in the Alps with smaller relative seasonal *Q* variations, downstream signals could dominate the overall trajectories, and leading to faster high-flow concentration responses. For the Armorican Massif, high-flow concentration responding first to changes in dominant diffuse N-input could cause the clockwise hysteresis patterns. This is supported by generally higher deep and lower shallow groundwater concentrations causing dilution patterns which could result from long-term N-inputs and large legacy stores (Dupas et al., 2020). On the other hand, within the dominant archetype of synchronous average *C*-*Q* seasonality, the heterogeneity in trajectories and controls was high and no dominant general pattern and control was detectable in this study (as discussed above).

In essence, the seasonality trajectory and its corresponding hysteresis integrate all the above mentioned processes. The missing dominance emphasizes that over the study domain multiple controls are relevant and hierarchies vary. Many settings can lead to the same response pattern and seasonality trajectory.

4.3. Spatial Variability Larger and Better Predictable Than Long-Term Temporal Variability of Nitrate Seasonality

Spatial variability of seasonality among the catchments is larger than the long-term temporal variability of most catchments, even when including significant trends in the logarithmic seasonal ratio. Although the number of significant long-term trends in the seasonal ratio $\log(C_{HF}/C_{LF})$ (76%) and hysteresis patterns (59%) reveal distinct changes in NO_3^- seasonality on multi-decadal time scales in the majority of catchments, inter-catchment variability across the study area largely exceeded the temporal variability within a catchment. Dupas et al. (2019) and Abbott, Gruau, et al. (2018) also report examples of higher spatial than temporal variability, resulting in spatial persistence, that is stable spatial patterns among catchments through time. These two studies, based on shorter periods of six (Dupas et al., 2019) and 12 years (Abbott, Gruau, et al., 2018), include mainly seasonal variations. Our finding thus extends the spatial persistence concept for NO_3^- seasonality to decadal trajectories across a wide range of Western European catchments.

At the same time, we can better explain the spatial variability of long-term average seasonality and *C*-*Q* dynamics among the catchments (Section 4.1). In contrast, the differences in trajectories resulting from different response times of low-flow and high-flow concentrations were only poorly predictable from the available data, and only small differences in catchment characteristics were apparent between the hysteresis classes (Section 4.2). This could be due to the fact that trajectories are affected by multiple controls with asynchronous source changes and seasonally variable responses, possibly masking each other. Further investigation may include temporarily variable catchment descriptors, such as long-term data on point source inputs, and time series of ecological in-stream metrics such as chlorophyll-a.

5. Conclusions

We characterized average long-term NO_3^--*Q* seasonalities and their trajectories from long-term time series in 290 French and German catchments covering a large variety in hydroclimate, topography, lithology and anthropogenic pressures. We implemented a novel hysteresis approach using low- and high-flow NO_3-N concentration trajectories. Our main findings are:

- We observed a widespread dominance of concurrent maxima of *Q* and NO_3-N in winter (84%), supporting our hypothesis. Deviations from this archetype of long-term average *C*-*Q* seasonality were linked to topography and hydroclimatic seasonality, and to source heterogeneity or lithology especially in the Armorican Massif
- Surprisingly, counterclockwise and clockwise hysteresis patterns of low-flow and high-flow NO_3-N concentrations occurred equally often, thus we had to reject our hypothesis about dominant occurrence of

Global Biogeochemical Cycles 10.1029/2021GB007050

faster response during high flow. We exemplarily showed that indeed counterclockwise hysteresis can be found in point source dominated and clockwise hysteresis in agricultural catchments. However, the lack of a consistent pattern in the French and German catchments suggests a high level of complexity and potential interactions in the controls over the wide range of catchments. These controls need to be further disentangled in a set of catchments with better known input time series. We point out that scarce data especially on point source loads (including their temporal evolution) is limiting the understanding of catchment functioning across a large sample. Therefore monitoring efforts and data use policies should be improved

- Overall, we found that spatial variability of long-term average *C*-*Q* seasonality between the catchments was larger and easier to predict than its long-term temporal evolution at a single station

Our large sample study has several implications for water quality management. The dominant spatial variability indicates that (a) uniform regulations may not be appropriate but need to take the spatial variability into account and should target the management regionally, and (b) short-term monitoring can already be useful to characterize the overall system functioning. The distinction between low- and high-flow trajectories can guide ecological assessment and water quality management considering that aquatic ecosystems are more prone to eutrophication during low flow, while exported loads are more susceptible to changes in high flows.

Conflict of Interest

The authors declare no conflicts of interest relevant to this study.

Data Availability Statement

Datasets used for this research are available at Ebeling and Dupas (2021), Musolff et al. (2020 original data in institutional repository), Musolff (2020), http://naiades.eaufrance.fr/ and http://hydro.eaufrance.fr/, Ehrhardt et al., 2021. References to further original datasets used for the catchment characteristics repository are given in the Table S1.

Acknowledgments
The authors acknowledge the E-OBS data set from the EU-FP6 project UERRA (http://www.uerra.eu) and the Copernicus Climate Change Service, and the data providers in the ECA&D project (https://eca.knmi.nl). The authors further acknowledge several organizations for providing data products used in the catchment characteristics data set, including the BGR, EEA, FAO, IIASA, ISRIC, ISSCAS and JRC. The authors greatly appreciate the funding by the Deutsche Forschungsgemeinschaft - DFG (Dominant controls on catchment water quality dynamics—a Germany-wide analysis using data-driven models, DFG 392886738) and the Initiative and Networking Fund of the Helmholtz Association through the project Advanced Earth System Modelling Capacity (ESM) (www.esmproject.net). B.A was supported by the US National Science Foundation award number EAR 2011439. Open access funding enabled and organized by Projekt DEAL.

References

Abbott, B. W., Bishop, K., Zarnetske, J. P., Hannah, D. M., Frei, R. J., Minaudo, C., et al. (2019). A water cycle for the Anthropocene. *Hydrological Processes*, *33*(23), 3046–3052. https://doi.org/10.1002/hyp.13544

Abbott, B. W., Gruau, G., Zarnetske, J. P., Moatar, F., Barbe, L., Thomas, Z., et al. (2018). Unexpected spatial stability of water chemistry in headwater stream networks. *Ecology Letters*, *21*(2), 296–308. https://doi.org/10.1111/ele.12897

Abbott, B. W., Moatar, F., Gauthier, O., Fovet, O., Antoine, V., & Ragueneau, O. (2018). Trends and seasonality of river nutrients in agricultural catchments: 18 years of weekly citizen science in France. *Science of the Total Environment*, *624*, 845–858. https://doi.org/10.1016/j.scitotenv.2017.12.176

Altmann, A., Toloşi, L., Sander, O., & Lengauer, T. (2010). Permutation importance: A corrected feature importance measure. *Bioinformatics*, *26*(10), 1340–1347. https://doi.org/10.1093/bioinformatics/btq134

Aquilina, L., Roques, C., Boisson, A., Vergnaud-Ayraud, V., Labasque, T., Pauwels, H., et al. (2018). Autotrophic denitrification supported by biotite dissolution in crystalline aquifers (1): New insights from short-term batch experiments. *Science of the Total Environment*, *619*, 842–853. https://doi.org/10.1016/j.scitotenv.2017.11.079

Ascott, M. J., Gooddy, D. C., Wang, L., Stuart, M. E., Lewis, M. A., Ward, R. S., & Binley, A. M. (2017). Global patterns of nitrate storage in the vadose zone. *Nature Communications*, *8*(1), 1416. https://doi.org/10.1038/s41467-017-01321-w

Aubert, A. H., Gascuel-Odoux, C., Gruau, G., Akkal, N., Faucheux, M., Fauvel, Y., et al. (2013). Solute transport dynamics in small, shallow groundwater-dominated agricultural catchments: Insights from a high-frequency, multisolute 10 yr-long monitoring study. *Hydrology and Earth System Sciences*, *17*(4), 1379–1391. https://doi.org/10.5194/hess-17-1379-2013

Benettin, P., Bailey, S. W., Rinaldo, A., Likens, G. E., McGuire, K. J., & Botter, G. (2017). Young runoff fractions control streamwater age and solute concentration dynamics. *Hydrological Processes*, *31*(16), 2982–2986. https://doi.org/10.1002/hyp.11243

Benettin, P., Fovet, O., & Li, L. (2020). Nitrate removal and young stream water fractions at the catchment scale. *Hydrological Processes*, *34*(12), 2725–2738. https://doi.org/10.1002/hyp.13781

Berghuijs, W. R., Harrigan, S., Molnar, P., Slater, L. J., & Kirchner, J. W. (2019). The relative importance of different flood-generating mechanisms across Europe. *Water Resources Research*, *55*(6), 4582–4593. https://doi.org/10.1029/2019WR024841

Blaszczak, J. R., Delesantro, J. M., Urban, D. L., Doyle, M. W., & Bernhardt, E. S. (2019). Scoured or suffocated: Urban stream ecosystems oscillate between hydrologic and dissolved oxygen extremes. *Limnology and Oceanography*, *64*(3), 877–894. https://doi.org/10.1002/lno.11081

Blöschl, G., Hall, J., Parajka, J., Perdigão, R. A. P., Merz, B., Arheimer, B., et al. (2017). Changing climate shifts timing of European floods. *Science*, *357*(6351), 588–590. https://doi.org/10.1126/science.aan2506

Botter, M., Li, L., Hartmann, J., Burlando, P., & Fatichi, S. (2020). Depth of solute generation is a dominant control on concentration-discharge relations. *Water Resources Research*, *56*, e2019WR026695. https://doi.org/10.1029/2019WR026695

Global Biogeochemical Cycles 10.1029/2021GB007050

Bouraoui, F., & Grizzetti, B. (2011). Long term change of nutrient concentrations of rivers discharging in European seas. *Science of the Total Environment*, *409*(23), 4899–4916. https://doi.org/10.1016/j.scitotenv.2011.08.015

Bouwman, A. F., Bierkens, M. F. P., Griffioen, J., Hefting, M. M., Middelburg, J. J., Middelkoop, H., & Slomp, C. P. (2013). Nutrient dynamics, transfer and retention along the aquatic continuum from land to ocean: Towards integration of ecological and biogeochemical models. *Biogeosciences*, *10*(1), 1–22. https://doi.org/10.5194/bg-10-1-2013

Bowes, M. J., Smith, J. T., Neal, C., Leach, D. V., Scarlett, P. M., Wickham, H. D., et al. (2011). Changes in water quality of the River Frome (UK) from 1965 to 2009: Is phosphorus mitigation finally working? *Science of the Total Environment*, *409*(18), 3418–3430. https://doi.org/10.1016/j.scitotenv.2011.04.049

Casquin, A., Gu, S., Dupas, R., Petitjean, P., Gruau, G., & Durand, P. (2020). River network alteration of C-N-P dynamics in a mesoscale agricultural catchment. *Science of the Total Environment*, *749*, 141551. https://doi.org/10.1016/j.scitotenv.2020.141551

CLC. (2006). *CORINE land cover*. Retrieved from https://land.copernicus.eu/pan-european/corine-land-cover

Condon, L. E., Markovich, K. H., Kelleher, C. A., McDonnell, J. J., Ferguson, G., & McIntosh, J. C. (2020). Where is the bottom of a watershed? *Water Resources Research*, *56*(3), e2019WR026010. https://doi.org/10.1029/2019WR026010

Cornes, R. C., van der Schrier, G.,van den Besselaar, E. J. M., & Jones, P. D. (2018). An ensemble version of the E-OBS temperature and precipitation data sets. *Journal of Geophysical Research: Atmospheres*, *123*, 9391–9409. https://doi.org/10.1029/2017jd028200

Diaz, R. J., & Rosenberg, R. (2008). Spreading dead zones and consequences for marine ecosystems. *Science*, *321*(5891), 926–929. https://doi.org/10.1126/science.1156401

Duncan, J. M., Band, L. E., Groffman, P. M., & Bernhardt, E. S. (2015). Mechanisms driving the seasonality of catchment scale nitrate export: Evidence for riparian ecohydrologic controls. *Water Resources Research*, *51*, 3982–3997. https://doi.org/10.1002/2015WR016937

Dupas, R., Ehrhardt, S., Musolff, A., Fovet, O., & Durand, P. (2020). Long-term nitrogen retention and transit time distribution in agricultural catchments in western France. *Environmental Research Letters*, *15*(11), 115011. https://doi.org/10.1088/1748-9326/abbe47

Dupas, R., Jomaa, S., Musolff, A., Borchardt, D., & Rode, M. (2016). Disentangling the influence of hydroclimatic patterns and agricultural management on river nitrate dynamics from sub-hourly to decadal time scales. *Science of the Total Environment*, *571*, 791–800. https://doi.org/10.1016/j.scitotenv.2016.07.053

Dupas, R., Minaudo, C., & Abbott, B. W. (2019). Stability of spatial patterns in water chemistry across temperate ecoregions. *Environmental Research Letters*, *14*(7), 074015. https://doi.org/10.1088/1748-9326/ab24f4

Dupas, R., Minaudo, C., Gruau, G., Ruiz, L., & Gascuel-Odoux, C. (2018). Multidecadal trajectory of riverine nitrogen and phosphorus dynamics in rural catchments. *Water Resources Research*, *54*, 5327–5340. https://doi.org/10.1029/2018WR022905

Dupas, R., Musolff, A., Jawitz, J. W., Rao, P. S. C., Jäger, C. G., Fleckenstein, J. H., et al. (2017). Carbon and nutrient export regimes from headwater catchments to downstream reaches. *Biogeosciences*, *14*(18), 4391–4407. https://doi.org/10.5194/bg-14-4391-2017

Ebeling, P. (2021). *CCDB - Catchment characteristics database Germany, HydroShare*. [Dataset]. https://doi.org/10.4211/hs.0fc1b5b1be4a475aacfd9545e72e6839

Ebeling, P., & Dupas, R. (2021). *CCDB - Catchment characteristics data base France and Germany, HydroShare*. [Dataset]. https://doi.org/10.4211/hs.c7d4df3ba74647f0aa83ae92be2e294b

Ebeling, P., Kumar, R., Weber, M., Knoll, L., Fleckenstein, J. H., & Musolff, A. (2021). Archetypes and controls of riverine nutrient export across German catchments. *Water Research*. e2020WR028134. https://doi.org/10.1029/2020WR028134

EEA. (2013). *DEM over Europe from the GMES RDA project (EU-DEM, resolution 25m) - version 1*. Dataset.

EEC. (1991a). *Council Directive 91/271/EEC of 21 May 1991 concerning urban wastewater treatment*. European Economic Community.

EEC. (1991b). *Council Directive 91/676/EEC of 12 December 1991 concerning the protection of waters against pollution caused by nitrates from agricultural sources*. European Economic Community.

Ehrhardt, S., Ebeling, P., & Dupas, R. (2021). *Exported French water quality and quantity data, HydroShare*. [Dataset]. https://doi.org/10.4211/hs.d8c43e1e8a5a4872bc0b75a45f350f7a

Ehrhardt, S., Ebeling, P., Dupas, R., Kumar, R., Fleckenstein, J., & Musolff, A. (2020). Nitrate transport and retention in Western European catchments are shaped by hydroclimate and subsurface properties. *Earth and Space Science Open Archive*. https://doi.org/10.1002/essoar.10505117.4

Ehrhardt, S., Kumar, R., Fleckenstein, J. H., Attinger, S., & Musolff, A. (2019). Trajectories of nitrate input and output in three nested catchments along a land use gradient. *Hydrology and Earth System Sciences*, *23*(9), 3503–3524. https://doi.org/10.5194/hess-23-3503-2019

Fovet, O., Humbert, G., Dupas, R., Gascuel-Odoux, C., Gruau, G., Jaffrezic, A., et al. (2018). Seasonal variability of stream water quality response to storm events captured using high-frequency and multi-parameter data. *Journal of Hydrology*, *559*, 282–293. https://doi.org/10.1016/j.jhydrol.2018.02.040

Frei, R. J., Abbott, B. W., Dupas, R., Gu, S., Gruau, G., Thomas, Z., et al. (2020). Predicting nutrient incontinence in the Anthropocene at watershed scales. *Frontiers in Environmental Science*, *7*(200). https://doi.org/10.3389/fenvs.2019.00200

Gnann, S. J., Howden, N. J. K., & Woods, R. A. (2020). Hydrological signatures describing the translation of climate seasonality into streamflow seasonality. *Hydrology and Earth System Sciences*, *24*(2), 561–580. https://doi.org/10.5194/hess-24-561-2020

Godsey, S. E., Kirchner, J. W., & Clow, D. W. (2009). Concentration-discharge relationships reflect chemostatic characteristics of US catchments. *Hydrological Processes*, *23*(13), 1844–1864. https://doi.org/10.1002/hyp.7315

Guillemot, S., Fovet, O., Gascuel-Odoux, C., Gruau, G., Casquin, A., Curie, F., et al. (2021). Spatio-temporal controls of C–N–P dynamics across headwater catchments of a temperate agricultural region from public data analysis. *Hydrology and Earth System Sciences*, *25*(5), 2491–2511. https://doi.org/10.5194/hess-25-2491-2021

Gupta, H. V., Perrin, C., Bloschl, G., Montanari, A., Kumar, R., Clark, M., & Andreassian, V. (2014). Large-sample hydrology: A need to balance depth with breadth. *Hydrology and Earth System Sciences*, *18*(2), 463–477. https://doi.org/10.5194/hess-18-463-2014

Hamilton, S. K. (2012). Biogeochemical time lags may delay responses of streams to ecological restoration. *Freshwater Biology*, *57*(s1), 43–57. https://doi.org/10.1111/j.1365-2427.2011.02685.x

Hirsch, R. M., & De Cicco, L. A. (2015). User Guide to Exploration and Graphics for RivEr Trends (EGRET) and dataRetrieval: R Packages for Hydrologic Data. *U.S. Geological Survey Techniques and Methods Book 4, 4*. Chap. A10, 93. https://doi.org/10.3133/tm4A10

Hirsch, R. M., Moyer, D. L., & Archfield, S. A. (2010). Weighted Regressions on time, discharge, and season (WRTDS), with an application to Chesapeake Bay river inputs. *JAWRA Journal of the American Water Resources Association*, *46*(5), 857–880. https://doi.org/10.1111/j.1752-1688.2010.00482.x

Howden, N. J. K., Burt, T. P., Worrall, F., Whelan, M. J., & Bieroza, M. Z. (2010). Nitrate concentrations and fluxes in the River Thames over 140 years (1868–2008): Are increases irreversible? *Hydrological Processes*, *24*(18), 2657–2662. https://doi.org/10.1002/hyp.7835

Jawitz, J. W., Desormeaux, A. M., Annable, M. D., Borchardt, D., & Dobberfuhl, D. (2020). Disaggregating landscape-scale nitrogen attenuation along hydrological flow paths. *Journal of Geophysical Research: Biogeosciences*, *125*, e2019JG005229. https://doi.org/10.1029/2019JG005229

Kolbe, T., de Dreuzy, J.-R., Abbott, B. W., Aquilina, L., Babey, T., Green, C. T., et al. (2019). Stratification of reactivity determines nitrate removal in groundwater. *Proceedings of the National Academy of Sciences*, *116*(7), 2494–2499. https://doi.org/10.1073/pnas.1816892116

Kolbe, T., Marçais, J., Thomas, Z., Abbott, B. W., de Dreuzy, J.-R., Rousseau-Gueutin, P., et al. (2016). Coupling 3D groundwater modeling with CFC-based age dating to classify local groundwater circulation in an unconfined crystalline aquifer. *Journal of Hydrology*, *543*, 31–46. https://doi.org/10.1016/j.jhydrol.2016.05.020

Krueger, T., Quinton, J. N., Freer, J., Macleod, C. J. A., Bilotta, G. S., Brazier, R. E., et al. (2009). Uncertainties in data and models to describe event dynamics of agricultural sediment and phosphorus transfer. *Journal of Environmental Quality*, *38*(3), 1137–1148. https://doi.org/10.2134/jeq2008.0179

Kuentz, A., Arheimer, B., Hundecha, Y., & Wagener, T. (2017). Understanding hydrologic variability across Europe through catchment classification. *Hydrology and Earth System Sciences*, *21*(6), 2863–2879. https://doi.org/10.5194/hess-21-2863-2017

Kumar, R., Heße, F., Rao, P. S. C., Musolff, A., Jawitz, J. W., Sarrazin, F., et al. (2020). Strong hydroclimatic controls on vulnerability to subsurface nitrate contamination across Europe. *Nature Communications*, *11*(1), 6302. https://doi.org/10.1038/s41467-020-19955-8

Kumar, R., Samaniego, L., & Attinger, S. (2013). Implications of distributed hydrologic model parameterization on water fluxes at multiple scales and locations. *Water Resources Research*, *49*(1), 360–379. https://doi.org/10.1029/2012wr012195

Lang, M., Binder, M., Richter, J., Schratz, P., Pfisterer, F., Coors, S., et al. (2019). MLR3: A modern object-oriented machine learning framework in R. *Journal of Open Source Software*, *4*, 1903. https://doi.org/10.21105/joss.01903

Le Moal, M., Gascuel-Odoux, C., Ménesguen, A., Souchon, Y., Étrillard, C., Levain, A., et al. (2019). Eutrophication: A new wine in an old bottle? *Science of the Total Environment*, *651*, 1–11. https://doi.org/10.1016/j.scitotenv.2018.09.139

Li, L., Sullivan, P. L., Benettin, P., Cirpka, O. A., Bishop, K., Brantley, S. L., et al. (2021). Toward catchment hydro-biogeochemical theories. *WIREs Water*, *8*(1), e1495. https://doi.org/10.1002/wat2.1495

Lloyd, C. E. M., Freer, J. E., Johnes, P. J., & Collins, A. L. (2016). Technical Note: Testing an improved index for analysing storm discharge–concentration hysteresis. *Hydrology and Earth System Sciences*, *20*(2), 625–632. https://doi.org/10.5194/hess-20-625-2016

Lutz, S. R., Trauth, N., Musolff, A., Van Breukelen, B. M., Knöller, K., & Fleckenstein, J. H. (2020). How important is denitrification in riparian zones? Combining end-member mixing and isotope modeling to quantify nitrate removal from riparian groundwater. *Water Resources Research*, *56*, e2019WR025528. https://doi.org/10.1029/2019wr025528

Marçais, J., Gauvain, A., Labasque, T., Abbott, B. W., Pinay, G., Aquilina, L., et al. (2018). Dating groundwater with dissolved silica and CFC concentrations in crystalline aquifers. *Science of the Total Environment*, *636*, 260–272. https://doi.org/10.1016/j.scitotenv.2018.04.196

Martin, C., Aquilina, L., Gascuel-Odoux, C., Molénat, J., Faucheux, M., & Ruiz, L. (2004). Seasonal and interannual variations of nitrate and chloride in stream waters related to spatial and temporal patterns of groundwater concentrations in agricultural catchments. *Hydrological Processes*, *18*(7), 1237–1254. https://doi.org/10.1002/hyp.1395

Martin, C., Molénat, J., Gascuel-Odoux, C., Vouillamoz, J. M., Robain, H., Ruiz, L., et al. (2006). Modelling the effect of physical and chemical characteristics of shallow aquifers on water and nitrate transport in small agricultural catchments. *Journal of Hydrology*, *326*(1), 25–42. https://doi.org/10.1016/j.jhydrol.2005.10.040

Meals, D. W., Dressing, S. A., & Davenport, T. E. (2010). Lag time in water quality response to best management practices: A review. *Journal of Environmental Quality*, *39*(1), 85–96. https://doi.org/10.2134/jeq2009.0108

Minaudo, C., Abonyi, A., Leitão, M., Lançon, A. M., Floury, M., Descy, J.-P., & Moatar, F. (2020). Long-term impacts of nutrient control, climate change, and invasive clams on phytoplankton and cyanobacteria biomass in a large temperate river. *Science of the Total Environment*. https://doi.org/10.1016/j.scitotenv.2020.144074

Minaudo, C., Dupas, R., Gascuel-Odoux, C., Roubeix, V., Danis, P.-A., & Moatar, F. (2019). Seasonal and event-based concentration-discharge relationships to identify catchment controls on nutrient export regimes. *Advances in Water Resources*, *131*, 103379. https://doi.org/10.1016/j.advwatres.2019.103379

Minaudo, C., Meybeck, M., Moatar, F., Gassama, N., & Curie, F. (2015). Eutrophication mitigation in rivers: 30 years of trends in spatial and seasonal patterns of biogeochemistry of the Loire River (1980–2012). *Biogeosciences*, *12*(8), 2549–2563. https://doi.org/10.5194/bg-12-2549-2015

Moatar, F., Abbott, B. W., Minaudo, C., Curie, F., & Pinay, G. (2017). Elemental properties, hydrology, and biology interact to shape concentration-discharge curves for carbon, nutrients, sediment, and major ions. *Water Resources Research*, *53*, 1270–1287. https://doi.org/10.1002/2016wr019635

Musolff, A. (2020). WQQDB - Water quality and quantity data base Germany: Metadata. *HydroShare*. Dataset. https://doi.org/10.4211/hs.a42addcbd59a466a9aa56472dfef8721

Musolff, A., Grau, T., Weber, M., Ebeling, P., Samaniego-Eguiguren, L., & Kumar, R. (2020). *WQQDB: Water quality and quantity data base Germany*. Dataset. Retrieved from http://www.ufz.de/record/dmp/archive/7754

Musolff, A., Schmidt, C., Rode, M., Lischeid, G., Weise, S. M., & Fleckenstein, J. H. (2016). Groundwater head controls nitrate export from an agricultural lowland catchment. *Advances in Water Resources*, *96*, 95–107. https://doi.org/10.1016/j.advwatres.2016.07.003

Musolff, A., Schmidt, C., Selle, B., & Fleckenstein, J. H. (2015). Catchment controls on solute export. *Advances in Water Resources*, *86*, 133–146. https://doi.org/10.1016/j.advwatres.2015.09.026

Newcomer, M. E., Bouskill, N. J., Wainwright, H., Maavara, T., Arora, B., Siirila-Woodburn, E. R., et al. (2021). Hysteresis patterns of watershed nitrogen retention and loss over the Past 50 years in United States hydrological basins. *Global Biogeochemical Cycles*, *35*(4), e2020GB006777. https://doi.org/10.1029/2020GB006777

Raymond, P. A., Saiers, J. E., & Sobczak, W. V. (2016). Hydrological and biogeochemical controls on watershed dissolved organic matter transport: Pulse-shunt concept. *Ecology*, *97*(1), 5–16. https://doi.org/10.1890/14-1684.1

Samaniego, L., Kumar, R., & Attinger, S. (2010). Multiscale parameter regionalization of a grid-based hydrologic model at the mesoscale. *Water Resources Research*, *46*. https://doi.org/10.1029/2008WR007327

Sebilo, M., Mayer, B., Nicolardot, B., Pinay, G., & Mariotti, A. (2013). Long-term fate of nitrate fertilizer in agricultural soils. *Proceedings of the National Academy of Sciences*, *110*(45), 18185–18189. https://doi.org/10.1073/pnas.1305372110

Seibert, J., Grabs, T., Köhler, S., Laudon, H., Winterdahl, M., & Bishop, K. (2009). Linking soil- and stream-water chemistry based on a riparian flow-concentration integration model. *Hydrology and Earth System Sciences*, *13*(12), 2287–2297. https://doi.org/10.5194/hess-13-2287-2009

Sen, P. K. (1968). Estimates of the regression coefficient based on Kendall's Tau. *Journal of the American Statistical Association*, *63*(324), 1379–1389. https://doi.org/10.1080/01621459.1968.10480934

Global Biogeochemical Cycles 10.1029/2021GB007050

Steffen, W., Richardson, K., Rockstrom, J., Cornell, S. E., Fetzer, I., Bennett, E. M., et al. (2015). Sustainability. Planetary boundaries: Guiding human development on a changing planet. *Science*, *347*(6223), 1259855. https://doi.org/10.1126/science.1259855

Van Meter, K. J., & Basu, N. B. (2015). Catchment legacies and time lags: A parsimonious watershed model to predict the effects of legacy storage on nitrogen export. *PloS One*, *10*(5), e0125971. https://doi.org/10.1371/journal.pone.0125971

Van Meter, K. J., & Basu, N. B. (2017). Time lags in watershed-scale nutrient transport: An exploration of dominant controls. *Environmental Research Letters*, *12*(8), 084017. https://doi.org/10.1088/1748-9326/aa7bf4

Van Meter, K. J., Basu, N. B., Veenstra, J. J., & Burras, C. L. (2016). The nitrogen legacy: Emerging evidence of nitrogen accumulation in anthropogenic landscapes. *Environmental Research Letters*, *11*(3), 035014. https://doi.org/10.1088/1748-9326/11/3/035014

Van Meter, K. J., Chowdhury, S., Byrnes, D. K., & Basu, N. B. (2020). Biogeochemical asynchrony: Ecosystem drivers of seasonal concentration regimes across the Great Lakes Basin. *Limnology and Oceanography*, *65*(4), 848–862. https://doi.org/10.1002/lno.11353

Vitousek, P. M., Mooney, H. A., Lubchenco, J., & Melillo, J. M. (1997). Human Domination of Earth's Ecosystems. *Science*, *277*(5325), 494–499. https://doi.org/10.1126/science.277.5325.494

Wang, L., Stuart, M. E., Lewis, M. A., Ward, R. S., Skirvin, D., Naden, P. S., et al. (2016). The changing trend in nitrate concentrations in major aquifers due to historical nitrate loading from agricultural land across England and Wales from 1925 to 2150. *Science of the Total Environment*, *542*(Pt), 694–705. https://doi.org/10.1016/j.scitotenv.2015.10.127

Westphal, K., Andreas, M., Daniel, G., & Dietrich, B. (2020). Controls of point and diffuse sources lowered riverine nutrient concentrations asynchronously, thereby warping molar N:P ratios. *Environmental Research Letters*. Retrieved from http://iopscience.iop.org/10.1088/1748-9326/ab98b6

Winter, C., Lutz, S. R., Musolff, A., Kumar, R., Weber, M., & Fleckenstein, J. H. (2020). Disentangling the impact of catchment heterogeneity on nitrate export dynamics from event to long-term time scales*n/a*(n/a). *Water Resources Research*, e2020WR027992. https://doi.org/10.1029/2020WR027992

Withers, P. J. A., & Jarvie, H. P. (2008). Delivery and cycling of phosphorus in rivers: A review. *Science of the Total Environment*, *400*(1), 379–395. https://doi.org/10.1016/j.scitotenv.2008.08.002

Wollheim, W. M., Mulukutla, G. K., Cook, C., & Carey, R. O. (2017). Aquatic nitrate retention at river network scales across flow conditions determined using nested in situ sensors. *Water Resources Research*, *53*, 9740–9756. https://doi.org/10.1002/2017wr020644

Wright, M. N., & Ziegler, A. (2017). Ranger: A fast implementation of random forests for high dimensional data in C++ and R. *Journal of Statistical Software*, *77*(1), 17. https://doi.org/10.18637/jss.v077.i01

Yang, J., Heidbüchel, I., Musolff, A., Reinstorf, F., & Fleckenstein, J. H. (2018). Exploring the dynamics of transit times and subsurface mixing in a small agricultural catchment. *Water Resources Research*, *54*, 2317–2335. https://doi.org/10.1002/2017WR021896

Zarnetske, J. P., Bouda, M., Abbott, B. W., Saiers, J., & Raymond, P. A. (2018). Generality of hydrologic transport limitation of watershed organic carbon flux across ecoregions of the United States. *Geophysical Research Letters*, *45*, 11702–11711. https://doi.org/10.1029/2018gl080005

Zhi, W., & Li, L. (2020). The shallow and deep hypothesis: Subsurface vertical chemical contrasts shape nitrate export patterns from different land uses. *Environmental Science & Technology*, *54*, 11915–11928. https://doi.org/10.1021/acs.est.0c01340

Global Biogeochemical Cycles

Supporting Information for

Long-term Nitrate Trajectories Vary by Season in Western European Catchments

Pia Ebeling[1], Rémi Dupas[2], Benjamin Abbott[3], Rohini Kumar[4], Sophie Ehrhardt[1], Jan H. Fleckenstein[1,5], Andreas Musolff[1]

[1]Department of Hydrogeology, Helmholtz Centre for Environmental Research - UFZ, Leipzig, Germany.

[2]UMR SAS, INRAE, Institut Agro, 35000, Rennes, France.

[3]Department of Plant and Wildlife Sciences, Brigham Young University, Provo, UT, USA.

[4]Department of Computational Hydrosystems, Helmholtz Centre for Environmental Research - UFZ, Leipzig, Germany.

[5]Bayreuth Center of Ecology and Environmental Research (BayCEER), University of Bayreuth, Bayreuth, Germany.

Contents of this file

Introduction

This supporting information provides additional figures and one table with details on the used catchment characteristics.

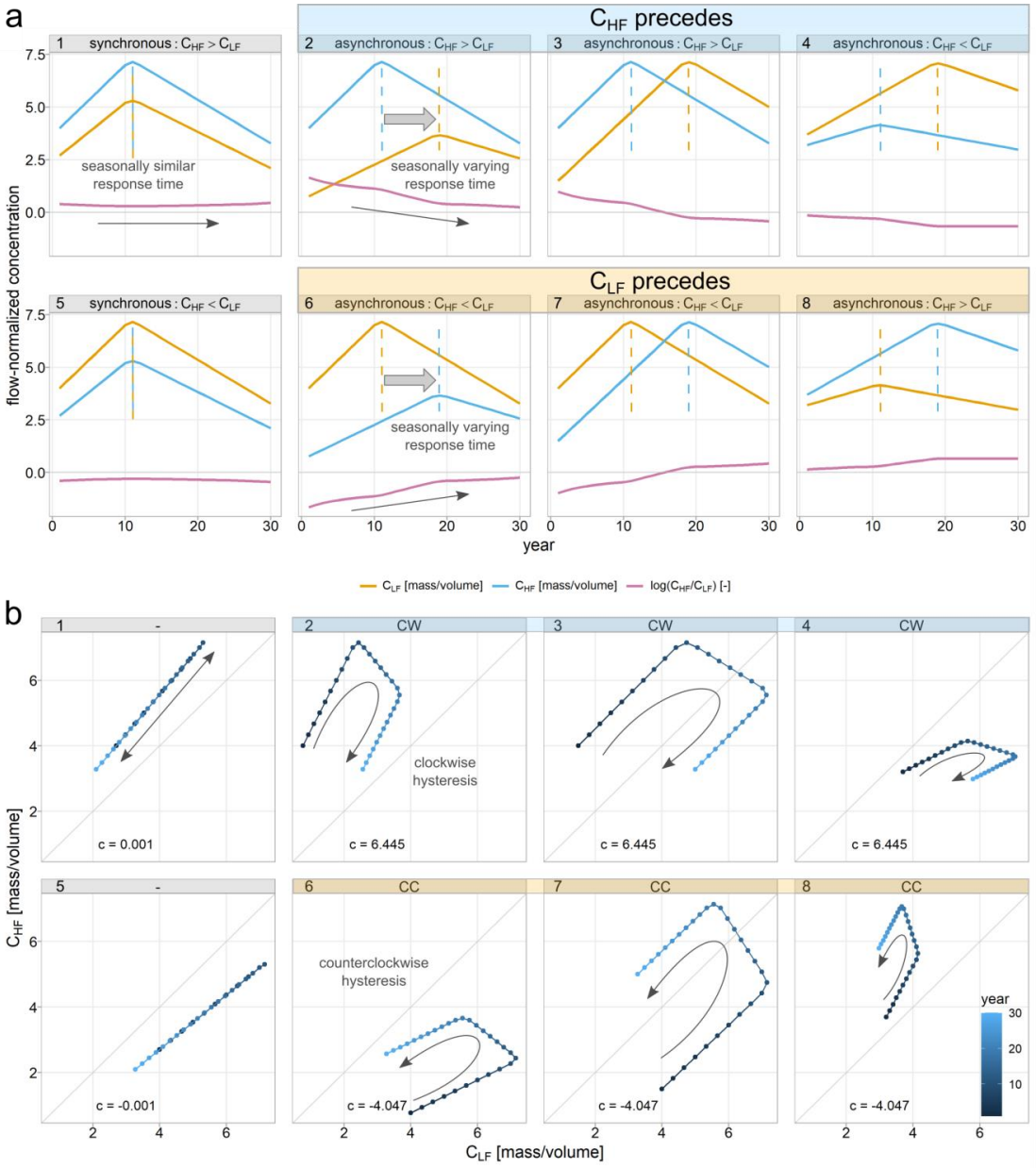

Figure S1. Conceptual framework of hysteresis between C_{LF} and C_{HF} extended from three (cases 1, 2 and 6 shown in main manuscript Figure 2) to eight synthetic time series of distinct C-Q trajectories: (a) time series of C_{LF} and C_{HF}, and the seasonal logarithmic ratio log(C_{HF}/C_{LF}), (b) corresponding hysteresis loops.

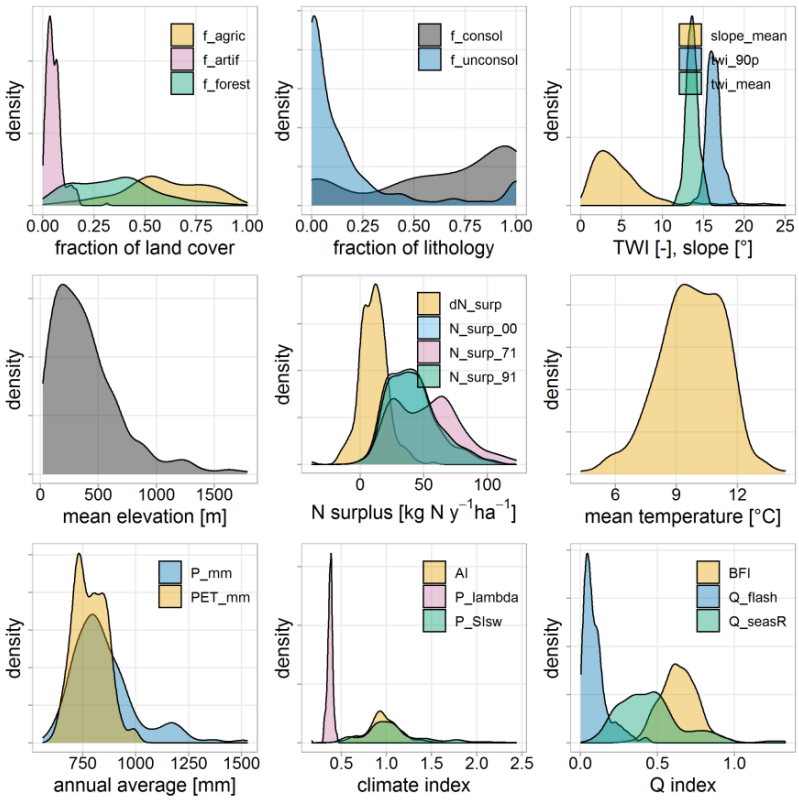

Figure S2. Density distributions of catchment characteristics covered by study catchments (n=290). For details on the descriptor variables see Table S1.

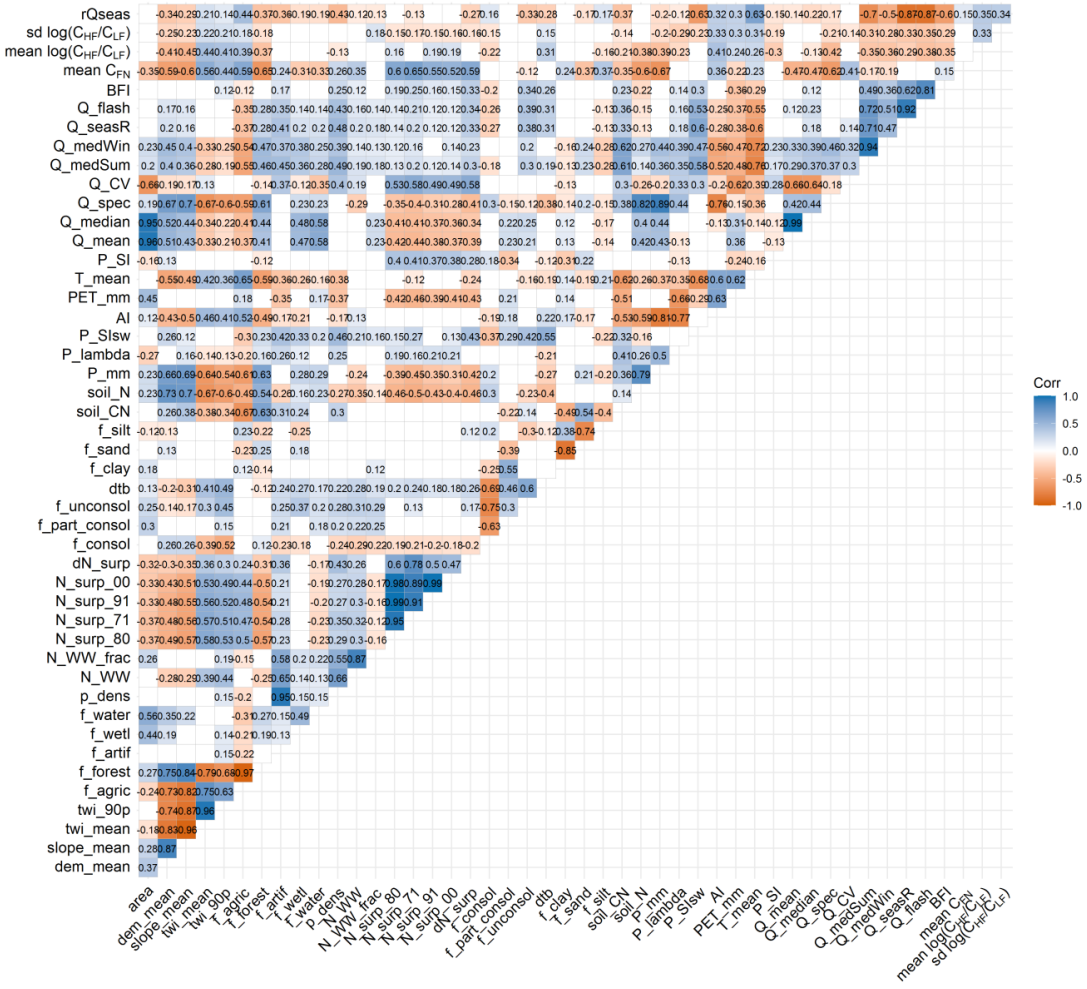

Figure S3. Spearman rank correlation matrix for seasonality metrics and catchment descriptors of the study catchments (n=290). Numbers indicate significant correlation coefficients and blank fields indicate non-significant correlations (significance level of 0.05). For descriptions of variables refer to Table S1.

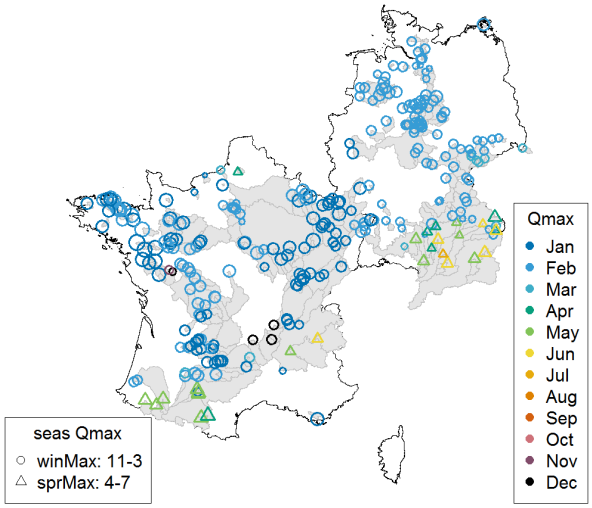

Figure S4. Spatial patterns of timing of Q maximum (colors), the corresponding Q seasonality class (shape) and relative Q seasonality rQseas (size).

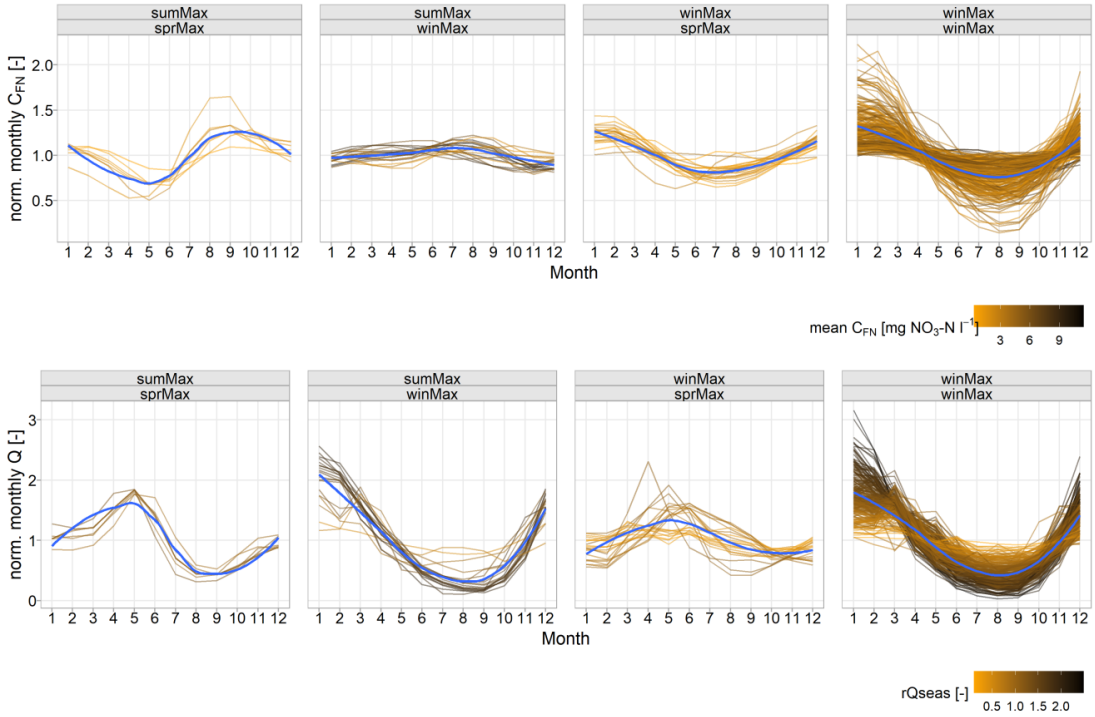

Figure S5. Normalized long-term average NO_3-N C_{FN} (top) and Q (bottom) seasonality (as monthly averages divided by long-term mean). Upper labels in each subplot refer to the class of NO_3-N seasonal timing of the maximum and below for the class of seasonal timing Q (with sumMax: Apr-Oct; winMax: Nov-Mar; sprMax: Apr-Jul), colors long-term mean C_{FN} (top) and mean relative Q seasonal amplitude rQseas (bottom).

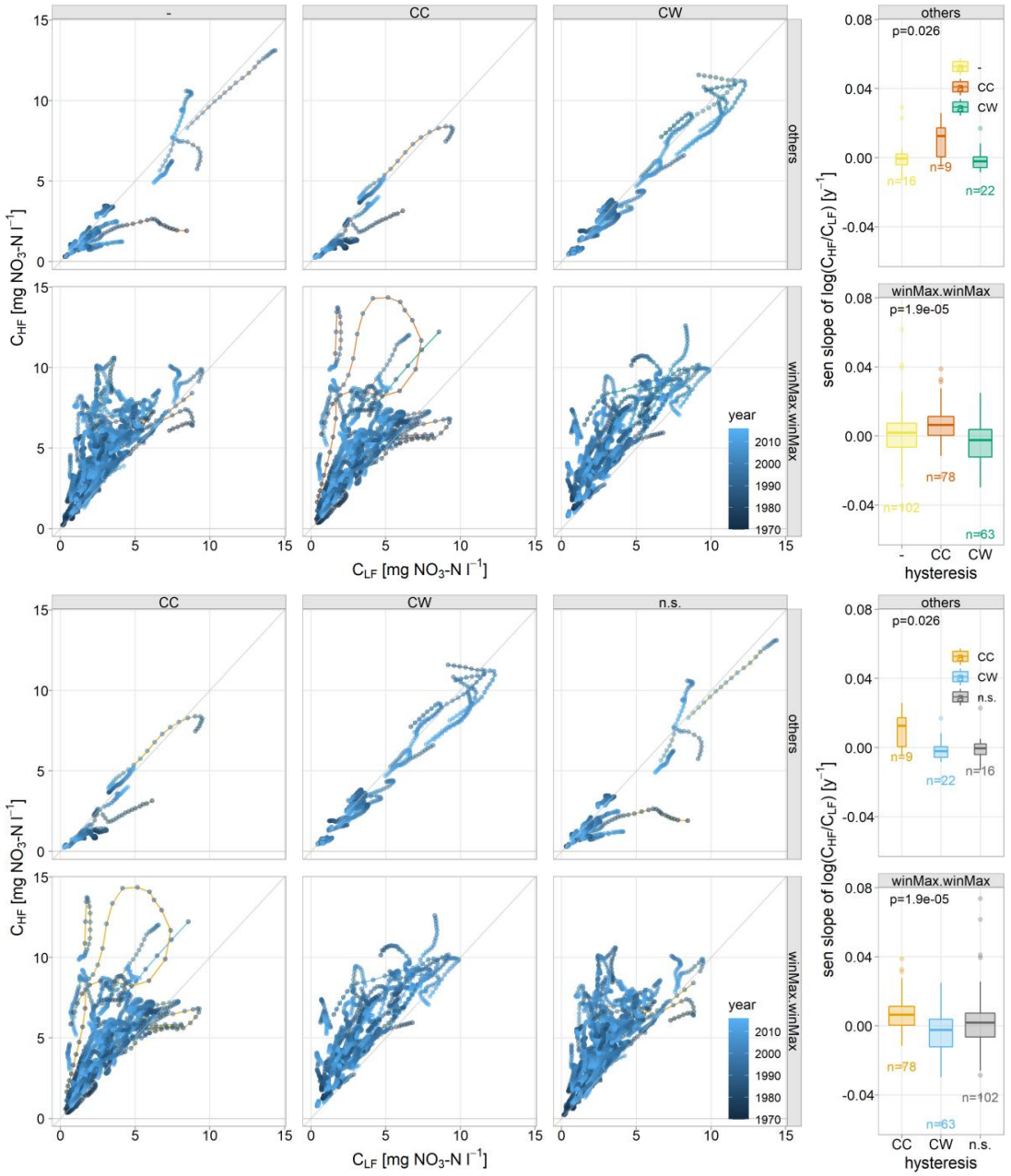

Figure S6. Hysteresis between NO_3-N C_{LF} and C_{HF} (a) and boxplots of sen slopes of monotonic trends of logarithmic seasonal ratio log(C_{HF}/C_{LF}) (b) for study catchments by classes of long-term average C-Q seasonality with winMax of both NO_3-N and Q (bottom) and all other classes (top) and hysteresis (columns). Point colors in (a) indicate the corresponding water year. Line colors in (a) indicate the monotonic trend class of the seasonal ratio trajectories, which corresponds to the color of the hysteresis class in (b) with the same prevalent trend (yellow - no trend, red - positive trend, green - negative trend).

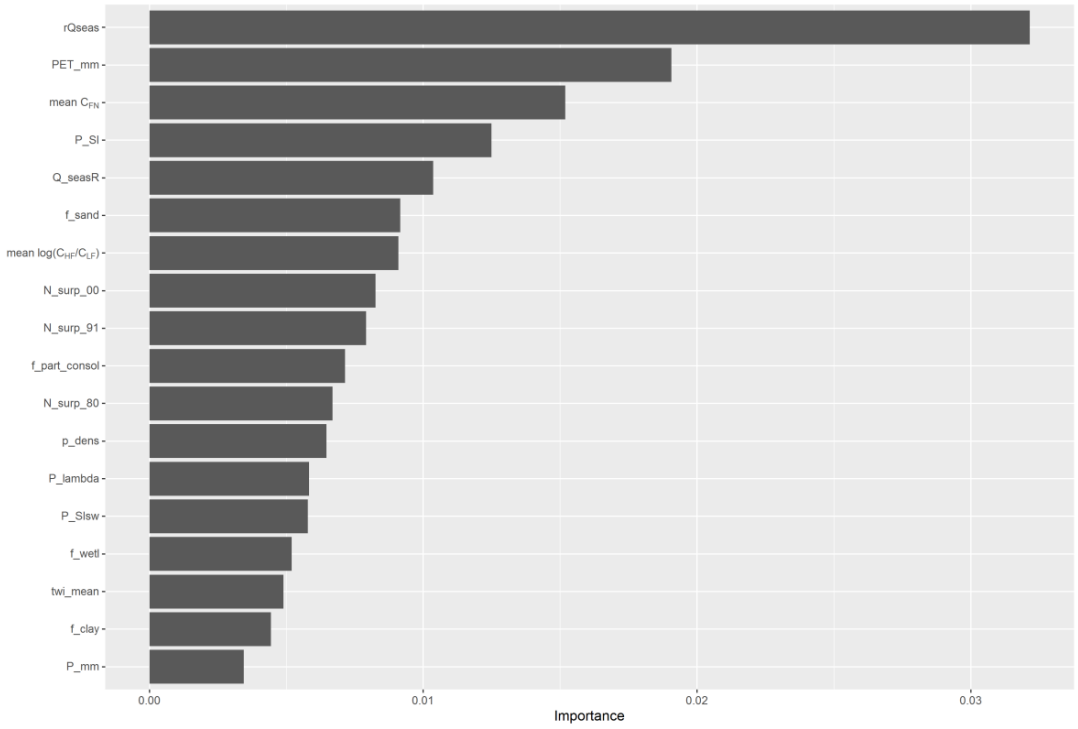

Figure S7. Feature importances from permutation of random forest classification model for CC and CW hysteresis (number of trees num.trees=500, mtry=6). For details on variables refer to Table 1 and S1.

Table S1. Catchment Characteristics, Associated Methods and Data Sources. For the Complete Data Set of Characteristics Refer to the Repository at Ebeling and Dupas (2021).

Category	Variable	Unit	Description and method	Data source
General	area	km²	Catchment area	
Topography	dem_mean	mamsl	Mean elevation of catchment, from DEM rescaled from 25 to 100 m resolution using average	EEA (2013)
	slope_mean	°	Mean topographic slope of catchment, from DEM	EEA (2013)
	twi_mean	-	Mean topographic wetness index (TWI, Beven & Kirkby, 1979)	EEA (2013)
	twi_90p	-	90th percentile of the TWI as a proxy for riparian wetlands (following Musolff et al., 2018)	EEA (2013)
Land cover	f_artif	-	Fraction of artificial land cover (Class 1 Level 1 CORINE)	EEA (2016)
	f_agric	-	Fraction of agricultural land cover (Class 2 Level 1 CORINE)	EEA (2016)
	f_forest	-	Fraction of forested land cover (Class 3 Level 1 CORINE)	EEA (2016)
	f_wetl	-	Fraction of wetland cover (Class 4 Level 1 CORINE)	EEA (2016)
	f_water	-	Fraction of surface water cover (Lass 5 Level 1 CORINE)	EEA (2016)
	p_dens	inhabitants	Mean population density	*CIESIN (2017)*

		km^{-2}		
Nutrient sources	N_surp_71	kg N ha^{-1} y^{-1}	Mean nitrogen (N) surplus per catchment from 1971 to 1990 (including the N surplus on agricultural land and atmospheric N deposition and biological N fixation on non-agricultural areas). For details on the N input data refer to Ehrhardt et al. (2020) and Ebeling and Dupas (2021).	Bach et al. (2006); Bach and Frede (1998); Bartnicky and Benedictow (2017); Bartnicky and Fagerli (2006); Behrendt et al. (1999); Cleveland et al. (1999); Häußermann et al. (2019); Poisvert et al. (2017); Van Meter et al. (2017)
	N_surp_80	kg N ha^{-1} y^{-1}	Mean N surplus per catchment from 1980 to 2015	See N_surp_80
	N_surp_91	kg N ha^{-1} y^{-1}	Mean N surplus per catchment from 1991 to 2015	See N_surp_80
	N_surp_00	kg N ha^{-1} y^{-1}	Mean N surplus per catchment from 2000 to 2015	See N_surp_80
	dN_surp	kg N ha^{-1} y^{-1}	Change in mean N surplus between the periods 1971-1990 and 1991-2015, i.e. dN_surp = N_surp_71 – N_surp_91	See N_surp_80
	N_WW	t N km^{-2} y^{-1}	Mean N input from point sources (from EU-DWE data base)	Vigiak et al. (2019); Vigiak et al. (2020)
	N_WW_frac	-	Fraction of point source loads from total N input loads N_WW_frac = N_WW*10 / (N_WW*10 + N_surp_80)	
Lithology and soils	f_consol	-	Fraction of consolidated rocks (Lithology Level 5)	BGR & UNESCO (eds.) (2014)
	f_part_consol	-	Fraction of partly consolidated rocks (Lithology Level 5)	BGR & UNESCO (eds.) (2014)
	f_unconsol	-	Fraction of unconsolidated rocks (Lithology Level 5)	BGR & UNESCO (eds.) (2014)
	dtb	cm	Median depth to bedrock in the catchment	Shangguan et al. (2017)
	f_sand	-	Mean fraction of sand in soil horizons of the top 100 cm	FAO/IIASA/ISRIC/ISSCAS/JRC (2012)
	f_silt		Mean fraction of silt in soil horizons of the top 100 cm	
	f_clay		Mean fraction of clay in soil horizons of the top 100 cm	
	soil_N	g kg^{-1}	Mean top soil N in catchment	Ballabio et al. (2019)
	soil_CN	-	Mean top soil C/N ratio in catchment	Ballabio et al. (2019)
Hydrology	Q_mean	m^3 s^{-1}	Mean discharge (from 1986, if available)	For Germany: Musolff (2020); Musolff et al. (2020); for France http://hydro.eaufrance.fr/
	Q_median	m^3 s^{-1}	Median discharge	See Q_mean
	Q_spec	mm	Mean annual specific discharge	See Q_mean
	Q_CV	-	Coefficient of variation of time series of daily Q	See Q_mean
	Q_medSum	m^3 s^{-1}	Median discharge in summer months	See Q_mean
	Q_medWin	m^3 s^{-1}	Median discharge in winter months	See Q_mean
	Q_seasR	-	Seasonality index of Q, as ratio between Q_medSum/Q_medWin	See Q_mean
	BFI	-	Base flow index calculated according to WMO [2008] with lfstat package (version 0.9.4) in R	See Q_mean
	Q_flash	-	Flashiness index of Q as the ratio between 5% percentile and 95% percentile of Q time series	See Q_mean
Climate	P_mm	mm	Mean annual precipitation (period 1986-2015 used for all climatic variables)	Cornes et al. (2018)
	P_SIsw	-	Seasonality of precipitation as the ratio between mean summer (Jun-Aug) and winter (Dec-Feb) precipitation	Cornes et al. (2018)
	P_SI	-	Seasonality index of precipitation as the mean difference between monthly P averages and year average	Cornes et al. (2018)
	P_lambda	-	Mean precipitation frequency λ as used by Botter et al. (2013)	Cornes et al. (2018)
	PET_mm	mm	Mean potential evapotranspiration	Cornes et al. (2018)
	AI	-	Aridity index as AI=PET_mm/P_mm	Cornes et al. (2018)
	T_mean	°C	Mean annual temperature	Cornes et al. (2018)

Bach, M., Breuer, L., Frede, H. G., Huisman, J. A., Otte, A., & Waldhardt, R. (2006). Accuracy and congruency of three different digital land-use maps. *Landscape and Urban Planning, 78*(4), 289-299. http://www.sciencedirect.com/science/article/pii/S0169204605001581

Bach, M., & Frede, H.-G. (1998). Agricultural nitrogen, phosphorus and potassium balances in Germany —Methodology and trends 1970 to 1995. *Zeitschrift für Pflanzenernährung und Bodenkunde, 161*(4), 385-393. https://onlinelibrary.wiley.com/doi/abs/10.1002/jpln.1998.3581610406

Ballabio, C., Lugato, E., Fernández-Ugalde, O., Orgiazzi, A., Jones, A., Borrelli, P., et al. (2019). Mapping LUCAS topsoil chemical properties at European scale using Gaussian process regression. *Geoderma, 355*, 113912. http://www.sciencedirect.com/science/article/pii/S0016706119304768

Bartnicky, J., & Benedictow, A. (2017). Atmospheric Deposition of Nitrogen to OSPAR Convention waters in the period 1995–2014. *EMEP/MSC-W Technical Report, 1/2007, Meteorological Synthesizing Centre-West (MSC-W), Norwegian Meteorological Institute, Oslo*. https://emep.int/publ/reports/2017/MSCW_technical_1_2017.pdf

Bartnicky, J., & Fagerli, H. (2006). Atmospheric Nitrogen in the OSPAR Convention Area in the Period 1990–2004. Summary Report for the OSPAR Convention. *EMEP/MSC-W Technical Report, 4/2006, Meteorological Synthesizing Centre-West (MSC-W) of EMEP, Oslo*. https://www.ospar.org/documents?v=7064

Behrendt, H., Huber, P., Opitz, D., Schmoll, O., Scholz, G., & Uebe, R. (1999). Nutrient emissions into river basins of Germany. *UBA-Texte, 75/99*. https://www.umweltbundesamt.de/en/publikationen/naehrstoffbilanzierung-flussgebiete-deutschlands

Beven, K. J., & Kirkby, M. J. (1979). A physically based, variable contributing area model of basin hydrology / Un modèle à base physique de zone d'appel variable de l'hydrologie du bassin versant. *Hydrological Sciences Bulletin, 24*(1), 43-69.

BGR & UNESCO (eds.). (2014). *International Hydrogeological Map of Europe 1 : 1,500,000 (IHME1500). Digital map data v1.1.* Retrieved from: http://www.bgr.bund.de/ihme1500/

Botter, G., Basso, S., Rodriguez-Iturbe, I., & Rinaldo, A. (2013). Resilience of river flow regimes. *Proc Natl Acad Sci U S A, 110*(32), 12925-12930. https://www.ncbi.nlm.nih.gov/pubmed/23878257

Center for International Earth Science Information Network - CIESIN - Columbia University. (2017). *Gridded Population of the World, Version 4 (GPWv4): Population Density, Revision 10*. Retrieved from: https://doi.org/10.7927/H4DZ068D

Cleveland, C. C., Townsend, A. R., Schimel, D. S., Fisher, H., Howarth, R. W., Hedin, L. O., et al. (1999). Global patterns of terrestrial biological nitrogen (N2) fixation in natural ecosystems. *Global Biogeochemical Cycles, 13*(2), 623-645. https://agupubs.onlinelibrary.wiley.com/doi/abs/10.1029/1999GB900014

Cornes, R. C., van der Schrier, G., van den Besselaar, E. J. M., & Jones, P. D. (2018). An Ensemble Version of the E-OBS Temperature and Precipitation Data Sets.

Journal of Geophysical Research: Atmospheres, 123(17), 9391-9409. https://agupubs.onlinelibrary.wiley.com/doi/abs/10.1029/2017JD028200

Ebeling, P., & Dupas, R. (2021). *CCDB - catchment characteristics data base France and Germany, HydroShare*. Retrieved from: http://www.hydroshare.org/resource/c7d4df3ba74647f0aa83ae92be2e294b

EEA. (2013). *DEM over Europe from the GMES RDA project (EU-DEM, resolution 25m) - version 1, Oct. 2013*.

EEA. (2016). *CORINE Land Cover 2012 v18.5*. Retrieved from: https://land.copernicus.eu/pan-european/corine-land-cover

Ehrhardt, S., Ebeling, P., Dupas, R., Kumar, R., Fleckenstein, J., & Musolff, A. (2020). Nitrate transport and retention in Western European catchments are shaped by hydroclimate and subsurface properties. *Earth and Space Science Open Archive*. https://doi.org/10.1002/essoar.10505117.4

FAO/IIASA/ISRIC/ISSCAS/JRC. (2012). *Harmonized World Soil Database (version 1.2)*. Retrieved from: https://webarchive.iiasa.ac.at/Research/LUC/External-World-soil-database/HTML/

Häußermann, U., Bach, M., Klement, L., & Breuer, L. (2019). Stickstoff-Flächenbilanzen für Deutschland mit Regionalgliederung Bundesländer und Kreise – Jahre 1995 bis 2017. Methodik, Ergebnisse und Minderungsmaßnahmen. *Texte, 131/2019*. https://www.umweltbundesamt.de/sites/default/files/medien/1410/publikationen/2019-10-28_texte_131-2019_stickstoffflaechenbilanz.pdf

Musolff, A. (2020). *WQQDB - water quality and quantity data base Germany: metadata, HydroShare*. Retrieved from: https://doi.org/10.4211/hs.a42addcbd59a466a9aa56472dfef8721

Musolff, A., Fleckenstein, J. H., Opitz, M., Büttner, O., Kumar, R., & Tittel, J. (2018). Spatio-temporal controls of dissolved organic carbon stream water concentrations. *Journal of Hydrology, 566*, 205-215. https://doi.org/10.1016/j.jhydrol.2018.09.011

Musolff, A., Grau, T., Weber, M., Ebeling, P., Samaniego-Eguiguren, L., & Kumar, R. (2020). *WQQDB: water quality and quantity data base Germany*. Retrieved from: http://www.ufz.de/record/dmp/archive/7754

Poisvert, C., Curie, F., & Moatar, F. (2017). Annual agricultural N surplus in France over a 70-year period. *Nutrient Cycling in Agroecosystems, 107*(1), 63-78. https://doi.org/10.1007/s10705-016-9814-x

Shangguan, W., Hengl, T., Mendes de Jesus, J., Yuan, H., & Dai, Y. (2017). Mapping the global depth to bedrock for land surface modeling. *Journal of Advances in Modeling Earth Systems, 9*(1), 65-88. https://agupubs.onlinelibrary.wiley.com/doi/abs/10.1002/2016MS000686

Van Meter, K. J., Basu, N. B., & Van Cappellen, P. (2017). Two centuries of nitrogen dynamics: Legacy sources and sinks in the Mississippi and Susquehanna River Basins. *Global Biogeochemical Cycles, 31*(1), 2-23. https://agupubs.onlinelibrary.wiley.com/doi/abs/10.1002/2016GB005498

Vigiak, O., Grizzetti, B., Zanni, M., Aloe, A., Dorati, C., Bouraoui, F., & Pistocchi, A. (2019). *Domestic waste emissions to European freshwaters in the 2010s (v. 1.0)*. Retrieved from: https://data.jrc.ec.europa.eu/dataset/0ae64ac2-64da-4c5e-8bab-ce928897c1fb

Vigiak, O., Grizzetti, B., Zanni, M., Aloe, A., Dorati, C., Bouraoui, F., & Pistocchi, A. (2020). Domestic waste emissions to European waters in the 2010s. *Scientific Data*, *7*(1), 33. https://doi.org/10.1038/s41597-020-0367-0

Study 3: QUADICA: water QUAlity, DIscharge and Catchment Attributes for large-sample studies in Germany

Status:	Published in Earth System Science Data
DOI:	10.5194/essd-14-3715-2022
Authors:	Pia Ebeling, Rohini Kumar, Stefanie R. Lutz, Tam V. Nguyen, Fanny Sarrazin, Michael Weber, Olaf Büttner, Sabine Attinger, Andreas Musolff

PE carried out the study, processed and curated the data and created the figures and tables. PE, AM and RK conceptualized and designed the study following initial ideas and acquired funding from AM and SA. Several authors contributed to the data collection and processing: RK provided the gridded meteorological time series, simulated discharge data and atmospheric deposition data, MW provided time series of N surplus data for the catchments, OB collected the point source data for Germany. PE produced the original draft of the manuscript with contributions of AM and RK. All authors contributed to the reviewing and editing of the manuscript.

Own contribution:

Study concept and design:	80 %
Data preparation and analysis:	90 %
Preparation of figures and tables:	100 %
Interpretation of the results:	80 %
Preparation of the manuscript:	90 %

Earth Syst. Sci. Data, 14, 3715–3741, 2022
https://doi.org/10.5194/essd-14-3715-2022

Open Access Earth System Science Data

QUADICA: water QUAlity, DIscharge and Catchment Attributes for large-sample studies in Germany

Pia Ebeling[1], Rohini Kumar[2], Stefanie R. Lutz[1,3], Tam Nguyen[1], Fanny Sarrazin[2], Michael Weber[2], Olaf Büttner[4], Sabine Attinger[2], and Andreas Musolff[1]

[1]Department of Hydrogeology, Helmholtz Centre for Environmental Research – UFZ, Leipzig 04318, Germany
[2]Department of Computational Hydrosystems, Helmholtz Centre for Environmental Research – UFZ, Leipzig 04318, Germany
[3]Copernicus Institute of Sustainable Development, Utrecht 3584 CB, the Netherlands
[4]Department of Aquatic Ecosystems Analysis and Management, Helmholtz Centre for Environmental Research – UFZ, Magdeburg 39114, Germany

Correspondence: Pia Ebeling (pia.ebeling@ufz.de)

Received: 5 January 2022 – Discussion started: 1 March 2022
Revised: 30 June 2022 – Accepted: 15 July 2022 – Published: 17 August 2022

Abstract. Environmental data are the key to defining and addressing water quality and quantity challenges at the catchment scale. Here, we present the first large-sample water quality data set for 1386 German catchments covering a large range of hydroclimatic, topographic, geologic, land use, and anthropogenic settings. QUADICA (water QUAlity, DIscharge and Catchment Attributes for large-sample studies in Germany) combines water quality with water quantity data, meteorological and nutrient forcing data, and catchment attributes. The data set comprises time series of riverine macronutrient concentrations (species of nitrogen, phosphorus, and organic carbon) and diffuse nitrogen forcing data (nitrogen surplus, atmospheric deposition, and fixation) at the catchment scale. Time series are generally aggregated to an annual basis; however, for 140 stations with long-term water quality and quantity data (more than 20 years), we additionally present monthly median discharge and nutrient concentrations, flow-normalized concentrations, and corresponding mean fluxes as outputs from Weighted Regressions on Time, Discharge, and Season (WRTDS). The catchment attributes include catchment nutrient inputs from point and diffuse sources and characteristics from topography, climate, land cover, lithology, and soils. This comprehensive, freely available data collection with a large spatial and temporal coverage can facilitate large-sample data-driven water quality assessments at the catchment scale as well as mechanistic modeling studies. QUADICA is available at https://doi.org/10.4211/hs.0ec5f43e43c349ff818a8d57699c0fe1 (Ebeling et al., 2022b) and https://doi.org/10.4211/hs.88254bd930d1466c85992a7dea6947a4 (Ebeling et al., 2022a).

1 Introduction

Understanding hydrological and biogeochemical processes at various spatiotemporal scales is a major goal in catchment hydrology and is particularly relevant for robust predictions of water quantity and quality as well as adequate catchment management. Analyzing observations of the spatial and temporal dynamics of water quantity and quality at the catchment scale can give insights into relevant processes using a "pattern to process" approach (Sivapalan, 2006). Especially large-sample studies covering a wide range of catchments can advance our knowledge on patterns across scales, catchment similarity, and dominant processes, beyond a single catchment or local behavior (Addor et al., 2020; Kingston et al., 2020). Such studies allow for generalizable theories and applications by "balancing depth with breadth" and facilitate classifications, regionalization, and a better understanding of uncertainty in model predictions (Gupta et al., 2014). Thus, environmental data are the key for process understanding and hypothesis testing (Li et al., 2021). The col-

Published by Copernicus Publications.

lection and availability of water quantity and quality data are steadily increasing with technological advances (Rode et al., 2016), but particularly harmonized and quality-controlled large-sample data sets of water quality and quantity along with catchment attributes are needed. These enable the identification and characterization of water quality and quantity response patterns and relationships with potential controls, facilitate hypothesis testing, and, thus, advance our understanding of the complex coupled hydrological and biogeochemical systems across larger samples and domains (Li et al., 2021).

In recent years, the application of large-sample studies has been advancing fast for (surface) water quantity studies investigating dominant processes and drivers of water flow characteristics. Gupta et al. (2014) provided an overview of such studies, with the first of them being published in the 1990s. These publications have been followed by a recent surge in studies documenting and analyzing large-sample hydrologic data sets, such as Newman et al. (2015), Kuentz et al. (2017), Do et al. (2017), Gnann et al. (2020), Tarasova et al. (2020), and Merz et al. (2020). These studies have identified catchment typologies, archetypal behavior, and underlying controls, such as discharge variability across Europe (Kuentz et al., 2017), catchments with similar runoff event types (Tarasova et al., 2020), or how catchment discharge attenuates and shifts climate seasonality (Gnann et al., 2020).

In contrast, large-sample studies for water quality are less common. Nevertheless, some recent large-sample water quality studies have provided a basis for enhancing our understanding of catchment functioning in terms of the mobilization, transport, and environmental fate of solutes and particulates as well as the generality of these functions. For example, Monteith et al. (2007) linked widespread positive trends in dissolved organic carbon (DOC) concentrations observed in Europe and North America with decreasing atmospheric sulfur and chloride deposition. Godsey et al. (2009, 2019) provided wide evidence that weathering-derived solutes are mostly exported chemostatically with low concentration variance. Basu et al. (2010) derived the hypothesis of chemostatic nutrient export resulting from homogenized sources due to the legacy of high inputs. More recently, Zarnetske et al. (2018) and Ebeling et al. (2021a) both provided evidence of widespread transport-limited DOC export from small to large catchments. However, several questions regarding general patterns, catchment similarities and typologies, and the underlying controls of the aforementioned factors remain open – for example, questions concerning the extent and recovery of nutrient legacy for both nitrogen (N) and phosphorous (P) (Chen et al., 2018), the extent of macronutrient interactions in differing landscape and anthropogenic settings as well as throughout the river network (Wollheim et al., 2018), and the impact of climate change on water quality trajectories in various catchments (Kaushal et al., 2018).

At the moment, large-sample studies are still hampered by limited availability (e.g., the number of stations, number of samples, and covered regions) and accessibility of spatially and temporally harmonized large-sample data collections (e.g., Addor et al., 2020), despite recent efforts to make consistent large-sample data sets of catchment hydrology for both water quantity and water quality in streams publicly available (e.g., Virro et al., 2021). Prominent examples of large-sample hydrological data sets including catchment attributes are the Catchment Attributes and MEteorology for Large-sample Studies (CAMELS) data sets, available for the USA (Addor et al., 2017), Chile (Alvarez-Garreton et al., 2018), Brazil (Chagas et al., 2020), Great Britain (Coxon et al., 2020), and Australia (Fowler et al., 2021). More recently, the multinational LArge-SaMple DAta for Hydrology and Environmental Sciences (LamaH; Klingler et al., 2021) initiative has provided hydrometeorological time series at an hourly resolution along with catchment attributes. For stream water quality, currently available large-sample data sets focus on water quality time series only but lack additional data. Recently, two global databases of surface water quality were published that combine data from several existing databases in homogenized and quality-checked form: the Surface Water Chemistry database (SWatCh; Rotteveel and Sterling, 2022), with a focus on variables relevant to acidification, and the Global River Water Quality Archive (GRQA; Virro et al., 2021), with a focus on macronutrients. Both include the global databases Global Freshwater Quality Database (GEMStat; UNEP, 2018) and the GLObal RIver CHemistry database (GLORICH; Hartmann et al., 2014) as well as the European Waterbase (EEA, 2020) database, although the spatiotemporal coverage of the data varies strongly. These are important recent advances towards open science in water quality research. However, to the authors' knowledge, there is currently no combined, ready-to-use data set of metrics of water quality, quantity, catchment attributes, and forcing data (such as meteorological and nutrient inputs), which would allow for the investigation of water quality dynamics and their controls. Moreover, large-sample and cross-regional studies are especially challenging in countries like Germany, where data responsibility is scattered between federal states and data are often not freely available nor homogenized between water quantity and quality stations. Nevertheless, a few Germany-wide water quality studies on groundwater (Knoll et al., 2020) and surface water (Ebeling et al., 2021a) have recently been carried out.

The key objective here is to provide a spatially and temporally consistent comprehensive data set of joint water quality and quantity data, catchment attributes, and nutrient inputs for German catchments that is ready to use and freely available, supporting the open science philosophy and FAIR (findability, accessibility, interoperability, and reuse) data principles. In this "Water QUAlity, DIscharge and Catchment Attributes for large-sample studies in Germany" (QUADICA) data set, we have complemented available data sets of catchment attributes with new data on water quality and water quantity. These data include delineated catchment bound-

aries, catchment responses in terms of macronutrient concentrations (species of N; P; and organic carbon, OC) and discharge (Q), forcing data in terms of meteorological and diffuse nitrogen inputs, and average catchment attributes. We distinguish stations with a high data availability, which allows further estimation of daily concentrations and fluxes using a regression approach, and stations with lower availability, for which aggregated observed concentrations are reported. For water quality (Sect. 3.1) and water quantity (Sect. 3.2), we provide the following:

1. time series of annual medians of observed macronutrient concentrations (dissolved and total forms of N, P, and OC) and of observed discharge,
2. time series of monthly and annual medians of estimated daily macronutrient concentrations and flow-normalized concentrations as well as mean nutrient fluxes and medians of observed discharge for stations with high data availability,
3. monthly medians and the monthly 25th and 75th percentiles of observed concentrations and discharge over the whole time series.

Additionally, we provide time series of driving forces (Sect. 3.3 and 3.4) and catchment attributes (Sect. 4):

4. time series of observed monthly meteorological forcing variables as catchment averages (Sect. 3.3),
5. time series of estimated annual net diffuse nitrogen inputs to the catchments (Sect. 3.4),
6. average catchment attributes, i.e., topography, land cover, nutrient sources, lithology and soils, and hydroclimate (Sect. 4).

We envision that the QUADICA data set will directly enable large-sample assessments of mean concentrations and fluxes; their variability in terms of long-term trends, seasonality, and relationships to discharge; and their relationships to catchment attributes. We believe that the data set will allow a better understanding of catchment functioning and water management beyond regional scales and stimulate provisioning and analysis of further water quality data at national to continental scales.

2 Catchment selection and delineation

The station selection and catchment delineation have been presented in a previous study (Ebeling et al., 2021a) and data repository (Ebeling, 2021) and are now included in the new QUADICA data set. All data sets use the same unique identifier (OBJECTID) for the stations and corresponding catchments. The station selection is based on riverine water quality data assembled from the German federal state environmental authorities, who are responsible for the routine monitoring of water quality in Germany (Musolff et al., 2020; Musolff, 2020) and take grab samples at approximately monthly intervals.

The following preprocessing steps were applied for each station and compound separately: we removed duplicate, negative, and zero values and applied an outlier test for each time series (removing values above mean concentration and 4 times the standard deviation in logarithmic space, i.e., confidence level $> 99.99\,\%$ for lognormally distributed data). Finally, 1386 stations met the criteria concerning water quality data and catchment delineation (Fig. 1) as described in the following: in the first step, water quality data cover at least 3 years, include a minimum of 70 samples from 2000 to 2015 after preprocessing, and cover all seasons, i.e., seasonal coverage of at least 10 % of the samples in each quarter considering all possible combinations of 3 consecutive months (criteria one to three as described in Ebeling et al., 2021a). These criteria should ensure that a representative amount of data is available. Stations fulfilling these water quality data criteria for nitrate (NO_3-N) or phosphate (PO_4-P) were preselected (i.e., 1692 stations). Other variables (e.g., total phosphorus, TP; total nitrogen, TN; and DOC) were not used in this initial step of station selection.

In the second step, we delineated the catchment area from topography for these preselected stations and verified them as described here. The topographic catchment boundaries were delineated based on a 100 m flow accumulation grid derived from a digital elevation model (DEM; resampled from 25 to 100 m using the average; EEA, 2013) using spatial analysis tools and a D8 flow direction type. The river network from the Rivers and Catchments of Europe – Catchment Characterisation Model (De Jager and Vogt, 2007) was used to burn by 10 m into the DEM before deriving the flow accumulation. The stations were snapped or manually moved towards the representative flow accumulation stream to define the catchment outlets (pour points). The resulting topography-based catchment polygons were quality-controlled manually by a comparison to the real river network. In case of major deviations, a few manual adaptations of the burned river segments were done if they substantially improved the overlap without hindering neighboring catchment delineations. In case of insufficient spatial overlap that could not be improved, stations were discarded from the selection. This resulted in a final set of 1386 catchments. The DEM, flow direction, and flow accumulation raster used as well as the modified station locations and the river network are also provided in the data repository for further use.

The varying density of stations across Germany (Fig. 1a) has two main reasons: firstly, the provision of raw data varied with respect to the number of stations, number of samples per compound and station, and time series length among the federal states; secondly, the topographic delineation of catchment boundaries was more successful where the topography is more pronounced, giving less delineable catchments in northern Germany. The delineated catchment boundaries

are provided with the data set and enable the user to develop further geoinformation routines (e.g., to extract characteristics from other geographic data sets).

3 Time series

For the 1386 delineated catchments, riverine concentration time series of nitrate (NO_3-N), mineral nitrogen (N_{min}), total nitrogen (TN), phosphate (PO_4-P), total phosphorus (TP), dissolved organic carbon (DOC), and total organic carbon (TOC) are provided (Table 1). They are supplemented by time series of discharge (where available) and forcing variables (meteorological drivers and diffuse N input). Due to limited data availability, not all variables can be provided for all stations.

3.1 Water quality time series

3.1.1 Annual median concentrations

Annual medians of concentration data are presented for time series of the 1386 stations fulfilling the water quality criteria (as done for the catchment selection criteria described in Sect. 2). To calculate summary statistics, we substituted concentration values below the detection limit (left-censored data) with half the detection limit.

The resulting data density distributions over time and the number of years covered by each variable show the highest data availability for TOC, PO_4-P, and NO_3-N in more recent years (Fig. 2). An overview of the time series statistics for each variable is given in Table 2, and time series are shown in Appendix A (Fig. A1). For NO_3-N concentrations, the number of stations with available data is 1339, and the median number of samples per station is 157. The earliest time series starts in 1954, but the median start across stations is in 1994. The median time series length is 19 years, and the maximum time series length is 61 years. For PO_4-P concentrations, the number of stations with available data is 1330, and the median number of samples per station is 152. The earliest time series starts in 1965, but the median start across stations is in 1993. The median time series length is 20 years, and the maximum time series length is 48 years. For TOC concentrations, the number of stations with available data is 1296, and the median number of samples per station is 139. The earliest time series starts in 1979, but the median start across stations is in 1999. The median time series length is 15 years, and the maximum time series length is 36 years. For all water quality variables, the median of the first year of the time series is in the 1990s, and the median number of samples per station and year is 12, indicating that grab samples were taken on a monthly basis on average. Note that the number of samples underlying the median values can differ between the different nutrient species so that the fraction of TN present as NO_3-N or TP present as PO_4-P may show inconsistencies for single stations (e.g., values above one).

3.1.2 Monthly median concentrations and mean fluxes for stations with high data availability

For the subset of stations with high data availability, a Weighted Regressions on Time, Discharge, and Season (WRTDS; Hirsch et al., 2010) analysis was applied using the "EGRET" R package (version 3.0.2; Hirsch and De Cicco, 2015). We refer to these stations as "WRTDS stations" for short. WRTDS represents long-term trends, seasonal components, and discharge-related variability in the water quality variables (Hirsch et al., 2010). The criteria for a WRTDS application were checked for each station and compound separately using the preprocessed data, as described in Sect. 2. The criteria were a time series of at least 20 years length, at least 150 samples of water quality, no data gaps larger than 20 % of the total time series length, and a complete time series of daily discharge (see also Sect. 3.2.2). The number of WRTDS stations varies between 44 for TN and 126 for PO_4-P (Table 3), and the fraction of stations with high data availability varies between 4.9 % for TOC and 11.7 % for TP.

For WRTDS stations, we provide the monthly and annual median estimated water quality and observed quantity data in addition to the annual observed data (see above). More specifically, we provide monthly and annual median concentration and flow-normalized concentration as well as mean flux estimates from the WRTDS model output and median observed discharge (see Sect. 3.2.2) if data are available for at least 80 % of the respective time frame. The median R^2 between WRTDS-modeled and observed concentrations varies between 0.44 for DOC and TOC and 0.75 for TN (Table 3); overall, 69.3 % of the catchment and compound combinations have a median R^2 of at least 0.5. The median bias varies between −1.4 % for PO_4-P (negative values indicate overestimation) and 0.2 % for NO_3-N (positive values indicate underestimation); overall, 51 % of the catchments have a bias below 1 %, and 95 % of the catchments have a bias below 5 %. An overview of the availability of WRTDS stations and model performance is given in Table 3 and shown in Fig. A2, their locations are shown in Fig. 1a, and their performance is provided in the data repository.

3.1.3 Monthly median concentrations over the time series

Next to annual and monthly time series, we provide long-term monthly medians over the complete time series of each station, enabling assessments of average seasonal variability. We also include the 25th and 75th percentiles to reflect the long-term variability in a given month. The provided data frame in QUADICA indicates the number of samples available for the corresponding month across the years, based on which representativeness can be assessed and quality criteria can be defined.

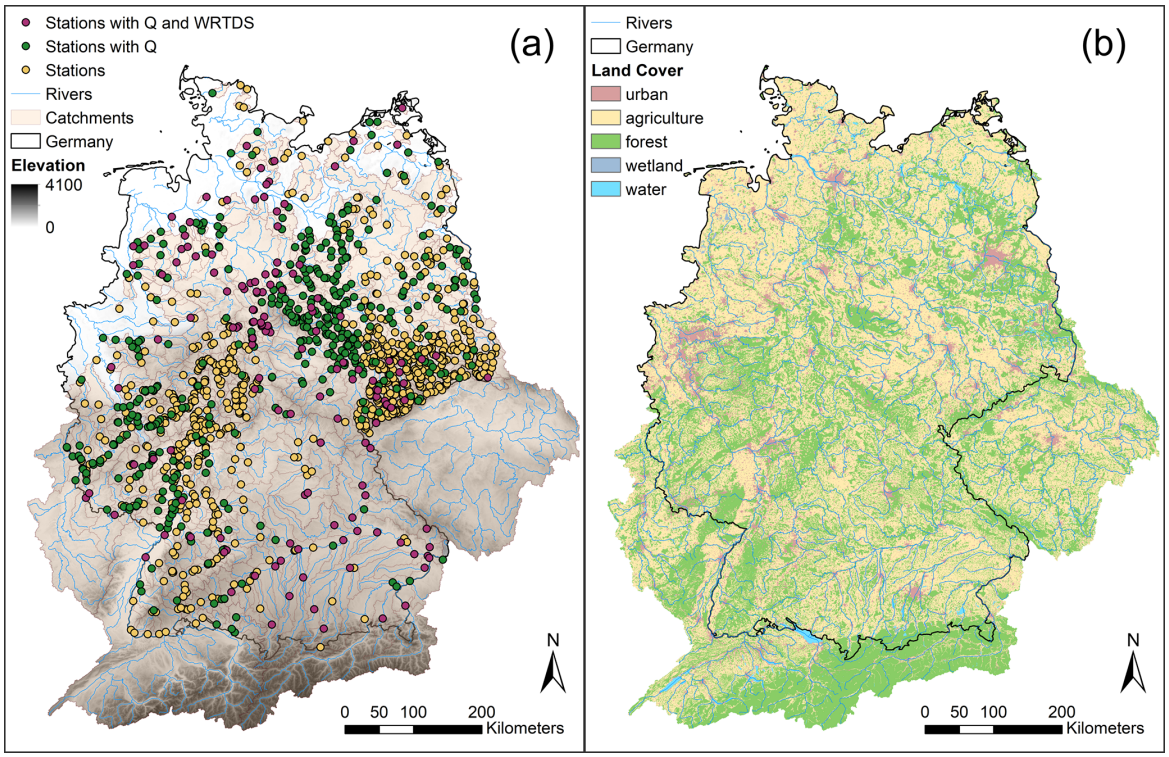

Figure 1. Map of **(a)** water quality stations, catchments, and elevation (EEA, 2013) and **(b)** map of land cover (EEA, 2016a). The colors in panel **(a)** distinguish between stations with (green) and without (yellow) discharge (Q) data and stations with high data availability of concentration and discharge (purple, WRTDS stations; for details, see Sect. 3.1). WRTDS refers to Weighted Regressions on Time, Discharge, and Season.

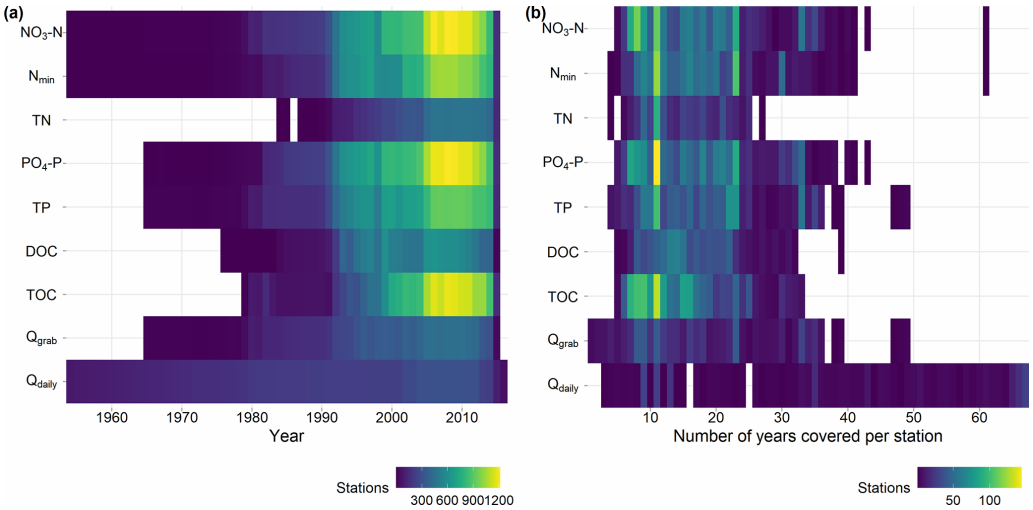

Figure 2. Heat map of **(a)** the number of stations with available annual medians over time and per variable and **(b)** the number of years covered by each station. Q_{grab} refers to the median discharge (Q) from grab sample dates, and Q_{daily} refers to median Q from daily discharge (see Sect. 3.2.1 for details). For visualization purposes, in panel **(a)**, station counts from 1954 are shown, omitting one concentration and a few Q_{daily} records before 1954; in panel **(b)**, counts up to 67 years are shown, omitting three longer Q_{daily} records.

Table 1. Provided time series data as well as their basis (observed or estimated), aggregation type, temporal resolution, and source of original data, which was used to calculate the aggregated data provided here.

Variable	Section	Data basis	Temporal (Spatial) aggregation	Temporal resolution	Source
Concentration of NO_3-N, N_{min}, TN, PO_4-P, TP, DOC, and TOC	3.1	Observed	Median	Annual	Musolff et al. (2020); Musolff (2020)
		Estimated daily using WRTDS	Median	Monthly	Musolff et al. (2020); Musolff (2020)
		Observed	Long-term median	Monthly	Musolff et al. (2020); Musolff (2020)
Discharge	3.2	Observed	Median	Annual	Musolff et al. (2020); Musolff (2020)
		Observed	Median	Monthly	Musolff et al. (2020); Musolff (2020)
		Observed	Long-term median	Monthly	Musolff et al. (2020); Musolff (2020)
Precipitation	3.3	Observed gridded	Sum (Average)	Monthly	E-OBS v18.0e, Cornes et al. (2018)
Potential evapotranspiration	3.3	Estimated	Sum (Average)	Monthly	E-OBS v18.0e, Cornes et al. (2018)
Mean air temperature	3.3	Observed gridded	Average (Average)	Monthly	E-OBS v18.0e, Cornes et al. (2018)
Diffuse N input as total	3.4	Estimated	(Average)	Annual	See Sect. 3.4
Diffuse N input from agricultural areas	3.4	Estimated	(Average)	Annual	See Sect. 3.4

The abbreviations used in the table are as follows: nitrate (NO_3-N); mineral nitrogen (N_{min}); total nitrogen (TN); phosphate (PO_4-P); total phosphorus (TP); dissolved organic carbon (DOC); total organic carbon (TOC); and Weighted Regressions on Time, Discharge, and Season.

3.2 Water quantity time series

For about 43 % of the water quality stations ($n = 590$), information on discharge is available (Fig. 1a) and is provided harmonized with the water quality data (i.e., at the annual and monthly resolution). The discharge information is a collection of data provided by the federal states along with the concentration data, either as daily discharge time series or for the times of grab sampling of water quality. Additionally, we integrated daily discharge data from 53 stations available from the Global Runoff Data Center (GRDC) to increase the number of stations with available discharge time series. We matched GRDC gauging stations to the existing water quality stations using a search radius of 500 m. For each match, we checked the consistency of river names and visually confirmed the locations. The corresponding GRDC station numbers are indicated in the metadata of the water quality and quantity data set (Musolff, 2020). For the original daily discharge data, the reader may refer to the regularly published and accessible data at the GRDC portal (https://portal.grdc.bafg.de, last access: 8 August 2022).

3.2.1 Annual median discharge

Annual median discharge is aggregated from available observed discharge data. For 324 water quality stations, a co-located Q station with a continuous daily Q record is available. However, the time series may include data gaps, and the time series of discharge and concentration data do not overlap at all for nine of the co-located discharge stations. For an additional 266 stations, Q data were only available at the time that the grab samples were taken. This resulted in a set of 581 stations for which Q data were available on the sampling dates of concentration data. We extracted annual me-

Table 2. The number of stations with available data for the water quality compounds and discharge during grab sampling dates, the earliest and median start year of time series, the maximum and median time series length and covered years (i.e., years with available data), the median number of samples per stations and per station and year, and the number of outliers removed.

Variable Unit	NO_3-N mg L^{-1}	N_{min} mg L^{-1}	TN mg L^{-1}	PO_4-P mg L^{-1}	TP mg L^{-1}	DOC mg L^{-1}	TOC mg L^{-1}	Q_{grab} m^3 s^{-1}	Q_{daily} m^3 s^{-1}
Number of stations	1339	1149	514	1330	1046	744	1296	581	324
Earliest start	1954*	1954	1984	1965	1965*	1976	1979	1965*	1893
Median start year	1994	1993	1999	1994	1993	1993	1999	1993	1975
Median time series length per station (years covered)	19 (16)	21 (16)	15 (13)	20 (16)	21 (17)	20 (15)	15 (13)	19 (16)	38 (38)
Maximum time series length per station (years covered)	61* (61)	61 (61)	31 (27)	48 (43)	49* (49)	39 (39)	36 (33)	49* (49)	123 (123)
Total number of samples (including outliers)	309 965	235 015	92 876	297 591	258 059	139 440	239 282	156 388	$> 4 \times 10^6$
Median number of samples per station	157	153	149	152	165	164	139	170	13 388
Median number of samples per station and year	12	12	12	12	12	12	12	13	365
Number of outliers	59	52	45	68	326	257	795	–	–
Maximum fraction of outliers per station (%)	1.7	1.7	1.7	1.7	2.5	3.1	3.6	–	–

* Omitting one sample from 1900. The abbreviations used in the table are as follows: nitrate (NO_3-N), mineral nitrogen (N_{min}), total nitrogen (TN), phosphate (PO_4-P), total phosphorus (TP), dissolved organic carbon (DOC), total organic carbon (TOC), the median discharge (Q) from grab sample dates (Q_{grab}), and the median Q from daily discharge (Q_{daily}).

Table 3. The number of stations with high data availability (WRTDS stations) for each compound and the median coefficient of determination for WRTDS models.

Variable Unit	Total	NO_3-N mg L^{-1}	N_{min} mg L^{-1}	TN mg L^{-1}	PO_4-P mg L^{-1}	TP mg L^{-1}	DOC mg L^{-1}	TOC mg L^{-1}
Number of WRTDS stations	140	125	97	44	126	122	61	64
Median R^2	0.61	0.63	0.71	0.75	0.69	0.53	0.44	0.44
Median bias (%)	−0.3	0.2	0.1	0.1	−1.4	−0.9	−0.6	−0.6

The abbreviations used in the table are as follows: nitrate (NO_3-N); mineral nitrogen (N_{min}); total nitrogen (TN); phosphate (PO_4-P); total phosphorus (TP); dissolved organic carbon (DOC); total organic carbon (TOC); and Weighted Regressions on Time, Discharge, and Season (WRTDS).

dian discharge from both continuous daily data (Q_{daily}) and dates when the water quality sample was taken (Q_{grab}, with a median of 13 values per year; Table 2) for the water quality stations. The density distribution of stations with available annual discharge over time is shown in Fig. 2a. Similar to the concentration data, the data availability is higher in more recent years, with a maximum of 449 stations in 2010. The number of years covered is, however, higher compared with water quality data for several stations (Fig. 2b). For stations with available daily discharge data, both annual median values of the daily data and the data from grab sample days were compared (Fig. A3). Our results suggest that annual median values from grab sample dates can be considered to be robust estimates of annual median discharge as they have a negligible bias (bias $= -0.5\,\%$) and low scatter around the 1 : 1 line ($R^2 > 0.99$). The time series are shown in Appendix A

(Fig. A1). The data set additionally provides the number of samples used to calculate the medians as a measure of robustness.

3.2.2 Monthly median discharge

Monthly median discharge is provided for WRTDS stations. To fill gaps in the daily discharge time series of the 45 stations required for WRTDS models (see Sect. 3.1.2), we used simulated discharge from the mesoscale hydrological model (mHM) (Kumar et al., 2013; Samaniego et al., 2010; Zink et al., 2017) if the regression coefficient (R^2) between observed and simulated discharge for the station was greater than 0.6. Subsequently, modeled discharge was bias-corrected with piecewise linear regressions and used for gap filling (Ebeling et al., 2021b; Ehrhardt et al., 2021a). If modeled discharge was not available, small gaps (up to 7 days) were interpolated with fixed-interval smoothing using the "baytrends" R package (Murphy et al., 2019). Note that the gap-filled discharge time series are used for the WRTDS models only. This includes the monthly and annual discharge data provided with the WRTDS data tables (as described in Sect. 3.1.2).

3.2.3 Monthly median discharge over the time series

As for the water quality metrics (see Sect. 3.1.3), we provide long-term monthly median discharge and the 25th and 75th percentile over the whole time series, if available, for the station representing average discharge seasonality. The number of samples used for the calculation of medians is indicated as a measure of accuracy.

3.3 Meteorological time series

Meteorological time series are provided as spatial catchment averages at a monthly resolution. We used the daily gridded product of climate variables (precipitation and maximum, minimum, and average air temperature) from the "European Climate Assessment & Dataset" (ECA&D) project (E-OBS, v18.0e; Cornes et al., 2018). The advantage of a European data set is the coverage of transnational catchments, such as the Elbe or the Rhine. The data sets are available at a spatial resolution of 0.1° over the period from 1950 to 2018. The interpolation approach employed to create the gridded fields uses a stochastic technique based on Gaussian random field and involves several ground-based observation networks distributed across Europe (see Cornes et al., 2018, for more details). The daily fields of potential evapotranspiration are derived based on the method from Hargreaves and Samani (1985) at the same spatial resolution (0.1°) using the daily (maximum, minimum, and average) air temperature data sets. We then calculated the spatial averages of daily climate variables (precipitation, air temperature, and potential evapotranspiration) for all water quality stations, considering the corresponding (upstream) catchment area. Monthly estimates of total precipitation and potential evapotranspiration as well as average air temperatures were subsequently calculated for each study basin.

3.4 Time series of net N input from diffuse sources

For the period from 1950 to 2015, we provide time series of catchment-scale N surplus (i.e., the net diffuse N input), which is the sum of N inputs minus the sum of N outputs from harvesting. At the catchment scale, the N surplus is the sum of N surplus from agricultural areas (N_{agri}; kg yr^{-1} ha^{-1}) and nonagricultural areas ($N_{nonagri}$; kg yr^{-1} ha^{-1}) normalized to the catchment area. For transboundary catchments with area outside of Germany, N surplus is normalized to the German part only. For nonagricultural areas, the N surplus is composed of atmospheric N deposition and biological N fixation. For agricultural areas, the N surplus includes additional N inputs (i.e., mineral fertilizer and manure applications) and N outputs from harvesting.

For agricultural land, the N surplus data stem from two data sets: one at the state level provided for the period from 1950 to 1998 (Behrendt et al., 2003, which builds on Bach and Frede, 1998, and Behrendt et al., 2000) and one at the county level provided for the period from 1995 to 2015 (Häußermann et al., 2019). To create a consistent long-term data set (1950–2015), we harmonized the county- and state-level data sets based on the overlapping years (1995–1998) and downscaled the state-level data to the county level for the period from 1950 to 1994. Specifically, we bias-corrected the state-level data of Behrendt et al. (2003) using proportions, as they commonly underestimated the values provided by Häußermann et al. (2019) for the period from 1995 to 1998. To downscale the bias-corrected state-level N surplus (1950–1994) to the county level, we used a linear regression between the county and state totals for the period from 1995 to 2015 (data from Häußermann et al., 2019). As data for city states (Berlin, Bremen, and Hamburg) are not provided in the state-level data set, we used the average value from 1995 to 1998 for the period from 1950 to 1994 under the assumption that the error is acceptable considering the small agricultural areas. The N surplus data comprise values for 5 of the 11 agricultural land classes in the CORINE (Coordination of Information on the Environment) Land Cover (CLC) inventory (EEA, 2016a): nonirrigated arable land, vineyards, fruit trees and berry plantations, pastures, and complex cultivation patterns. The data include N inputs from applications of fertilizers in mineral and organic forms, from seeds and planting material (county-level data only), from N deposition, and from biological N fixation as well as N outputs from harvested crops. To upscale agricultural N surplus from the county level to the catchment level, we used the fraction of agricultural area provided by CLC and a scaling factor. As CLC overestimates agricultural areas compared with the census data at the county level (Bach et al., 2006), we scaled the agricultural areas from CLC in each county by the mean ratio

between the agricultural area from census data (Häußermann et al., 2019) and the CLC maps (years 2000, 2006, and 2012; median ratio of 1.24 across counties).

For nonagricultural land (CLC forest, water bodies, wetlands, and grassland classes) and the remaining agricultural land CLC classes not covered by the N surplus data described above (e.g., permanently irrigated land), we used the atmospheric N deposition data from the Meteorological Synthesizing Centre – West (MSC-W) of the European Monitoring and Evaluation Programme (EMEP; Simpson et al., 2012). The EMEP database uses a chemical transport model to generate a consistent gridded field of Europe-wide wet and dry as well as oxidized and reduced atmospheric N deposition (Simpson et al., 2012). The model assimilates varying levels of observational information on different atmospheric chemicals (e.g., Bartnicki and Benedictow, 2017; Bartnicki and Fagerli, 2006). The data were available for the period from 1980 to 1995 with 5-year time steps, which we linearly interpolated to obtain an annual time series, and with annual time steps for the period from 1995 to 2015. For the data before 1980, we assumed constant values from 1980 due to missing information. Deposition on urban sealed surfaces was neglected, as we assume that this component is collected by the sewer system and transported to the wastewater treatment plants. Thus, we assume it is not a diffuse N source but part of the point sources (Sect. 4.3). In contrast, deposition on urban grassland, like public parks, was considered. To account for the overestimated area of the five agricultural CLC classes in the agricultural N surplus data (see above), we added the corresponding missing fraction proportionally to the remaining land cover classes. We estimated terrestrial biological N fixation by plants for nonagricultural, vegetated areas using land-use-specific rates provided by Cleveland et al. (1999) and Van Meter et al. (2017).

The catchment-scale N surplus time series were calculated by intersecting the two N surplus components (N_{agri} and $N_{nonagri}$) with the respective land use and catchment area components. As the N surplus data were only available within Germany, data from transboundary catchments (e.g., the main stretch of the Elbe or Rhine rivers) need to be used cautiously, with higher uncertainty for catchments with a higher fraction of the catchment area outside of Germany (Sect. 4.3). Figure 3 shows the resulting N input time series of all catchments. The majority of N input stems from agriculture, with a median of 64 % of the total catchment N surplus stemming from N_{agri} across all catchments (averages between 1950 and 2015). The agricultural N surplus (N_{agri}) and its fraction per catchment were highest during the 1980s, with a median across catchments of 52 kg ha^{-1} yr^{-1} and 76 % (average between 1980 and 1989), respectively. The highest mean agricultural N surplus and annual fraction across all catchments were reached in 1988, with respective values of 60.7 kg ha^{-1} yr^{-1} and 74 %, although these values were already above 50 kg ha^{-1} yr^{-1} and 70 % from 1976 to 1989. For the total N surplus, the mean annual values across catchments were above 70 kg ha^{-1} yr^{-1} during the same period (1976–1989), although values were above 50 kg ha^{-1} yr^{-1} from 1969, and the maximum of 76.7 kg ha^{-1} yr^{-1} occurred in 1980.

4 Catchment attributes

The provided catchment attributes characterize the catchments in terms of topography, land cover, nutrient sources, lithology and soils, and hydroclimate. The attributes were chosen with a focus on macronutrient sources and transport in line with the data set. Figure 4 shows the spatial distribution of a set of selected catchment attributes. All attributes, their variable names, original data sources, and methods are listed in Appendix B (Table B1) and the data repository (Ebeling et al., 2022a). This repository of catchment attributes is a composite of attributes from two existing repositories (Ebeling and Dupas, 2021; Ebeling, 2021).

4.1 Location and topography

Catchment size was calculated from the delineated catchment boundaries described in Sect. 2. Catchment size ranges from 0.9 to 123 012 km^2, with a median of 171.2 km^2 , a 25th percentile of 53.6, and a 75th percentile of 634.4 km^2. Additionally, the fraction of the catchment area lying within German borders was calculated (f_AreaGer). Mean and median catchment elevation and topographic slope were extracted from the DEM with a 100 m resolution (see also Sect. 2; EEA, 2013). A 100 m grid of the topographic wetness index (TWI) was calculated from the DEM by relating the upstream area (from flow accumulation) to the local slope at each grid cell, following Beven and Kirkby (1979). For each catchment, we extracted mean, median, and 90th percentile TWI values. The 90th percentile has been shown to be a proxy for the abundance of riparian wetlands in a catchment (Musolff et al., 2018). Drainage density, defined as the length of surface waters per area, closely relates to topography. Drainage density was calculated and provided in two ways: as the catchment average of the gridded drainage density (cell size 0.012°) provided in the Hydrologischer Atlas Deutschland (BMU, 2000) and as the river length from EU-Hydro River Network Database (EEA, 2019) within the catchment divided by its area. For the latter, the level of detail was too coarse to yield plausible values for all catchments, which is why values are missing for 27 of the smaller catchments. However, the EU-Hydro River Network Database provides further stream attributes such as the Strahler order.

4.2 Land cover and population density

The fractions of land cover classes were calculated from the level 1 classification of the CLC data set for 2012 (artificial, agricultural, forested land, wetland, and surface water cover) (EEA, 2016a). For a finer distinction within these overall

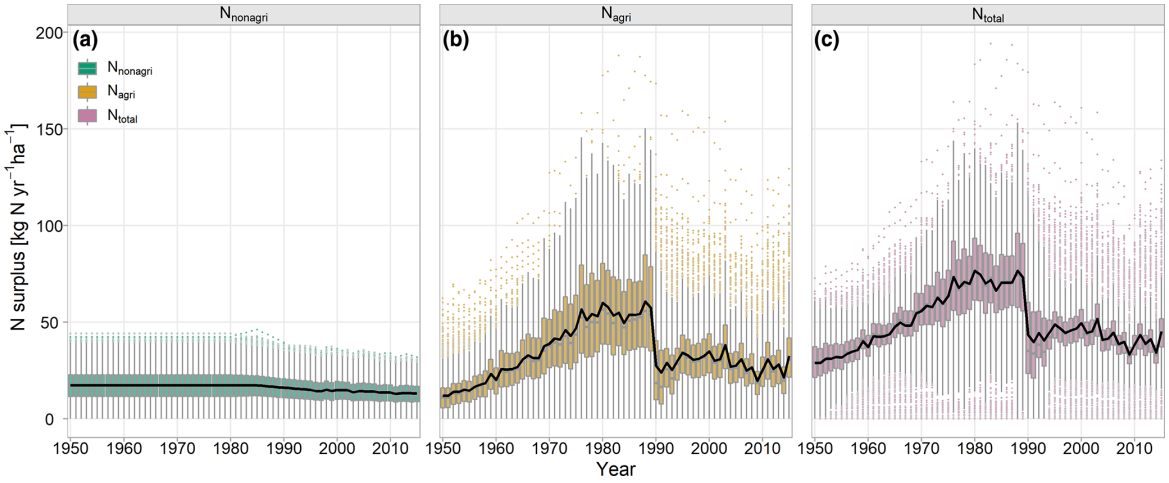

Figure 3. Time series of annual N surplus for all catchments for the different N surplus components: N surplus for nonagricultural areas **(a)**, N surplus for agricultural areas **(b)**, and total N surplus for both nonagricultural and agricultural areas **(c)**. Box plots represent the distribution of the annual N surplus as averages of the German catchment area across all catchments showing summary statistics (median, quartiles, and quartiles ±1.5 times the interquartile range) and individual points outside these ranges. The black lines represent the mean annual values for each N surplus component across the catchments.

classes, fractions of land cover classes were additionally calculated from level 2 data. Note that there can be an overestimation of agricultural areas from these CLC land cover classes when compared with census data as described by Bach et al. (2006) and considered for N surplus time series (Sect. 3.4). Nevertheless, we expect that the relative distribution of agricultural fractions among the catchments is well captured. The mean catchment population density was calculated from the Gridded Population of the World data set (CIESIN, 2017) for 2010.

4.3 Nutrient sources

The input from point sources is calculated as the sum of the N and P load from wastewater treatment plants (WWTPs) with more than 2000 population equivalents (PEs) from the database of the European Environment Agency (EEA, 2017) and data collected from 13 German federal states covering smaller WWTPs (PE $<$ 2000) within Germany (Büttner, 2020). One PE is defined as the organic biodegradable load having a 5-day biochemical oxygen demand (BOD5) of 60 g of oxygen per day (EC, 1991a). As a second data source, we calculated catchment averages of the European domestic waste emissions database (Vigiak et al., 2019, 2020) for N, P, and BOD5 inputs from point sources. The average N, P, and BOD5 input per person was estimated using the point source input divided by the number of inhabitants according to the population density. The advantage of these European data is the consistency for an extended transnational data set – for example, it is available for German and French catchments (Ebeling and Dupas, 2021).

The net N input from diffuse sources was determined as temporal averages of diffuse N surplus time series (Sect. 3.4) for different periods, representing the main sampling period with historic inputs (1980–2015) and the current period (2000–2015). We also calculated averages for the periods before (1971–1990) and after (1991–2015) the EU 91/676/EEC Nitrates Directive (EC, 1991b) as well as the difference between them, which was used as a characteristic of net input change. Note that the N surplus data used only cover Germany, but catchments can be transnational. The uncertainty increases for larger areas outside of Germany, for which f_AreaGer can be used as a measure. To estimate source apportionment between point and diffuse N sources, we calculated the fraction of catchment point source N loads (N_WW_frac) from total catchment N input as the sum of catchment point source N loads from domestic waste emissions (N_T_YKM2) and N surplus (here using Nsurp80_15 for the period from 1980 to 2015) on average:

$$\text{N\_WW\_frac} = \text{N\_T\_YKM2}/(\text{N\_T\_YKM2} + \text{Nsurp80\_15}).$$

We defined horizontal and vertical source heterogeneity in catchments to quantify the spatial distribution of diffuse nutrient sources with a focus on NO_3-N (Ebeling et al., 2021a). The horizontal source heterogeneity describes the distribution of agricultural land use in a catchment in relation to the stream network. We used the horizontal flow distance of the 100 m DEM (EEA, 2013; Sect. 2) to the EU-Hydro River Network Database (EEA, 2019) and a highly resolved land use map of 2015 provided by Pflugmacher et al. (2018). We divided the grid into classes of flow distance to stream with 400 m steps. Subsequently, we fitted a linear regression to

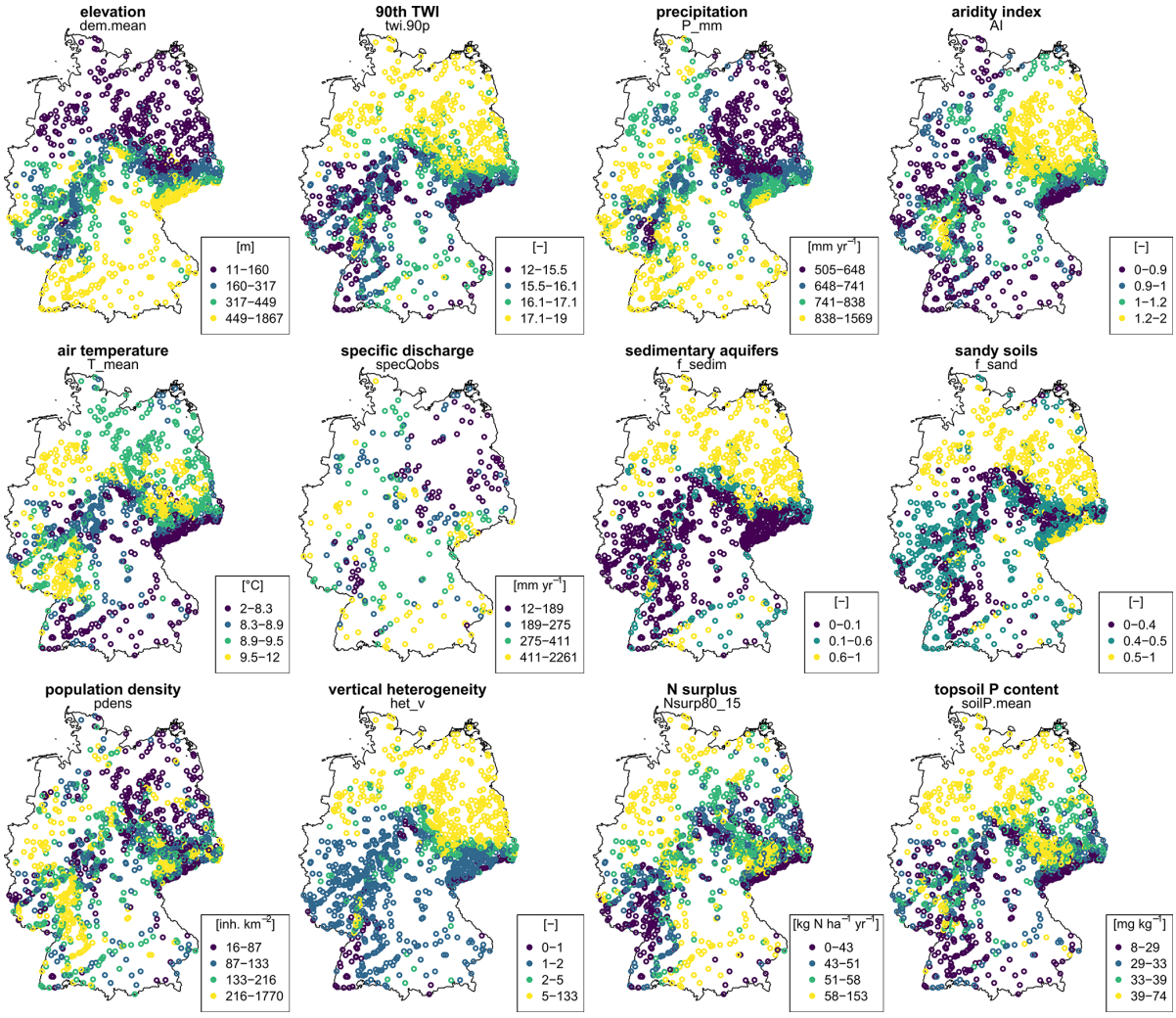

Figure 4. Maps of selected catchment attributes. Each dot represents one station, and the color represents the attribute of the corresponding catchment. Colors are according to the quartiles of the data distribution of each attribute. The attributes shown are as follows: dem.mean – average elevation [m], twi.90p – 90th percentile of the topographic wetness index [–], P_mm – mean annual precipitation [mm yr^{-1}], AI – aridity index [–], T_mean – mean air temperature [°C], specQobs – specific annual discharge [mm yr^{-1}], f_sedim – fraction of sedimentary aquifer [–], f_sand – fraction of sandy soils [–], pdens – population density [inhabitants km^{-2}], het_v – vertical concentration heterogeneity [–], Nsurp80_15 – mean N surplus from 1980 to 2015 [kg N ha^{-1} yr^{-1}], and soilP.mean – phosphorus content in topsoil [mg kg^{-1}]. For more details on the attributes, the reader is referred to the text in Sect. 4 and Table B1.

the share of agricultural source areas in each of the distance classes and the mean distance of the range of each distance class (i.e., 200 m for the class 0–400 m) weighted by the abundance of that specific class. The slope of the resulting linear model het_h characterizes if agricultural source areas tend to be located close to the stream network (het_h < 0), equally distributed (het_h $= 0$), or located far away from the stream network (het_h > 0). For more details, the reader is referred to Ebeling et al. (2021a). The vertical source heterogeneity het_v is the ratio of the shallow to deep NO_3-N concentrations. Shallow NO_3-N concentrations are estimated on a 1 km grid by Knoll et al. (2020) using a 10-year average of N surplus and average groundwater recharge. This can be seen as a potential leachate concentration, as denitrification in the soil's root zone and horizontal transport are not accounted for. The deep NO_3-N concentrations are estimated on the same grid using a random forest model that is trained on observed concentrations in groundwater (Knoll et al., 2020). The ratio of both was averaged across the catchment to yield het_v reported here. A ratio of 1 describes a

catchment that has a vertical homogeneity in NO_3-N concentrations, whereas a ratio above 1 describes stronger vertical concentration gradients.

4.4 Lithology and hydrogeology

To characterize the lithological and the hydrogeological settings of the catchments, we used the International Hydrogeological Map of Europe 1 : 1 500 000 (BGR and UNESCO, 2014). For the lithological settings, we derived the fraction of area covered by calcareous rocks, calcareous rocks and sediments, magmatic rocks, metamorphic rocks, siliciclastic rocks, siliciclastic rocks and sediments, and sediments (based on level 4 lithology data). Additionally, we determined the fractions of the more aggregated lithological classes (from level 5 lithology), i.e., consolidated, partly consolidated, and unconsolidated rocks. Furthermore, we quantified the areal fraction of aquifer type in the catchment, differentiating between porous aquifers, fissured hard-rock aquifers (including karst), and locally aquiferous or non-aquiferous rocks. Finally, we extracted the catchment median estimate of depth to bedrock from the global map from Shangguan et al. (2017).

4.5 Soil properties

We calculated the fraction of the catchment covered with hydromorphic soils (Stagnosols, semiterrestrial, semisubhydric, subhydric, and peat soils) from the German soil map (1 : 250 000; BGR, 2018). As this data source only covers Germany, data might not be reliable for transboundary catchments (see also Sect. 4.3). We also calculated the average fraction of sand, silt, and clay averaged across the soil horizons of the top 1 m based on the Harmonized World Soil Database (HWSD; v1.2) available as a 30 arcsec raster database (FAO/IIASA/ISRIC/ISSCAS/JRC, 2012). We first estimated vertically weighted soil textural properties from the original HWSD data provided for two soil layers (upper 30 and 30–100 cm). Next, we calculated the areal averages of respective properties considering the boundary (polygon) of each study catchment.

We estimated the porosity of soil profiles (thetaS) based on the pedotransfer function of Zacharias and Wessolek (2007) and the root zone plant-available water content (WaterRoots), which reflects the difference in water content between the field capacity and permanent wilting point. The field capacity is calculated based on a flux-based estimation approach proposed by Twarakavi et al. (2009) corresponding to a minimum drainage flux of 1 mm d^{-1}. The estimate of the permanent wilting point is derived using the van Genuchten (1980) model of the matric potential at −1500 kPa and the corresponding model parameters calculated from pedotransfer functions of Zacharias and Wessolek (2007). Similar to soil textural properties, for each of these soil hydraulic parameters (porosity, field capacity, and permanent wilting point), we calculated areal averages of the vertically weighted estimates for the upper 1 m of the soil profile for each study catchment. More details on this method of using pedotransfer functions and subsequent aggregations can be found in Livneh et al. (2015). Furthermore, we estimated average catchment soil chemistry of the topsoil (first 20 cm) for the year 2009 from the European soil chemistry map, which is based on the LUCAS (Land Use and Cover Area frame Survey) database (Ballabio et al., 2019). For this, we calculated the mean C / N ratio, nitrogen content, and phosphorus content from the maps for each catchment.

4.6 Hydroclimatic characteristics

Long-term average hydroclimatic characteristics were derived from the meteorological (Sect. 3.3) and discharge time series. All climatic characteristics were calculated for a period of 30 years from 1986 to 2015 based on the E-OBS data set from the ECA&D project (v18.0e; Cornes et al., 2018). First, we provide mean annual precipitation, mean annual potential evapotranspiration, mean annual air temperature, and the aridity index as the ratio between potential evapotranspiration and precipitation. The variability in precipitation is further characterized by the mean precipitation frequency and depth (Botter et al., 2013) as well as by two seasonality indices, i.e., the ratio between summer (June–August) and winter (December–February) precipitation (P_SIsw) and the average difference between average daily precipitation within each month and within a year (P_SI).

The hydrologic properties were characterized from stations with observed daily discharge data (Sect. 3.2) for different time periods according to the available data and study purposes of the original data sets. For current properties, daily discharge data from November 1999 (hydrological year 2000) were used for calculations (309 stations). Additionally, the hydrologic characteristics calculated from daily discharge data starting in 1986 are provided (319 stations), which are possibly more relevant for studies with a long-term perspective. If there were only data before 1986, we used the available time period (four stations). The actual starting and ending dates of the time series finally used for calculations are provided to inform the user of the exact time periods (StartQobs and EndQobs or Q_StartDate and Q_EndDate, respectively, refer to Table B1). Provided average characteristics include mean, median, median summer (May–October), median winter (November–April), and specific discharge. For the variability in discharge, we provide the coefficient of variation, the base flow index (according to WMO, 2008), and the flashiness index based on flow percentiles (ratio of the 5th to the 95th percentile) as well as discharge seasonality in terms of the ratio between summer and winter median discharge and the runoff coefficient (discharging fraction of precipitation).

5 Limitations

The presented data set has several limitations. More than half of the stations do not a have co-located gauging station and the ones that do are not homogeneously distributed across Germany. Existing concentration time series would benefit from available discharge data, as this allows the characterization of concentration-discharge relationships as well as the estimation of daily concentration, flow-normalized concentration and flux data for stations with high data availability using the WRTDS method. Generally, modeled discharge from hydrological models such as mHM (Sect. 3.2.2) or estimated discharge using other (mechanistic or statistical modeling) techniques could serve to extend the data set of joint water quality and water quantity and overcome missing station matches or data gaps. Other limitations are linked to data policies by federal state authorities, which sometimes do not permit publication of raw quality and quantity data. However, we aimed to make a virtue of necessity by providing aggregated data and further ready-to-use metrics of water quality and quantity (e.g., annual median concentrations and monthly median concentrations over the whole time series). Attributes derived from exclusively national data sets, such as N surplus, underlie higher uncertainties in transboundary catchments, as data outside Germany are either not available or not consistent. Additionally, there is uncertainty in the attributes, stemming from the inherent uncertainties in the data sets and the catchment boundaries. However, the provided description and references of the methods and the underlying data sources should enable users to evaluate the reliability of each descriptor in the data set and exclude stations from the analyses if necessary. This also leaves room for further improvements and extensions when new data and knowledge become available. Besides a higher number of water quality stations, longer time series and more co-located discharge data, it would be especially interesting to add time series of nutrient inputs from point sources and from diffuse P sources, as well as information on tile drainage locations to the catchment attributes. For a better linkage of chemical water quality with ecological research questions, biological water quality variables such as chlorophyll-*a* concentrations would be highly valuable as well.

6 Data availability

The QUADICA data set presented here is freely available from two online repositories. The water quality and water quantity data described in this paper as well as the time series of meteorological and diffuse nitrogen input can be accessed at https://doi.org/10.4211/hs.0ec5f43e43c349ff818a8d57699c0fe1 (Ebeling et al., 2022b). The catchment data, including the catchment attributes, boundaries, and stations, have been published at https://doi.org/10.4211/hs.88254bd930d1466c85992a7dea6947a4 (Ebeling et al., 2022a). Due to license agreements, the raw concentration and raw discharge data provided by the German federal states cannot made public, but they have been deposited in an institutional repository (Musolff et al., 2020). The metadata of the data and stations, however, are available from https://doi.org/10.4211/hs.a42addcbd59a466a9aa56472dfef8721 (Musolff, 2020).

7 Conclusions

In this study, we provide a comprehensive homogenized data set with a large spatial and temporal coverage of both water quality and quantity observations along with catchment attributes. Specifically, the data set includes time series of water quality, co-located discharge, hydroclimatic data, and diffuse nitrogen inputs as well as catchment boundaries and more than 100 catchment attributes for 1386 German catchments. The presented QUADICA (water QUAlity, DIscharge and Catchment Attributes for large-sample studies in Germany) data set offers the opportunity to identify spatial and temporal patterns of water quality along with water quantity. This allows one to formulate and test hypotheses on underlying processes by linking observed responses to the driving forces and catchment attributes. QUADICA also opens up opportunities to calibrate and validate water and solute transport models at the single- and multiple-catchment scales as well as at the national scale. Consequently, the data set has the potential to advance our understanding of water quality processes across scales. More specifically, the data can be used to examine various spatiotemporal water quality patterns such as average concentrations, trends, and average seasonality. For stations with high data availability, analyses can be extended to trajectories of seasonality, flow-normalized concentrations, and mass fluxes. The patterns can be investigated for the three different macronutrients, nitrogen, phosphorus, and organic carbon; their species; and for nutrient ratios. In addition, interactions between the nutrients and their spatiotemporal patterns can be assessed. In the context of comparative large-sample hydrology (e.g., Gupta et al., 2014), the spatiotemporal water quality patterns can be linked to catchment attributes to identify underlying processes. This can, for example, support quantification of the impact of human disturbances on nutrient cycles and their interactions with natural controls. Some studies have recently investigated spatiotemporal patterns and underlying controls in large-sample approaches using parts of the provided data set. For example, Ebeling et al. (2021a) assessed average nutrient concentrations and export dynamics, Ebeling et al. (2021b) evaluated long-term trajectories of nitrate seasonality, Ehrhardt et al. (2021b) quantified nitrogen legacies using nitrogen input and export time series, and Yang et al. (2021) modeled the impact of phosphorus inputs on stream network algae growth. These assessments and the derived hypotheses can be further explored and extended with

the provided data to increase our knowledge on catchment functioning.

Furthermore, the provided data can be merged with other water quality and quantity data sets – for example, to enable assessments across transnational scales and an even larger variability in catchment attributes. Here, we hope to stimulate other researchers or environmental authorities to provide similar data sets of joint water quality and quantity data to make the wealth of spatiotemporal water quality data available, including long-term data that have been collected during research projects and regular monitoring activities, such as for the 2000/60/EC EU Water Framework Directive (EC, 2000). Therefore, we call for joint efforts to further increase opportunities for catchment-scale water quality assessments and modeling activities on regional, transnational, and even continental scales.

Appendix A

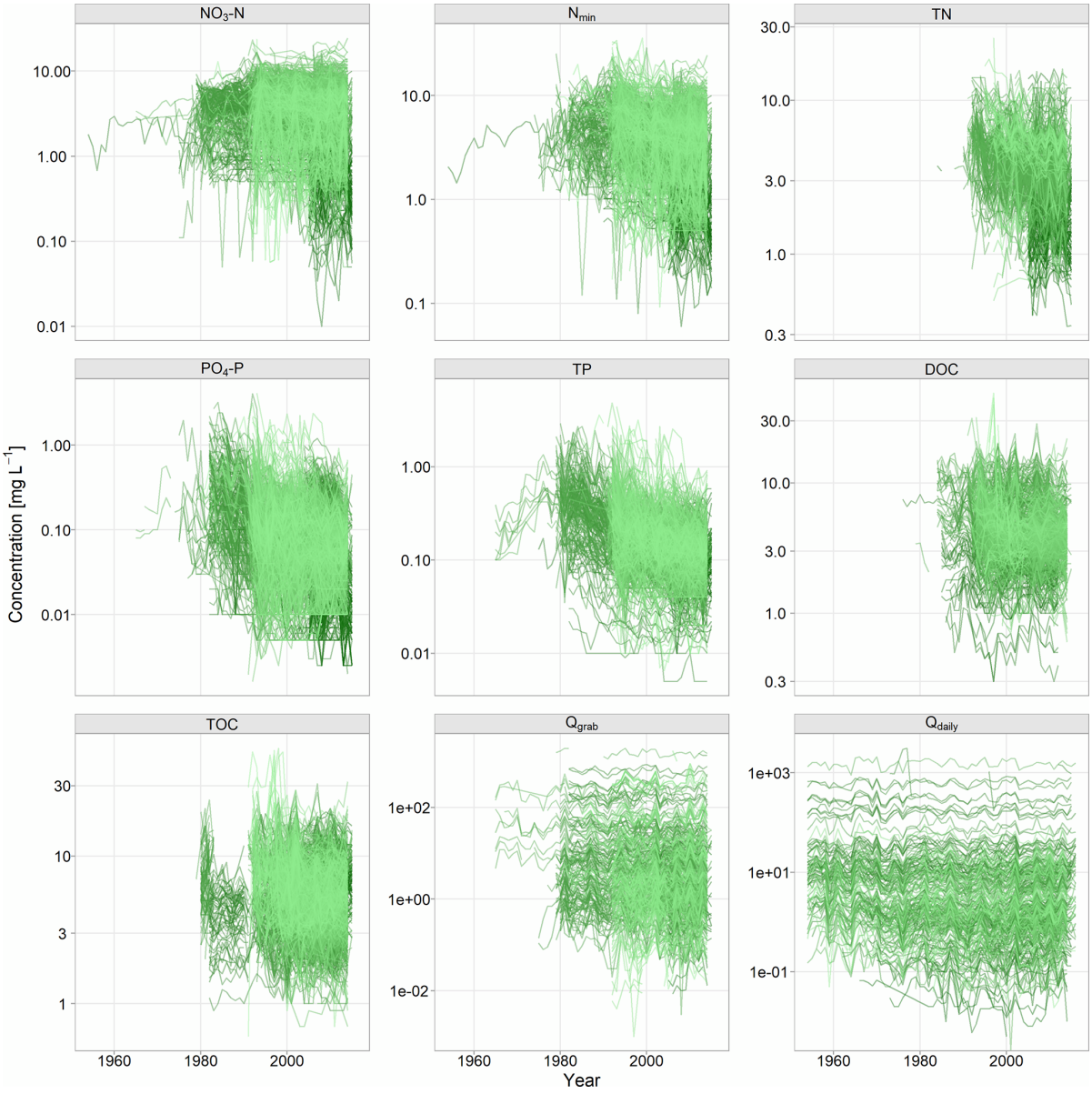

Figure A1. Time series of annual median concentrations and discharge observed at the 1386 water quality stations during grab sampling, as shown in Table 1 and Fig. 1 and described in Sect. 3.1. Note that, for visualization purposes, values before 1954 and values $> 40\,\mathrm{mg\,L^{-1}}$ for N species (i.e., five NO_3-N, seven N_{min}, and zero TN values) are not shown.

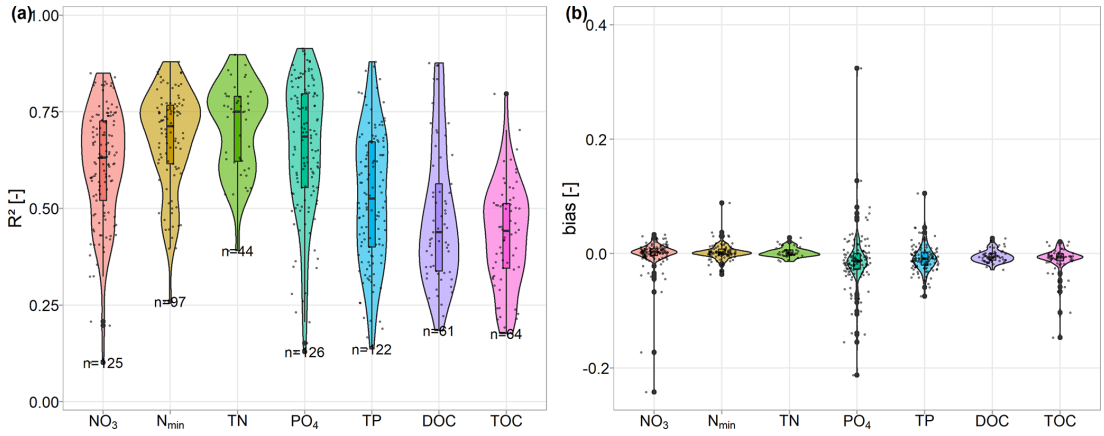

Figure A2. Distribution of the performance of WRTDS models by compound based on the coefficient of determination R^2 **(a)** and bias **(b)**. Boxes highlight the median and quartiles of each distribution, and points display the performance values of single catchments. Note that, for visualization purposes, one bias value > 0.4 is not shown for TOC.

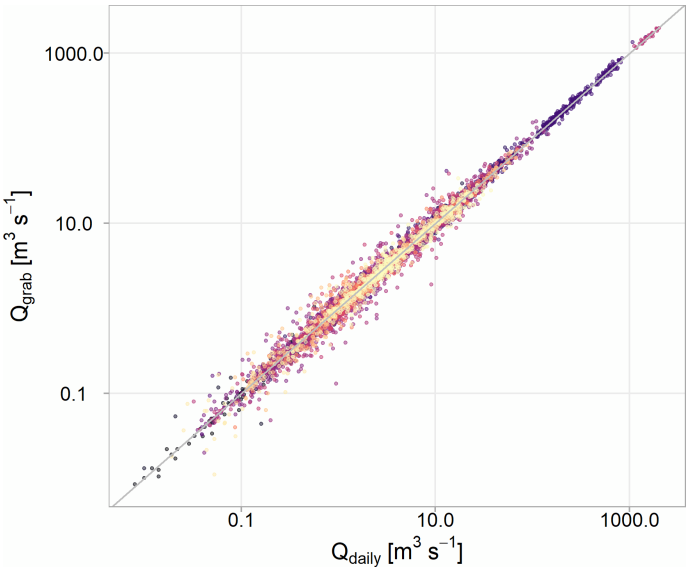

Figure A3. Comparison of annual medians from continuous daily discharge (Q_{daily}) and discharge at the dates grab samples were taken (Q_{grab}). Colors represent different catchments.

Appendix B

Table B1. Catchment attributes, associated methods, and original data sources used for calculating the attributes (Ebeling et al., 2022a). This collection of catchment attributes is merged and adapted from existing repositories (Ebeling, 2021; Ebeling and Dupas, 2021) and the related publications (Ebeling et al., 2021a, b). For more details, the reader is referred to Sect. 4.

Category	Variable	Unit	Description and method	Data source
General	OBJECTID	–	Unique identifier	
	Station	–	Station name	
	Area_km2	km^2	Catchment area	
	f_AreaGer	–	Fraction of catchment area within Germany	
Topography	dem.mean	m a.m.s.l.	Mean elevation of catchment, from the DEM rescaled from a 25 to 100 m resolution using the average	EEA (2013)
	dem.median	m a.m.s.l.	Median elevation of catchment, from the DEM rescaled from a 25 to 100 m resolution using the average	EEA (2013)
	slo.mean	°	Mean topographic slope of catchment, from the DEM (100 m resolution)	EEA (2013)
	slo.median	°	Median topographic slope of catchment, from the DEM (100 m resolution)	EEA (2013)
	twi.mean	–	Mean topographic wetness index (TWI; Beven and Kirkby, 1979)	EEA (2013)
	twi.med	–	Median topographic wetness index (TWI; Beven and Kirkby, 1979)	EEA (2013)
	twi.90p	–	The 90th percentile of the TWI as a proxy for riparian wetlands (following Musolff et al., 2018)	EEA (2013)
	ddhad	km^{-1}	Average drainage density of the catchment. Gridded drainage density is provided as the length of surface waters (rivers and lakes) per area from a 75 km^2 circular area centered around each cell.	BMU (2000)
	DrainDens	km^{-1}	Average drainage density of the catchment, calculated from the EU-Hydro River Network Database and intersection with catchment polygons (contains several implausible values, and values are often overly small due to the coarser resolution of the river network)	EEA (2019)
Land cover	f_artif	–	Fraction of artificial land cover	EEA (2016a)
	f_agric	–	Fraction of agricultural land cover	EEA (2016a)
	f_forest	–	Fraction of forested land cover	EEA (2016a)
	f_wetl	–	Fraction of wetland cover	EEA (2016a)
	f_water	–	Fraction of surface water cover	EEA (2016a)
	f_urban	–	Fraction of class 11, level 2 of the CORINE Land Cover data set	EEA (2016a)
	f_industry	–	Fraction of class 12, level 2 of the CORINE Land Cover data set	EEA (2016a)

Table B1. Continued.

Category	Variable	Unit	Description and method	Data source
	f_mine	–	Fraction of class 13, level 2 of the CORINE Land Cover data set	EEA (2016a)
	f_urban_veg	–	Fraction of class 14, level 2 of the CORINE Land Cover data set	EEA (2016a)
	f_arable	–	Fraction of class 21, level 2 of the CORINE Land Cover data set	EEA (2016a)
	f_agri_perm	–	Fraction of class 22, level 2 of the CORINE Land Cover data set	EEA (2016a)
	f_pastures	–	Fraction of class 23, level 2 of the CORINE Land Cover data set	EEA (2016a)
	f_agri_hetero	–	Fraction of class 24, level 2 of the CORINE Land Cover data set	EEA (2016a)
	f_fores	–	Fraction of class 31, level 2 of the CORINE Land Cover data set	EEA (2016a)
	f_scrub	–	Fraction of class 32, level 2 of the CORINE Land Cover data set	EEA (2016a)
	f_open	–	Fraction of class 33, level 2 of the CORINE Land Cover data set	EEA (2016a)
	pdens	inhabitants km^{-2}	Mean population density	CIESIN (2017)
Nutrient sources	Nsurp00_15	kg N ha^{-1} yr^{-1}	Mean nitrogen (N) surplus per catchment during the sampling period (2000–2015) including the N surplus from agricultural land and atmospheric N deposition as well as biological N fixation from nonagricultural areas. Details on the N surplus data are given in Sect. 3.4.	Bach et al. (2006); Bach and Frede (1998); Bartnicki and Benedictow (2017); Bartnicki and Fagerli (2006); Behrendt et al. (1999); Cleveland et al. (1999); Häußermann et al. (2019); Van Meter et al. (2017)
	Nsurp91_15	kg N ha^{-1} yr^{-1}	Mean N surplus per catchment from 1991 to 2015 (after the 91/676/EEC Nitrates Directive was introduced)	See Nsurp00_15
	Nsurp80_15	kg N ha^{-1} yr^{-1}	Mean N surplus per catchment from 1980 to 2015 (main sampling period)	See Nsurp00_15
	Nsurp71_90	kg N ha^{-1} yr^{-1}	Mean N surplus per catchment from 1971 to 1990 (historic (legacy) inputs)	See Nsurp00_15
	dNsurp71_91	kg N ha^{-1} yr^{-1}	Change in mean N surplus between the periods from 1971 to 1990 and from 1991 to 2015, i.e., dNsurp71_91 = Nsurp71_90 – Nsurp91_15	See Nsurp00_15
	N_WW	kg N ha^{-1} yr^{-1}	Sum of N input from point sources including wastewater treatment plants (WWTPs) > 2000 person equivalents from the database of the European Environment Agency covering areas beyond Germany and data collected from 13 federal German states covering smaller WWTPs within Germany	Büttner (2020)

Table B1. Continued.

Category	Variable	Unit	Description and method	Data source
	P_WW	kg P ha^{-1} yr^{-1}	Sum of P input from WWTPs analogous to N_WW	Büttner (2020)
	N_T_YKM2	t N km^{-2} yr^{-1}	Mean N input from point sources summing all N emission values provided in the EU domestic waste emissions database	Vigiak et al. (2019, 2020)
	P_T_YKM2	t P km^{-2} yr^{-1}	Mean P input from point sources summing all P emission values provided in the EU domestic waste emissions database	Vigiak et al. (2019, 2020)
	BOD_T_YKM2	t O km^{-2} yr^{-1}	Mean 5-day biochemical oxygen demand (BOD) input from point sources summing all BOD emission values provided in the EU domestic waste emissions database	Vigiak et al. (2019, 2020)
	N_T_YEW	t N inhabitant $^{-1}$ yr^{-1}	Calculated N input per person (from EU domestic waste emissions database): N_T_YEW = N_T_YKM2/nEW · Area_km2	Vigiak et al. (2019, 2020)
	P_T_YEW	t P inhabitant $^{-1}$ yr^{-1}	Calculated P input per person (from EU domestic waste emissions database): P_T_YEW = P_T_YKM2/nEW · Area_km2	Vigiak et al. (2019, 2020)
	nEW	–	Calculated number of inhabitants: nEW = pdens · Area_km2	CIESIN (2017)
	n_UWWTP	–	Number of point sources from the European WWTP database	EEA (2017)
	N_WW_frac	–	Fraction of point source loads from total N input loads: N_ WW_frac = N_T_YKM2 / (N_T_YKM2 + Nsurp80_15)	
	f_sarea	–	Fraction of source area in the catchment. Source areas were defined as seasonal and perennial cropland and grassland land cover classes using a highly resolved land use map (Pflugmacher et al., 2018)	Source areas based on Pflugmacher et al. (2018)
	het_h	m^{-1}	Slope of relative frequency of source areas in classes of flow distances to stream as a proxy for horizontal source heterogeneity. For details, the reader is referred to Ebeling et al. (2021a)	Source areas based on Pflugmacher et al. (2018)
	R2_het_h	–	Coefficient of determination of horizontal source heterogeneity het_h	
	sdist_mean	m	Mean lateral flow distance of source areas to stream. For details, the reader is referred to Ebeling et al. (2021a)	Source areas based on Pflugmacher et al. (2018)
	het_v	–	Mean ratio between potential seepage and groundwater NO_3-N concentrations as proxy for vertical concentration heterogeneity. For details, the reader is referred to Ebeling et al. (2021a)	Knoll et al. (2020)

Table B1. Continued.

Category	Variable	Unit	Description and method	Data source
Lithology and soils	f_calc	–	Fraction of calcareous rocks (lithology level 4)	BGR and UNESCO (2014)
	f_calc_sed	–	Fraction of calcareous rocks and sediments (lithology level 4, coarse and fine sediments aggregated)	BGR and UNESCO (2014)
	f_magma	–	Fraction of magmatic rocks (lithology level 4)	BGR and UNESCO (2014)
	f_metam	–	Fraction of metamorphic rocks (lithology level 4)	BGR and UNESCO (2014)
	f_sedim	–	Fraction of sedimentary aquifer (lithology level 4, coarse and fine sediments aggregated)	BGR and UNESCO (2014)
	f_silic	–	Fraction of siliciclastic rocks (lithology level 4)	BGR and UNESCO (2014)
	f_sili_sed	–	Fraction of siliciclastic rocks and sediments (lithology level 4, coarse and fine sediments aggregated)	BGR and UNESCO (2014)
	f_consol	–	Fraction of consolidated rocks (lithology Level 5)	BGR and UNESCO (2014)
	f_part_consol	–	Fraction of partly consolidated rocks (lithology level 5)	BGR and UNESCO (2014)
	f_unconsol	–	Fraction of unconsolidated rocks (lithology level 5)	BGR and UNESCO (2014)
	f_porous	–	Fraction of porous aquifer (code 1 and 2 of aquifer type)	BGR and UNESCO (2014)
	f_porous1	–	Fraction of porous aquifer (code 1 of aquifer type)	BGR and UNESCO (2014)
	f_porous2	–	Fraction of porous aquifer (code 2 of aquifer type)	BGR and UNESCO (2014)
	f_fissured	–	Fraction of fissured aquifer (code 3 and 4 of aquifer type)	BGR and UNESCO (2014)
	f_fiss1	–	Fraction of fissured aquifer (code 3 of aquifer type)	BGR and UNESCO (2014)
	f_fiss2	–	Fraction of fissured aquifer (code 4 of aquifer type)	BGR and UNESCO (2014)
	f_hard	–	Fraction of locally aquiferous and non-aquiferous aquifer (code 5 and 6 of aquifer type)	BGR and UNESCO (2014)
	f_hard1	–	Fraction of locally aquiferous rocks (code 5 of aquifer type)	BGR and UNESCO (2014)
	f_hard2	–	Fraction of non-aquiferous rocks (code 6 of aquifer type)	BGR and UNESCO (2014)
	f_inwater	–	Fraction of inland water (code 200 of aquifer type)	BGR and UNESCO (2014)
	f_ice	–	Fraction of snow or ice field (code 300 of aquifer type)	BGR and UNESCO (2014)

Table B1. Continued.

Category	Variable	Unit	Description and method	Data source
	dtb.median	cm	Median depth to bedrock in the catchment	Shangguan et al. (2017)
	f_gwsoils	–	Fraction of water-impacted soils in the catchment (from 1 : 250 000 soil map), including Stagnosols, semiterrestrial, semi-subhydric, subhydric, and moor soils	BGR (2018)
	f_sand f_silt f_clay	–	Mean fraction of sand in soil horizons of the top 100 cm Mean fraction of silt in soil horizons of the top 100 cm Mean fraction of clay in soil horizons of the top 100 cm	FAO/IIASA/ISRIC/ ISSCAS/JRC (2012)
	f_clay_agri	–	Mean fraction of clay in soil horizons of the top 100 cm for agricultural land use (class 2, level 1 CORINE; see f_clay and f_agric)	FAO/IIASA/ISRIC/ ISSCAS/JRC (2012); EEA (2016a)
	WaterRoots	mm	Mean available water content in the root zone from pedotransfer functions	Livneh et al. (2015); Samaniego et al. (2010); Zink et al. (2017)
	thetaS	–	Mean porosity in catchment from pedotransfer functions	Livneh et al. (2015); Samaniego et al. (2010); Zink et al. (2017)
	soilN.mean	$g\,kg^{-1}$	Mean topsoil N in catchment	Ballabio et al. (2019)
	soilP.mean	$mg\,kg^{-1}$	Mean topsoil P in catchment	Ballabio et al. (2019)
	soilCN.mean	–	Mean topsoil C / N ratio in catchment	Ballabio et al. (2019)
Hydrology	StartQobs	YYYY-MM-DD	Starting date of Q time series used for calculating hydrological indices (1999-11-01 or start of time series)	
	EndQobs	YYYY-MM-DD	End date of Q time series used for calculating hydrological indices	
	meanQobs	$m^3\,s^{-1}$	Mean discharge (period from StartQobs to EndQobs)	Musolff (2020); Musolff et al. (2020)
	medQobs	$m^3\,s^{-1}$	Median discharge (period from StartQobs to EndQobs)	Musolff (2020); Musolff et al. (2020)
	specQobs	$mm\,yr^{-1}$	Mean annual specific discharge (period from StartQobs to EndQobs)	Musolff (2020); Musolff et al. (2020)
	CVQobs	–	Coefficient of variation of time series of daily Q (period from StartQobs to EndQobs)	Musolff (2020); Musolff et al. (2020)
	medSuQobs	$m^3\,s^{-1}$	Median summer discharge (months May–October; period from StartQobs to EndQobs)	Musolff (2020); Musolff et al. (2020)
	medWiQobs	$m^3\,s^{-1}$	Median winter discharge (months November–April; period from StartQobs to EndQobs)	Musolff (2020); Musolff et al. (2020)
	seasRQobs	–	Seasonality index of Q, as a ratio between median summer and median winter Q (period from StartQobs to EndQobs)	Musolff (2020); Musolff et al. (2020)

Table B1. Continued.

Category	Variable	Unit	Description and method	Data source
	BFIQobs	–	Base flow index calculated according to WMO (2008) with the "lfstat" package (version 0.9.4) in R (period from StartQobs to EndQobs)	Musolff (2020); Musolff et al. (2020)
	flashQobs	–	Flashiness index of Q as the ratio between the 5th percentile and the 95th percentile of the Q time series (period from StartQobs to EndQobs)	Musolff (2020); Musolff et al. (2020)
	RCQobs	–	Runoff coefficient (fraction of mean annual precipitation discharging as specific discharge, specQobs/P_mm) (period from StartQobs to EndQobs)	Musolff (2020); Musolff et al. (2020)
	Q_StartDate	YYYY-MM-DD	Starting date of Q time series used for calculating hydrological indices (from 1986, if possible, and using at least 3 years of data; in few cases, only earlier data were available)	
	Q_EndDate	YYYY-MM-DD	End date of Q time series used for calculating hydrological indices (as available)	
	Q_mean	$m^3\ s^{-1}$	Mean discharge (data for the period Q_ StartDate–Q_EndDate)	Musolff (2020); Musolff et al. (2020)
	Q_median	$m^3\ s^{-1}$	Median discharge (data for the period Q_ StartDate–Q_ EndDate)	Musolff (2020); Musolff et al. (2020)
	Q_spec	$mm\ yr^{-1}$	Mean annual specific discharge (data for the period Q_ StartDate–Q_EndDate)	Musolff (2020); Musolff et al. (2020)
	Q_CVQ	–	Coefficient of variation of time series of daily Q (data for the period Q_StartDate–Q_EndDate)	Musolff (2020); Musolff et al. (2020)
	Q_medSum	$m^3\ s^{-1}$	Median summer discharge (months May–October; data for the period Q_StartDate–Q_EndDate)	Musolff (2020); Musolff et al. (2020)
	Q_medWin	$m^3\ s^{-1}$	Median winter discharge (months November–April; data for the period Q_StartDate–Q_EndDate)	Musolff (2020); Musolff et al. (2020)
	Q_Sum2Win	–	Seasonality index of Q, as a ratio between median summer and median winter Q (data for the period Q_StartDate–Q_EndDate)	Musolff (2020); Musolff et al. (2020)
	BFI	–	Base flow index calculated according to WMO (2008) with the lfstat package (version 0.9.4) in R (data for the period Q_ StartDate–Q_EndDate)	Musolff (2020); Musolff et al. (2020)
	flashi	–	Flashiness index of Q as the ratio between the 5th percentile and the 95th percentile of the Q time series (data for the period Q_ StartDate–Q_EndDate)	Musolff (2020); Musolff et al. (2020)
Climate	P_mm	$mm\ yr^{-1}$	Mean annual precipitation (period 1986–2015)	Cornes et al. (2018)

Table B1. Continued.

Category	Variable	Unit	Description and method	Data source
	P_SIsw	–	Seasonality of precipitation as the ratio between mean summer (June–August) and winter (December–February) precipitation (period 1986–2015)	Cornes et al. (2018)
	P_SI	–	Seasonality index of precipitation as the mean difference between monthly averages of daily precipitation and the annual average of daily precipitation (period 1986–2015)	Cornes et al. (2018)
	P_lambda	d^{-1}	Mean precipitation frequency λ as used by Botter et al. (2013) with rain days for precipitation above 1 mm (period 1986–2015)	Cornes et al. (2018)
	P_alpha	$mm\,d^{-1}$	Mean precipitation depth as used by Botter et al. (2013) with rain days for precipitation above 1 mm (period 1986–2015)	
	PET_mm	$mm\,yr^{-1}$	Mean annual potential evapotranspiration (period 1986–2015)	Cornes et al. (2018)
	AI	–	Aridity index: AI=PET_mm/P_mm (period 1986–2015)	Cornes et al. (2018)
	T_mean	°C	Mean annual air temperature (period 1986–2015)	Cornes et al. (2018)

Author contributions. PE carried out the study, processed and curated the data, and created the figures and tables. PE, AM, and RK conceptualized and designed the study; AM and SA provided the initial ideas for the study and obtained funding. Several authors contributed to the data collection and processing: RK provided the gridded meteorological time series, simulated discharge data, and atmospheric deposition data; MW provided time series of N surplus data for the catchments; and OB collected the point source data for Germany. PE produced the original draft of the paper with contributions from AM and RK. All authors contributed to reviewing and editing the manuscript.

Competing interests. The contact author has declared that none of the authors has any competing interests.

Disclaimer. Publisher's note: Copernicus Publications remains neutral with regard to jurisdictional claims in published maps and institutional affiliations.

Acknowledgements. The authors gratefully thank all data collectors, processors, and providers, including the federal state environmental agencies and all contributors to this data set. We are especially grateful to Thomas Grau, Teresa Nitz, Joni Dehaspe, Stefanie Breese, and Sophie Ehrhardt for their contributions to data processing. The authors wish to thank the two anonymous reviewers for their valuable comments. Moreover, we gratefully acknowledge Martin Bach and Uwe Häußermann (Justus-Liebig-Universität Giessen) for the provision of the two data sets on the agricultural N surplus data for Germany. We acknowledge the E-OBS data set from the EU FP6 project UERRA (http://www.uerra.eu, last access: 8 August 2022) and the Copernicus Climate Change Service, and the data providers for the ECA&D project (https://www.ecad.eu, last access: 8 August 2022). The authors additionally acknowledge several organizations responsible for the data products used here, including the BfG, BGR, SGD, EEA, FAO, IIASA, ISRIC, ISSCAS, and JRC.

Financial support. This research has been supported by the Deutsche Forschungsgemeinschaft (grant no. 392886738).

Review statement. This paper was edited by David Carlson and reviewed by two anonymous referees.

References

Addor, N., Newman, A. J., Mizukami, N., and Clark, M. P.: The CAMELS data set: catchment attributes and meteorology for large-sample studies, Hydrol. Earth Syst. Sci., 21, 5293–5313, https://doi.org/10.5194/hess-21-5293-2017, 2017.

Addor, N., Do, H. X., Alvarez-Garreton, C., Coxon, G., Fowler, K., and Mendoza, P. A.: Large-sample hydrology: recent progress, guidelines for new datasets and grand challenges, Hydrolog. Sci. J., 65, 712–725, https://doi.org/10.1080/02626667.2019.1683182, 2020.

Alvarez-Garreton, C., Mendoza, P. A., Boisier, J. P., Addor, N., Galleguillos, M., Zambrano-Bigiarini, M., Lara, A., Puelma, C., Cortes, G., Garreaud, R., McPhee, J., and Ayala, A.: The CAMELS-CL dataset: catchment attributes and meteorology for large sample studies – Chile dataset, Hydrol. Earth Syst. Sci., 22, 5817–5846, https://doi.org/10.5194/hess-22-5817-2018, 2018.

Bach, M. and Frede, H.-G.: Agricultural nitrogen, phosphorus and potassium balances in Germany – Methodology and trends 1970 to 1995, Z. Pflanz. Bodenkunde, 161, 385–393, https://doi.org/10.1002/jpln.1998.3581610406, 1998.

Bach, M., Breuer, L., Frede, H. G., Huisman, J. A., Otte, A., and Waldhardt, R.: Accuracy and congruency of three different digital land-use maps, Landscape Urban Plan., 78, 289–299, https://doi.org/10.1016/j.landurbplan.2005.09.004, 2006.

Ballabio, C., Lugato, E., Fernández-Ugalde, O., Orgiazzi, A., Jones, A., Borrelli, P., Montanarella, L., and Panagos, P.: Mapping LUCAS topsoil chemical properties at European scale using Gaussian process regression, Geoderma, 355, 113912, https://doi.org/10.1016/j.geoderma.2019.113912, 2019.

Bartnicki, J. and Benedictow, A.: Atmospheric Deposition of Nitrogen to OSPAR Convention waters in the period 1995–2014, EMEP/MSC-W Technical Report, 1/2007, Meteorological Synthesizing Centre-West (MSC-W), Norwegian Meteorological Institute, Oslo, https://emep.int/publ/reports/2017/MSCW_technical_1_2017.pdf (last access: 11 August 2022), 2017.

Bartnicki, J. and Fagerli, H.: Atmospheric Nitrogen in the OSPAR Convention Area in the Period 1990–2004. Summary Report for the OSPAR Convention, EMEP/MSC-W Technical Report, 4/2006, Meteorological Synthesizing Centre-West (MSC-W) of EMEP, Oslo, https://www.ospar.org/documents?v=7064 (last access: 12 August 2022), 2006.

Basu, N. B., Destouni, G., Jawitz, J. W., Thompson, S. E., Loukinova, N. V., Darracq, A., Zanardo, S., Yaeger, M., Sivapalan, M., Rinaldo, A., and Rao, P. S. C.: Nutrient loads exported from managed catchments reveal emergent biogeochemical stationarity, Geophys. Res. Lett., 37, L23404, https://doi.org/10.1029/2010gl045168, 2010.

Behrendt, H., Huber, P., Opitz, D., Schmoll, O., Scholz, G., and Uebe, R.: Nutrient emissions into river basins of Germany, UBA-Texte, 75/99, https://www.umweltbundesamt.de/en/publikationen/naehrstoffbilanzierung-flussgebiete-deutschlands (last access: 8 August 2022), 1999.

Behrendt, H., Huber, P., Opitz, D., Schmoll, O., Scholz, G., and Uebe, R.: Nutrient emissions into river basins of Germany, UBA-Texte, 23/00, https://www.umweltbundesamt.de/en/publikationen/nutrient-emissions-into-river-basins-of-germany (last access: 9 August 2022), 2000.

Behrendt, H., Bach, M., Kunkel, R., Opitz, D., Pagenkopf, W.-G., Scholz, G., and Wendland, F.: Nutrient Emissions into River Basins of Germany on the Basis of a Harmonized Procedure UBA-Texte, 82/03, https://www.umweltbundesamt.de/en/publikationen/nutrient-emissions-into-river-basins-of-germany-on (last access: 9 August 2022), 2003.

Beven, K. J. and Kirkby, M. J.: A physically based, variable contributing area model of basin hydrology/Un modèle à base physique de zone d'appel variable de l'hydrologie du bassin versant, Hydrol. Sci. B., 24, 43–69, https://doi.org/10.1080/02626667909491834, 1979.

BGR: Bodenübersichtskarte der Bundesrepublik Deutschland 1:250.000 (BUEK250). Soil map of Germany 1:250,000, Federal Institute for Geosciences and Natural Resources (BGR) [data set], https://produktcenter.bgr.de/terraCatalog/Start.do (last access: 9 August 2022), 2018.

BGR and UNESCO (Eds.): International Hydrogeological Map of Europe 1:1 500 000 (IHME1500). Digital map data v1.1. [data set], http://www.bgr.bund.de/ihme1500/ (last access: 9 August 2022), 2014.

BMU (Bundesministerium Für Umwelt) (Ed.): Hydrologischer Atlas von Deutschland, Datenquelle: Hydrologischer Atlas von Deutschland/BfG, 2000, Bonn, Berlin, https://geoportal.bafg.de/mapapps/resources/apps/HAD/index.html (last access: 9 August 2022), 2000.

Botter, G., Basso, S., Rodriguez-Iturbe, I., and Rinaldo, A.: Resilience of river flow regimes, P. Natl. Acad. Sci. USA, 110, 12925–12930, https://doi.org/10.1073/pnas.1311920110, 2013.

Büttner, O.: DE-WWTP – data collection of wastewater treatment plants of Germany (status 2015, metadata), HydroShare [data set], https://doi.org/10.4211/hs.712c1df62aca4ef29688242eeab7940c, 2020.

Center for International Earth Science Information Network – CIESIN – Columbia University: Gridded Population of the World, Version 4 (GPWv4): Population Density, Revision 10, NASA Socioeconomic Data and Applications Center (SEDAC) [data set], https://doi.org/10.7927/H4DZ068D, 2017.

Chagas, V. B. P., Chaffe, P. L. B., Addor, N., Fan, F. M., Fleischmann, A. S., Paiva, R. C. D., and Siqueira, V. A.: CAMELS-BR: hydrometeorological time series and landscape attributes for 897 catchments in Brazil, Earth Syst. Sci. Data, 12, 2075–2096, https://doi.org/10.5194/essd-12-2075-2020, 2020.

Chen, D., Shen, H., Hu, M., Wang, J., Zhang, Y., and Dahlgren, R. A.: Chapter Five – Legacy Nutrient Dynamics at the Watershed Scale: Principles, Modeling, and Implications, in: Advances in Agronomy, edited by: Sparks, D. L., Academic Press, 237–313, https://doi.org/10.1016/bs.agron.2018.01.005, 2018.

Cleveland, C. C., Townsend, A. R., Schimel, D. S., Fisher, H., Howarth, R. W., Hedin, L. O., Perakis, S. S., Latty, E. F., Von Fischer, J. C., Elseroad, A., and Wasson, M. F.: Global patterns of terrestrial biological nitrogen (N2) fixation in natural ecosystems, Global Biogeochem. Cy., 13, 623–645, https://doi.org/10.1029/1999GB900014, 1999.

Cornes, R. C., van der Schrier, G., van den Besselaar, E. J. M., and Jones, P. D.: An Ensemble Version of the E-OBS Temperature and Precipitation Data Sets, J. Geophys. Res.-Atmos., 123, 9391–9409, https://doi.org/10.1029/2017jd028200, 2018.

Coxon, G., Addor, N., Bloomfield, J. P., Freer, J., Fry, M., Hannaford, J., Howden, N. J. K., Lane, R., Lewis, M., Robinson, E. L., Wagener, T., and Woods, R.: CAMELS-GB: hydrometeorological time series and landscape attributes for 671 catchments in Great Britain, Earth Syst. Sci. Data, 12, 2459–2483, https://doi.org/10.5194/essd-12-2459-2020, 2020.

De Jager, A. and Vogt, J.: Rivers and Catchments of Europe – Catchment Characterisation Model (CCM) (2.1), European Commission, Joint Research Centre (JRC) [data set], http://data.europa.eu/89h/fe1878e8-7541-4c66-8453-afdae7469221 (last access: 9 August 2022), 2007.

Do, H. X., Westra, S., and Leonard, M.: A global-scale investigation of trends in annual maximum streamflow, J. Hydrol., 552, 28–43, https://doi.org/10.1016/j.jhydrol.2017.06.015, 2017.

Ebeling, P.: CCDB – catchment characteristics data base Germany, HydroShare [data set], https://doi.org/10.4211/hs.0fc1b5b1be4a475aacfd9545e72e6839, 2021.

Ebeling, P. and Dupas, R.: CCDB – catchment characteristics data base France and Germany, HydroShare [data set], https://doi.org/10.4211/hs.c7d4df3ba74647f0aa83ae92be2e294b, 2021.

Ebeling, P., Kumar, R., Weber, M., Knoll, L., Fleckenstein, J. H., and Musolff, A.: Archetypes and Controls of Riverine Nutrient Export Across German Catchments, Water Resour. Res., 57, e2020WR028134, https://doi.org/10.1029/2020WR028134, 2021a.

Ebeling, P., Dupas, R., Abbott, B., Kumar, R., Ehrhardt, S., Fleckenstein, J. H., and Musolff, A.: Long-Term Nitrate Trajectories Vary by Season in Western European Catchments, Global Biogeochem. Cy., 35, e2021GB007050, https://doi.org/10.1029/2021GB007050, 2021b.

Ebeling, P., Kumar, R., and Musolff, A.: CCDB – catchment characteristics data base Germany, HydroShare [data set], https://doi.org/10.4211/hs.88254bd930d1466c85992a7dea6947a4, 2022a.

Ebeling, P., Kumar, R., Weber, M., and Musolff, A.: QUADICA – water quality, discharge and catchment attributes for large-sample studies in Germany, HydroShare [data set], https://doi.org/10.4211/hs.0ec5f43e43c349ff818a8d57699c0fe1, 2022b.

EC: Council Directive 91/271/EEC of 21 May 1991 concerning urban waste water treatment, Official Journal of the European Communities, http://data.europa.eu/eli/dir/1991/271/oj (last access: 9 August 2022), 1991a.

EC: Council Directive 91/676/EEC of 12 December 1991 concerning the protection of waters against pollution caused by nitrates from agricultural sources, Official Journal of the European Communities, http://data.europa.eu/eli/dir/1991/676/oj (last access: 9 August 2022), 1991b.

EC: Directive 2000/60/EC of the European Parliament and of the Council of 23 October 2000 establishing a framework for Community action in the field of water policy, Official Journal of the European Communities, L 327, 1–73, http://data.europa.eu/eli/dir/2000/60/oj (last access: 9 August 2022), 2000.

EEA: DEM over Europe from the GMES RDA project (EU-DEM, resolution 25 m) – version 1, European Environment Agency [data set], https://www.eea.europa.eu/data-and-maps/data/eu-dem (last access: 9 August 2022), 2013.

EEA: CORINE Land Cover 2012 v18.5, European Environment Agency [data set], https://land.copernicus.eu/pan-european/corine-land-cover/clc-2012 (last access: 11 August 2022), 2016.

EEA: Waterbase – UWWTD: Urban Waste Water Treatment Directive – reported data (v5), European Environment Agency [data set], https://www.eea.europa.eu/data-and-maps/data/waterbase-uwwtd-urban-waste-water-treatment-directive-5 (last access: 9 August 2022), 2017.

EEA: EU-Hydro – River Network Database (v1), European Environment Agency [data set], https://land.copernicus.eu/imagery-in-situ/eu-hydro/eu-hydro-river-network-database (last access: 9 August 2022), 2019.

EEA: Waterbase – Water Quality ICM, European Environment Agency [data set], https://www.eea.europa.eu/data-and-maps/data/waterbase-water-quality-icm-2 (last access: 9 August 2022), 2020.

Ehrhardt, S., Ebeling, P., and Dupas, R.: Exported french water quality and quantity data, HydroShare [data set], https://doi.org/10.4211/hs.d8c43e1e8a5a4872bc0b75a45f350f7a, 2021a.

Ehrhardt, S., Ebeling, P., Dupas, R., Kumar, R., Fleckenstein, J. H., and Musolff, A.: Nitrate Transport and Retention in Western European Catchments Are Shaped by Hydroclimate and Subsurface Properties, Water Resour. Res., 57, e2020WR029469, https://doi.org/10.1029/2020WR029469, 2021b.

FAO/IIASA/ISRIC/ISSCAS/JRC: Harmonized World Soil Database (version 1.2), FAO, Rome, Italy and IIASA, Laxenburg, Austria [data set], https://webarchive.iiasa.ac.at/Research/LUC/External-World-soil-database/HTML/ (last access: 11 August 2022), 2012.

Fowler, K. J. A., Acharya, S. C., Addor, N., Chou, C., and Peel, M. C.: CAMELS-AUS: hydrometeorological time series and landscape attributes for 222 catchments in Australia, Earth Syst. Sci. Data, 13, 3847–3867, https://doi.org/10.5194/essd-13-3847-2021, 2021.

Gnann, S. J., Howden, N. J. K., and Woods, R. A.: Hydrological signatures describing the translation of climate seasonality into streamflow seasonality, Hydrol. Earth Syst. Sci., 24, 561–580, https://doi.org/10.5194/hess-24-561-2020, 2020.

Godsey, S. E., Kirchner, J. W., and Clow, D. W.: Concentration-discharge relationships reflect chemostatic characteristics of US catchments, Hydrol. Process., 23, 1844–1864, https://doi.org/10.1002/hyp.7315, 2009.

Godsey, S. E., Hartmann, J., and Kirchner, J. W.: Catchment chemostasis revisited: Water quality responds differently to variations in weather and climate, Hydrol. Process., 33, 3056–3069, https://doi.org/10.1002/hyp.13554, 2019.

Gupta, H. V., Perrin, C., Blöschl, G., Montanari, A., Kumar, R., Clark, M., and Andréassian, V.: Large-sample hydrology: a need to balance depth with breadth, Hydrol. Earth Syst. Sci., 18, 463–477, https://doi.org/10.5194/hess-18-463-2014, 2014.

Hargreaves, G. H. and Samani, Z. A.: Reference Crop Evapotranspiration from Temperature, Appl. Eng. Agric., 1, 96–99, https://doi.org/10.13031/2013.26773, 1985.

Hartmann, J., Lauerwald, R., and Moosdorf, N.: A Brief Overview of the GLObal RIver Chemistry Database, GLORICH, Proced. Earth Plan. Sc., 10, 23–27, https://doi.org/10.1016/j.proeps.2014.08.005, 2014.

Häußermann, U., Bach, M., Klement, L., and Breuer, L.: Stickstoff-Flächenbilanzen für Deutschland mit Regionalgliederung Bundesländer und Kreise – Jahre 1995 bis 2017. Methodik, Ergebnisse und Minderungsmaßnahmen, Texte, 131/2019, https://www.umweltbundesamt.de/sites/default/files/medien/1410/publikationen/2019-10-28_texte_131-2019_stickstoffflaechenbilanz.pdf (last access: 9 August 2022), 2019.

Hirsch, R. M. and De Cicco, L. A.: User Guide to Exploration and Graphics for RivEr Trends (EGRET) and dataRetrieval: R Packages for Hydrologic Data, U.S. Geological Survey Techniques and Methods book 4, chap. A10, 93, https://doi.org/10.3133/tm4A10, 2015.

Hirsch, R. M., Moyer, D. L., and Archfield, S. A.: Weighted Regressions on Time, Discharge, and Season (WRTDS), with an Application to Chesapeake Bay River Inputs, J. Am. Water Resour. As., 46, 857-880, https://doi.org/10.1111/j.1752-1688.2010.00482.x, 2010.

Kaushal, S. S., Gold, A. J., Bernal, S., and Tank, J. L.: Diverse water quality responses to extreme climate events: an introduction, Biogeochemistry, 141, 273–279, https://doi.org/10.1007/s10533-018-0527-x, 2018.

Kingston, D. G., Massei, N., Dieppois, B., Hannah, D. M., Hartmann, A., Lavers, D. A., and Vidal, J. P.: Moving beyond the catchment scale: Value and opportunities in large-scale hydrology to understand our changing world, Hydrol. Process., 34, 2292–2298, https://doi.org/10.1002/hyp.13729, 2020.

Klingler, C., Schulz, K., and Herrnegger, M.: LamaH-CE: LArge-SaMple DAta for Hydrology and Environmental Sciences for Central Europe, Earth Syst. Sci. Data, 13, 4529–4565, https://doi.org/10.5194/essd-13-4529-2021, 2021.

Knoll, L., Breuer, L., and Bach, M.: Nation-wide estimation of groundwater redox conditions and nitrate concentrations through machine learning, Environ. Res. Lett., 15, 064004, https://doi.org/10.1088/1748-9326/ab7d5c, 2020.

Kuentz, A., Arheimer, B., Hundecha, Y., and Wagener, T.: Understanding hydrologic variability across Europe through catchment classification, Hydrol. Earth Syst. Sci., 21, 2863–2879, https://doi.org/10.5194/hess-21-2863-2017, 2017.

Kumar, R., Samaniego, L., and Attinger, S.: Implications of distributed hydrologic model parameterization on water fluxes at multiple scales and locations, Water Resour. Res., 49, 360–379, https://doi.org/10.1029/2012wr012195, 2013.

Li, L., Sullivan, P. L., Benettin, P., Cirpka, O. A., Bishop, K., Brantley, S. L., Knapp, J. L. A., van Meerveld, I., Rinaldo, A., Seibert, J., Wen, H., and Kirchner, J. W.: Toward catchment hydro-biogeochemical theories, WIREs Water, 8, e1495, https://doi.org/10.1002/wat2.1495, 2021.

Livneh, B., Kumar, R., and Samaniego, L.: Influence of soil textural properties on hydrologic fluxes in the Mississippi river basin, Hydrol. Process., 29, 4638–4655, https://doi.org/10.1002/hyp.10601, 2015.

Merz, R., Tarasova, L., and Basso, S.: The flood cooking book: ingredients and regional flavors of floods across Germany, Environ. Res. Lett., 15, 114024, https://doi.org/10.1088/1748-9326/abb9dd, 2020.

Monteith, D. T., Stoddard, J. L., Evans, C. D., de Wit, H. A., Forsius, M., Høgåsen, T., Wilander, A., Skjelkvåle, B. L., Jeffries, D. S., Vuorenmaa, J., Keller, B., Kopácek, J., and Vesely, J.: Dissolved organic carbon trends resulting from changes in atmospheric deposition chemistry, Nature, 450, 537–540, https://doi.org/10.1038/nature06316, 2007.

Murphy, R., Perry, E., Keisman, J., Harcum, J., and Leppo, E. W.: baytrends: Long Term Water Quality Trend Analysis. R package version 1.1.0, https://CRAN.R-project.org/package=baytrends (last access: 9 August 2022), 2019.

Musolff, A.: WQQDB – water quality and quantity data base Germany: metadata, HydroShare [data set], https://doi.org/10.4211/hs.a42addcbd59a466a9aa56472dfef8721, 2020.

Musolff, A., Fleckenstein, J. H., Opitz, M., Büttner, O., Kumar, R., and Tittel, J.: Spatio-temporal controls of dissolved organic carbon stream water concentrations, J. Hydrol., 566, 205–215, https://doi.org/10.1016/j.jhydrol.2018.09.011, 2018.

Musolff, A., Grau, T., Weber, M., Ebeling, P., Samaniego-Eguiguren, L., and Kumar, R.: WQQDB: water quality and quantity data base Germany [data set], http://www.ufz.de/record/dmp/archive/7754 (last access: 9 August 2022), 2020.

Newman, A. J., Clark, M. P., Sampson, K., Wood, A., Hay, L. E., Bock, A., Viger, R. J., Blodgett, D., Brekke, L., Arnold, J. R., Hopson, T., and Duan, Q.: Development of a large-sample watershed-scale hydrometeorological data set for the contiguous USA: data set characteristics and assessment of regional variability in hydrologic model performance, Hydrol. Earth Syst. Sci., 19, 209–223, https://doi.org/10.5194/hess-19-209-2015, 2015.

Pflugmacher, D., Rabe, A., Peters, M., and Hostert, P.: Pan-European land cover map of 2015 based on Landsat and LUCAS data, PANGAEA [data set], https://doi.org/10.1594/PANGAEA.896282, 2018.

Rode, M., Wade, A. J., Cohen, M. J., Hensley, R. T., Bowes, M. J., Kirchner, J. W., Arhonditsis, G. B., Jordan, P., Kronvang, B., Halliday, S. J., Skeffington, R. A., Rozemeijer, J. C., Aubert, A. H., Rinke, K., and Jomaa, S.: Sensors in the Stream: The High-Frequency Wave of the Present, Environ. Sci. Technol., 50, 10297–10307, https://doi.org/10.1021/acs.est.6b02155, 2016.

Rotteveel, L. and Sterling, S. M.: The Surface Water Chemistry (SWatCh) database: A standardized global database of water chemistry to facilitate large-sample hydrological research, Earth Syst. Sci. Data Discuss. [preprint], https://doi.org/10.5194/essd-2021-43, in review, 2022.

Samaniego, L., Kumar, R., and Attinger, S.: Multiscale parameter regionalization of a grid-based hydrologic model at the mesoscale, Water Resour. Res., 46, W05523, https://doi.org/10.1029/2008WR007327, 2010.

Shangguan, W., Hengl, T., Mendes de Jesus, J., Yuan, H., and Dai, Y.: Mapping the global depth to bedrock for land surface modeling, J. Adv. Model. Earth Sy., 9, 65–88, https://doi.org/10.1002/2016ms000686, 2017.

Simpson, D., Benedictow, A., Berge, H., Bergström, R., Emberson, L. D., Fagerli, H., Flechard, C. R., Hayman, G. D., Gauss, M., Jonson, J. E., Jenkin, M. E., Nyíri, A., Richter, C., Semeena, V. S., Tsyro, S., Tuovinen, J.-P., Valdebenito, Á., and Wind, P.: The EMEP MSC-W chemical transport model – technical description, Atmos. Chem. Phys., 12, 7825–7865, https://doi.org/10.5194/acp-12-7825-2012, 2012.

Sivapalan, M.: Pattern, Process and Function: Elements of a Unified Theory of Hydrology at the Catchment Scale, in: Encyclopedia of Hydrological Sciences, edited

by: Anderson, M. G. and McDonnell, J. J., Wiley, https://doi.org/10.1002/0470848944.hsa012, 2006.

Tarasova, L., Basso, S., Wendi, D., Viglione, A., Kumar, R., and Merz, R.: A Process-Based Framework to Characterize and Classify Runoff Events: The Event Typology of Germany, Water Resour. Res., 56, e2019WR026951, https://doi.org/10.1029/2019WR026951, 2020.

Twarakavi, N. K. C., Sakai, M., and Šimůnek, J.: An objective analysis of the dynamic nature of field capacity, Water Resour. Res., 45, W10410, https://doi.org/10.1029/2009WR007944, 2009.

UNEP: GEMStat database of the Global Environment Monitoring System for Freshwater (GEMS/Water) Programme, United Nations Environment Programme [data set], https://gemstat.org (last access: 9 August 2022), 2018.

van Genuchten, M. T.: A Closed-form Equation for Predicting the Hydraulic Conductivity of Unsaturated Soils, Soil Sci. Soc. Am. J., 44, 892–898, https://doi.org/10.2136/sssaj1980.03615995004400050002x, 1980.

Van Meter, K. J., Basu, N. B., and Van Cappellen, P.: Two centuries of nitrogen dynamics: Legacy sources and sinks in the Mississippi and Susquehanna River Basins, Global Biogeochem. Cy., 31, 2–23, https://doi.org/10.1002/2016GB005498, 2017.

Vigiak, O., Grizzetti, B., Zanni, M., Aloe, A., Dorati, C., Bouraoui, F., and Pistocchi, A.: Domestic waste emissions to European freshwaters in the 2010s (v. 1.0), European Commission, Joint Research Centre (JRC) [data set], https://data.jrc.ec.europa.eu/dataset/0ae64ac2-64da-4c5e-8bab-ce928897c1fb (last access: 9 August 2022), 2019.

Vigiak, O., Grizzetti, B., Zanni, M., Aloe, A., Dorati, C., Bouraoui, F., and Pistocchi, A.: Domestic waste emissions to European waters in the 2010s, Sci. Data, 7, 33, https://doi.org/10.1038/s41597-020-0367-0, 2020.

Virro, H., Amatulli, G., Kmoch, A., Shen, L., and Uuemaa, E.: GRQA: Global River Water Quality Archive, Earth Syst. Sci. Data, 13, 5483–5507, https://doi.org/10.5194/essd-13-5483-2021, 2021.

WMO: Manual on Low-flow Estimation and Prediction, Operational Hydrology Report (OHR), Volume No. 50, Series Volume No. 1029, World Meteorological Organization, ISBN 978-92-63-11029-9, https://library.wmo.int/doc_num.php?explnum_id=7699 (last access: 9 August 2022), 2008.

Wollheim, W. M., Bernal, S., Burns, D. A., Czuba, J. A., Driscoll, C. T., Hansen, A. T., Hensley, R. T., Hosen, J. D., Inamdar, S., Kaushal, S. S., Koenig, L. E., Lu, Y. H., Marzadri, A., Raymond, P. A., Scott, D., Stewart, R. J., Vidon, P. G., and Wohl, E.: River network saturation concept: factors influencing the balance of biogeochemical supply and demand of river networks, Biogeochemistry, 141, 503–521, https://doi.org/10.1007/s10533-018-0488-0, 2018.

Yang, S., Bertuzzo, E., Büttner, O., Borchardt, D., and Rao, P. S. C.: Emergent spatial patterns of competing benthic and pelagic algae in a river network: A parsimonious basin-scale modeling analysis, Water Res., 193, 116887, https://doi.org/10.1016/j.watres.2021.116887, 2021.

Zacharias, S. and Wessolek, G.: Excluding Organic Matter Content from Pedotransfer Predictors of Soil Water Retention, Soil Sci. Soc. Am. J., 71, 43–50, https://doi.org/10.2136/sssaj2006.0098, 2007.

Zarnetske, J. P., Bouda, M., Abbott, B. W., Saiers, J., and Raymond, P. A.: Generality of Hydrologic Transport Limitation of Watershed Organic Carbon Flux Across Ecoregions of the United States, Geophys. Res. Lett., 45, 11702–11711, https://doi.org/10.1029/2018gl080005, 2018.

Zink, M., Kumar, R., Cuntz, M., and Samaniego, L.: A high-resolution dataset of water fluxes and states for Germany accounting for parametric uncertainty, Hydrol. Earth Syst. Sci., 21, 1769–1790, https://doi.org/10.5194/hess-21-1769-2017, 2017.

List of publications

Publications included in this thesis

Ebeling, P., Kumar, R., Lutz, S. R., Nguyen, T., Sarrazin, F., Weber, M., Büttner, O., Attinger, S., Musolff, A. (2022). 'QUADICA: water QUAlity, DIscharge and Catchment Attributes for large-sample studies in Germany'. *Earth Syst. Sci. Data* 14(8), 2022, 3715-3741. https://doi.org/10.5194/essd-14-3715-2022

Ebeling, P., Dupas, R., Abbott, B., Kumar, R., Ehrhardt, S., Fleckenstein, J. H. and Musolff, A. (2021), 'Long-Term Nitrate Trajectories Vary by Season in Western EuropeanCatchments', *Global Biogeochemical Cycles* 35(9), e2021GB007050. https://doi.org/10.1029/2021GB007050

Ebeling, P., Kumar, R., Weber, M., Knoll, L., Fleckenstein, J. H. and Musolff, A. (2021),'Archetypes and Controls of Riverine Nutrient Export Across German Catchments', *Water Resources Research* 57(4), e2020WR028134. https://doi.org/10.1029/2020WR028134

Other peer-reviewed publications

Ehrhardt, S., **Ebeling, P.**, Dupas, R., Kumar, R., Fleckenstein, J. H. and Musolff, A. (2021), 'Nitrate Transport and Retention in Western European Catchments Are Shaped by Hydroclimate and Subsurface Properties', *Water Resources Research* 57(10), e2020WR029469. https://doi.org/10.1029/2020WR029469

Ebeling, P., Händel, F., and Walther, M. (2019), 'Potential of mixed hydraulic barriers to remediate seawater intrusion', *Science of The Total Environment*, 693, 133478. https://doi.org/10.1016/j.scitotenv.2019.07.284

Data products published in repositories

Ebeling, P., Kumar, R., Weber, M. and Musolff, A. (2022), 'QUADICA - water quality, discharge and catchment attributes for large-sample studies in Germany, HydroShare' https://doi.org/10.4211/hs.0ec5f43e43c349ff818a8d57699c0fe1

Ebeling, P., Kumar, R. and Musolff, A. (2022), 'CCDB - catchment characteristics database Germany, HydroShare' https://doi.org/10.4211/hs.88254bd930d1466c85992a7dea6947a4

Ebeling, P. and Dupas, R. (2021), 'CCDB - catchment characteristics data base France and Germany, HydroShare' https://doi.org/10.4211/hs.c7d4df3ba74647f0aa83ae92be2e294b

(Eidesstattliche) Versicherungen und Erklärungen

(§ 8 Satz 2 Nr. 3 PromO Fakultät)

Hiermit versichere ich eidesstattlich, dass ich die Arbeit selbstständig verfasst und keine anderen als die von mir angegebenen Quellen und Hilfsmittel benutzt habe (vgl. Art. 64 Abs. 1 Satz 6 BayHSchG).

(§ 8 Satz 2 Nr. 3 PromO Fakultät)

Hiermit erkläre ich, dass ich die Dissertation nicht bereits zur Erlangung eines akademischen Grades eingereicht habe und dass ich nicht bereits diese oder eine gleichartige Doktorprüfung endgültig nicht bestanden habe.

(§ 8 Satz 2 Nr. 4 PromO Fakultät)

Hiermit erkläre ich, dass ich Hilfe von gewerblichen Promotionsberatern bzw. –vermittlern oder ähnlichen Dienstleistern weder bisher in Anspruch genommen habe noch künftig in Anspruch nehmen werde.

(§ 8 Satz 2 Nr. 7 PromO Fakultät)

Hiermit erkläre ich mein Einverständnis, dass die elektronische Fassung der Dissertation unter Wahrung meiner Urheberrechte und des Datenschutzes einer gesonderten Überprüfung unterzogen werden kann.

(§ 8 Satz 2 Nr. 8 PromO Fakultät)

Hiermit erkläre ich mein Einverständnis, dass bei Verdacht wissenschaftlichen Fehlverhaltens Ermittlungen durch universitätsinterne Organe der wissenschaftlichen Selbstkontrolle stattfinden können.

…….
Ort, Datum, Unterschrift